Materials Sciences Corporation

ANALYSIS OF WOVEN FABRICS FOR REINFORCED COMPOSITE MATERIALS

Technical Final Report

MSC TFR 1715/0210

August, 1987

Prepared by:

Norris F. Dow
V. Ramnath
B. Walter Rosen

Prepared for:

National Aeronautics and Space Administration
Langley Research Center
Hampton, Virginia 23665-5225

Gwynedd Plaza II, Bethlehem Pike, Spring House, PA • 215-542-8400

PREFACE

This report, covering the work done for the NASA Langley Research Center on Contract NAS1-17205 during the period November 3, 1982 through April 30, 1987, was prepared by the Principal Investigator for MSC, Mr. Norris Dow, in collaboration with Mr. V. Ramnath and the Program Manager for MSC, Dr. B. Walter Rosen and other members of the MSC staff. The authors wish to express their appreciation to their collaborators and to Mr. H. Benson Dexter, who was the NASA Technical Representative, for their many contributions and technical discussions.

APPROVED BY;

B. Walter Rosen
Program Manager

TABLE OF CONTENTS

TABLE OF CONTENTS, (Cont'd)

TABLE OF CONTENTS, (Cont'd)

LIST OF SYMBOLS

(As used in main text, tables, and figures)

A	area
E	Young's modulus
G	shear modulus
I_P^*	indicator number for plate efficiency, $I_P^* = \dfrac{E_P^{1/6}\sigma_{cu}^{1/2}}{\rho}$
	where, $E_P = 1/2 \dfrac{\sqrt{E_x E_y}}{1-\sqrt{\nu_{xy}\nu_{yx}}} + G_{xy}$
L	length
v	volume
ν	Poisson's ratio
ρ	density
σ	stress
ϕ	direction angle for reinforcement

SUBSCRIPTS AND SUPERSCRIPTS

cu	compressive ultimate stress
f	fiber
fb	fraction fiber in fiber bundle
fp	fraction packing of fiber bundles
IC	measure of impact damage resistance
m	matrix
su	shear ultimate stress
tu	tensile ultimate stress
x,y,z; 1,2,3	axis directions

INTRODUCTION

A courtship is in progress between the centuries-old technology of textiles and the decades-old technology of composites. Stimulated initially by potential economies offered by the ease of handling stable, woven constructions (to begin with primarily 8-harness satins), and encouraged by their performance in prototype composite structures (for example, ref. 1), a beneficent interaction between these two technologies has been developing. Resulting, on the textile side, are advances in weaving capabilities to make available multi-directional (ref. 2) and complex three-dimensional configurations (ref. 3). On the composite side are: (1) advances in analysis methodology as required for the complex configurations becoming available, including effects due to yarn out-of-straightness (crimp) due to weaving and composite lay-up; (2) progress toward development of criteria for thru the thickness reinforcement to reduce both interlaminar shear and damage resulting from lateral impact (refs. 4 & 5); and (3) generation of guidelines for improved three-dimensional (multi-directional) weaves.

The present report covers activities in all three of the latter categories. Interactions with textile technology are suggested as appropriate.

The question indubitably arises - apart from economies from ease of handling in manufacture, why woven instead of the obviously superior straight filaments? Importantly, as will be shown, if the detail designs of weave and composite are proper - providing gently crimped yarns and avoiding matrix pockets and voids, there should be no loss in overall properties for wovens compared to straight filaments in multi-directional arrays. The total potential reinforcement for a given volume fraction is a constant, and actually, as will become increasingly evident in succeeding sections of this report, there are a number of corollary potentials for multi-directional properties offered by woven fabrics: -

(1) Multi-directional reinforcement in a single ply
(2) Potentials for interweaving two or more plies to eliminate interlaminar weaknesses
(3) Possibilities of weaving each lamina's reinforcement to nest with adjacent laminae, to yield constructions of tailorable thicknesses with enhanced thru the thickness properties.

OBJECTIVES

The first objective of this study was the development of improved analytical methods for the prediction of the physical behavior of woven fabric reinforced composites. Here the interaction between textiles and composites is indeed important. Photomicrographs of fabric reinforced composites (Figure 1) reveal significant changes in reinforcement geometry from idealized weave structure. Emphasis was accordingly first directed toward the development of realistic models of the actual resulting constructions to use as bases for analyses. Analysis development was undertaken for all aspects of mechanical behavior. Progress toward that goal is reported in the sections "DEVELOPMENT OF ANALYTICAL METHODS FOR WOVEN-FABRIC REINFORCED COMPOSITE STIFFNESS PROPERTIES" AND "DEVELOPMENT OF ANALYTICAL METHODS FOR WOVEN-FABRIC REINFORCED COMPOSITE STRENGTHS." Comparison of the resulting property predictions with experiments and with predictions of previously available analysis are given in the following section .

Because of the demonstrated susceptibility of conventional composite laminates to damage from lateral impact (for example, ref. 5) studies were made of the influence of thru the thickness running reinforcement elements for the enhancement of thickness direction composite properties. Trade-offs among longitudinal, transverse (widthwise), and transverse (thicknesswise) properties were quantified. The objectives here were adequate definitions of both the potentials for property improvements in the thickness direction and types of configurations appropriate to provide such improvements. Thus a framework was established within which desired interactions between composite and textile design technologies might develop. Studies relating to the thru the thickness reinforcement problem are found in all sections of this report, including the composite/textile technology interactions in the sections "DEVELOPMENT OF ADVANCED WEAVES" and "GUIDELINES FOR IMPROVED FABRIC DESIGNS".

Improved fabric designs comprise the main objective. Through improvement in understanding of the detailed mechanics of reinforcement, combined with advances in fabric formation techniques, it does appear that impact-resistant composites of enhanced performance capabilities can become accessible. Indeed progress is in evidence in both these areas: for example, the mechanics of in-plane reinforcement by fabrics as influenced by fineness of weave has been demonstrated (ref. 6); the mechanics of thru the thickness reinforcement by finely spaced stitches has been demonstrated (ref. 7); and the weaving of triaxial fabrics hitherto considered not feasible has been demonstrated (ref. 8). Studies directed toward improved fabric reinforcement designs are presented in the final sections of this report.

APPROACH

The woven fabrics problem was divided into three areas, to be attacked sequentially:

(1) Development of Analytical Methodology
(2) Evaluations of Performance Potentials
(3) Development of Advanced Weaves

At the outset it appeared that the state of the art of analysis of woven fabric reinforced composites needed to be both reviewed and supplemented to provide an adequately sound basis for the attack upon the following areas of investigation. The approach elected was a combined analytical/experimental investigation. The analysis was derived in large measure from the accumulated composite analysis technology that had led to references 9 and 10 and that has been incorporated in MSC's X-CAP computer code. Experiments were conducted at the Langley Research Center to help guide and confirm the further development of analytical methodology. Similarly, for the determination of performance potentials, structural/material efficency analysis procedures presented in references 11 and 12 were used as the starting point for extension to the 3-D regime of thru the thickness reinforced composites. Thus in both the analysis development and the performance evaluation areas the approaches used were essentially a typical build-on-developed-technology approach. For the development of advanced weaves, however, a rather different approach was required.

Weavers, like magicians, are not wont to divulge their methodologies. Reference material corresponding to that available for analysis development and performance evaluation was not available to delineate the limits of weaving capabilities. Accordingly, the approach used for this third and most important phase of the problem was the two-fold one of

(1) Defining desirable weave configurations, based on the results of the first two areas of investigation.
(2) Determining or inventing ways in which such configurations can be made.

As will be seen, limitations arising because of lack of weaving capability related almost entirely to fineness of weave. The ordinary multi-harness loom can weave an astonishing variety of three-dimensional configurations. The recent development of a multi-harness triaxial loom (ref. 8) further extends the capability. Advanced textile technology appears capable of supporting advanced composite reinforcement technology.

RESULTS

The results obtained in each of the categories "Analysis Methodology", "Potentials for Performance", and "Development of Advanced Weaves" are summarized below. More detailed discussion of the development and implications of these results will be found in the body of the report.

ANALYSIS METHODOLOY

1. A realistic model was generated to use as the basis for development of the analysis of the properties of woven-fabric reinforced composites. This model was derived based on photomicrographic studies (for example Fig. 1) of various woven-reinforced composites performed at the Langley Research Center. Use of this model led to the development of analytical procedures yielding elastic property predictions in good agreement with experiments for satin weaves in tension but less satisfactory agreement for plain weaves and in compression.

2. A sequential failure analysis, similar to sequential ply failure analysis for 2-D composite laminates, was developed for 3-D constructions. This analysis utilized "Average Stresses" on fibers and matrix (as described herein) to determine regions of first and subsequent fracture, and established methodology for accounting for resulting property degradations. Satisfactory correlations with experiment were demonstrated for this analysis in tension, - less so in compression.

3. The MSC NDPROP computer code was modified to incorporate the foregoing results. Thus stiffness and strength properties of composites incorporating multi-directional woven reinforcements are readily accessible. A copy of this code has been furnished to NASA Langley.

POTENTIALS FOR PERFORMANCE

1. Invariance

The fact that certain combinations of calculated stiffness properties of composites are invariant for a fixed volume fraction reinforcement was employed to assist in the evaluation of trade-offs in properties resulting from configuration changes. It was shown, for example, in reference 13, that if the reinforcing configuration provides three-dimensional isotropy, the magnitudes of the elastic properties achieved are identical regardless of the specifics of the configuration used. Similarly, it can be shown that the sum of the stiffnesses in the stiffness matrix (usually C_{11}, C_{12} etc. in the literature, $\$_1$, $\$_2$ etc. herein) is another such invariant - hence, the enhancement of any one stiffness (such as the thru the thickness stiffness $\$_6$) can only be done at the expense of other stiffnesses.

2. For Composites in Tension

a. The most effective approach for evaluating performance potentials of various configurations in tension was found to be a plot of tensile stress/density ratio $\frac{\sigma_x}{\rho}$ (as ordinate) vs. <u>both</u> shear stiffness/density ratio $\frac{G_{xy}}{\rho}$ and axial stiffness ratio $\frac{E_x}{\rho}$ (as abscissae) so that the ordinate value for a given configuration identifies both its shear and extensional properties. On such a plot, maximum values of $\frac{\sigma_x}{\rho}$ which meet required stiffness $\frac{G_{xy}}{\rho}$ and $\frac{E_x}{\rho}$ represent minimum weight. (For example figure 2. Detailed discussion of such evaluations is given in the section "Methodologies for Structural Efficiency Evaluations.") Figure 2 is a summary plot of this type, embodying many of the results of the evaluations performed, as noted in the following discussion.

(1) Maximum values of $\frac{\sigma_x}{\rho}$ (highest strength/weight ratio and lightest structure) always correspond to minimum shear stiffness requirements $\frac{G_{xy}}{\rho}$ but not to minimum axial stiffness requirements $\frac{E_x}{\rho}$). As is to be expected, appropriate reinforcement configurations approach simple unidirectionals as shear stiffness requirements decrease.

(2) As shear stiffness requirements increase, off-axis reinforcements are needed and values of $\frac{\sigma_x}{\rho}$ decrease. Up to shear stiffness requirements approximately 2 to 2 1/2 times that provided by unidirectional reinforcements, simple angle-ply (up to about ±15°) constructions are the lightest. For higher shear stiffness, $\pm\phi°/90°$ configurations emerge as most efficient (as shown in figure 3 for T-300; also found true for Kevlar, as noted in the section "Parametric Studies of Properties"; further, for the same shear stiffness T-300 yielded substantially lighter weights then Kevlar - the margin increasing with increasing stiffness requirements; hybrids were intermediate - Figures 4 and 5.

b. A plot such as figure 2 is also useful for comparing various approaches to design for tension with requirements for stiffness in shear - a common problem encountered in aircraft wings, helicopter rotor blades, propellers, etc. Thus, for example, figure 2 provides the following comparisons:

(1) Aluminum alloy (7075-T6) is not in contention with T-300/5208 in either the $\pm\phi°$ or the $\pm\phi°/90°$

configuration. If additional requirements such as 3-D isotropy are encountered, however, the aluminum alloy emerges superior. Similarly, if substantial thru the thickness reinforcement is required, the advantage of T-300/5208 over aluminum is greatly reduced or lost completely. For example, the Omniweave braids (ref.14) either in the basic "diagonals of a cube" configuration (OM_4 in fig. 2) or with a fifth (axial) reinforcement direction added (OM_5), while providing good tensile strength values if loaded along a reinforcement direction, are deficient in shear stiffness. If the braids are oriented for maximum shear stiffness (the bottom point on the figure) they are deficient in tensile strength.

(2) If stiffness is not a criterion, figure 2 shows that E-Glass is in contention for tensile loadings. The tensile strength/density ratio is superior to aluminum, but the strain at failure is approximately five times as much. Axial stiffness is more apt to be a limitation for glass than for aluminum or for any of the other fibers considered.

c. The invariance of the sum of the terms in the stiffness matrix demands a penalty in other stiffnesses for an increase in thru the thickness stiffness. This penalty is rather attenuated by being distributed among the various other stiffnesses so that the effect on any one - such as the longitudinal or shear stiffness is relatively small. For example, for a typical quasi-isotropic 2-D configuration the transfer of enough reinforcement material to the thru the thickness direction to produce a 1% increase in the thru the thickness-direction stiffness, E_z, results in less than 0.1% decrease in axial stiffness, E_x, and shear stiffness, G_{xy}. (See the section "Effects of thru the thickness Reinforcements" herein.)

While such stiffness penalties are orderly and small, effects on structural performance in some cases can be substantial and cannot be readily anticipated. The addition of thru the thickness-running elements can induce new failure modes which can be particularly degrading of most efficient configurations. For example, for a 0°/±15° 2-D configuration putting 10% of the reinforcement material in the thru the thickness direction can reduce the value of axial strength/density, $\frac{\sigma_x}{\rho}$, by 25% (see figure 6) approximately. While the corresponding reduction for a ±15°/90° configuration is only about 16% (see figure 7), it is still greater than the percentage of material employed thru the thickness. Thru the thickness reinforcement demands thorough design and analysis for most effective performance.

Hybrids play a role in the thru the thickness reinforcement problem. Here again adequate design and analysis is important. For example, 0°/±15° T-300 composites with 10% Kevlar thru the thickness show only about 11% loss in $\frac{\sigma_x}{\rho}$ compared to the simple 2-D configuration (c.f. 25% for all T-300 as above). Reversing the constituents to 0°/+15° Kevlar with 10% T-300 thru the thickness, however, is a disaster - nearly 50% loss in $\frac{\sigma_x}{\rho}$ due to the reduced overall stiffnesses provided by the Kevlar and the reduced compliance to transverse cracking provided by the T-300. See figures 8 and 9. Totally apart from its inherent toughness, Kevlar appears most promising, if properly used, as a thru the thickness constituent.

3. <u>For Composites in Compression</u>

(a) In compression, material strength/density values ($\frac{-\sigma_x}{\rho}$) are not the adequate measures of performance that values of $\frac{\sigma_x}{\rho}$ are in tension. A measure that accounts for buckling resistance as well as strength is required. Such a measure is the "Indicator Number" derived in reference 15 and used extensively in references 12 and 16. The plate buckling Indicator Number $I_p^* = \frac{E_p^{1/6}\ \sigma_{cu}^{1/2}}{\rho}$, considered in detail in the section "Parametric Studies of Properties" herein, is accordingly used here to provide a plot for compressive properties (figure 10) similar to Figure 2 for tension.

Results of evaluations from Figure 10 are as follows:

(1) Maximum values of I_p^* (lightest structures) always correspond to minimum shear stiffness requirements $\frac{G_{xy}}{\rho}$ (but not to minimum axial stiffness requirements $\frac{E_x}{\rho}$). As is to be expected, configurations appropriate for such requirements approach simple unidirectionals.

(2) As shear stiffness requirements increase, off-axis reinforcements are needed and values of I_p^* decrease. The $\pm\phi°/90°$ configuration was found to be the most effective for all shear stiffness requirements with either graphite or Kevlar reinforcements.

(3) Comparisons of Indicator Numbers for T-300/5208 2-D constructions with other reinforcement configurations and aluminum alloy confirm the superiority of T-300 for compressive applications. The gains possible compared to aluminum or 3-D constructions like Omniweave (OM_4, OM_5) are indeed substantial.

(4) The Indicator Number provides a direct measure of the performance penalty associated with the addition of thru the thickness reinforcement. The magnitude of the decrease is summarized by the plot of Figure 11 for a 2-D quasi-isotropic configuration. The value of the

decrement in I_P^* for an increment in thru the thickness reinforcement increases as the amount of thru the thickness reinforcement increases. When the total amount of thru the thickness reinforcement is 1/10 of the total in the configuration, the decrement is 1/10 of 1% for each 1% increment in the amount of thru the thickness reinforcement. When the amount of thru the thickness reinforcement is 4/10 of the total, the decrement in I_P^* increases to 3/10 of 1%. Typical results of deploying 1/10 and 2/10 of the total volume fraction reinforcement thru the thickness are illustrated in Figure 12 for the $\pm\phi°/90°$ configuration.

ADVANCED WEAVES

Progress was made toward the definition of weaving concepts which both capitalize on advances in textile technology and are most appropriate for composite reinforcement, as follows:

(1) Nesting. In order to take advantage of the inherent flexibility of construction provided by laminations, a "bumpy" fabric construction was proposed (Figure 13) comprising auxiliary warps running atop, or on both faces of an essentially plain weave base fabric. Stacking such constructions provides overlapping, thru the thickness yarns as illustrated in Figure 14. First samples of such constructions, woven of T-300 carbon yarns by Textile Technologies, Inc., showed adequate dimensional consistency for nesting, volume fraction reinforcements of over 50 percent and performance characteristics consistent with such volume fractions (see Figures 2 and 10). While the area of damage from lateral impact for the nested construction was found to be smaller than for equivalent ordinary laminates, strengths after such damage were not increased. Photomicrographs suggested that the bumps were not bumpy enough. In addition, the weaver suggested that the tightly woven plain weave base fabric (18 x 18 yarns/inch) may

have suffered substantial fiber damage during the weaving operation.

(2) Second Generation Bumpy Fabric. A second generation bumpy fabric was designed in light of the foregoing observations (Figure 15). In this design the auxiliary warps are stacked two high and the spaces between them laterally reduced substantially compared to those of Figures 13 and 14. This constuction is currently being tested.

(3) Bulbous Blade Bumpy (BBB) Fabrics. A bumpy fabric construction to provide even greater thru the thickness reinforcement than provided by the simple auxiliary warps of (1) or (2) above has been designed. This construction both increases the bumpy overlap and provides for a kind of interference fit between laminae (Figure 16). This construction has not yet been woven. A patent has been applied for covering these bumpy constructions.

(4) Triaxial Weaves. Triaxial weaves combine potential for multi-directional reinforcement within a single ply, and, in some configurations such as the Substrate Weave, potentials for high volume fraction reinforcement. The substrate weave with auxiliary warps as shown in Figure 17 has been woven by Richard Dow on NASA Contract NAS1-17877. A corresponding fabric with BBB has been designed (Figure 18).

(5) Stitchbase Weaves. The "locked intersection" characteristic of many triaxial weaves provides a dimensional stability to the construction adequate to insure that stacked configurations can be precisely matched. Thus weaves with regular holes could be stitched through the holes for thru the thickness reinforcement without damage to the yarns in the fabric. Example Stitchbase Weaves are shown in Figure 19.

(6) Fine Weave. A related study (ref. 6) has shown a substantial "size effect" for fine weaves as reinforcements. The use of such

construction is proposed for special applications such as at bolted or riveted joints. The new developments in triaxial weaving that led to the capability to weave the Substrate Weave make fine triaxial weaves a possibility for such applications.

DEVELOPMENT OF ANALYTICAL METHODS FOR THE CALCULATION OF WOVEN-FABRIC-REINFORCED COMPOSITE STIFFNESS PROPERTIES

The mechanics of woven-fabric-reinforced composites are not as well understood as those for tape-reinforced laminates. The behavior of woven-fabric-reinforced composites is related to the additional geometric parameters introduced by the complexity of the weave construction and modifications caused by the composite fabrication process. A methodology was therefore developed, based on extensive photomicrographs of various woven reinforcements provided by NASA Langley, to establish a realistic base for the development of the detailed analytical three-dimensional treatment required to account properly for this complexity. The development of this analysis for both biaxial and triaxial weaves is described herewith.

BIAXIAL WEAVES

Various analytical models exist in the literature for the prediction of woven-fabric reinforced composite elastic properties, references 17 and 18. Three different models --- "the mosaic model", "the fiber undulation model" and "the bridging model" have been used by Chou and Ishikawa for predicting fabric thermoelastic properties. Each of these approaches is based on a one or two dimensional representation of the woven fabrics.

During the course of the present program, a number of different mathematical models have been formulated. A detailed account of the approach, the modeling assumptions and results for standard biaxial fabrics is given in Appendix A. Comparison with experimental data indicated that the "NDPROP" model was the most suitable for the desired purpose.

"NDPROP" MODEL

An important aspect of the development of this model was the formulation of a rational geometric configuration to represent the various fabrics under consideration. The geometric models were based on photomicrographs similar to the ones shown in Figure 20. As seen in the photomicrographs, the yarns assume several cross-sectional shapes and flatten out to fill space almost completely. Very small amounts of matrix interstitial pockets can be seen with the result that high fiber volume fraction reinforcements can occur. The "NDPROP" geometry developed to correspond to these photomicrographs is shown in cross-section in Figure 21 and the variation in shape of a given yarn bundle along its length is shown for two different weaves in Figure 22. Based upon the geometry of Figure 22, the yarn bundle can be represented as an assemblage of short unidirectional fiber reinforced composites oriented in various directions. This geometric assemblage represents the input to the "NDPROP" code to be used for calculation of elastic stiffnesses.

Properties can be obtained from the code for either an Upper Bound (using assumed displacement fields and minimizing the strain energy) or a Lower Bound (using assumed traction fields and minimizing the complementary energy). For relatively small amounts of yarn waviness and small amounts of interstitial matrix material the Upper Bound yields results that are closer to experimentally determined values. Typical results generated using the Upper Bound are shown for T-300/Epoxy (v_f=0.6) composites for selected weaves in Table 1. The trends of increasing in-plane and decreasing thru the thickness moduli as the harness number of the weave increases can be observed. The eight harness satin fabric properties are similar to the properties of a cross-plied (0°/90°) laminate, properties of which are also shown in Table 1. Similar trends can also be observed for in-plane and thru the thickness shear moduli. Detailed correlations between predicted and measured fabric properties are presented in the section entitled "Experimental Program".

TRIAXIAL WEAVES

A related approach to that used for biaxial fabrics was used for triaxial fabrics. Here analyses were based on a first approximation assumption of elliptical yarn cross-sections. A cross-sectional view of triaxial weave with such a yarn is shown in Figure 23. The procedure for determining the yarn geometry and volume fraction of reinforcement is also outlined in Figure 23. The approach is first to assume the volume fraction of yarn within the yarn bundle and then solve a transcendental equation to determine the yarn geometrical parameters. The overall volume fraction of fiber within the fabric is finally computed and checked with the experimentally determined value.

From Figure 23, it can be observed that the yarn consists of a straight section of length ℓ and two curved segments of ellipses subtending angles of γ at their centers of curvature. For input to NDPROP the curved segments are divided into several smaller segments and given sets of direction numbers and volume fractions. Typical results generated using this code are shown for the BiPlain and Substrate Weaves (see Figure 24) in Table 2. The Substrate Weave has less crimp in the warp yarns than the BiPlain Weave. In the results shown in Table 2, the X-direction refers to the direction bisecting the +30 degree and -30 degree directions. The results are calculated for fiber volume fractions of 50%. Properties of a ±30°/90° laminate have also been listed for comparison purposes.

EFFECTS OF THRU THE THICKNESS RUNNING ELEMENTS

The procedure to analyze special weaves having thru the thickness running elements is essentially similar to that outlined above. The basic repeating elements of the weaves are first identified. The yarns are then divided into straight segments, curved segments or segments of any of the standard weaves described earlier. Further sub-division of the curved segments may be done as required. The sets of volume fractions and direction numbers of the various yarn bundle segments used to model the weave are used by "NDPROP" to calculate the elastic properties.

For filaments without curved segments algebraic equations representative of the NDPROP analysis were derived for the strength and stiffnesses properties of 3-D $0°/\pm\phi°/90°/90°$ configurations. These equations, are readily programmable for a hand-held calculator. Programs for the Hewlett-Packard 41-C are included with the equations in Appendix C.

DEVELOPMENT OF ANALYTICAL METHODS FOR THE CALCULATION OF WOVEN-FABRIC REINFORCED COMPOSITE STRENGTHS

Based on comparisons with other approaches and some experimental results, the "NDPROP" Upper Bound was selected as the approach to be followed for determining fabric stiffness properties. Efforts were then devoted to developing a corresponding consistent and realistic model for predicting strengths, based on the assumed geometric configurations for the various fabrics and the "NDPROP" Upper Bound.

Initially, the strength approach was formulated on a yarn bundle level. Three-dimensional stress analyses were conducted on the fabric composite modeled as an assemblage of oriented yarn bundles. Stresses on each yarn bundle in its local coordinate system were calculated and compared to input yarn bundle allowable strengths using the maximum stress failure criterion. One of the main disadvantages of this method lies in the fact that the input bundle allowable strengths have to be modified each time the assumed fiber volume fraction within the bundle is changed. While this is fairly straight-forward for axial strengths, no consistent procedure exists to define bundle transverse and shear strengths as a function of fiber volume fraction.

Accordingly, an "Average Stress Model" was used and the strength approach was formulated on an overall constituent fiber and matrix level. The yarn bundle stresses were broken down into constituent fiber and matrix stresses using the "Average Stress Model". That is, the bundle stresses and strains were equated to the volume averages of the corresponding fiber and matrix stresses and strains. Then, the constitutive stress-strain relations of the fiber, matrix and yarn bundle were used to compute constituent stresses. Thus, the matrix (or fiber) stresses could be determined as a function of the fiber volume fraction, compliance matrices of the fiber, matrix and unidirectional composite and the applied composite bundle stresses. Although the stress states in the fiber and matrix vary from point to point, failure analyses conducted on the basis of average states of stress may be more realistic. The input allowables for the fiber and matrix strengths were used to compute failure ratios for the fiber and matrix for tensile, compressive and shear failure modes. The strength approach was then extended into a sequential failure analysis mode wherein matrix dominated failures are considered not catastrophic. If the first failure is a matrix failure, the matrix properties for the appropriate yarn bundle are reduced and the analysis is continued until fiber failure occurs. Ultimate strength is characterized by fiber axial failure or sudden increase in strain levels due to stiffness reductions as a result of large numbers of transverse and shear failures. The details of the strength approach are relegated to Appendix B.

Typical results from this approach are shown for T-300/Epoxy biaxial and triaxial woven fabrics in Tables 3 and 4, respectively. Trends among the various fabrics styles are similar to those seen for the elastic properties. Discussions regarding the merits of the strength approach will be made in the section entitled "COMPARISONS OF ANALYSIS AND EXPERIMENT" wherein the results of data correlations between predicted and measured fabric strengths will be presented.

COMPARISONS OF ANALYSIS AND EXPERIMENT

An experimental program was conducted at NASA, Langley with the following objectives:

1. To verify the analytical predictions of standard woven fabric properties and strengths and to explore differences in toughness characteristics among the various fabric reinforced composites and compare them to those of equivalent tape laminates;
2. To serve as a guide for modifying the analytical models and methodology based upon the data correlations in 1;
3. To determine the properties and strengths of the advanced weaves developed in this program and compare them to those predicted analytically;
4. To determine possible enhancements in toughness characteristics among the newly developed advanced weaves in comparison with both tape laminates and standard weaves; and
5. To guide the development of advanced weaves based on the shortcomings or advantages experienced in 3 and 4.

The results presented in this section are arranged in two parts: those for standard biaxial and triaxial weaves and those for the newly developed advanced weaves.

Standard Weaves

Tests were conducted at NASA, Langley using T-300/934 graphite/epoxy material and the following fabric styles: Plain weave, Oxford weave, 5 Harness Satin weave, 8 Harness Satin weave and BiPlain Triaxial weave. Some Kevlar/934 triaxial weave samples were also available for testing.

Biaxial Weave Elastic Properties and Strengths

Calculations were made using the "NDPROP" code in order to perform data correlations with experimental results. The weave parameters used to model the geometry are shown in Table 5. Assuming that the overall fiber volume fraction within the bundle, v_f, is known from experimental measurements, the fiber volume fraction within the bundle, v_{fp}, and the packing fraction of yarns, v_{fp}, have to be adjusted to satisfy the relation:

$$v_f = v_{fb} \times v_{fp}$$

The experimentally observed in-plane elastic properties are shown in Table 6 along with "NDPROP" calculated values.

The measured data were obtained from the experimental program conducted at NASA, Langley. Both tabbed and untabbed specimens were used for the tension test. Gage section failures were consistently observed only for the untabbed specimens. Hence the reported tensile strengths are the averages of the untabbed specimen data. The tensile moduli have been calculated using both the untabbed and tabbed specimen data. The compression test data reported were obtained from the "Short Block Compression Test" method. The ±45° Tension test was used to determine the fabric in-plane shear properties. The calculated tensile moduli are about an average of 12% higher than measured values for the Oxford, 5 and 8 harness satin weaves. However, a large discrepancy (30%) exists in the case of the plain weave. This may have been caused by either or both of the following factors:

1. The plain weave sample may be of poor quality. C-scans of the material indicated damaged areas and the photomicrographs indicated areas with voids and resin rich areas.
2. The higher crimp in the plain weave may cause the measured values to be lower than predicted by the Upper Bound. Although the analytical model accounts for the crimp in the woven fabrics, the Upper Bound assumption tends to minimize the effects of high cross-over angles. The Upper Bound predictions thus represent properties attainable from good quality woven fabrics (fewer voids and damaged areas) having small amounts of yarn waviness.

For the plain weave, the tensile and compressive moduli are not significantly different. For the other weave styles, the compressive moduli are lower by an average of approximately 13%. The analysis does not distinguish between tensile and compressive moduli. A possible reason for the lower measured compressive moduli lies in the inherent complexity of compression testing of composites. This complexity arises because the test fixture and specimen must be designed so that buckling must not occur (unsupported length must be small) and the gage section stress state must be uniform and uniaxial (gage section must be sufficiently far from the supports).

The in-plane shear moduli are in good agreement for the five and eight harness satin weaves. For the Oxford weave, a balanced ±45° lay-up was not used, hence the data are not reported.

Comparisons between calculated and measured in-plane tensile, compressive and shear strengths of the same biaxial fabrics are shown in Table 7. Both the initial and ultimate failure stresses are reported in the table. It can be observed that the predicted tensile first failure occurs at a stress of approximately 70 ksi for all four fabric styles. For the 5HS and 8HS fabrics, the measured strengths are in good agreement with the predicted final failure stress (~110 ksi). However, for the plain weave and Oxford weave, the measured strengths are closer to the first failure stresses. A possible explanation is that the higher amounts of crimp in these two fabric styles cause matrix dominated failures to be more severe by not allowing the loads to get effectively redistributed among the fibers.

In the case of predicted shear strengths, the first failures are matrix dominated failures. Since the shear loads have to be primarily carried by the matrix in orthogonal biaxial fabrics, subsequent failures are also matrix failures and occur at stresses even lower than the first failure stress. Therefore the first failure stress represents the ultimate strength also since the fabric can no longer carry shear loads after the first matrix failure has occurred. The measured and predicted shear strengths are in good agreement, as can be observed from Table 7.

In the case of predicted compressive strengths, the first failure in each case is a fiber failure. Thus the initial and ultimate compressive strengths are the same for each of the four fabric styles. The results are in good agreement for the 5HS and 8HS weaves. The predicted values are much higher than the measured values for the plain weave and Oxford weave (warp direction). The reason for the large discrepancy can be explained in the following manner. For conventional tape laminates numerous studies have been carried out, aimed at deriving analytical expressions for the axial compressive strengths of unidirectional fiber bundles. These strengths are then used in laminate failure analyses. The axial compressive strength can be analytically shown to be equal to the unidirectional composite axial shear modulus. Measured strengths have consistently been much lower. It is postulated here that the discrepancy may be explained by a decrease in the matrix shear modulus because its proportional limit has been exceeded. For an absolutely straight fiber bundle under compression, the axial stress in the matrix is low due to the large ratio of fiber to matrix axial Young's modulus. Also, the shear stress in the matrix is zero.

Because of imperfections associated with fabrication, small amounts of waviness exist in the fibers (for conventional tape laminates). When these fibers are under compression, the states of stress in the matrix are a combination of normal and shear stresses. The shear stresses become significant even at small angles of waviness and cause the matrix to yield resulting in low compressive strengths. Accordingly, the allowables that are used for conventional laminate strength analyses reflect this knockdown.

Additional knockdowns in strength can occur if the crimp in the fabrics is high. This is because the matrix shear stresses are a strong function of the off-axis angle and may become more significant than the normal stresses in terms of causing the matrix to yield even at off-axis angles as low as

5°. Therefore, the compressive strength allowables that go in as input to the stress analysis have to be calculated as a function of the off-axis angle. More work is required in this area so that the postulate can be formalized and incorporated into the computer code.

Iosipescu shear tests were done on the fabrics at the University of Wyoming. Results are presented in reference 19. Both in-plane and transverse shear moduli and strengths are presented in Table 8 along with the predicted values. The predicted shear moduli in all cases are higher than the measured values by about 20-30%. The calculated in-plane shear strengths, however, under predict the measured values by about 20%. The predicted transverse shear strengths are in reasonable agreement with data. For in-plane moduli and strengths, the ±45° tension tests are generally more reliable than the Iosipeseu shear tests and those results were in better agreement with calculations, as indicated in Tables 6 and 7.

Triaxial Weave Elastic Properties and Strengths

The parameters used for modeling the T-300/934 and Kevlar/934 triaxial weaves are shown in Table 9. The comparisons between calculated and measured properties and strengths are shown in Table 10. The triaxial woven fabrics had essentially the same crimp as the plain weave biaxial fabrics discussed above and in addition had more resin rich areas (low values of v_f). The following conclusions may be made from the data:

1. Measured tensile and compressive moduli are almost identical. This is in agreement with the analytical model assumptions of equal tensile and compressive moduli.
2. Both moduli and strengths in the fill direction are higher than corresponding warp direction values by about 10-15%.
3. Measured compressive strengths are significantly higher than the tensile strengths (about 16-20%).

The comparisons between predicted and measured values indicate that the agreement is not as good as for biaxial weaves. The analysis predicts higher ultimate tensile and compressive strengths in the warp direction as compared to the fill direction, but measured data indicate otherwise. A possible explanation for the discrepancy in the tensile strength stems from the fact that the y-direction load is directly along the fiber; therefore, failure in this direction only occurs when axial fiber breakage occurs. In the warp direction, matrix failures may have caused material degradation leading to premature failures. The analytical model for triaxial weaves thus needs some modification and improvement.

Biaxial Weave Toughness Properties

In order to evaluate toughness properties of fabric composites, NASA Standard Toughness tests (reference 20) were done on the various types of fabrics. The results of the compression after impact tests are shown in Table 11. Results for the equivalent tape lay-up are also presented in the table. The results of the other toughness tests (Double Cantilever Beam, Open Hole Tension and Open Hole Compression) are shown in Table 12. Results for the corresponding tape lay-ups were obtained from reference 22 and are also presented in the same table.

The toughness tests generally indicated that fabrics possess better toughness characteristics as compared to conventional tape laminates as evidenced by higher strengths and ultimate strains for the "Compression after Impact" test and higher values of interlaminar fracture toughness (G_{IC}) as measured by the "Double Cantilever Beam" test. It was originally thought that open hole tension and compression strengths for fabrics may be higher than those for equivalent tape laminates because of the increased delamination resistance that the fabrics are likely to provide. It is possible that the increased resistance was not observed because the weave patterns were fairly coarse (small amounts of intersections of warp and fill yarns per square inch). Inhibition of the initial failures through the use of finer weaves was demonstrated in another research program, reference 6.

Advanced Weaves

As described in the section "Development of Advanced Weaves", some "Building Block" configurations were defined during the course of this program. The first configuration from this category is termed the "Auxiliary Warp Reinforcement Weave" and consists of two nested configurations --- "Nested face-ply" and "Nested Internal-ply" (see Figure 14).

Elastic property and strength calculations were made in order to assess the potential of these woven configurations.

Auxiliary Warp Reinforcement Weaves

Calculations were made based on the following specifications:

1. 3000 filaments/yarn;
2. Yarn count of 18 for the basic plain weave, and
3. T-300/Epoxy material.

The first task was the identification of the repeating volume element with realistic dimensions based on the photomicrographs and measured volume fractions. It was assumed that the area fraction of the fiber within the yarn was 70%.

The nested face-ply configuration contains within its repeating element, 8 yarns each in X and Y directions constituting the 18x18 plain weave, 6 circular section yarns (assumed straight) traveling in the X direction and 6 non-circular auxiliary yarns in the Y-direction holding the other yarns in place. The lengths and direction numbers of the plain weave were obtained based on the yarn count, cross-over angle and yarn cross-sectional area. Similar calculations were done for the auxiliary yarns, and curved segments were approximated by short straight segments to determine volume fractions and yarn orientations. The resulting set of direction numbers and volume fractions were fed into "NDPROP" in order to get an Upper Bound prediction on elastic properties and strengths.

A similar procedure was used to calculate properties of the nested internal-ply configuration. The repeating element in this case contains the same 8 yarns of the basic plain weave in the X and Y directions but contains 12 circular straight yarns in the X-direction and 12 auxiliary yarns in the Y-direction.

The materials that were tested were the nested face-ply, the 4-ply building block and the 12-ply building-block configurations. The 4-ply fabric consists of 1 nested face-ply and 1 nested internal-ply. The 12-ply fabric material consists of 1 nested face-ply and 5 nested internal-plies. The properties of these building-block configurations were generated from the basic face-ply and internal-ply properties. The results of these calculations are shown in Table 13. The comparison between predicted and measured values from tests conducted on these materials are shown in Table 14. In general, the measured tensile moduli and strengths and the measured compressive moduli are 20-30% lower than the calculated values. The major discrepancy is in the compressive strength values.

Because of these low values a new design of auxiliary warp weaves was developed based on the following considerations: (1) elimination of the resin-rich pockets as far as possible and (2) use of yarns with longer float lengths, minimizing crimp while retaining the basic features of the original building-block configuration. The following section contains the details of the Revised Design Auxiliary Warp reinforcement weaves.

Revised Design Auxiliary Warp Reinforcement Weaves

The building-block for the advanced weave also consists of the face-ply and internal-ply configurations. The modified face-ply design is shown in Figure 26. It can be observed that the basic weave corresponds to a four harness satin in the fill direction and a five harness satin in the warp direction. As before, a thread count of 18 per inch and 3000 filaments/yarn were assumed for the calculations.

The dimensions of the repeating element are 4Lx10L as can be seen from Figure 26. Different cross-sectional views of the face-ply and internal-ply configurations at various sections are shown in Figures 27 and 28, respectively. The repeating element contains two each of the yarns shown in sections B-B, C-C, D-D, and E-E, and one each of the yarns shown in sections A-A and F-F, see Figures 27 and 28. The nested face-ply and nested internal-ply configurations are shown in Figure 29. Property calculations were made by assuming a volume fraction of fiber within the yarn of 70%. The "NDPROP" Upper Bound results for the Revised Design Auxiliary Warp nested face-ply and nested internal-ply are shown in Table 11. Also listed are the properties for a 4-ply nested lay-up consisting of two face-plies and two internal-plies, shown in Figure 29. Test data on the revised weave design are awaited.

EVALUATION OF POTENTIALS FOR PERFORMANCE OF WOVEN FABRIC REINFORCEMENTS

Evaluation of the potentials for performance of woven-fabric reinforced composites is complicated by the fact that both strength and stiffness in various directions (including the thru the thickness direction) are variables dependent on the weave design. In general, therefore, as the following results will emphasize, trade-offs are needed among the pertinent variable properties to define most appropriate weave configurations. Likewise, the methodology of evaluation must be extended to include additional pertinent design parameters such as thru the thickness reinforcement, as will be shown.

APPROACH

The approach used to evaluate the potentials of woven reinforcement constructions was to utilize the NDPROP computer code to calculate properties for typical composites, with parametric variations of reinforcement configurations, and relate the results to the familiar standard, - 7075-T6 aluminum alloy. This baseline material has much to recommend it beside familiarity. For one thing, it is hard to beat, particularly, as will be seen, for three-dimensional properties. Thus composites offering potentials superior to the aluminum can be considered of interest. The fact that wovens of T-300 can indeed out-perform aluminum for many applications will be repeatedly demonstrated in the following evaluations.

Throughout these calculations the assumption is made that the woven (or braided) constructions are comparable to multi-harness weaves, having minimal crimp and accompanying maximum properties. (Similar assumptions have been employed successfully for 3-D carbon-carbon composites, for example, reference 21). Thus the potentials for performance are represented.

EVALUATION PROCEDURES

A wide range of reinforcement configurations, both 2-D and 3-D, was evaluated, as follows:

2-D (1) 0°/90°, of varying proportions

(2) $\pm\phi°$

(3) $\pm\phi°/90°$

(4) $0°/\pm\phi°$

3-D (1) The 2-D constructions with thru the thickness reinforcement.

(2) Omniweave

(3) Nested constructions

Primary constituents considered were T-300 and Kevlar 49 filaments in a 5208 resin matrix. Volume fractions were 60% throughout.

In accordance with the results found in the section "COMPARISONS OF ANALYSIS AND EXPERIMENT", with the assumption that woven constructions of minimal crimp are accessible, as they in general appear to be, the upper bound NDPROP analysis was employed for the evaluation of elastic properties. For strength, first failure rather than that for cumulative damage was the criterion, as representative of conservative design practice for repeated loading.

EVALUATION PARAMETERS

Tension

The important design parameters for tensile applications were determined to be:

(1) Tensile strength/density ratio $\frac{\sigma_x}{\rho}$ - a direct measure of weight of material required to carry a tensile load.

(2) Tensile stiffness/density ratio $\frac{E_x}{\rho}$ - a prime measure of weight of material required to limit the extension of a tensile element to some desired value.

(3) Shear stiffness/density ratio $\frac{G_{xy}}{\rho}$ - a measure of weight of material required to limit distortion of an element subject to shear.

Of these parameters (1) and (3) are generally most important. For tensile applications, the tensile load to be carried is the essence of the design. For many applications, - aircraft wings, helicopter rotor blades, propellers, etc., shear stiffness, relating to flutter and divergence, is also of major importance. Axial stiffness, relating to overall bending of the wing for example, may also be a design consideration, particularly for composites, because in general as the configuration is changed to increase shear stiffness the axial stiffness decreases, as the following plots will show.

Compression

The parameters for compression are similar to those for tension, but require an additional one to account for the possibility of compressive buckling, as follows:

(1) Compressive strength/density ratio $\frac{-\sigma_x}{\rho}$ - a direct measure of weight of material required to carry a compressive load.

(2) Compressive stiffness/density ratio $\frac{E_x}{\rho}$ - in general equal to $\frac{E_x}{\rho}$ for tension.

(3) Shear stiffness/density ratio $\frac{G_{xy}}{\rho}$ - in general equal to $\frac{G_{xy}}{\rho}$ for tension.

Additionally,

(4) Compressive buckling Indicator Number I_P^* - a value combining the material strength and stiffness properties to measure weight required to carry the applied load. Different formulations are required (see ref. 12) depending on whether a plate (I_P^*) or shell (I_S^*) construction is involved. Herein only I_P^* will be used; results for I_S^* while numerically different would lead to identical conclusions. The formulation for I_P^* is

$$I_P^* = \frac{E_P^{1/6} \sigma_{cu}^{1/2}}{\rho}, \quad \left(\frac{in^5}{lb}\right)^{1/3}$$

where:

E_P, plate buckling modulus, $= \frac{1}{2} \frac{\sqrt{E_x E_y}}{1-\sqrt{\nu_{xy}\nu_{yx}}} + G_{xy}$

with E_x, E_y longitudinal and transverse extensional moduli, psi

ν_{xy}, ν_{yx}, in-plane Poisson's ratios

G_{xy}, in-plane shear stiffness, psi

σ_{cu}, compressive strength, psi

ρ, density of material, pci

EVALUATIONS

Tension

Evaluations for tensile applications are presented in the format used in Figure 2 for the various materials and constructions considered. In every case the ultimate tensile strength/density ratio $\frac{\sigma_x}{\rho}$ is plotted against $\frac{G_{xy}}{\rho}$, the shear stiffness/density ratio and $\frac{E_x}{\rho}$ the axial stiffness/density ratio. Curves for shear stiffness are solid; for the axial stiffness dashed. Tick marks on the curves identify specific proportions, as indicated.

Biaxial 0°/90° Configurations

Evaluations begin (Figure 30 & 31) for a simple, biaxial configuration, representative of 5 harness or 8 harness satin weave, with various proportions of reinforcement in the warp and fill directions (see the vertical curve to the left on each of the figures). Such variations in proportions might be produced, for example, simply by changing the weft yarn count while holding the warp yarn count constant. The figures show that the simple 0°/90° configuration has a minimal shear stiffness/density ratio (25%

of that of aluminum, 15% for Kevlar) for all proportions, but enormous (up to 750%) improvement in strength/density ratio.

Biaxial Configurations.

For many, perhaps most, applications, shear stiffnesses greater than those attained by the biaxial 0°/90° reinforcement are required. Braided biaxial constructions making angles $\pm\phi°$ to the axial x-direction can provide such increases, as shown on Figures 30 and 31. For the T-300 braid at the same strength/density as aluminum the shear stiffness/density ratio is approximately 225% that of aluminum. For Kevlar the ratio is 130%. Strengthwise, for the same shear stiffness/density as aluminum the gains are even greater, being approximately 330% for T-300 and 80% for Kevlar.

Triaxial Configurations.

Shear stiffnesses greater than for the 0°/90° configuration are also obtainable with triaxial weaves in either $0°/\pm\phi°$ or $\pm\phi°/90°$ configuration. Rather surprisingly, the $\pm\phi°/90°$ arrangement is generally superior to the $0°/\pm\phi°$ configuration but there are exceptions for the latter, as the following comparisons bring out.

Numerical comparisons taken from figures 32-35 with nominal aluminum-alloy properties, are indicated in the table below

Property	Aluminum Alloy	T-300 and (Kevlar-49)		
		$\pm\phi°$	$\pm\phi°/90°$	$0°/\pm\phi°$
$\frac{G_{xy}}{\rho}$, in.	40,000,000	40,000,000	40,000,000	40,000,000
$\frac{\sigma_x}{\rho}$, in.	700,000	3,200,200[3] (1,300,000) @ $\phi=20°$	3,800,000[3] (570,000)[2] @ $\phi=20°$	3,300,000[3] (1,700,000) @ $\phi=20°$
$\frac{\sigma_x}{\rho}$, in.	700,000	700,000	700,000	700,000
$\frac{G_{xy}}{\rho}$, in.	40,000,000	87,000,000 @ $\phi=25°$ (39,000,000) @ $\phi=35°$	80,000,000 @ $\phi=40°$ (38,000,000) @ $\phi=30°$	82,000,000 @ $\phi=45°$ (52,000,000) @ $\phi=40°$

(1) The superiority of the braid for high shear stiffness (±45° is a maximum).

(2) Deficiency regions in the Kevlar construction due to the compressive weakness of Kevlar. In this case, Poisson contractions induce compressive failures in the 90° filaments.

(3) Minor but not substantial superiority of the ±ϕ°/90° configuration.

Both the ±ϕ°/90° and the 0°/±ϕ° configurations can be made with various proportions as shown in figures 32 to 35. For the ±ϕ°/90° configuration, highest values of $\frac{\sigma_x}{\rho}$ are achieved with most material in the ±ϕ° direction and also highest values of $\frac{G_{xy}}{\rho}$ are achieved with the highest fractions of material in the ±ϕ° direction (Figs. 32 & 33). The reverse is true for $\frac{\sigma_x}{\rho}$ for the 0°/±ϕ° cases (Figs. 34 & 35), hence specific comparisons such as those in the table above may be misleading unless truly optimized proportions of each approach for the application have been evaluated. The use of envelope curves such as those of figure 36 provides such optimization. From these envelopes it is evident that the ±ϕ°/90° configuration is indeed superior to the 0°/±ϕ° configuration except for the restricted area encountered in comparisons with aluminum for which ϕ approaches 45° and in which the curves come together.

<u>Effect of Use of First Failure Criterion in Evaluations</u>

As previously noted, the failure criterion used throughout these evaluations was that of first failure. In order to determine whether the use of this criterion unduly penalized the composite constructions, as for example in relation to their performance compared to aluminum, a few exploratory calculations were made using the cumulative damage failure criterion. Typical results are shown in Figure 37 for a ±ϕ°/90° construction. As would be expected, the final failure criterion is shown to raise the value of $\frac{\sigma_x}{\rho}$ for given values of $\frac{G_{xy}}{\rho}$ and $\frac{E_x}{\rho}$. Differences are not substantial - on the order of 10%. The conservative use of the first failure criterion for these evaluations appears to be appropriate.

Implications of Analytical Methodology Used (NDPROP, Equations of Appendix C) on Effects of Thru the Thickness Reinforcement

The addition of thru the thickness (TTT) reinforcement to planar reinforcement configurations is shown to be twofold: (1) it detracts from the volume fraction available for in-plane reinforcement, and (2) it introduces the possibility of new failure modes associated with the transverse (TTT) direction. The first of these effects is straightforward. One percent taken away from unidirectional (axial, 0°) stiffening and used TTT reduces the 0° stiffness slightly less than 1% (0.875% for T-300/5208 @ v_f=0.6) but increases the TTT stiffness by much more than 1% (12.5% for the same construction). Surprisingly, the in-plane transverse (90°) stiffness is also increased (by 1.72% due to Poisson's ratio effects). (These changes are not in contradiction to the theorem that the sum of the stiffness $ in the stiffness matrix for the material is invariant; 1% of the original <u>axial</u> stiffness is a quantity which is the same order of magnitude as 12.5% of the original <u>transverse</u> stiffness.) The effect on strength, however, can be substantial; instead of the 330,000 psi tensile strength of the unidirectional composite, the TTT configuration fails in a transverse mode at 220,000 psi. (Starting with a balanced 0°/90° T-300/5208, v_f = 0.6 configuration, removing 1% of the in-plane reinforcement, and adding it TTT, decreases both the 0° and 90° in-plane stiffnesses 0.66% and increases the TTT stiffness 11%).

Various combinations of woven reinforcements were investigated to evaluate the effects of thru the thickness reinforcement. Typical results are shown in Figures 38-41.

For both T-300 and Kevlar constructions the effects of adding thru the thickness reinforcements on resulting composite properties (both stiffness and strength) are shown to be orderly and not disproportionate to the percentage TTT addition as long as new failure modes are not encountered. New failure modes were encountered for the 0°/±ϕ° configurations in both T-300 and Kevlar for proportions having mostly 0° reinforcements. Accordingly calculations for strength of these configurations yielded substantially lower stresses than for the same configurations without TTT (see particularly figures 40 and 41 for low values of $\frac{G_{xy}}{\rho}$ and $\frac{v_{f_z}}{v_f}$).

If new failure modes are not introduced by TTT reinforcements the relationships between losses in tensile strengths and increases in thru the thickness reinforcement can be summarized on a simple plot of $\Delta\sigma_{x_{max}}$ vs. v_{f_z} (figure 42).

The figure shows that if the losses in tensile strength are to be kept under ten percent, even for simple, constant failure modes, the volume fraction of TTT reinforcement must also be kept below 10% of the total reinforcement.

Compression

Evaluations for compressive applications are presented in a similar format to that used for tension, i.e. plots of $\frac{-\sigma_x}{\rho}$ vs. the parameters $\frac{G_{xy}}{\rho}$ and $\frac{E_x}{\rho}$ with the curves for $\frac{-\sigma_x}{\rho}$ vs. $\frac{E_x}{\rho}$ as dashed lines indicative of the lesser role of E_x in most cases to that played by the shear stiffness G_{xy}. To evaluate buckling resistance, curves are also plotted of I_p^*, as discussed in the section on "EVALUATION PARAMETERS".

Biaxial 0°/90° and ±φ° Configurations.

For the simple biaxial configurations in compression the evaluations (figures 43 and 44) depict similar characteristics to those found in tension. The 0°/90° configuration is characterized by low shear stiffnesses; the ±φ configurations have reasonable combinations of compressive strength/density and shear stiffness/density - better than the aluminum alloy for T-300/Epoxy. The Kevlar suffers from its low compressive strength, and is not competitive in any of these simple configurations.

Evaluations with account taken of buckling characteristics utilizing I_p^* as the measurement parameter in place of $\frac{\sigma_x}{\rho}$ (figure 45) show that the ±φ° configuration can potentially be made in a plate structure to carry the same compressive loading, at the same shear stiffness, as aluminum alloy for 3/8 the weight.

Kevlar was not evaluated for use in plates in compression because its low compressive strength does not make it attractive for such application.

Triaxial Configurations.

As noted for tension, the use of triaxial weaves, either $0°/\pm\phi°$ or $\pm\phi°/90°$, can provide both high compressive strength/density ratios and high shear stiffness/density ratios, as the specific values (taken from figures 46 and 47) in the table below reveal.

Property	Aluminum alloy	T300/5208 $\pm\phi°$	T300/5208 $\pm\phi/90°$	T300/5208 $0°/\pm\phi°$
$\frac{G_{xy}}{\rho}$, in.	40,000,000	40,000,000	40,000,000	40,000,000
$\frac{-\sigma_x}{\rho}$, in.	600,000	2,900,000 @ $\phi \approx 20°$	2,900,000(2) @ $\phi \approx 20°$	2,500,000 @ $\phi = 25°$
$\frac{-\sigma_x}{\rho}$, in.	600,000	600,000	600,000	600,000
$\frac{G_{xy}}{\rho}$, in.	40,000,000	81,000,000(1) @ $\phi \approx 40°$	80,000,000 @ $\phi \approx 45°$	80,000,000 @ $\phi = 40°$

As previously found for tension, the table shows (1) superiority (though less than in tension) of the braid for high shear stiffnesses, and (2) minor but not substantial superiority of the $\pm\phi°/90°$ configuration over the $0°/\pm\phi°$ configuration.

Here again, however, as in tension, specific comparisons may be misleading. The best basis for evaluation appears to be by comparisons of the best against the best, using the most rigorous comparative parameters. Accordingly, envelope curves of I_P^* vs. $\frac{G_{xy}}{\rho}$ and $\frac{E_x}{\rho}$ were drawn for the various configurations and used as the basis for overall evaluations, as shown in Figure 48. The results of these overall evaluations are summarized below.

(1) The triaxial $\pm\phi°/90°$ weave provides superior performance in compression as measured by higher values of the Indicator Numbers I_p^*, for the range of shear stiffnesses achieved for $0°<\phi°<45°$, as compared to (a) 0°/90° biaxial weaves, (b) $\pm\phi°$ biaxial braids, (c) $0°/\pm\phi°$.

(2) The superiority of the $\pm\phi°/90°$ weave is greatest at shear stiffnesses corresponding to those achieved by the weave at intermediate angles of ϕ, as in the range $20°<\phi°<30°$. The superiority diminishes to zero as ϕ approaches 0° or 45°.

(3) The plot of figure 48 forms a basis for comparison of performance among various other materials and configurations. (Such comparisons are made and reported in the section "POTENTIALS FOR PERFORMANCE".)

HYBRIDS

Woven hybrid reinforcements are perhaps unduly intriguing because they are easy to make. In both biaxial and triaxial construction the use of different materials in warp and fill imposes no difficulty, indeed in some cases may make the weaving easier.

From a performance standpoint the prime motivation for hybrid constructions relates to the thru the thickness reinforcement problem. The use of fibers of higher "toughness" such as nylon or Kevlar appears appropriate for investigation even though as yet the relative roles of thru the thickness strength, stiffness, and toughness have not been adequately characterized. Further, the addition of any thru the thickness running element must be evaluated in terms of its possible influence on in-plane performance.

In-plane hybrids also deserve consideration. The basis for hope that some hybrid combination might prove more effective than either constituent follows some such pattern as the following: (1) the transverse stiffnesses of material (b) are much less than those of material (a) therefore, the use of (b) transversely will not as readily lead to premature cracking in tension as the use of (a) transversely, - so a combination of (b) with (a) should be better than (a) alone. While there may be merit to this argument, detailed analysis reveals that the benefits are limited, as will be shown.

Analyses were made of various hybrid combinations, following the same approach used for the performance evaluation of individual materials. In all cases the materials studied were T-300 and Kevlar-49. On all figures, tick marks on the curves denote angles of 15°, 30°, and 45°, as in Figure 2.

EVALUATIONS OF HYBRIDS

Tension

Biaxial 0°/90° Weaves

Evaluations begin (fig. 49) for a simple biaxial weave with T-300 in the warp (0°) direction and varying proportions of Kevlar-49 in the fill. (The reverse hybrid having Kevlar in the 0° direction was not considered because of the adversely high transverse stiffness of T-300. The damaging effect of this characteristic will be considered in the section "Thru the Thickness Reinforcements" to follow.) Figure 49 shows clearly the desired improvement in tensile properties for the hybrid over those for either T-300 or Kevlar alone. For both materials by themselves the smallest fraction of transverse fiber induces premature cracking whereas the Kevlar transverse fiber accommodates the low strain of the 0° T-300 environment.

With this encouraging result, the next question to be considered is "Can this same improvement be found in triaxial weaves providing increased shear stiffnesses compared to those for the biaxial constructions?"

Triaxial $\pm\phi$°/90° and 0°/$\pm\phi$° Weaves

Answers to the above question are explored in Figure 50 to 55. The overall answer is a negative one, for various reasons, such as:

(1) Putting a 90° Kevlar into a $\pm\phi$°/90° configuration ($\pm\phi$° being T-300) introduces a new failure mode, - compression in the Kevlar due to Poisson contraction, - with substantial strength reductions (Figure 50).

(2) Putting a 90° T-300 into a $\pm\phi°/90°$ configuration ($\pm\phi°$ being Kevlar) aggravates the transverse failure mode caused by the 90° element (Fig. 51).

(3) Putting a 0° Kevlar into a $0°/\pm\phi°$ configuration ($\pm\phi°$ being T-300) does not do much harm, but it does not do any good either (Fig. 52).

(4) Putting a 0° T-300 into a $0°/\pm\phi°$ configuration ($\pm\phi°$being Kevlar) does do much good, but not as much as putting T-300 all around (Fig. 53, and c.f. Fig. 34).

(5) Comparisons of the best - the envelope curves for hybrids and non-hybrids of both triaxial weaves show that the $\pm\phi°/90°$ T-300 is the best followed closely by the $0°/\pm\phi°$ T-300 (Figs. 54 and 55). The $\pm\phi°/90°$ Kevlar is the poorest, again due to the compressive failures induced in the 90° elements. The hybrids fall in all cases between the Kevlar and the T-300.

Thru the Thickness Reinforcements

Typical results of evaluations of the effects of using Kevlar reinforcements thru the thickness are shown by comparisons of Figures 56 and 57. Figure 56 shows losses in performance due to additions of T-300 thru the thickness reinforcement to a triaxial $0°/\pm\phi°$ configuration. Figure 57 shows lesser losses for the use of Kevlar TTT. Figure 58 and 59 indicate similar results when the base configuration is $\pm\phi°/90°$. Kevlar appears especially attractive as a TTT reinforcement material.

Compression

In compression, the evaluation results show that, as in tension, Kevlar has a role to play as a thru the thickness reinforcement but not as a booster of in-plane performance. Because of the similarity of these results to those for tension they will be summarized only briefly here before going on to treat the more complex problem not encountered in tension, of combined strength and buckling resistance.

Biaxial 0°/90° Weaves

Hybrid combinations of T-300 filaments in the warp (0°) direction and Kevlar in the fill (90°) direction are represented in Figure 60. No merit is evident for the hybrids compared to 100% T-300.

Triaxial ±ϕ°/90° and 0°/±ϕ° Weaves

For the 0°/±ϕ° configuration the Kevlar is least damaging if used in the ±ϕ° direction filaments (Figs. 61 and 62). For the ±ϕ°/90° configuration (Figs. 63 and 64), Kevlar in the 90° direction is nearly as effective as T-300, but used in the ±ϕ° directions it destroys the usefulness of the configuration. Because of the potential increased toughness of Kevlar, a ±ϕ°(T-300)/90° (Kevlar) hybrid may be of interest. The penalty to be paid in terms of potential $\frac{-\sigma_x}{\rho}$ values is 10% to 15% as shown by the envelope curves of Figure 65. Losses if used in the 0°/±ϕ° configuration (Fig. 66) are substantially higher.

Thru the Thickness Reinforcement

The most appropriate use for Kevlar as a hybrid with fibers like T-300 appears to be in the thru the thickness direction. Here the losses for the addition of small volume fractions of thru the thickness Kevlar are minimal (Figures 67 and 68) and less than those for all T-300 constructions (compare Figs. 8 and 67, for example).

Evaluations on the Basis of Indicator Numbers

If shear stiffnesses greater than one fourth those of aluminum are required so that a simple biaxial configuration is inadequate (Fig. 69), the only hybrids competitive with 100% T-300 are the ±ϕ°/90° configuration with Kevlar in the 90° direction (Fig. 70). Even here the best has the least Kevlar. The 0°/±ϕ° at proportions giving shear stiffness/density ratios about equal to aluminum are indeed much lighter than aluminum (Fig. 71), but lesser than the $\pm\phi°/90°$ configurations. As is to be expected, the mostly Kevlar hybrids (Figs. 72 and 73) are not competitive for these compressive loading with the mostly T-300 hybrids (Figs. 70 and 71).

Thru the thickness, however, Kevlar does a most effective job (Fig. 72). Reductions of only approximately 5% and 10% in I_p^* values accompany TTT Kevlar reinforcements in planar $\pm\phi°/90°$ T-300 weaves for 10% and 20% TTT Kevlar.

<u>DEVELOPMENT OF ADVANCED WEAVES</u>

Development of advanced weaves had the following two principal objectives superposed on the ongoing one of providing improved in-plane properties (compression, shear), namely:

(1) Weaves to facilitate enhancement and control of thru the thickness properties.

(2) Weaves to facilitate fabrication of composites for high load intensities (thick constructions), particularly weaves providing for tapering thickness to accommodate varying load intensities.

(3) Fiber architectures that inherently improve damage tolerance.

Three advanced weave concepts have been developed to meet the foregoing objectives. These weaves derive in part from the analyses described in the previous sections, in part from supporting studies and tests at the Langley Research Center, and in part from developments in related studies (refs.8 and 22). These concepts are the auxiliary warp (or "Bumpy Fabric") concept (Patent Applied for), the Stitchbase Weave, and the Multi-layer Triaxial, as described below.

BUMPY FABRICS

The Bumpy Fabric concept is simple. As illustrated in Figure 75 it proposes nesting configurations that overlap thru the thickness to provide increased interlaminar interface area and provide that separating forces be resisted by shear as well as tension. Such a configuration also makes accessible the same flexibility for tapering thickness that ordinary laminated construction provides.

While the concept is simple, the execution is not. First trial weaves (Figs. 76 and 77), adequately bumpy appearing on paper, turned out to be not very bumpy as fabricated. Further the intentionally widely spaced auxiliary warps (Fig. 77) did not spread laterally sufficiently during autoclave curing to fill the open spaces allotted for them. Voids and resin-rich areas that were created led to premature failures, especially in compression. Even so, lateral impact tests of bumpy fabric laminates using these initial samples did appear to show reduced areas of damage compared to comparable conventional laminates.

To increase the bumpiness, a revised design was made (Fig. 78). Again, the bumps appeared greater in cross-sections on paper than as woven. Tests have not yet been performed on the revised design material.

Because of the continued lack of bumpiness of the revised design, a concept similar to a blade-stiffened construction is proposed (Figure 79). The auxiliary warps are woven vertically, perpendicular to the base fabric, as shown. With the addition of a double thickness "bulb" to the tops of the blades, a truly interlocking construction is achieved. As the cross-sectional view reveals, the fill yarns that tie in the bumps truly provide thru the thickness reinforcement. This design has yet to be fabricated.

STITCHBASE WEAVES

In a study related to this program (ref. 7), Dexter and Funk found notable improvements in thru the thickness properties of laminates stitched together with closely-spaced Kevlar stitches. About the only drawback to this stitching approach appeared to be damage induced by stabbing the stitching needles through the reinforcing yarns. To overcome this drawback a "Stitchbase" woven construction is proposed. Examples of such weaves are shown in Figure 80.

Triaxial weaves can be woven with regularly spaced holes in a wide variety of configurations. The necessary accuracy of yarn spacing of the Barber-Colman type triaxial loom together with the high Young's modulus of composite reinforcement yarns and the "locked intersection" characteristic of the Stitchbase Weaves insures that such construction can be accurately stacked with holes matching holes. Thus the potential is created for stitching through the holes without yarn damage. Furthermore, technology is available, as from the computer industry, for positioning the stitching needles (e.g. the soldering or welding heads for computer chip connections) with precision.

No stitchbase weaves have been made, however, their development is recommended.

THICK TRIAXIAL WEAVES

Recent exploratory development of triaxial weaving equipment with multiple harnesses (like a biaxial Dobby loom) opens new possibilities for triaxial fabrics. Samples of the Substrate Weave with auxiliary warps (fig. 81) have already been woven (in ref. 8). The next step is weaving of a Substrate Weave with Bulbous Blade auxiliary warps (fig. 82). Constructions like this have the potential to provide thru the thickness reinforcement with tapered thickness constructions (as with ordinary laminates, by changing number of plies), together with multi-axial yarns for improved shear stiffness compared to biaxial weaves.

Thick triaxial constructions can also be woven on the multi-harness, Barber-Colman type machine, providing a multi-layer fabric with thru the thickness running yarns as shown in Figure 83. While tapering thickness could probably be programmed into the weaving, it would have to be done so specifically for the end application and would not have the generality of applicability of the Bumpy constructions.

THE PERFECT WEAVE

A corollary to the development of the multi-harness triaxial loom is the potential for weaving triaxially interwoven triaxial constructions such as that shown in Figure 84. This construction (1-up, 1-down in all three directions) is the most nearly perfect of the triaxial weaves, having symmetries in all three in-plane directions. It is perhaps of greater interest as a textile than as a composite reinforcement; emphasis on its development is not proposed or recommended. As textile technology continues to advance, however, to the point that such weaves can be woven with high yarn counts, they may find application in composites in such places as in the vicinity of joints or other points of stress concentration to take best advantage of the gain in ultimate strength recently found for finely woven reinforcements.

GUIDELINES FOR IMPROVED FABRIC DESIGNS

In this section a summary is made of unexplored areas which appear to offer promise of performance improvements of various kinds. In some cases weaving capability already exists to produce the weave described, in others extensions to textile technology are required as will be noted. In all cases an assessment of projected potentials is attempted.

BIAXIAL FABRICS

Float Length

The curves of Figure 85 suggest that, for conventional weave constructions as the float length decreases below about 3 yarn diameters (corresponding to 4 harness satins) losses in in-plane reinforcement effectivenesses begin to increase rapidly. The likely cause is the increasing ratio of crimped to straight yarn with diminishing float lengths, possibly exaggerated by the abruptness of the 8-up/1-down, 6-up/1-down, 4-up/1-down nature of satins. If the weaves were 8-up/2-down, 6-up/2-down, etc. the direction reversals would be less abrupt and in-plane yarn effectivenesses can be expected to improve. The magnitude of improvement can be readily explored both analytically, by extending the model of Figures 21 and 22, and experimentally with fabric woven on conventional looms.

Braids

Simple $\pm\phi$ reinforcement configurations have been shown (ref. 22) to provide maximum combinations of in-plane axial - and shear-stiffness/density ratios. Thus either by themselves (probably mostly at values of ϕ not greater than 20° to avoid excessive Poisson effects), or laminated with other configurations, they provide a maximum potential. To provide such configurations in any but small sizes, however, textile technology is deficient. Large braiding machines are not available. In this area machine development (perhaps borrowing from filament winding technology) must come first.

TRIAXIAL FABRICS

The development of multi-harness machinery to weave triaxial fabrics opens up new possibilities for triaxially woven reinforcements. Hitherto limited to the open Basic Weave and the 1-up, 1-down BiPlain Weave (Fig. 24), other more desirable configurations now become available. Guidelines for their development are given below.

Volume Fractions

Configurations are needed which provide maximum volume fraction reinforcement. The Substrate 2-up and 1-down Weave (Fig. 24) appears to be a step in that direction compared to the BiPlain. Much depends, however on the final resulting configurations of yarn cross-sections. Extensive photomicrographs, similar to Figure 1 for biaxial fabrics are needed. Longer float lengths than those in the Substrate Weave may be found preferable.

Bumpy Fabrics

Triaxial weaves provide a desirable base for the Bumpy Fabric constructions (Figs. 17 and 18), allowing shear properties to be designed into the woven configuration. Development requires photomicrograph studies to define models for analysis and direct configurations toward maximum volume fractions.

Stitchbase Weaves

The development of Stitchbase Weaves (Fig. 19) to provide thru the thickness holes for sewing plies together can also be used for cases in which substantial thru the thickness reinforcement is required. Both cases present problems: (1) for sewing, the problem is to make the holes small enough; (2) for TTT reinforcement, the problems are primarily those of insertion. Both problems appear solvable, but (1) may lead to the use of 1K carbon yarns in the base fabric and (2) may lead to the development of special insertion systems. Further study is needed to evaluate these problems.

Hybrids

The triaxial weave lends itself well to hybridization - carbon fiber in the warps, Kevlar in the fill. Although the evaluations herein showed that in-plane performance of the hybrids is generally less than for all carbon construction, the losses were in many cases minor and possibly more than compensated for by increased toughness. Guidelines here involve: (1) definitization of toughness criteria so that quantitative measures of toughness can be found by test; and (2) tests of representative triaxial hybrids to determine their performance utilizing the criteria developed.

Multilayer Constructions

The Substrate Weave lends itself well to multilayer constructions (Figure 83). Such constructions provide thru the thickness running yearns, and should not be prone to TTT failure. The TTT yarns can just as readily be hybridized, if desired, for further toughness increases. The recent advances in triaxial weaving technology make such weaves accessible.

These multilayer triaxial weaves embody all the desired directional reinforcement characteristics: (1) In plane axial, transverse and shear reinforcement, and (2) thru the thickness reinforcement. These individual properties may be traded off, one against another, but for the same volume fraction total these trade-offs involve no overall loss or gain; the sum total reinforcement remains the same. Lacking is only the flexibility of tapering provided by constructions like the Bumpy fabrics. The guidelines here are that both multi-layer and bumpy should be exploited.

OVERALL CONCLUSIONS AND RECOMMENDATIONS

ANALYSIS METHODOLOGY

Analysis methodology, culminating in the NDPROP Computer code, appears adequate for multi-harness weaves in tension, useful (with arbitrary knock-down factors) for plain weaves in tension and multi-harness weaves in compression, unconservative and to be used with caution for plain weaves in compression. Further research, both analytical and experimental, in this last area is recommended.

POTENTIALS FOR PERFORMANCE

The development of the NDPROP code makes possible an analytical assessment of the difference in potential for performance of woven constructions and unidirectional tape laminates. Results of such an assessment are shown in Figure 85. This upper bound assessment shows less than 4% loss in longitudinal stiffness and ultimate tensile strength for weaves having float lengths corresponding to three or more harnesses. Corresponding first failures (in the vicinity of yarn cross-over) are calculated to occur at stresses 6%-8% below those for unidirectional tape lay ups. Thus, inevitably, for in-plane, two-dimensional constructions, such minor losses in performance potentials are to be expected.

Three dimensional reinforcement constructions such as braids like Omniweave, configurations approaching 3-D isotropy, and the like are not competitive in performance with constructions which are primarily 2-D planar, with minimal thru the thickness reinforcement. Trade-offs in properties to maximize performance for 3-D constructions include the minimization of the thru the thickness elements to the extent possible without encountering thru the thickness weakness problems. Further research, both analytical and experimental is recommended to quantify criteria for the magnitude of thru the thickness reinforcement required.

ADVANCED WEAVES

Innovative approaches to the thru the thickness reinforcement problem, such as the Bumpy Fabric and the Stitchbase Weaves are in early stages of development. Continuing effort to bring them to fruition is recommended. Emphasis should be upon configurations providing angularly oriented in-plane yarns as needed for enhanced shear properties.

REFERENCES

1. Cominsky, A., et al., "Manufacturing Development of DC-10 Advanced Rudder", NASA Contractor Report 159060, May 1981.

2. Ko, F.K., and Pastore, C.M., "Design and Formation of 3-D Fabrics for Advanced Composites" in NASA Conference Publication 2420, 1986.

3. Crawford, James A., Jr., "Recent Developments in Multi-Directional Weaving" in NASA Conference Publication 2420, 1986.

4. Starnes, James H. Jr., Rhodes, Marvin D; and Williams, Jerry G., "The Effect of Impact Damage and Circular Holes on the Compressive Strength of a Graphite/Epoxy Laminate", NASA TM 78796, Oct. 1978.

5. Rhodes, Marvin D., and Williams, Jerry G., "Concepts for Improving The Damage Tolerance of Composite Compression Panels", NASA TM 85748, Feb. 1984.

6. Dow, N.F., and Rossi, G., et al., "Effect of Fineness of Weave on Crack Initiation and Ultimate Strength of E-Glass/Epoxy Woven Fabric Reinforced Composites in Tension at $\pm 45^{\circ}$ to Warp and Fill", Technical Final Report on Contract NAS1 17934, 1985.

7. Dexter, H. Benson, and Funk, Joan G., "Impact Resistance and Interlaminar Fracture Toughness of Through-the-Thickness Reinforced Graphite/Epoxy", presented at the 27th Structures, Structural Dynamics, and Materials Conference, May 19-21, 1986.

8. Dow, N.F., "Extension of Triaxial Weaving Technology for Improved Composite Reinforcement". Technical Final Report on Contract NAS1-17877, 1986.

9. Hashin, Z., "Theory of Fiber Reinforced Materials", NASA CR-1974, 1972.

10. Rosen, B.W., Chatterjee, S.N., and Kibler, J.J., "An Analysis Model for Spatially Oriented Fiber Composites", ASTM STP 617, 1977.

11. Dow, N.F., Derby, E., Ramkumar, R.L., and Rosen, B.W., "Theoretical Evaluation of Advanced Composites for Missile Structural Applications". Final Report on Contract N60921-77-C-0085, 1977.

12. Dow, N.F., Humphreys, E.A., and Rosen, B.W., "Guidelines for Composite Materials Research Related to General Aviation Aircraft". NASA CR 3720, 1983.

13. Dow, N.F., "Directions for 3-D Composite Reinforcement I: Intimations of Isotropy", presented at 21st Structures, Structural Dynamics and Materials Conference, Seattle, WA, May 12-14, 1980.

14. Stover, E.R., Mark, W.C., Marfowitz, I., and Mueller, W., "Preparation of an Omniweave-Reinforced Carbon-Carbon Cylinder as a Candidate for Evaluation in the Advanced Heat Shield Screening Program". AFML-TR-70-283, 1971.

15. Dow, N.F., Derby, E., Ramkumar, R.L., and Rosen, B.W., "Theoretical Evaluation of Advanced Composites for Missile Structural Applications", MSC Report No. TFR711/1143, 1978.

16. Dow, N.F., and Derby, E., "Survey of Metal Matrix Technology for Fabrication of Bridging Structures" Technical Final Report on Contract DAAG46-79-C-0067, 1980.

17. Ishikawa, Takashi, "Anti-Symmetric Elastic Properties of Composite Plates of Stain Weave Cloth," Fibre Science & Technology, 15, p. 127, 1981.

18. Ishikawa, Takashi and Chou Tsu-Wei, "Elastic Behavior of Woven Hybrid Composites," Journal of Composite Materials, 16, p. 2, 1982.

19. Walrath, David E., and Adams, Donald F., "Iosipescu Shear Properties of Graphite/epoxy Composite Laminates", NASA CR-176316, June 1985.

20. "Standard Tests for Toughened Composites", NASA Reference Publication 1092, 1983.

21. Williams, Jerry G., O'Brien, Kevin T., and Chapman III, A.J., "Comparison of Toughened Composite Laminates Using NASA Standard Damage Tolerance Tests", ACEE Composite Structures Technology Conference Proceedings, NASA CP 2321, 1984.

22. Dow, N.F., and Ramnath, V., "Evaluation and Criteria for 3-D Composites, in NASA Conference Publication 2420, 1985.

Table 1. Predicted Elastic Properties for Selected T300/Epoxy Biaxial Woven Fabrics, v_f=0.6

Property	Plain	3HS	5HS	8HS	0/90 Laminate
E_x, E_y, Msi	10.40	10.58	10.79	10.91	11.00
E_z, Msi	1.81	1.81	1.82	1.82	1.78
G_{xy}, Msi	1.00	0.95	0.87	0.80	0.69
G_{xz}, G_{yz}, Msi	0.77	0.72	0.68	0.66	0.62
ν_{xy}	0.064	0.061	0.056	0.052	0.045
ν_{xz}, ν_{yz}	0.456	0.436	0.420	0.415	0.414

Table 2. Predicted Elastic Properties for Selected T300/Epoxy Triaxial Woven Fabrics, v_f=0.5

Property	BiPlain	Substrate	±30/90 Laminate
E_x, Msi	6.29	6.50	6.56
E_y, Msi	6.29	5.97	6.56
E_z, Msi	1.65	1.65	1.54
G_{xy}, Msi	2.44	2.52	2.48
G_{yz}, Msi	0.86	0.83	0.51
G_{zx}, Msi	0.86	0.82	0.51
ν_{xy}	0.290	0.320	0.323
ν_{yz}	0.395	0.389	0.304
ν_{zx}	0.104	0.092	0.071

Table 3. Predicted Strengths for Selected T300/Epoxy Biaxial Woven Fabrics, $v_f=0.6$

Property	Plain	3HS	5HS	8HS	0/90 Laminate
σ_x^{tu}, σ_y^{tu}, ksi	100.2	100.7	101.7	104.5	106.5
σ_x^{cu}, σ_y^{cu}, ksi	102.2	103.5	105.6	106.9	107.9
σ_z^{tu}, ksi	9.9	9.9	9.9	9.9	9.9
σ_z^{cu}, ksi	32.1	32.3	32.3	32.4	38.3
τ_{xy}^{su}, ksi	15.9	15.3	14.0	13.0	12.2
τ_{yz}^{su}, τ_{zx}^{su}, ksi	12.2	11.5	11.0	10.7	11.0

Table 4. Predicted Strengths for Selected T300/Epoxy Triaxial Woven Fabrics, $v_f=0.5$

Property	BiPlain	Substrate	±30/90 Laminate
σ_x^{tu}, ksi	78.6	84.2	87.5
σ_x^{cu}, ksi	77.1	79.4	96.2
σ_y^{tu}, ksi	55.7	52.0	59.4
σ_y^{cu}, ksi	62.0	58.4	64.6
σ_z^{tu}, ksi	8.7	8.7	9.9
σ_z^{cu}, ksi	28.2	28.2	32.3
τ_{xy}^{su}, ksi	45.9	48.0	52.0
τ_{yz}^{su}, ksi	14.3	13.0	10.6
τ_{zx}^{su}, ksi	16.5	13.7	11.0

Table 5. Geometrical Parameters Used for Property Calculations of Biaxial Woven Fabrics

Weave Parameter	Plain	Oxford	5HS	8HS
Ply thickness, in	.01125	.0106	.0106	.0106
v_f	.667	.620	.640	.640
L, in	1/19	1/18 (warp)	1/18	1/18
A_f, in^2	.000175	.000175 (warp)	.000175	.00175
v_{fb}	.7428	.6457	.6857	.6857
v_{fp}	.8980	.9603	.9334	.9334
A, in^2	.000236	.000271 (warp)	.000255	.000255

Table 6. Comparison of Calculated versus Measured T300/Epoxy Biaxial Woven Fabric Elastic Properties

Property	Plain (v_f=.667)		Oxford (v_f=.620)		5HS(v_f=.640)		8HS (v_f=.640)	
	Calc.	Meas.	Calc.	Meas.	Calc.	Meas.	Calc.	Meas.
$E_x^{+(1)}$, Msi	11.62	9.13	10.69	9.63	11.56	10.05	11.61	10.59
$E_x^{-(2)}$, Msi	11.62	9.14	10.69	8.26	11.56	8.88	11.61	9.15
E_y^{+}, Msi	11.62	8.83	10.77	9.68	11.56	10.09	11.61	10.35
E_y^{-}, Msi	11.62	8.59	10.77	8.44	11.56	8.80	11.61	8.94
G_{xy}, Msi	1.17	-	10.99	-	10.89	0.810	0.90	0.811
ν_{xy}^{+}	0.061	0.113	0.062	0.057	0.051	0.056	0.052	0.054
ν_{xy}^{-}	0.061	0.084	0.062	0.063	0.051	0.056	0.052	0.056

(1) + indicates tension

(2) - indicates compression

Table 7. Comparison of Calculated versus Measured T300/Epoxy Biaxial Woven Fabric Strengths

Property	Plain (v_f=.667)		Oxford (v_f=.620)		5HS(v_f=.640)		8HS(v_f=.640)	
	Calc.	Meas.	Calc.	Meas.	Calc.	Meas.	Calc.	Meas.
$\sigma_x^{+(1)}$, ksi	$68.1^{(1)}/111.8$	79.8	$75.3^{(1)}/102.5$	90.5	$73.9^{(1)}/110.7$	105.7	$74.0^{(1)}/110.7$	121.3
$\sigma_x^{-(2)}$, ksi	114.1	57.9	105.0	73.3	113.3	100.7	113.6	118.6
σ_y^{+}, ksi	$68.1^{(1)}/111.8$	68.4	$70.5^{(1)}/103.6$	96.3	$73.9^{(1)}/110.7$	109.2	$74.0^{(1)}/110.7$	115.8
σ_y^{-}, ksi	114.1	53.2	105.7	101.6	113.3	109.8	113.6	112.8
τ_{xy}, ksi	15.1	-	16.1	-	13.3	16.0	13.5	16.1

(1) + Indicates tension
(2) - Indicates compression
(1) First Failure

Table 8. Calculated Versus Measured T300/Epoxy Fabric Shear Moduli and Strengths from Iosipescu Shear Tests

Property	Oxford Weave (v_f = .620)		5 Harness Weave (v_f = .640)		8 Harness Weave (v_f = .640)	
	Measured	Calculated	Measured	Calculated	Measured	Calculated
G_{xy}, Msi	0.770	0.990	0.760	0.894	0.978	0.901
G_{yz}, Msi	0.570	0.744	0.550	0.743	0.500	0.724
G_{zx}, Msi	0.680	0.806	0.610	0.743	0.490	0.724
τ_{xy}, ksi	16.5	16.1	18.5	13.3	19.4	13.4
τ_{yz}, ksi	10.6	11.9	10.9	11.0	11.0	10.8
τ_{zx}, ksi	11.0	13.1	10.9	11.0	10.2	10.8

xy - in-plane shear

yz,zx - transverse shear

Table 9. Geometrical Parameters Used for Property Calculations of Triaxial Woven Fabrics

Weave Parameter	T300/934	Kev/934
Ply thickness, in	.022	.025
v_f	.451	.389
L, in	1/18.5	1/18.5
A_f, in^2	.000175	.00017
v_{fb}	.7	.65
v_{fp}	.6429	.5980
A, in^2	.000250	.000262

Table 10. Comparison of Calculated Versus Measured Triaxial Woven Fabric Properties and Strengths

Property	T300/934 (v_f=.45)		Kev/934 (v_f=.39)	
	Calc.	Meas.	Calc.	Meas.
$E_x^{+(1)}$, Msi	5.64	4.60	2.63	1.81
$E_x^{-(2)}$, Msi	5.64	4.56	2.63	2.01
ν_y^+, Msi	5.64	5.05	-	-
E_y^-, Msi	5.64	5.13	-	-
ν_{xy}^+	0.284	0.234	0.293	0.256
ν_{xy}^-	0.284	0.232	0.293	0.305
ν_{yx}^+	0.284	0.250	-	-
ν_{yx}^-	0.284	0.268	-	-
σ_x^+, ksi	42.1/69.8	36.8	32.8	24.4
σ_x^-. ksi	68.3	42.7	14.1	18.5
σ_y^-, ksi	38.0/49.8	41.5	-	-
σ_y^-, ksi	55.5	49.6	-	-

(1) + indicates tension

(2) - indicates compression

Table 11. Comparison of Fabric Versus Tape Compression after Impact Test Data, T300/Epoxy

Property	Oxford Weave	5HS Weave	8HS Weave	Tape Laminate
v_f	.633	.669	.656	-
Failure Stress σ_x^c, ksi	25.75	26.78	26.40	21.00
Failure Strain, ε_x^c, %	.4196	.4152	.4010	.2887
Modulus ε_x^c, Msi	6.44	6.79	6.88	7.37

- Layup: $[+45/0/-45/90]_{3s}$ for fabrics

  $[+45/0/-45/90]_{6s}$ for tape

- Impact Energy 20 ft. - lb.

Table 12. Comparison of Fabric Versus Tape Data for NASA Standard Toughness Tests, T300/Epoxy

Property	Oxford Weave	5HS Weave	8HS Weave	Tape Laminate
Double Cantilever Beam				
G_{IC}, lb./in.[1]	2.23	1.85	2.25	0.44[3],
Open Hole Tension				
Failure Stress, ksi[1]	46.3	50.2	50.0	-
Failure Strain, %[1]	.4683	.4820	.4613	-
Failure Stress, ksi[2]	38.5	41.2	41.8	44.5[3]
Failure Strain, %[2]	.5560	.5780	.5600	-
Open Hole Compression				
Failure Stress, ksi[1]	25.8	30.2	30.9	-
Failure Strain, %[1]	.3180	.3628	.3633	-
Failure Stress, ksi[2]	30.0	35.9	38.2	36.5[3]
Failure Strain, %[2]	.4903	.5573	.5770	.5600[3]

1 - Layup: $[0^\circ]_{8s}$

2 - Layup: $[+45/0/-45/90]_{3s}$

3 - Tape Data From [21]

Table 13. Calculation of Elastic Properties and Strengths of Original "Building-Block" Auxiliary Warp Configuration

Property	Face-Ply	Internal-Ply	4-Ply	12-Ply
E_x, Msi	11.72	12.80	12.48	12.70
E_y, Msi	7.06	4.66	5.56	4.93
E_z, Msi	1.76	1.87	1.82	1.86
G_{xy}, Msi	0.69	0.64	0.66	0.65
G_{yz}, Msi	0.89	0.81	0.79	0.80
G_{zx}, Msi	0.76	0.64	0.74	0.67
ν_{xy}	0.032	0.069	0.050	0.063
ν_{yz}	0.499	0.431	0.432	0.431
ν_{zx}	0.057	0.041	0.051	0.044
σ_x^+, ksi	78.4/123.9	80.8/137.6	80.9/133.2	80.8/136.3
σ_y^+, ksi	51.4/67.6	29.1/40.3	34.6/50.6	30.7/43.4
σ_x^-, ksi	122.3	133.3	130.1	132.4
σ_y^-, ksi	73.8	48.7	58.0	51.5

+ indicates tension

- indicates compression

Table 14. Comparison of Predicted and Measured Properties and of Original "Building-Block" Auxiliary Warp Configuration

Property	Face-Ply		4-Ply		12-Ply	
	Predicted	Measured	Predicted	Measured	Predicted	Measured
E_x^+, Msi	11.72	8.60	12.48	9.11	12.70	9.66
E_y^+, Msi	7.06	5.92	5.56	5.19	4.93	4.48
E_x^-, Msi	11.72	--	12.48	--	12.70	8.81
E_y^-, Msi	7.06	--	5.56	--	4.93	4.67
ν_{xy}^+	0.032	0.148	0.050	0.150	0.063	0.134
ν_{yx}^+	0.019	0.098	0.022	0.083	0.024	0.080
ν_{xy}^-	0.032	--	0.050	--	0.063	0.136
ν_{yx}^-	0.019	--	0.022	--	0.024	0.031
σ_x^+, ksi	78.4/123.9	71.0	80.9/133.2	77.35	80.8/136.3	82.5
σ_y^+, ksi	51.4/67.6	45.2	34.6/50.6	37.86	30.7/43.4	34.9
σ_x^-, ksi	122.3	--	130.1	--	32.4	45.6
σ_y^-, ksi	73.8	--	58.0	--	51.5	34.9

\+ indicates tension

\- indicates compression

Table 15. Results of Elastic Property Calculations on Revised Design Auxililary Warp Reinforcement Weaves

Property	Nested Face-Ply	Nested Internal-Ply	Nested Face & Internal Files
E_x, Msi	11.93	13.03	12.56
E_y, Msi	6.67	5.30	5.89
E_z, Msi	1.71	1.73	1.72
G_{xy}, Msi	0.66	0.65	0.66
G_{yz}, Msi	0.62	0.59	0.60
G_{zx}, Msi	0.69	0.70	0.70
ν_{yx}	0.050	0.064	0.057
ν_{yz}	0.374	0.364	0.368
ν_{zx}	0.052	0.047	0.049
t, in	0.035	0.047	0.082
v_f	0.55	0.54	0.54

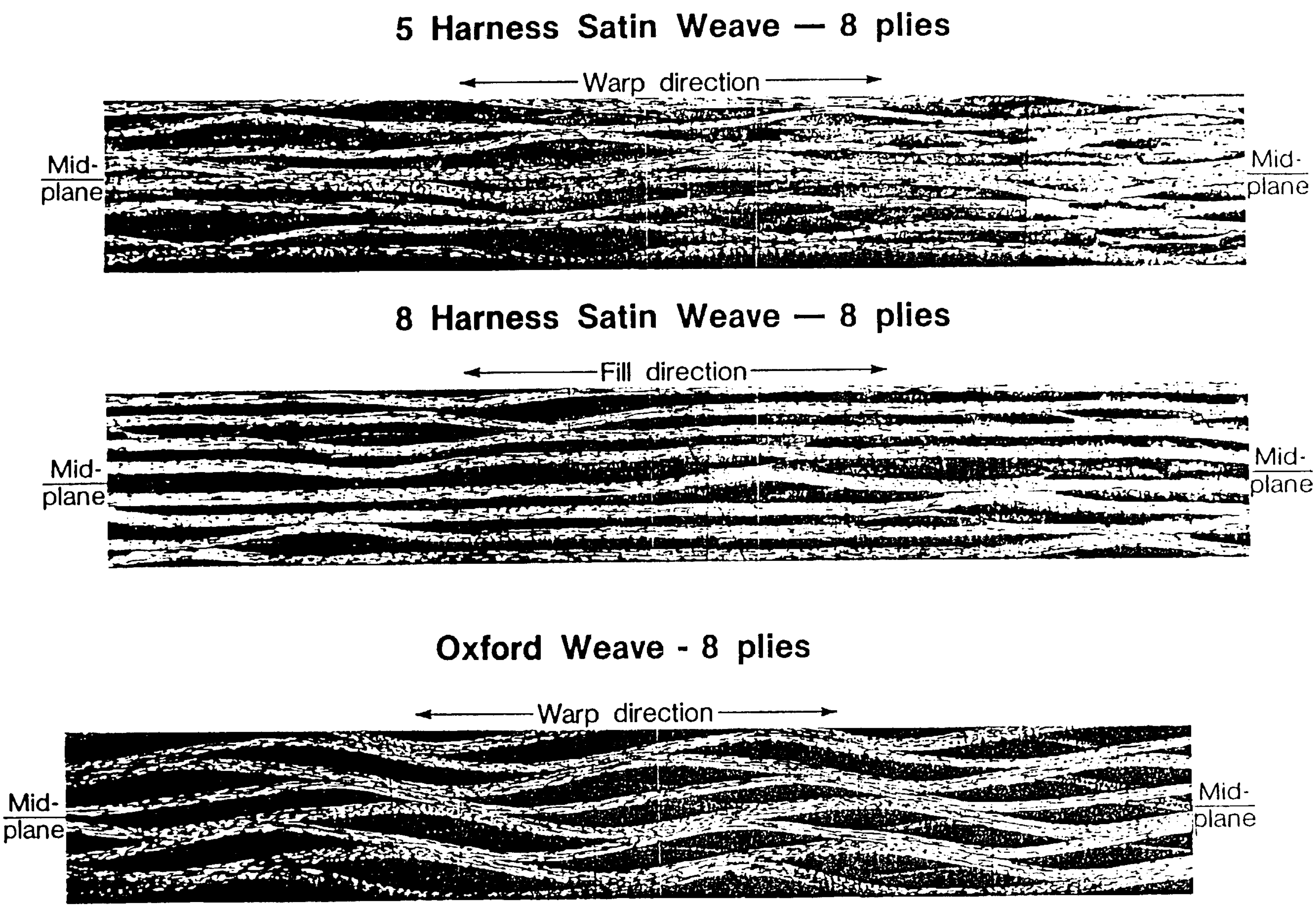

ORIGINAL PAGE IS OF POOR QUALITY

Figure 1. Photomicrographs of Typical T-300/Epoxy Composites Reinforced with Biaxial Woven Fabrics. Dark areas represent fibers running perpendicular to the plane of the paper. In all cases these fibers have conformed almost completely to the dark area shapes.

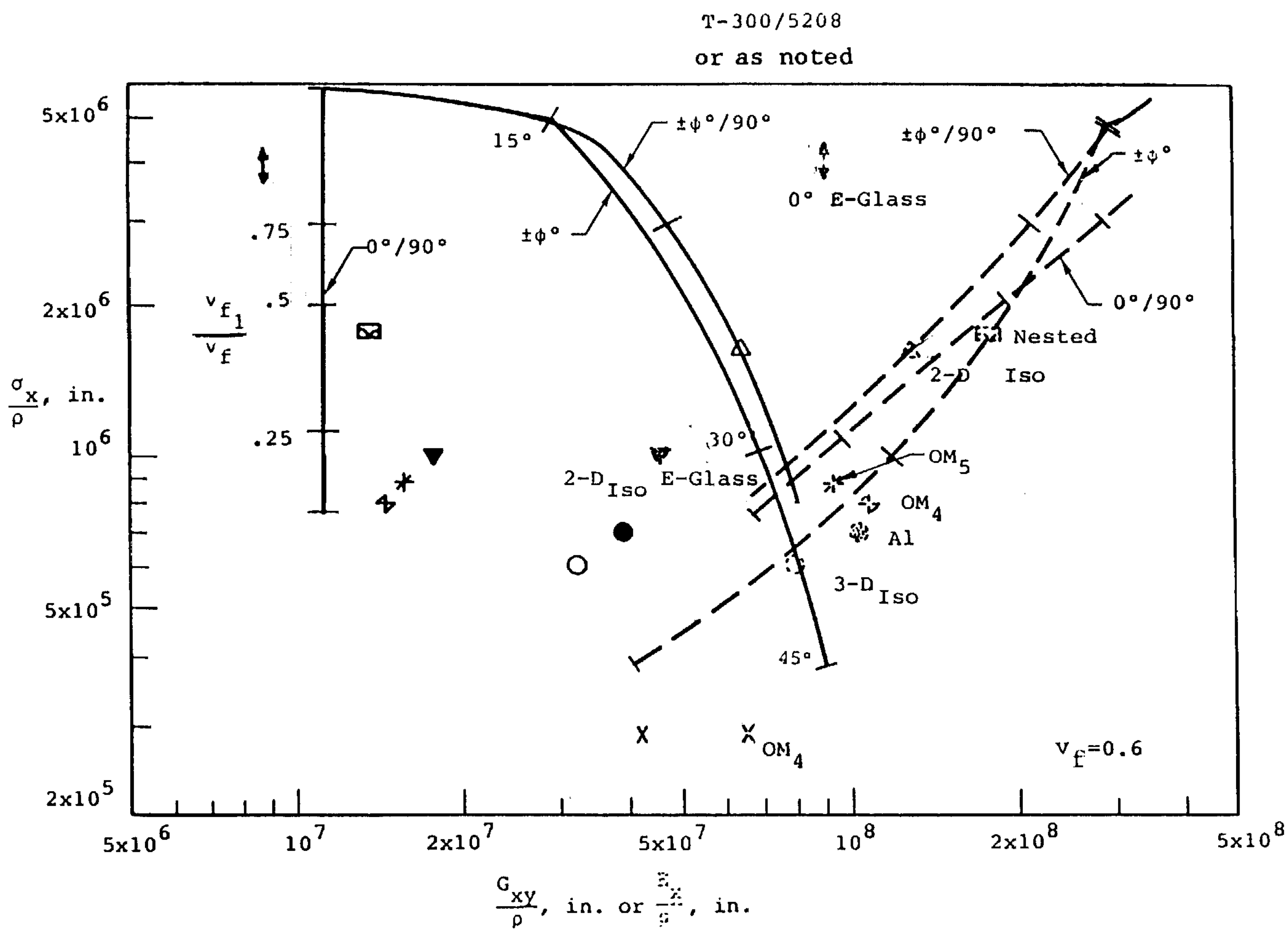

Figure 2. Tensile Performance Evaluations.-Various Materials and Configurations. Plotted is tensile strength/density ratio $\frac{\sigma_x}{\rho}$ to meet stiffness requirements in shear $\frac{G_{xy}}{\rho}$ and extension $\frac{E_x}{\rho}$. Shear stiffness is dominant; if zero shear stiffness is allowable, unidirectional reinforcement is most efficient. If the reinforcement is configured for high shear stiffness, however, the extensional stiffness may become critical.

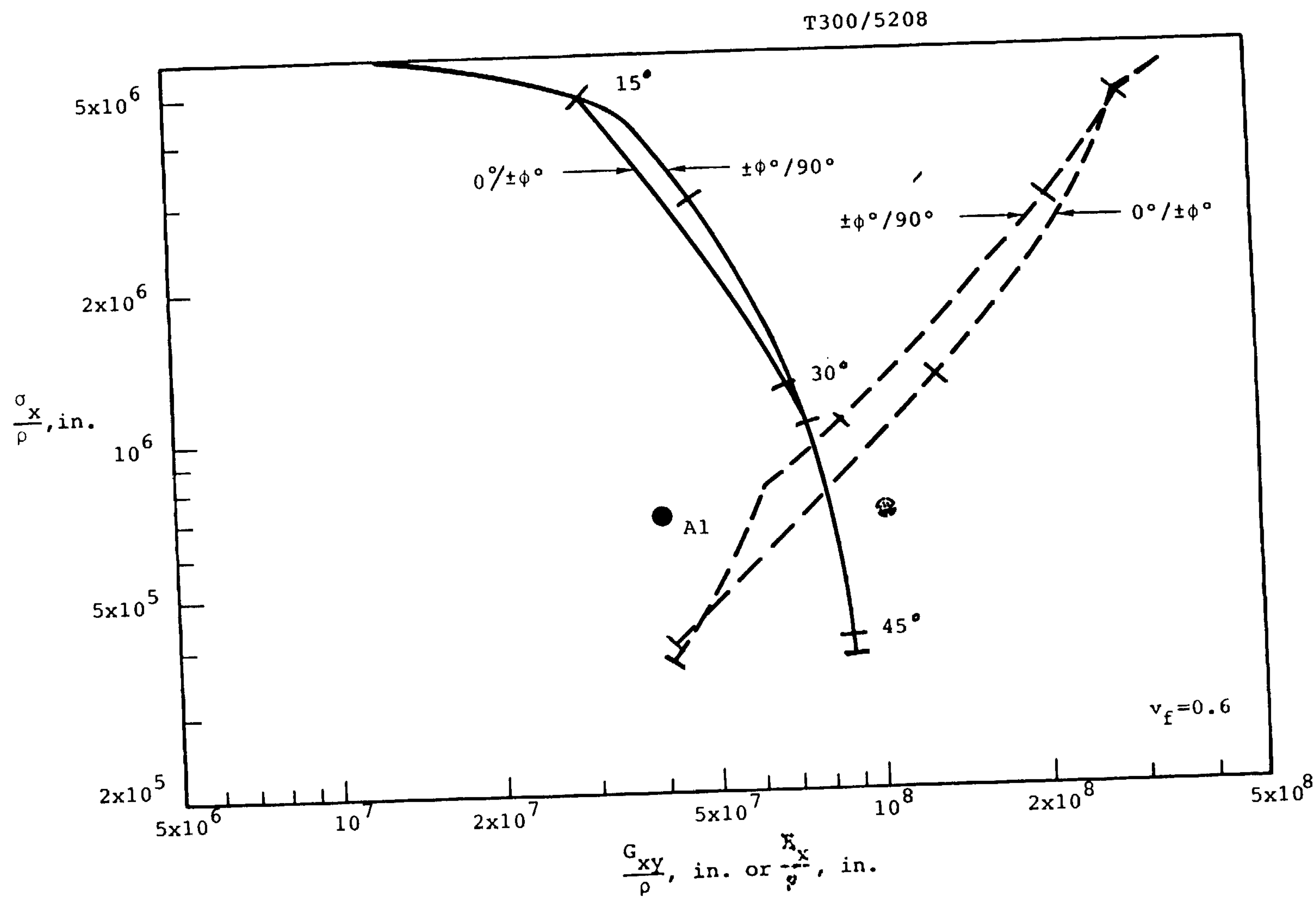

Figure 3. Tensile Performance Evaluations, - Comparison of $0°/\pm\phi°$ and $\pm\phi°/90°$ Configurations. The $\pm\phi°/90°$ configuration has higher strength/density values than the $0°/\pm\phi°$ configuration up to the maximum shear stiffness ($\phi=\pm45°$).

Envelopes

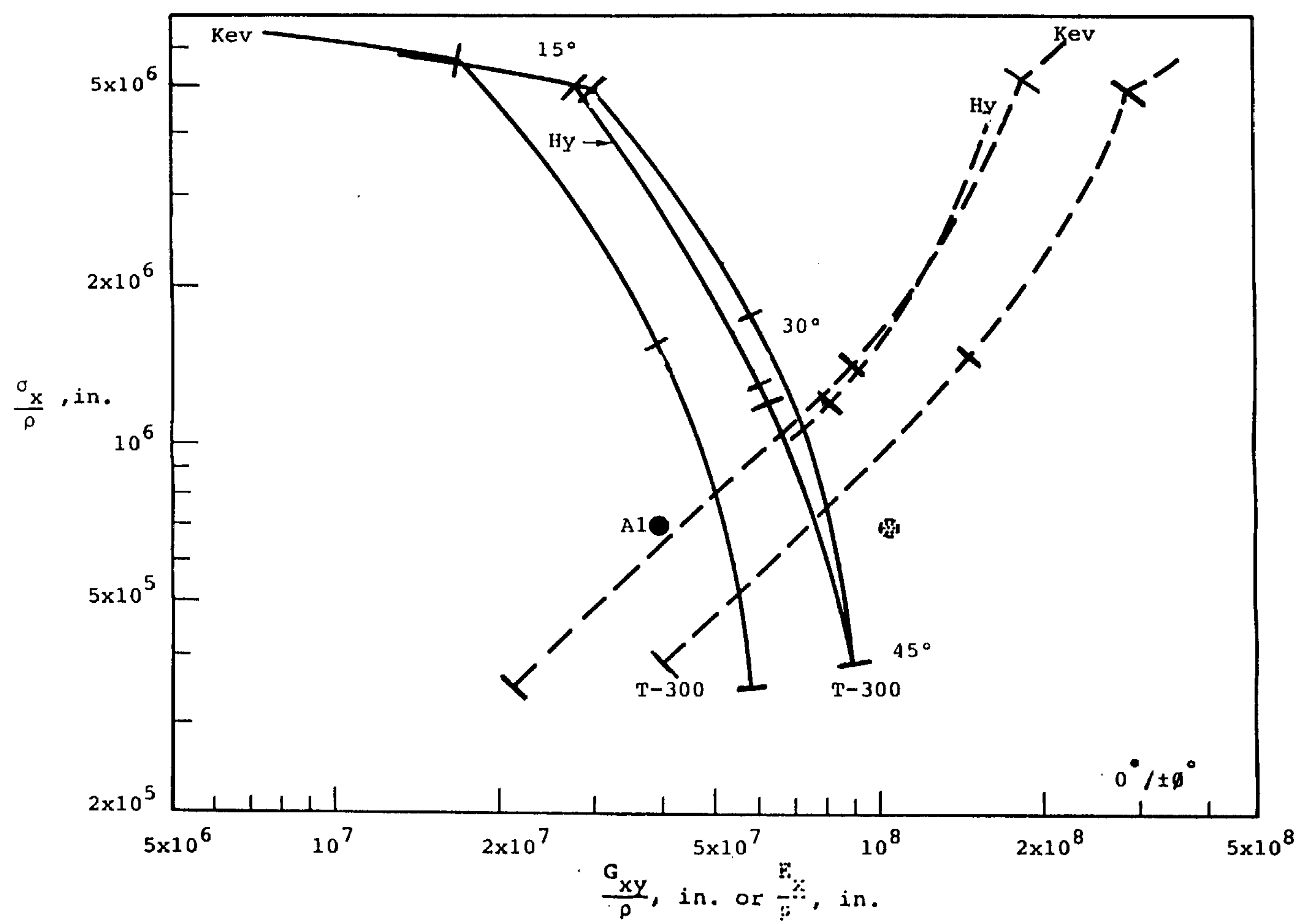

Figure 4. Tensile Performance Evaluations,-Comparisons of Envelope Curves for Various Proportions of $0^\circ/\pm\phi^\circ$, T-300, Kevlar, and Hybrids of T-300 and Kevlar. Except for the small region of required tensile stiffness between $\frac{E_x}{\rho}=12x10^8$ and $17x10^8$ in., hybrid properties all fall between those for T-300 and Kevlar. Kevlar can not compete with T-300 except for low shear stiffness requirements.

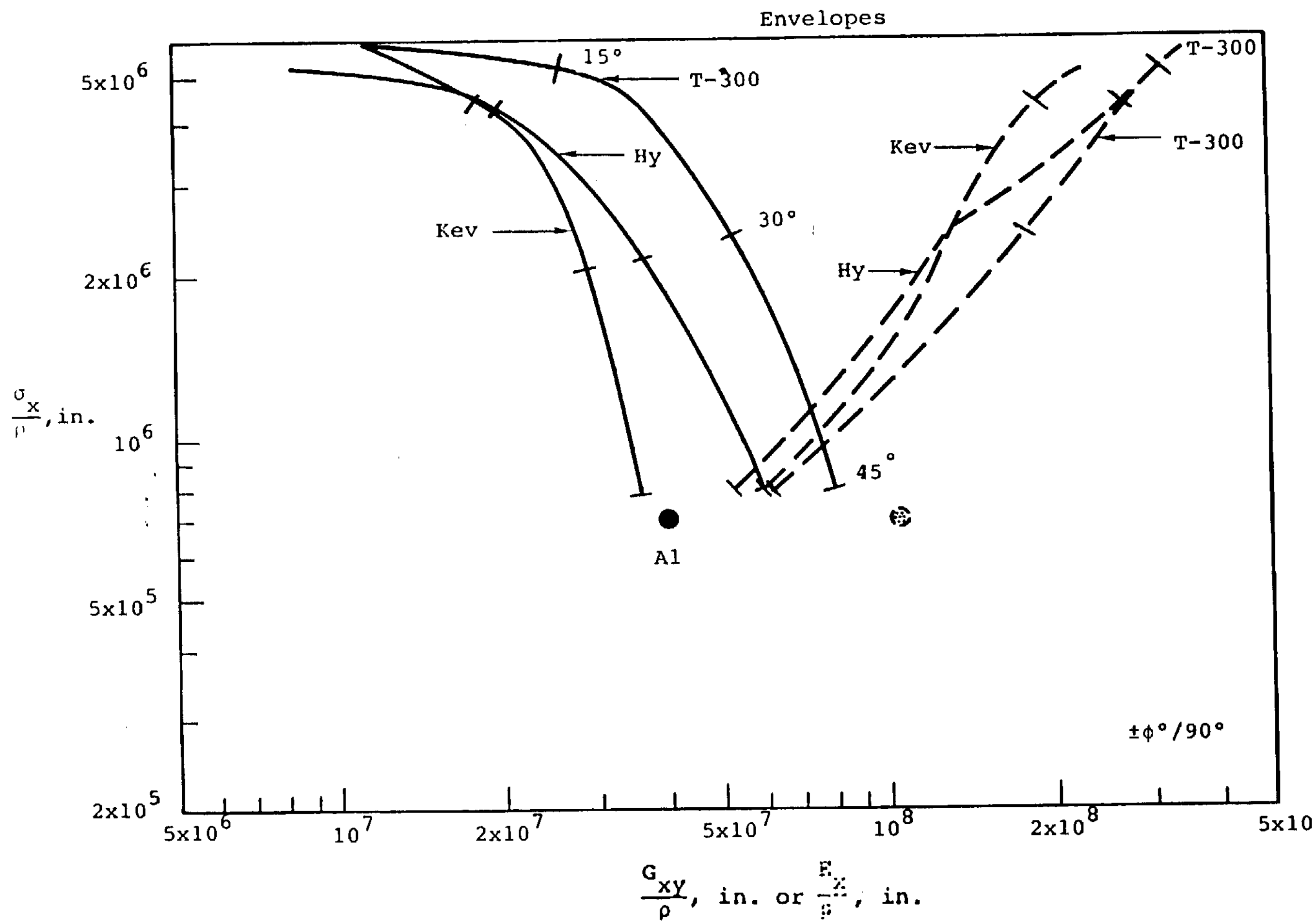

Figure 5. Tensile Performance Evaluations,- Comparisons of Envelope Curves for Various Proportions of $\pm\phi^\circ/90^\circ$ T-300, Kevlar, and Hybrids of T-300 and Kevlar. Except for the region of tensile stiffness requirements $5\times10^8 < \frac{E_x}{\rho} < 13\times10^8$ the hybrid properties all fall between those for T-300 and Kevlar. Kevlar can not compete with T-300 for any shear stiffness requirement.

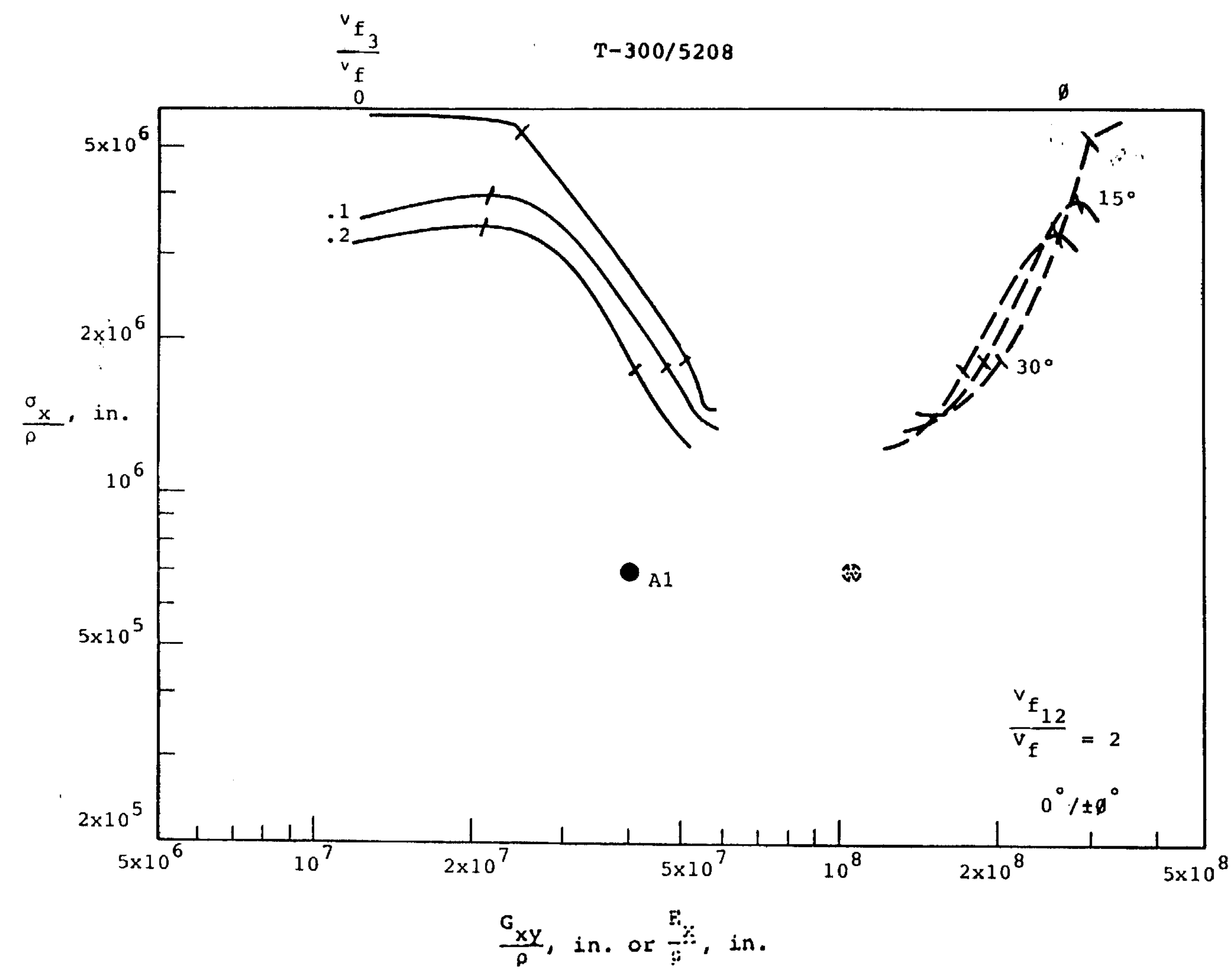

Figure 6. Tensile Performance Evaluations,-Effect of Adding Through-the-Thickness Reinforcements to 0°/±ϕ° 2-D Reinforcement Configurations Having Equal Volume Fraction Reinforcements in All Three Planar Directions. Performance losses due to TTT reinforcement are substantial for low shear stiffness requirements.

T-300/5208

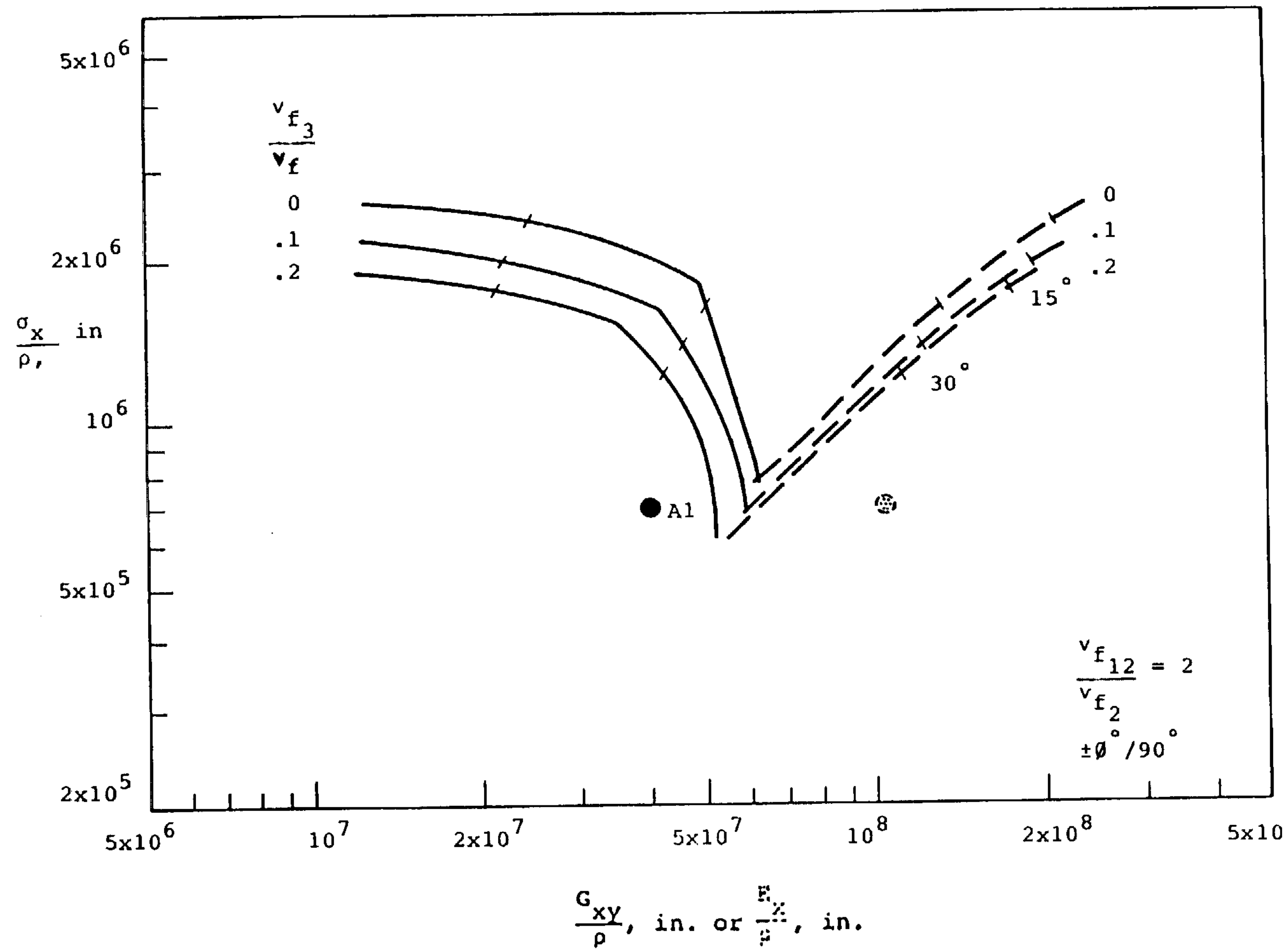

Figure 7. Tensile Performance Evaluations,-Effects of Adding Through-the-Thickness Reinforcements to $\pm\phi^\circ/90^\circ$ 2-D Reinforcement Configurations Having Equal Volume Fraction Reinforcements in the Three Planar Directions. Performance losses can be substantial for high shear stiffness requirements.

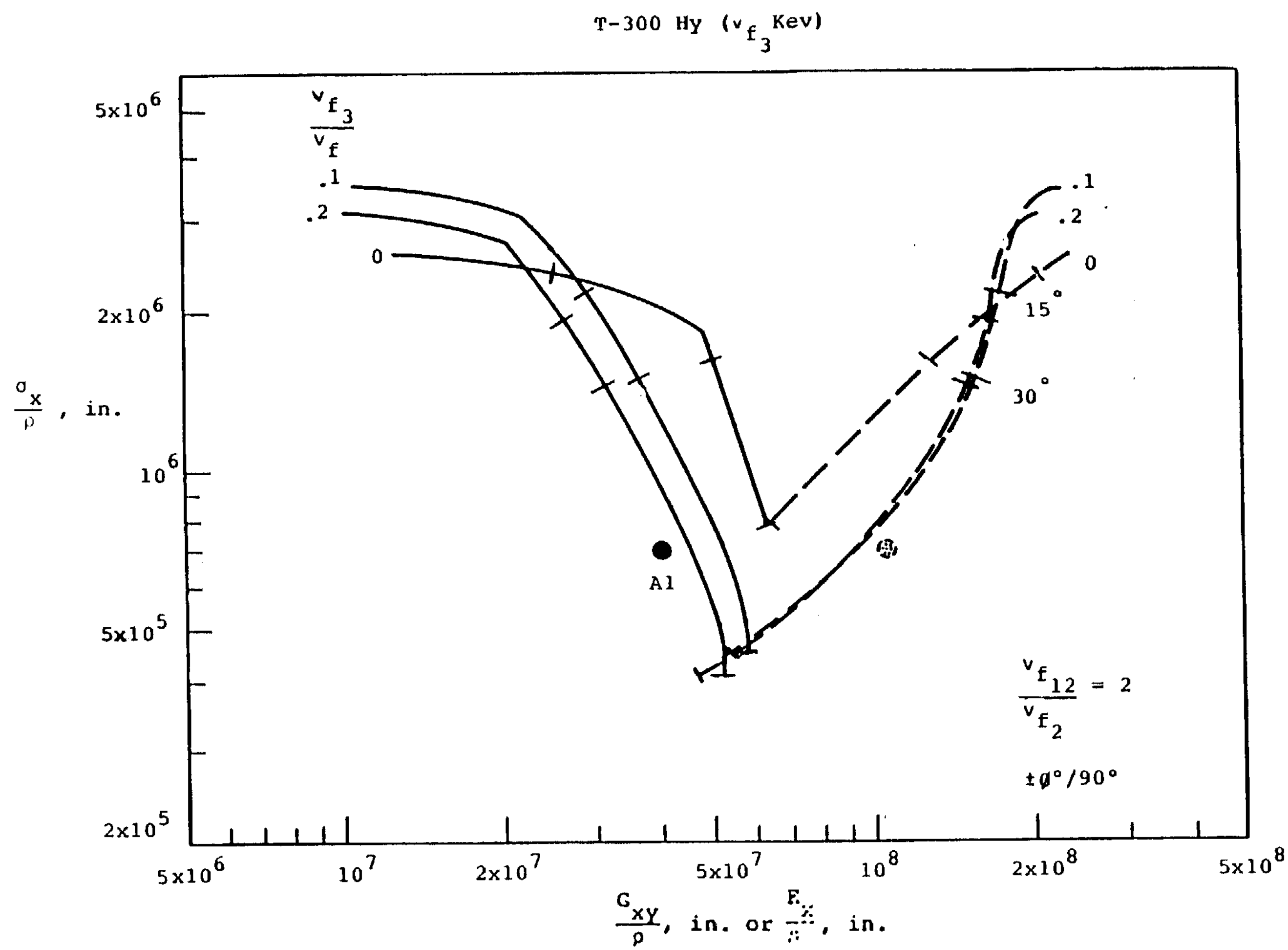

Figure 8. Tensile Performance Evaluations,-Effects of Adding Kevlar Through-the-Thickness Reinforcements to ±φ°/90° T-300 2-D Reinforcements Having Equal Volume Fraction Reinforcements in the Three Planar Direction.

While there is an actual gain in $\frac{\sigma_x}{\rho}$ for low shear stiffness requirements due to the delay of a premature transverse in-plane failure mode, there are substantial performance losses for the higher shear stiffness requirements.

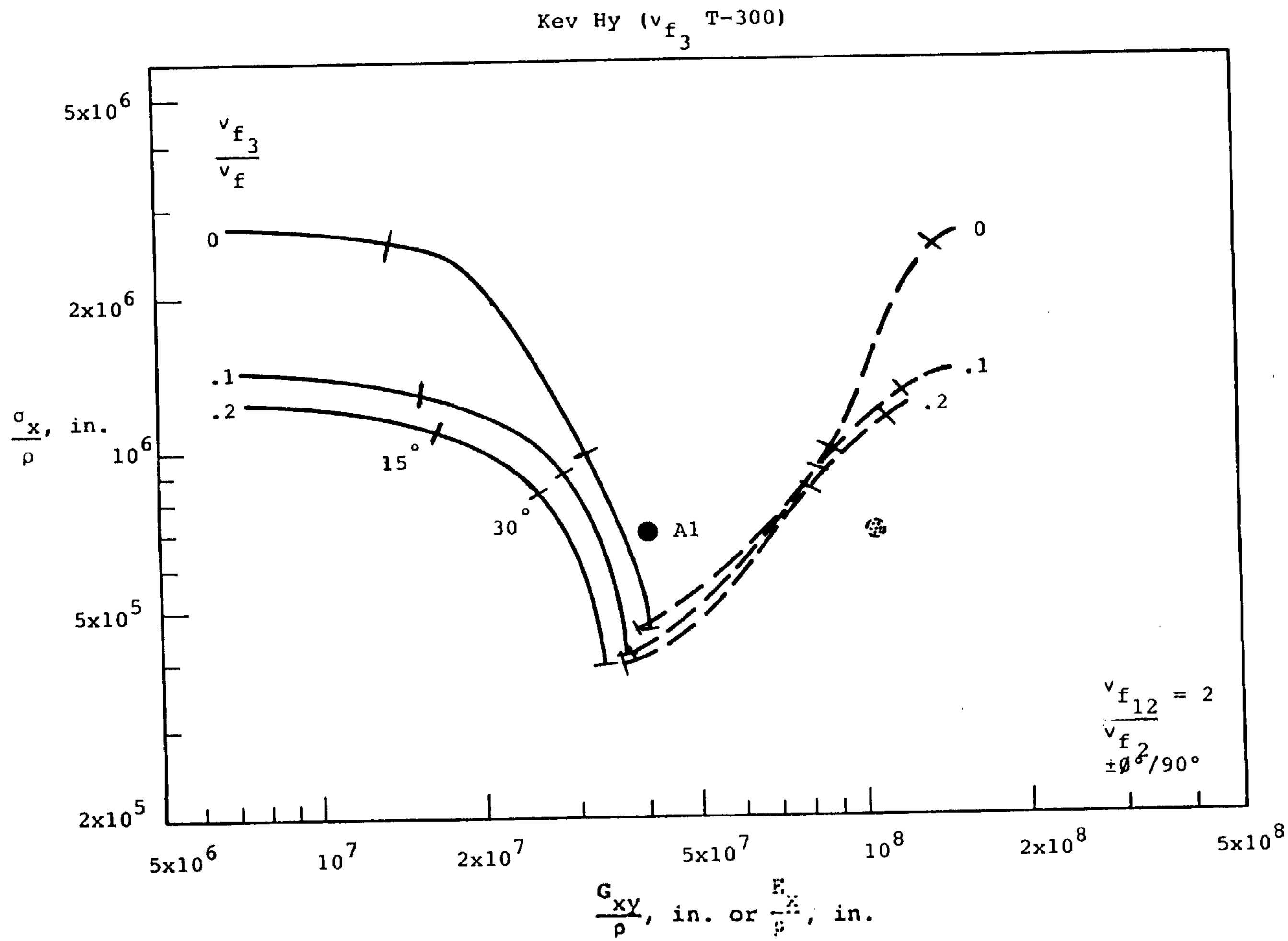

Figure 9. Tensile Performance Evaluations,-Effects of Adding T-300 Through-the-Thickness Reinforcements to $\mp\phi°/90°$ Kevlar 2-D Reinforcements Having Equal Volume Fraction Reinforcements in the Three Planar Directions. Performance losses are enormous for all shear stiffness requirements.

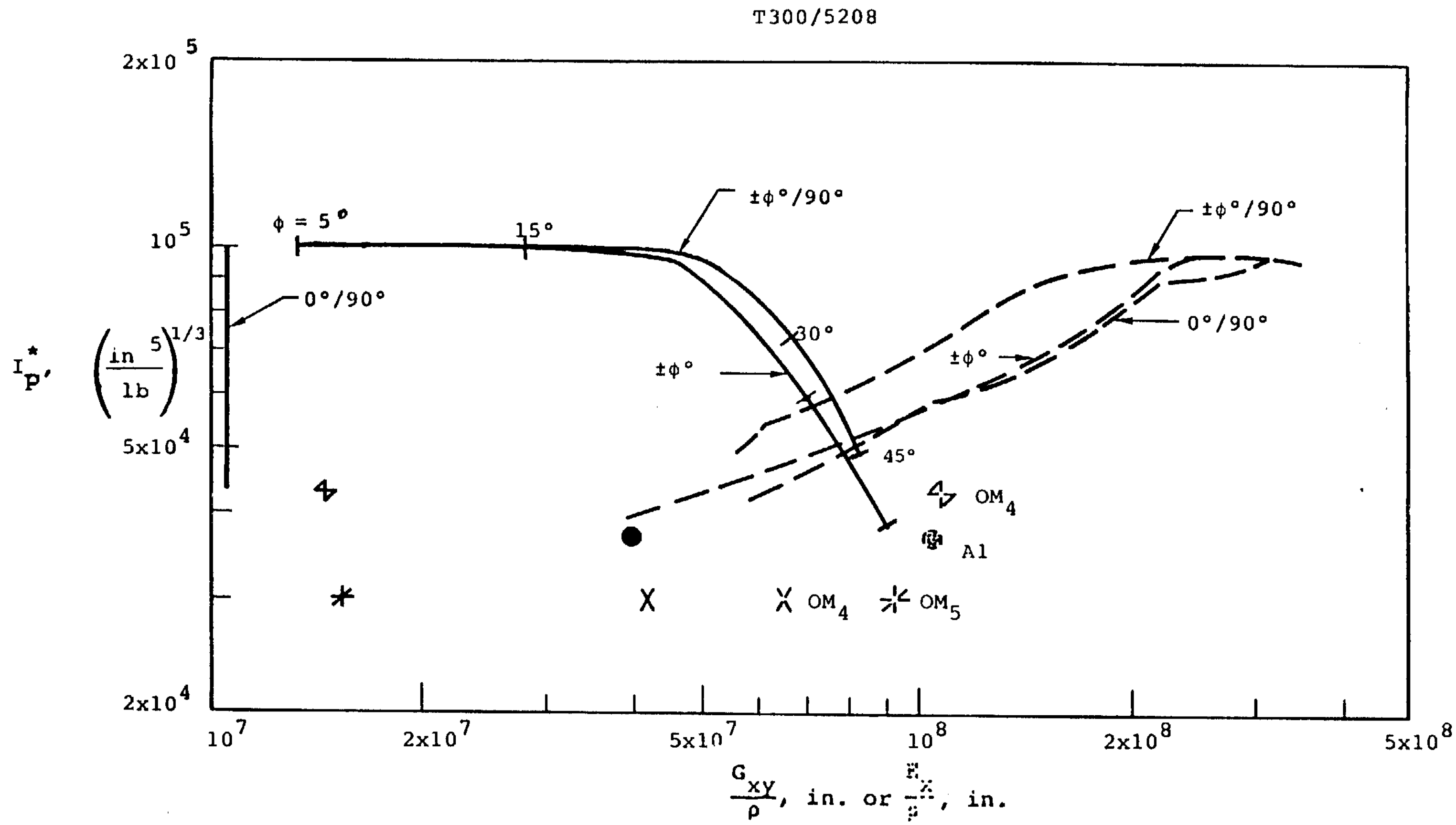

Figure 10. Compressive Performance Evaluations,-Various Materials and Configurations. Plotted is the indicator number I_p^* vs. shear and extensional stiffness/density ratios $\frac{G_{xy}}{\rho}$ and $\frac{E_x}{\rho}$. As in tension, shear is the dominant criterion. I_p^* is a combined measure of strength and buckling resistance for a given weight-the greater I_p^* the less the weight.

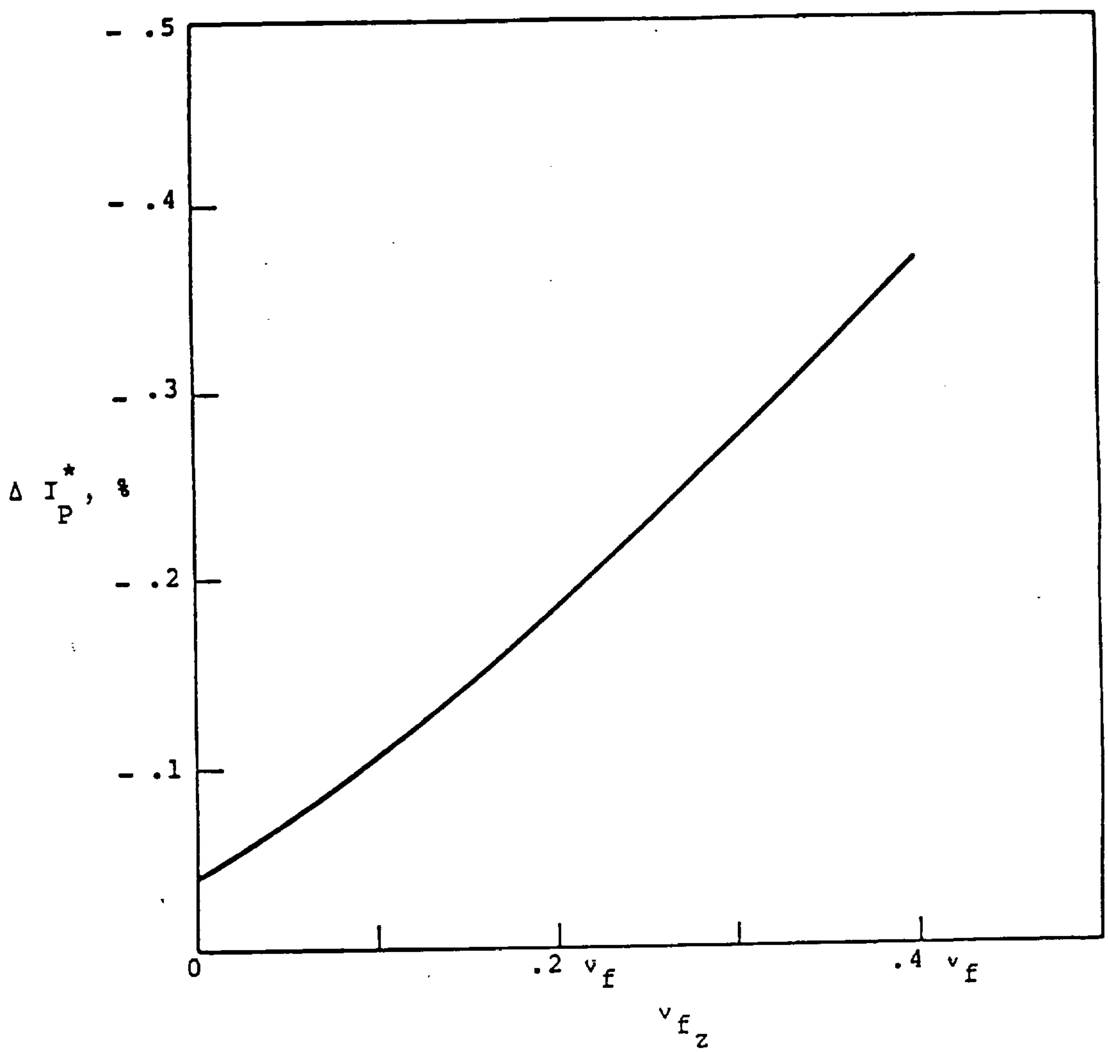

Figure 11. Summary Measure of Penalty $-\Delta I_P^*$ for Thru the Thickness Reinforcement v_{f_z} for Compressive Loadings. Curve is typical, though specifically accurate as drawn for $\pm 30^\circ/90^\circ/90^\circ$ quasi-isotropic in-plane reinforcement configurations. See also figure 12.

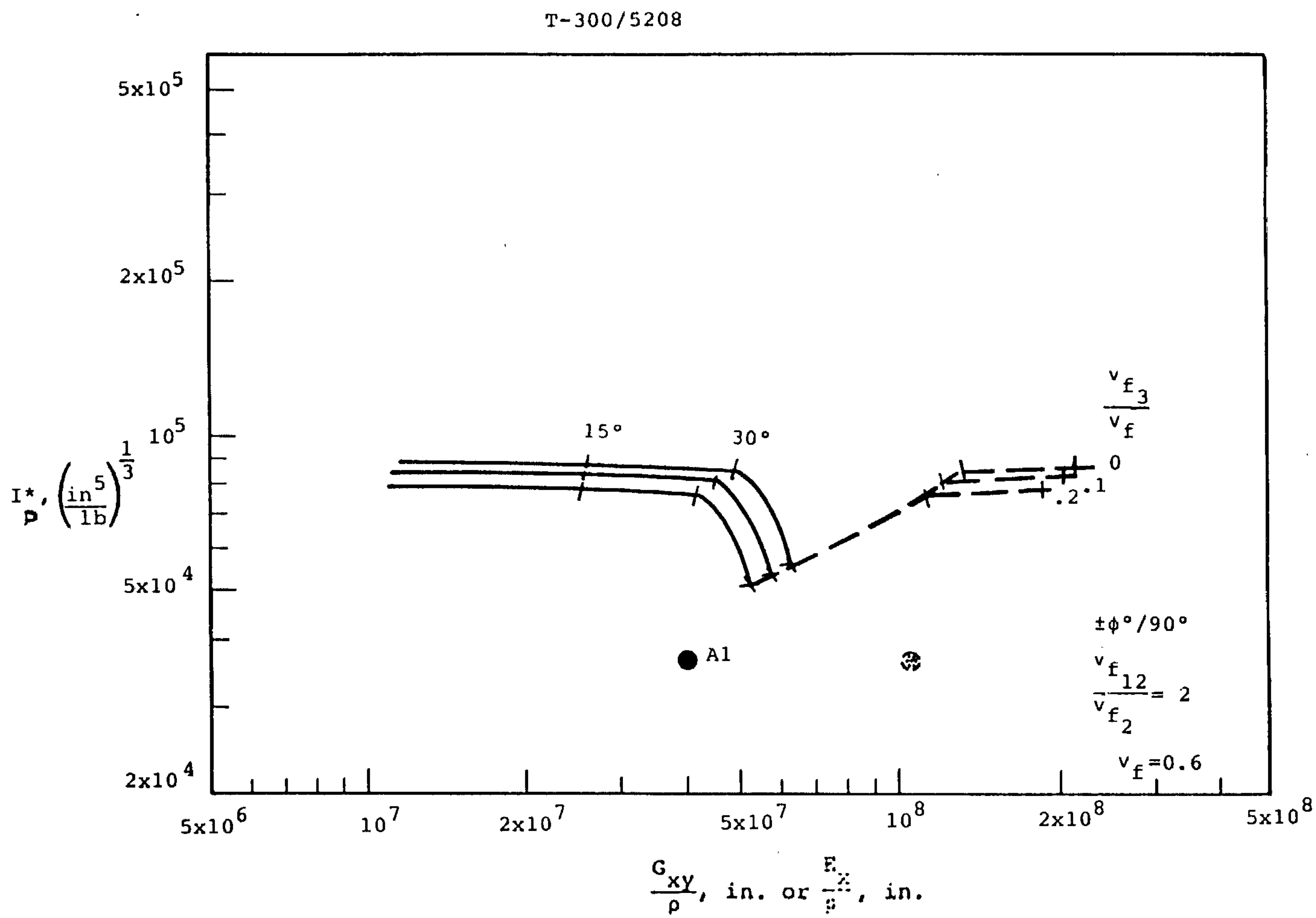

Figure 12. Detailed Representation of Penalties for Thru the Thickness Reinforcement for Compressive Loading of $\pm\phi°/90°$ 2-D Reinforcement Configurations.

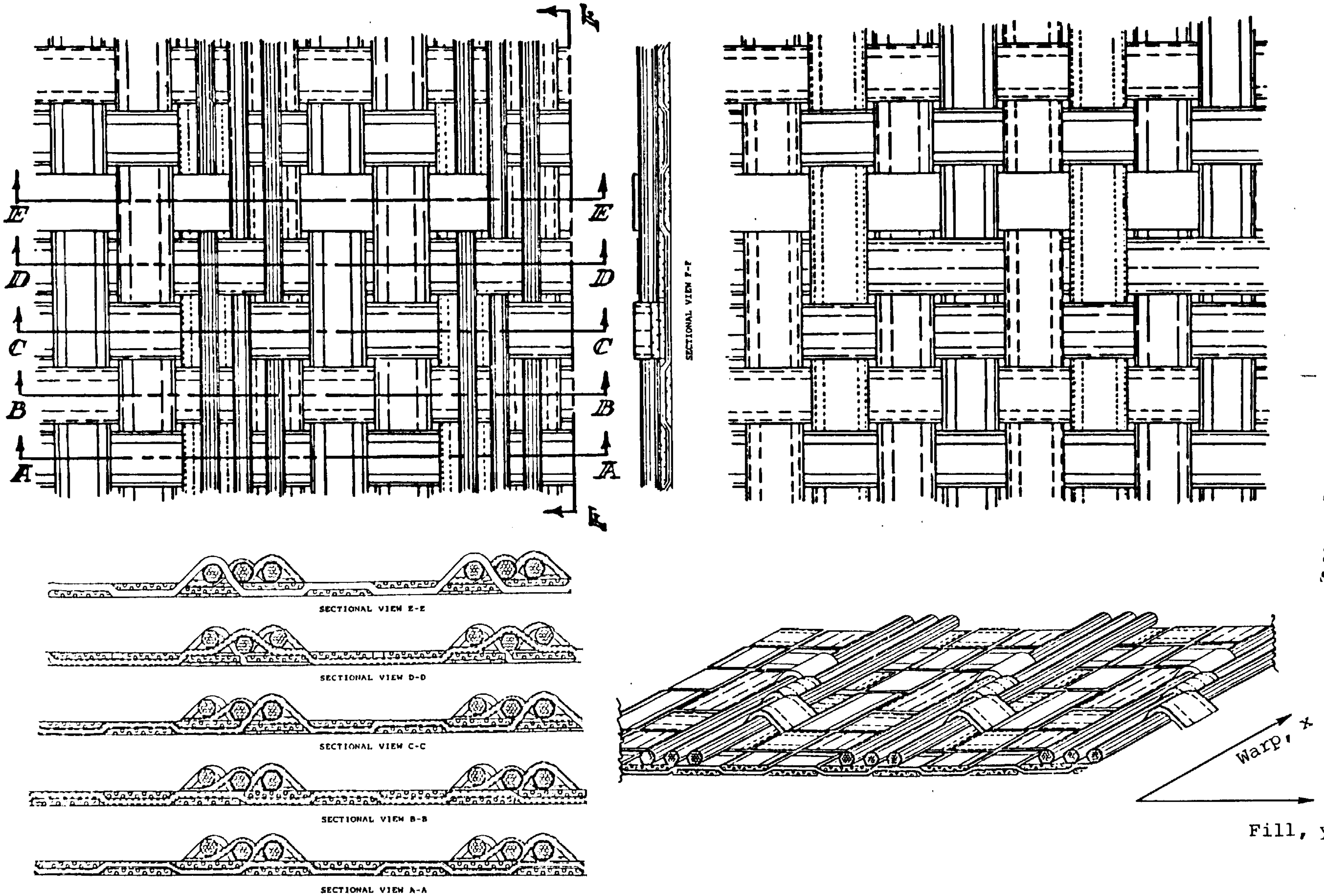

Figure 13. Plan Views from Above and Below, Sectional Views, and an Isometric of First Face-Ply-for-Nesting Constructions. The Auxiliary Warps atop the base weave are twisted before weaving to approach a circular cross section as shown.

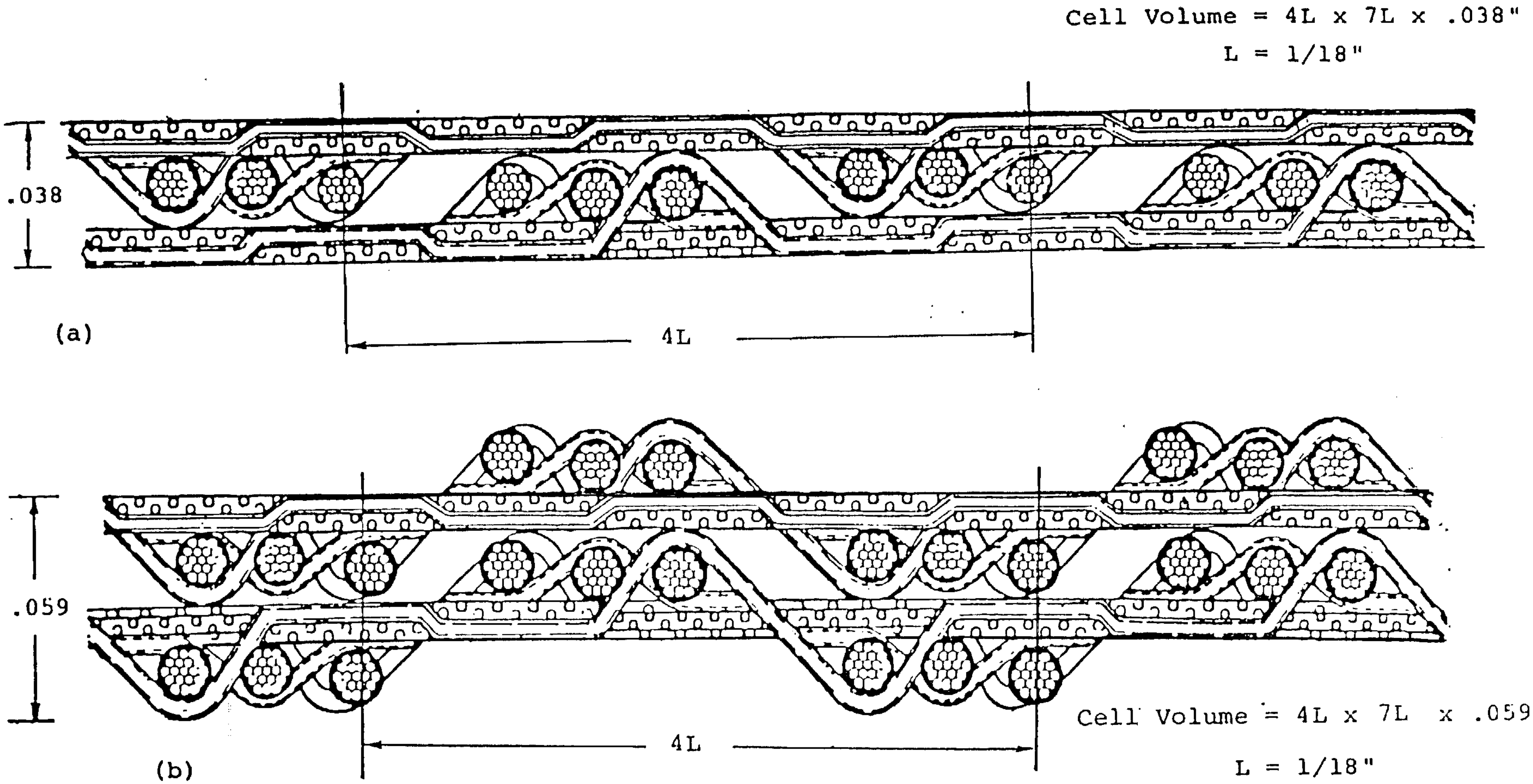

Figure 14. Detailed Cross Sectional Views of (a) Nested Face-Ply and (b) Nested Internal Play Configurations Showing Dimensions of First Woven Sample. In this first sample the auxiliary warps were deliberately spaced to allow for lateral growth during fabrication. As it turned out too much space was allowed and resin pockets resulted.

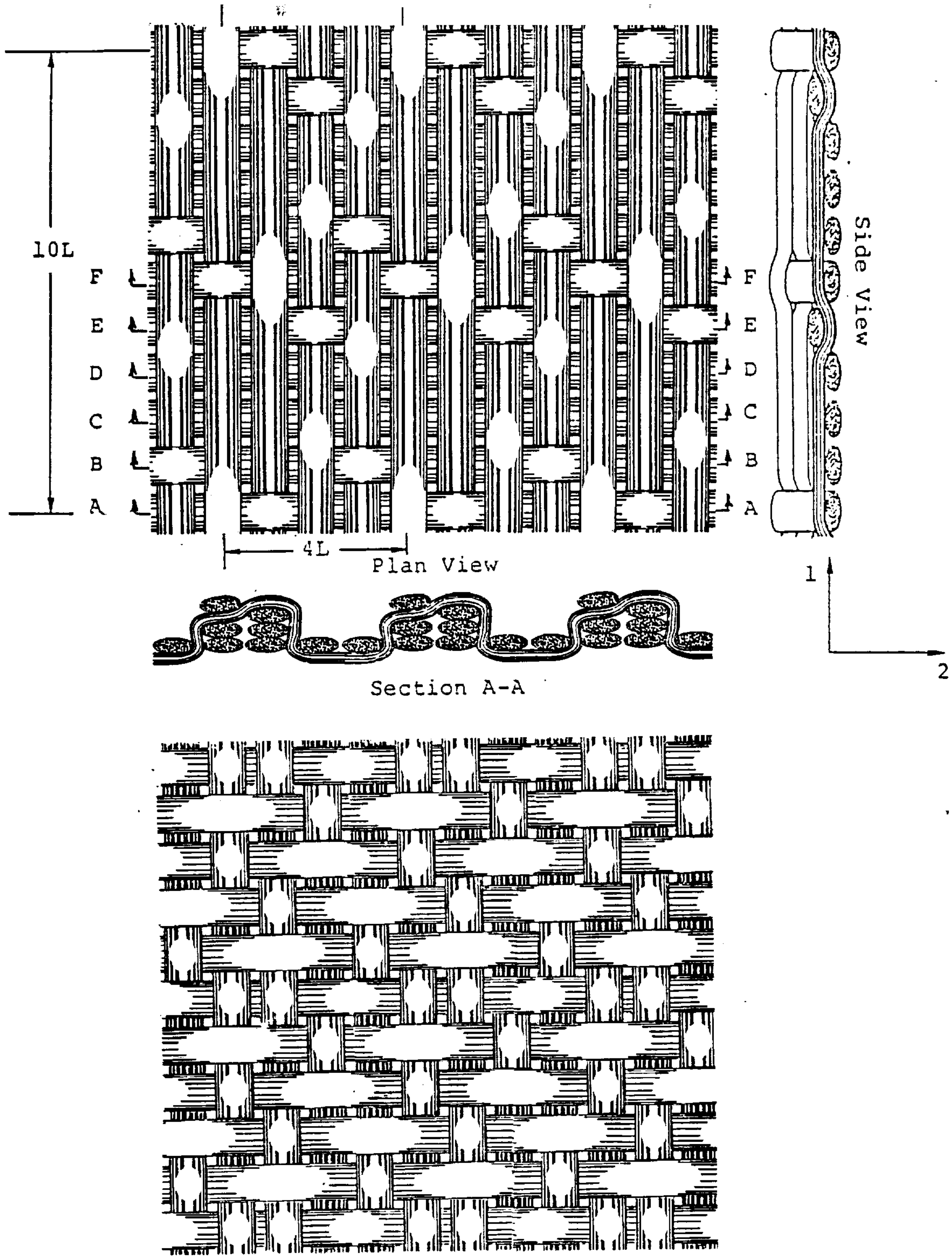

Figure 15. Revised (Mark II) Bumpy Fabric Stacked the Auxiliary Warps Two High, as Shown Here. Whether this is adequate to provide appreciable thru the thickness reinforcement is yet to be determined.

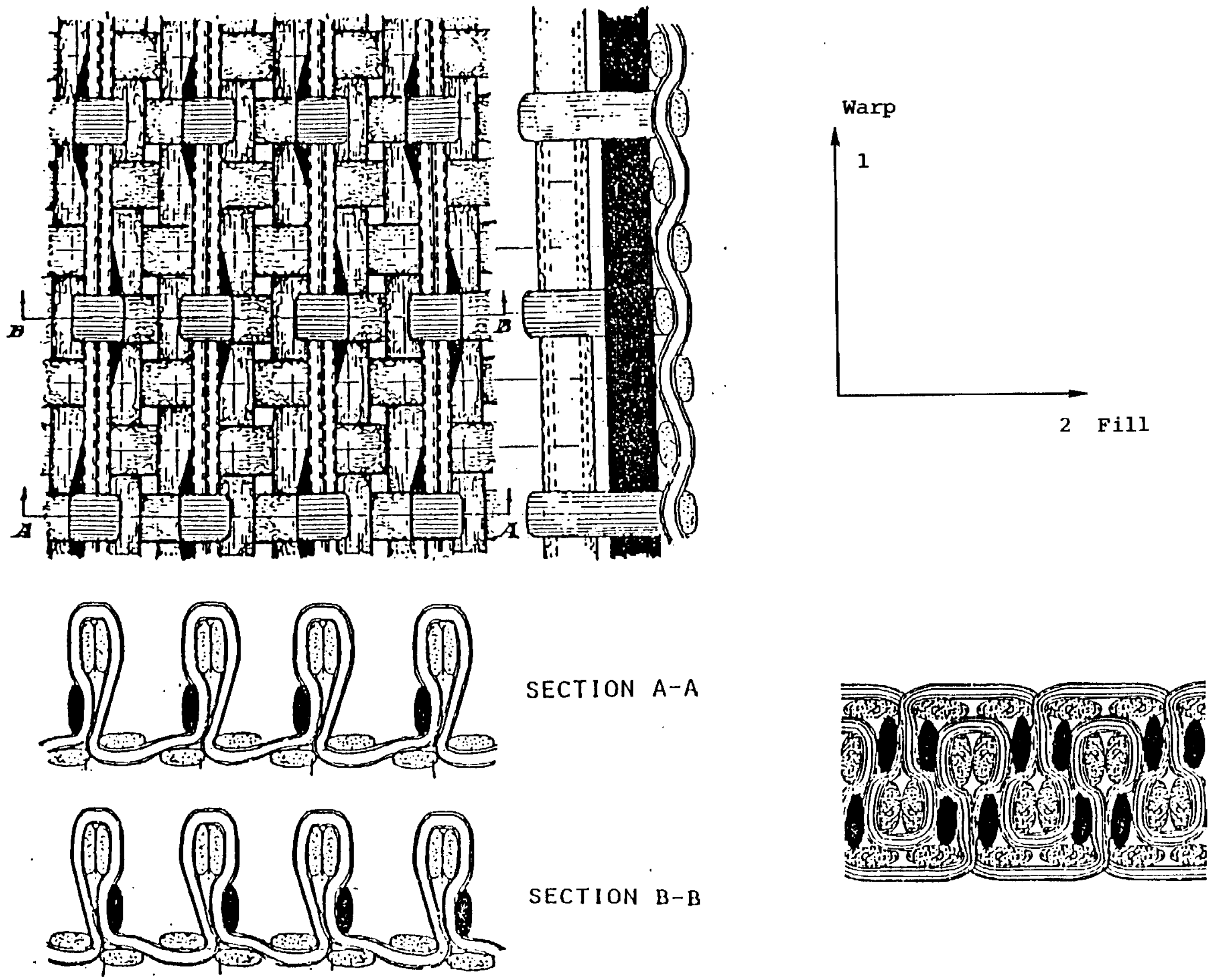

Figure 16. Bulbous Blade Bumpy Construction Woven with Auxiliary Warps Flat (Untwisted) and Oriented Vertically as Shown. Nesting provides snug overlapping of auxiliaries.

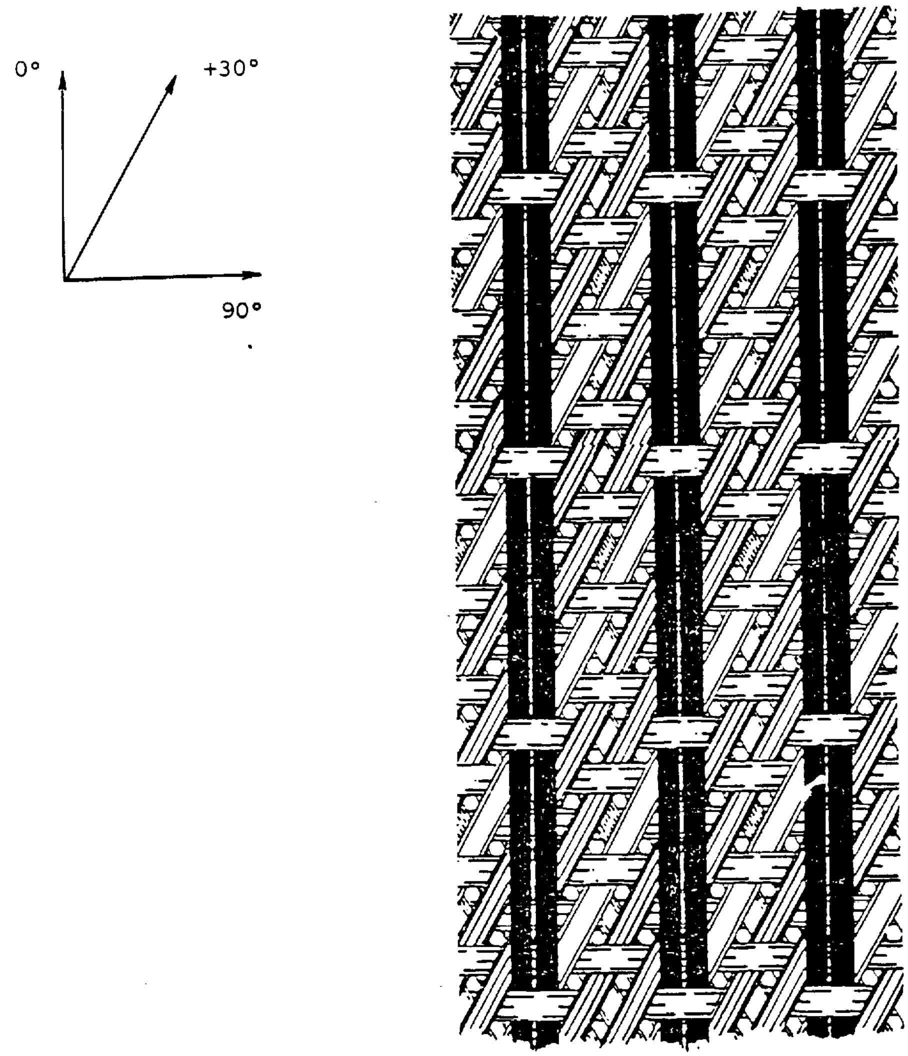

Figure 17. Substrate Triaxial Weave with Auxiliary Warps. The Substrate shown is loosely woven to a density equivalent to that of a tightly woven biaxial plain weave to illustrate the construction. Normally the Substrate would be snugly packed together so that the -30° warps would not be visible. (See also fig. 24).

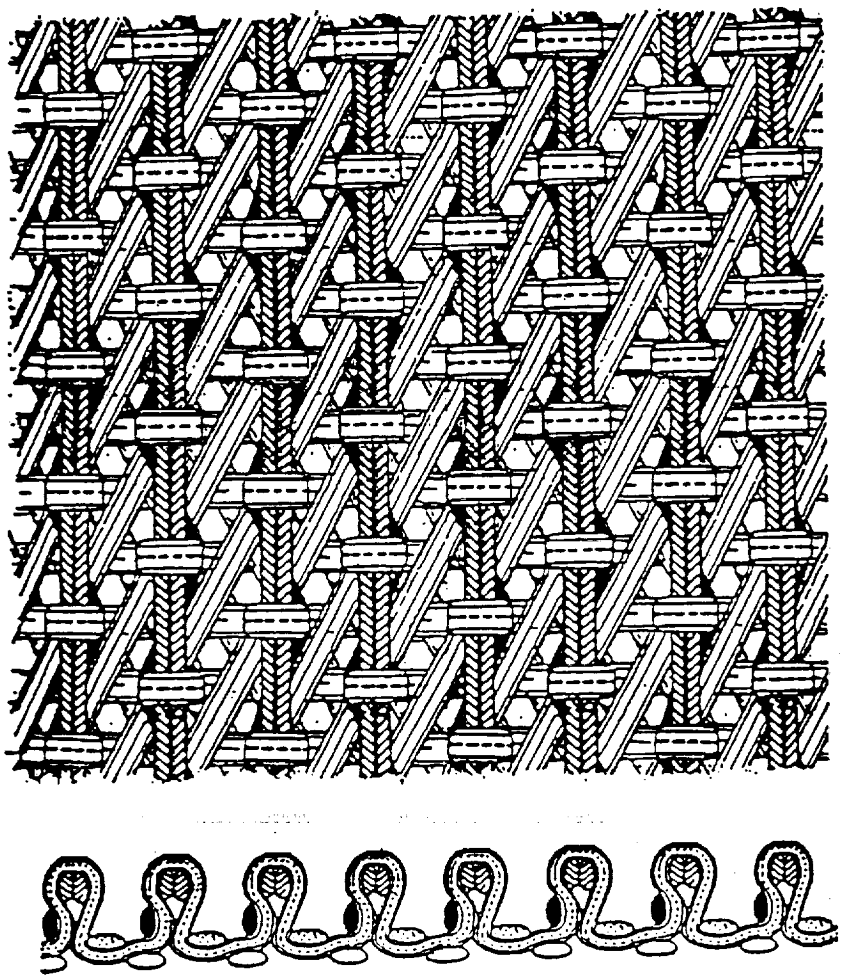

Figure 18. Bulbous Blade Auxiliary Warps in a Triaxial Substrate Weave Base. The Substrate Weave is shown loosely woven to permit the -30° yarns to appear.

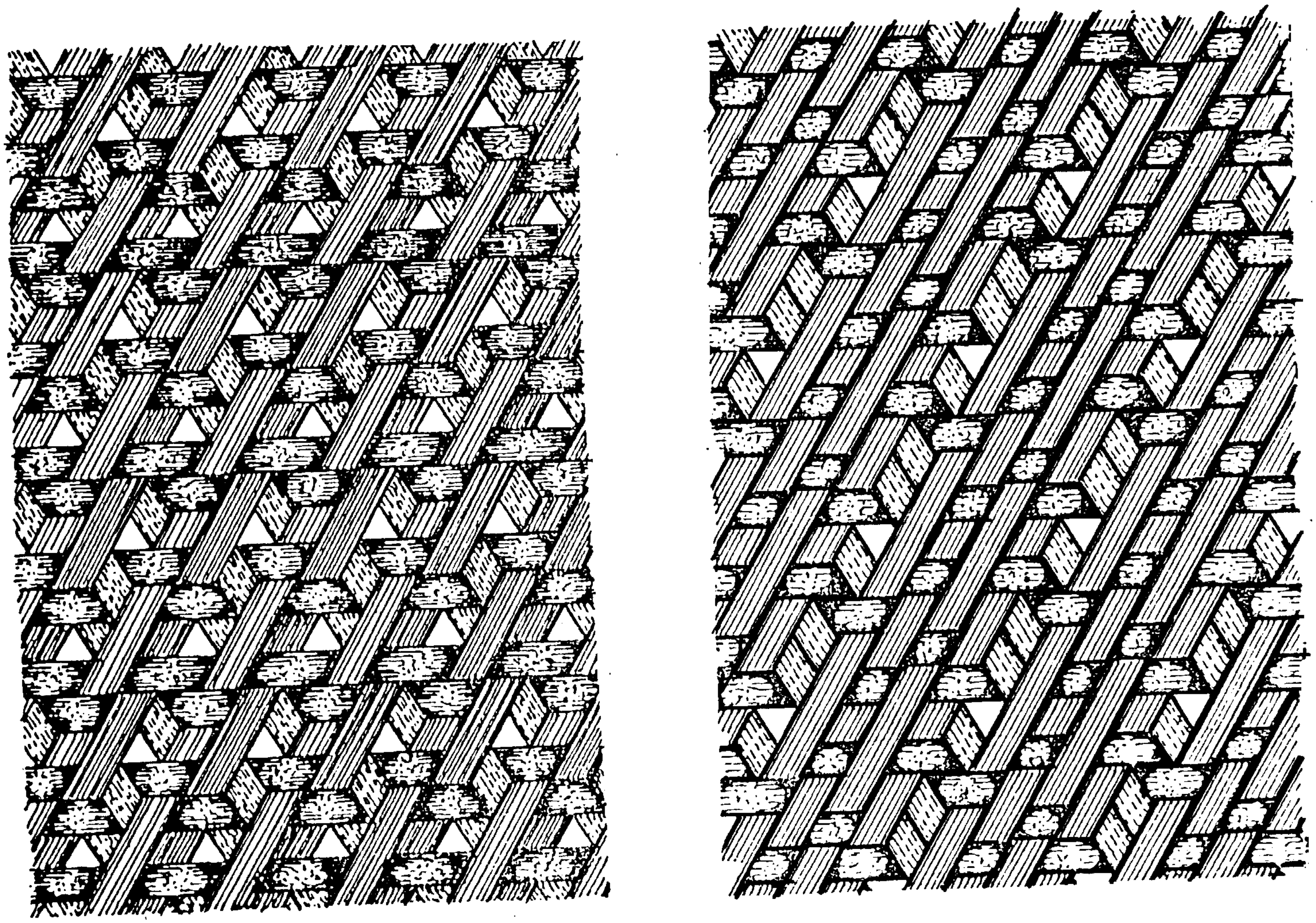

Figure 19. Examples of Triaxial Stitchbase Weaves, Providing Regularly Spaced Holes, Precisely Located by Locked Intersections of the Yarns, Through Which Stitching Can Be Done to Tie Plies Together Without Damage to the Yarns.

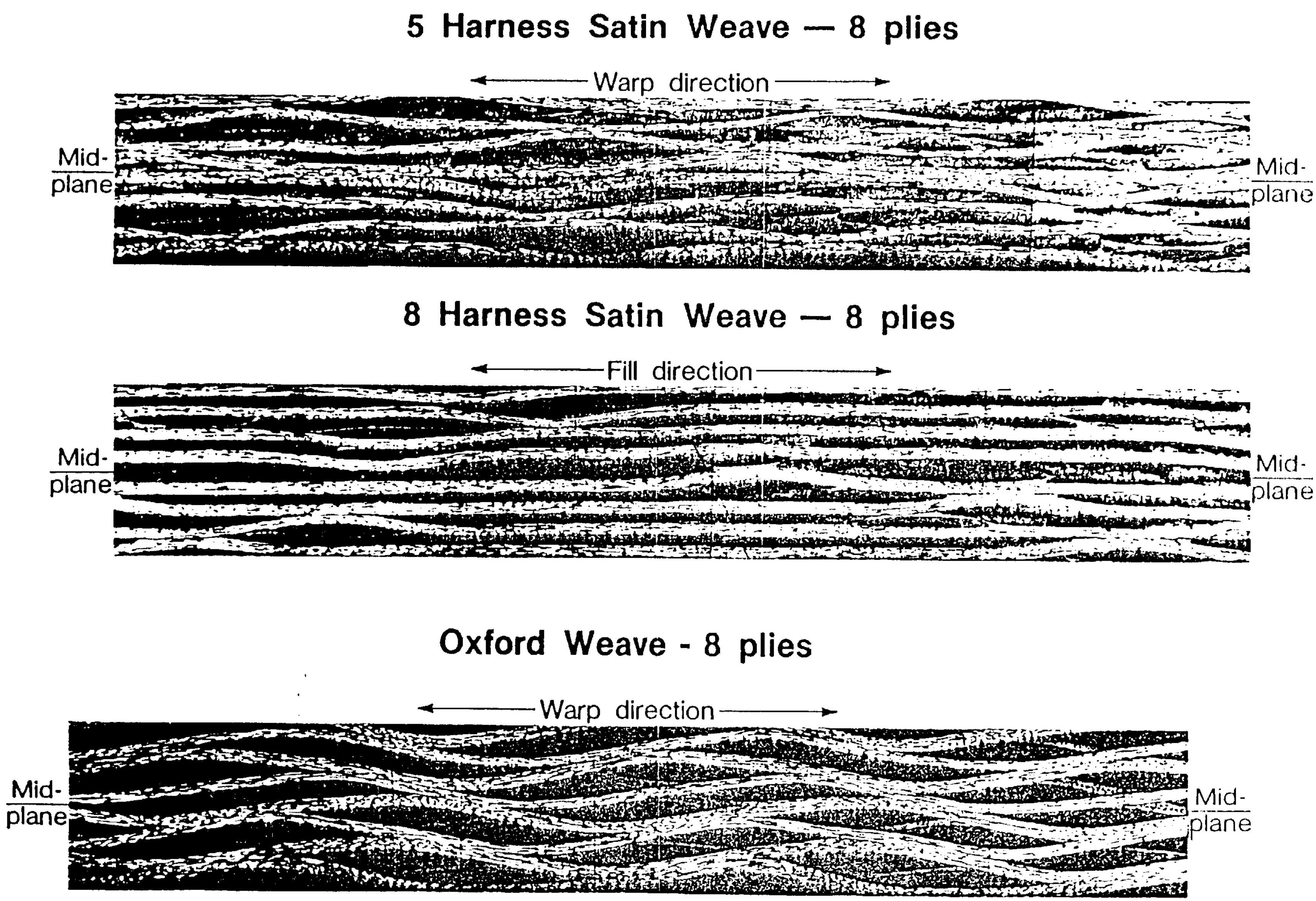

Figure 20. Repeat of Figure 1 for Convenience in Relating the Actual Cross Sectional Shapes Developed in Woven-Fabric-Reinforced Composites to the Shapes Modeled for Analysis (Figs.21 and 22).

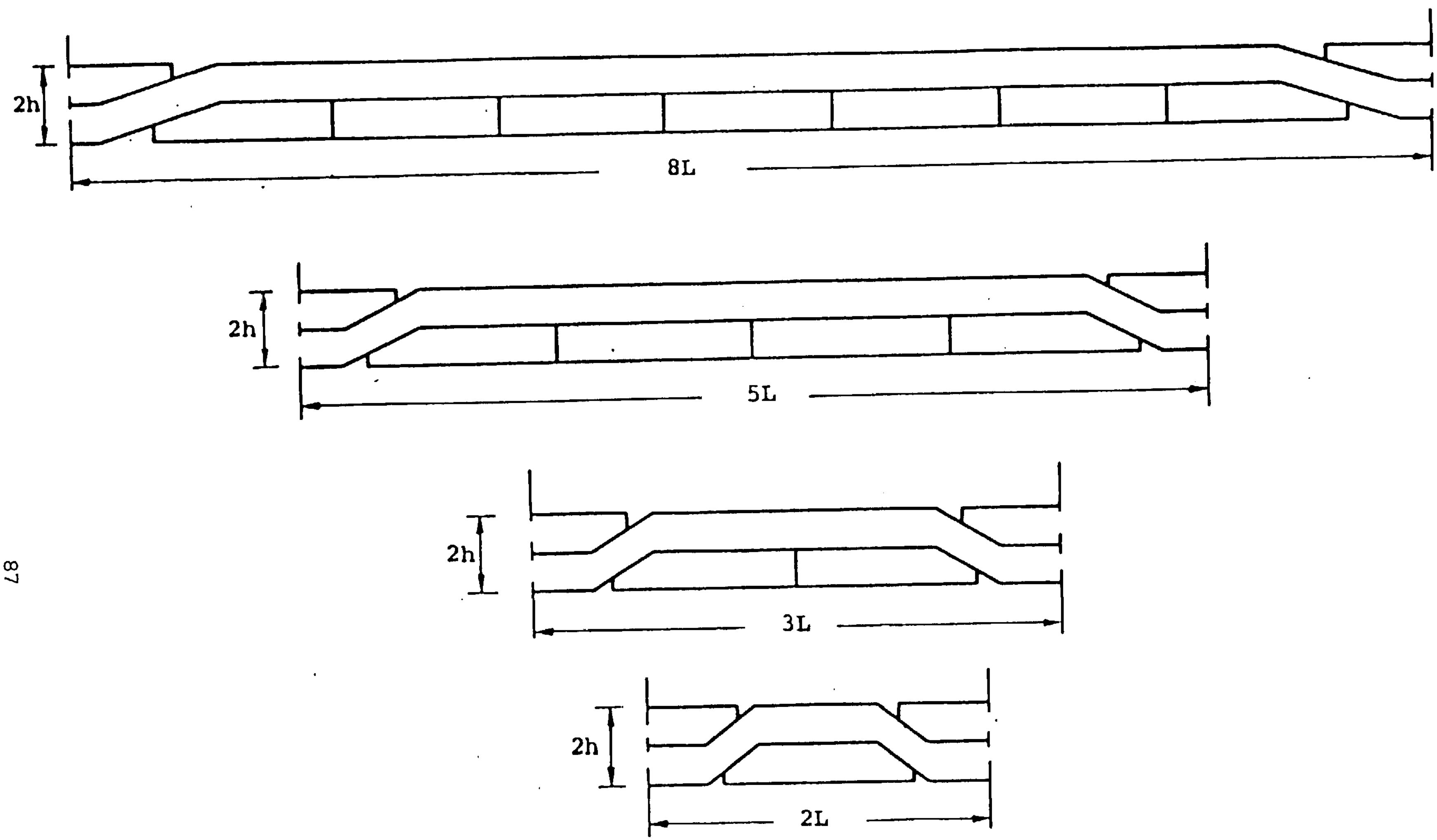

Figure 21. Representative Cross Sectional Area Elements of Woven Fabric of Various Float Lengths (i.e. Various Harness Numbers) as Used in NDPROP Analysis.

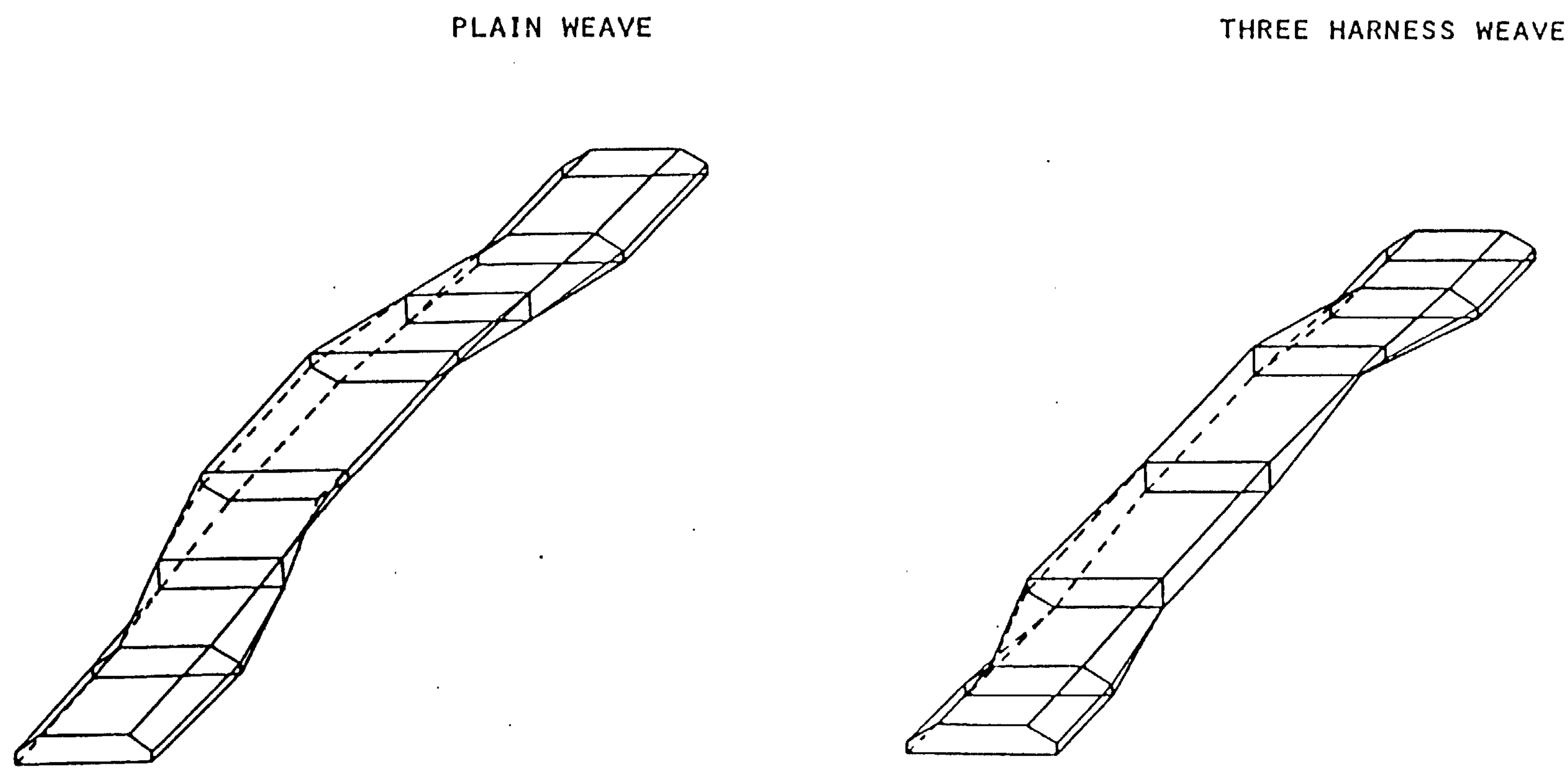

Figure 22. Representation of the Variation of Yarn Bundle Cross Sections at Yarn Cross-Over Points and Along Straight Floats as Modeled for NDPROP Analysis.

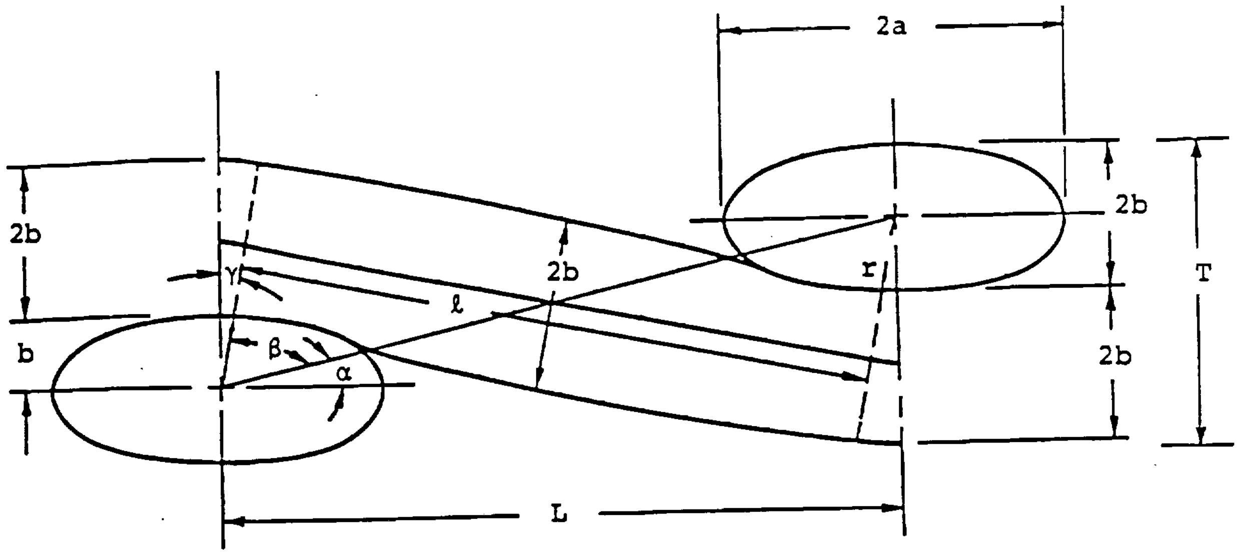

Definition of Symbols not defined in figure:

A_f :cross-sectional area of fibers in yarn

V_{fb}:volume fraction of fibers in yarn

V_f :overall fiber volume fraction

e :eccentricity of ellipse = b/a

V_{fp}:volume fraction of yarns within repeating element

Procedure: Given L, T and A_f

1. Calculate $b = 0.25\ T$

2. Assume V_{fb}

3. Calculate $e = \pi b^2 V_{fb}/A_f$

Figure 23. Cross Sectional View of Elliptical-Section Yarns for Triaxial Weaves and Procedures to Define Yarn Geometry.

4. Solve for r, where b < r < b/e :

$$\tan^{-1}\frac{2b}{L} + \tan^{-1}\sqrt{\frac{L^2-4r^2-2Tr}{2r+2b}} + \tan^{-1}\sqrt{\frac{r^2-b^2}{b^2-e^2r^2}} = 90°$$

5. Determine fabric geometrical parameters:

$$\alpha = \tan^{-1}\frac{2b}{L}$$

$$\beta = \tan^{-1}\sqrt{\frac{L^2-4r^2-2Tr}{2r+2b}}$$

$$\gamma = \tan^{-1}\sqrt{\frac{r^2-b^2}{b^2-e^2r^2}}$$

$$\ell = \sqrt{L^2-2Tr-4r^2}$$

6. Compute $$v_f = \frac{3A_f}{L^2T}\left[\ell + 2a_o \int_o^{\sin^{-1}\left(\frac{r_o}{a_o}\sin\gamma\right)} \sqrt{1-\sin^2\theta\sin^2\phi}\ d\phi\right]$$

where $r_o = r+b$;

$b_o = 2b$;

$$a_o = \frac{r_o b_o \sin\gamma}{\sqrt{b_o^2-r_o^2\cos^2\gamma}};$$

and $$\theta = \sin^{-1}\sqrt{1-\frac{b_o^2}{a_o^2}}$$

7. Calculate $v_{fp} = V_f/V_{fb}$

Figure 23. (cont'd) Cross Sectional View of Elliptical-Section Yarns for Triaxial Weaves, and Procedures to Define Yarn Geometry.

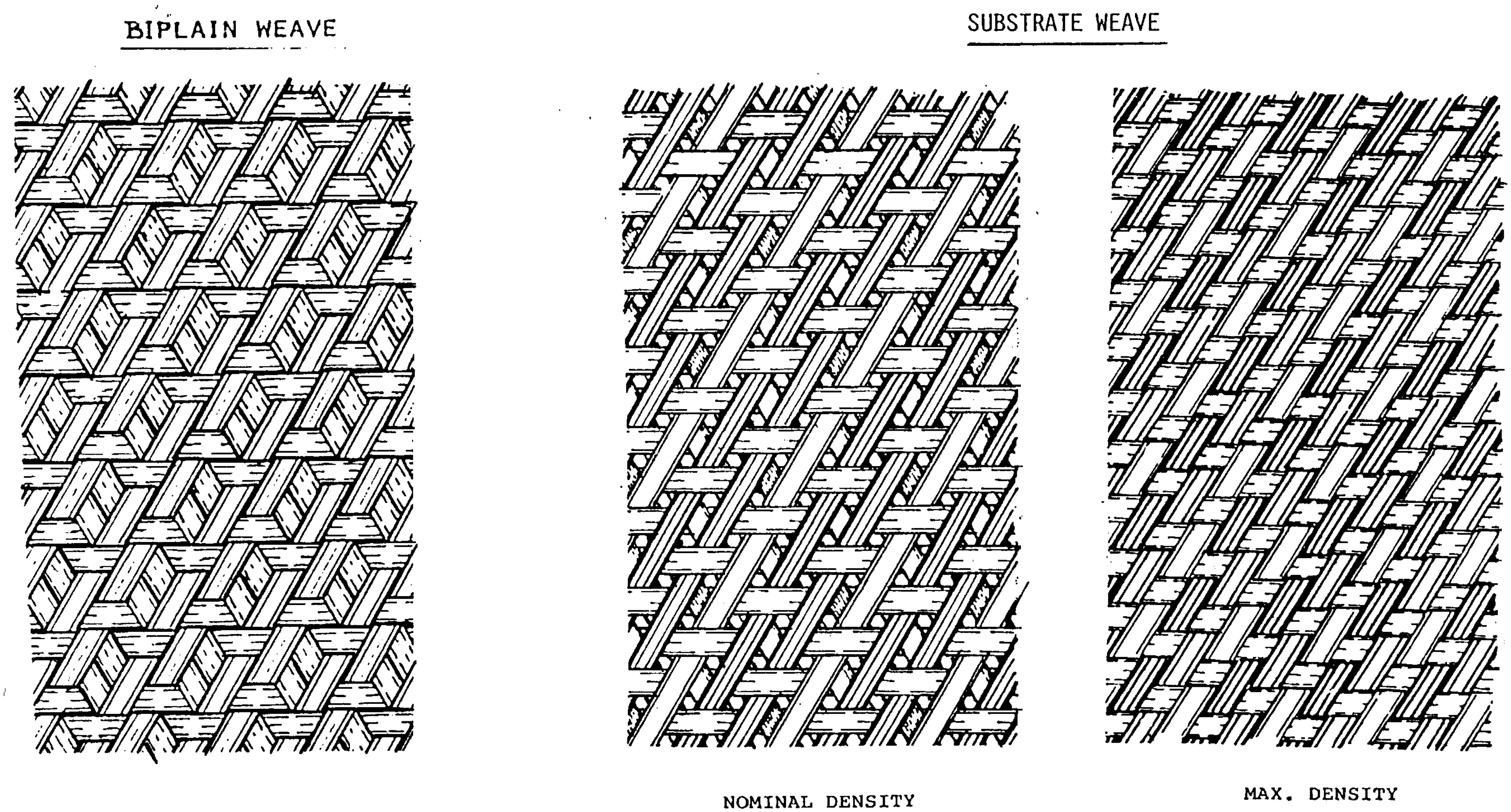

Figure 24. BiPlain and Substrate Triaxial Weaves. In the BiPlain the weave is one up and one down for the fill with each of the warps. In the Substrate the weave is one up and two down for the fill with each of the warps. The warps are not interwoven.

C-2

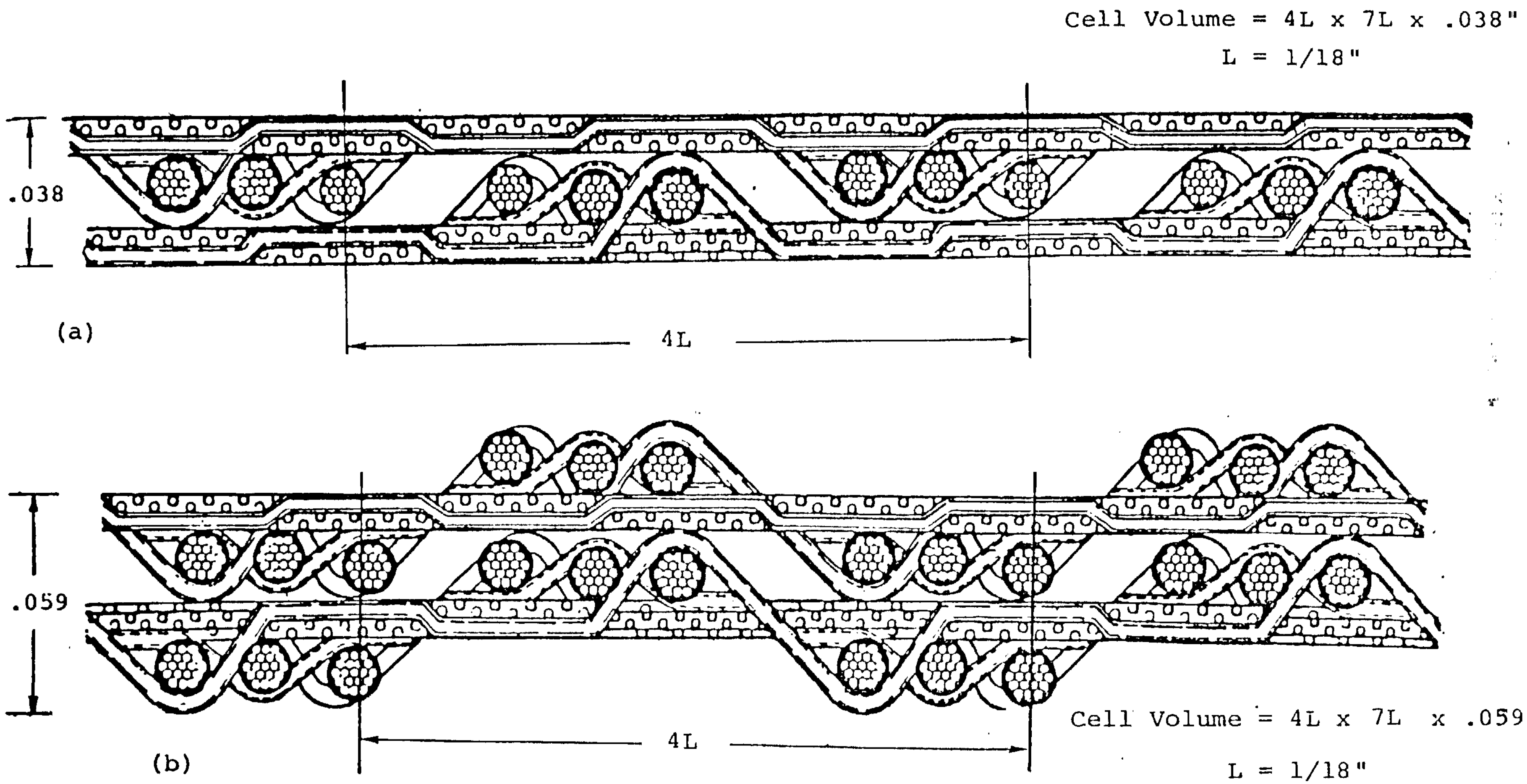

Figure 25. Repeat of Figure 15 Showing Dimensions and Repeating Element Used in Calculating Properties of First Nested Configurations.

ORIGINAL PAGE IS
OF POOR QUALITY

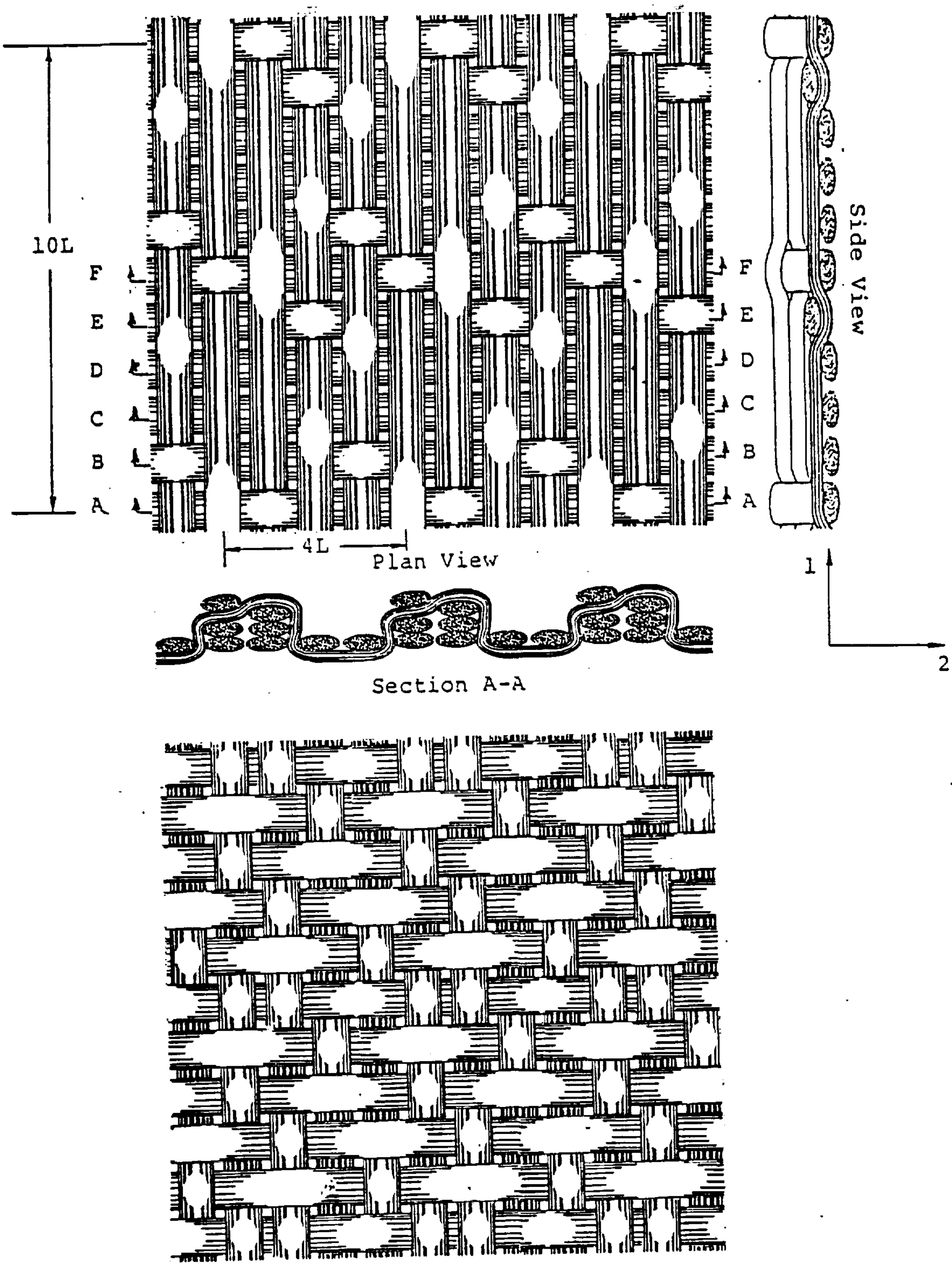

Figure 26. Revised Design Auxiliary Warp Construction. Revisions from first design include stacking of the auxiliary warps to make the fabric more bumpy and increasing float lengths to improve compressive properties.

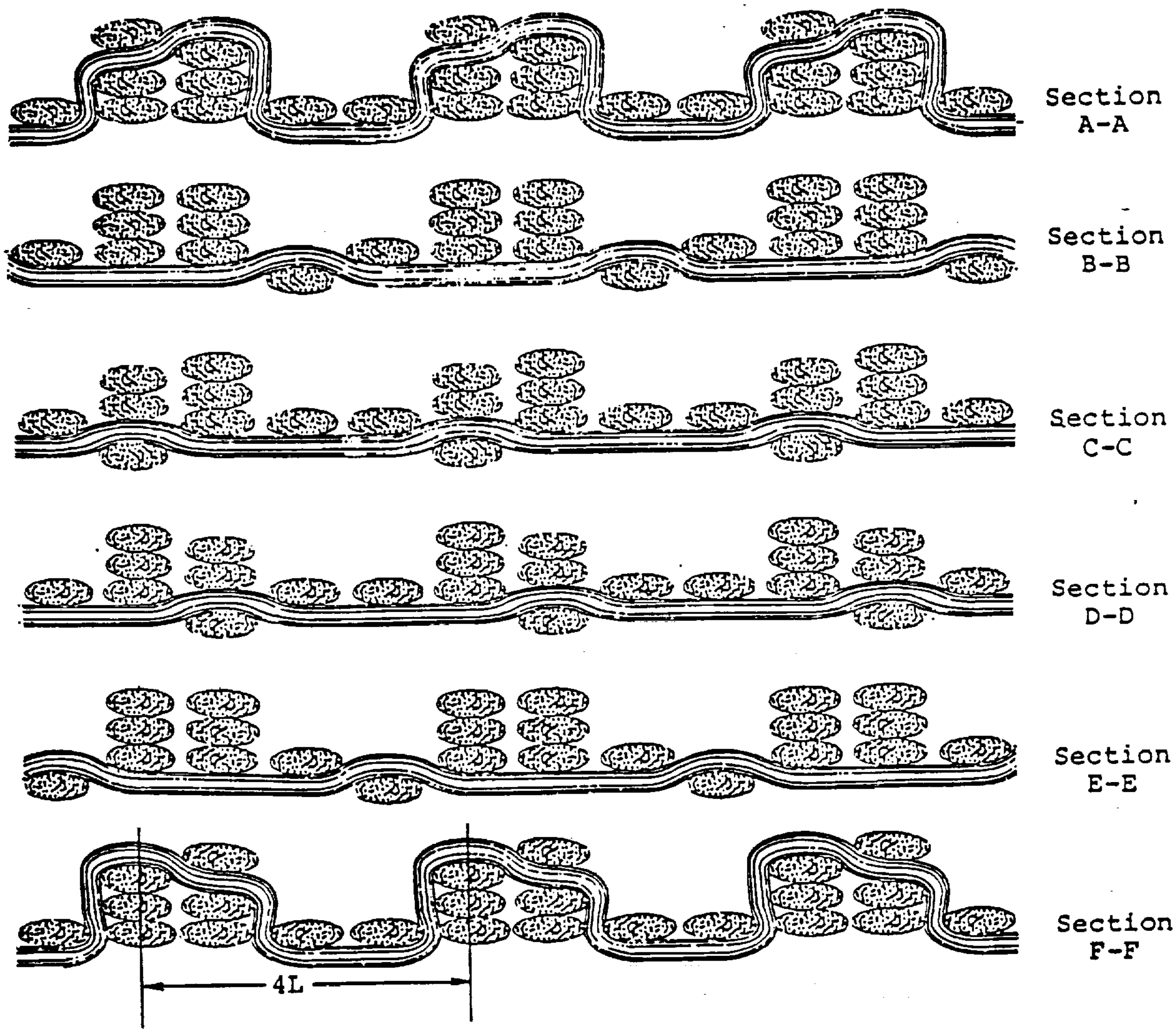

Figure 27. Cross Sections of Revised Face Ply Reinforcement Showing Auxiliary Warp Tie-Down Every Fifth Pick, Alternating Over-and-under the Individual Yarn Pairs of the Auxiliaries.

ORIGINAL PAGE IS
OF POOR QUALITY

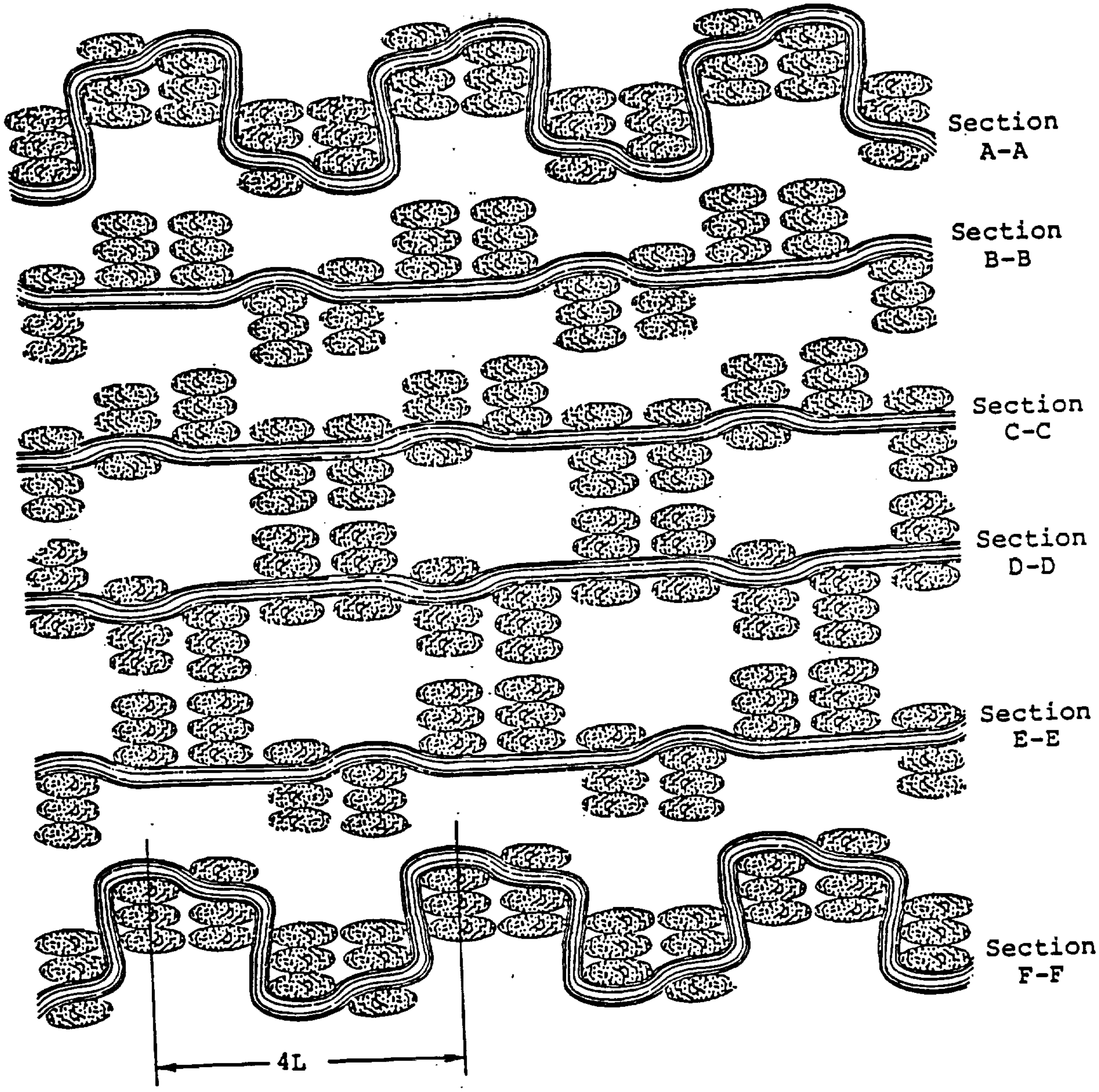

Figure 28. Cross Sections of Revised Internal Ply Reinforcement with Similar Tie-Downs for the Auxiliaries to Those in the Face Plies. From this figure the construction appears much more bumpy than the original auxiliary warp construction (fig. 14). As woven, however, the difference did not appear nearly as great.

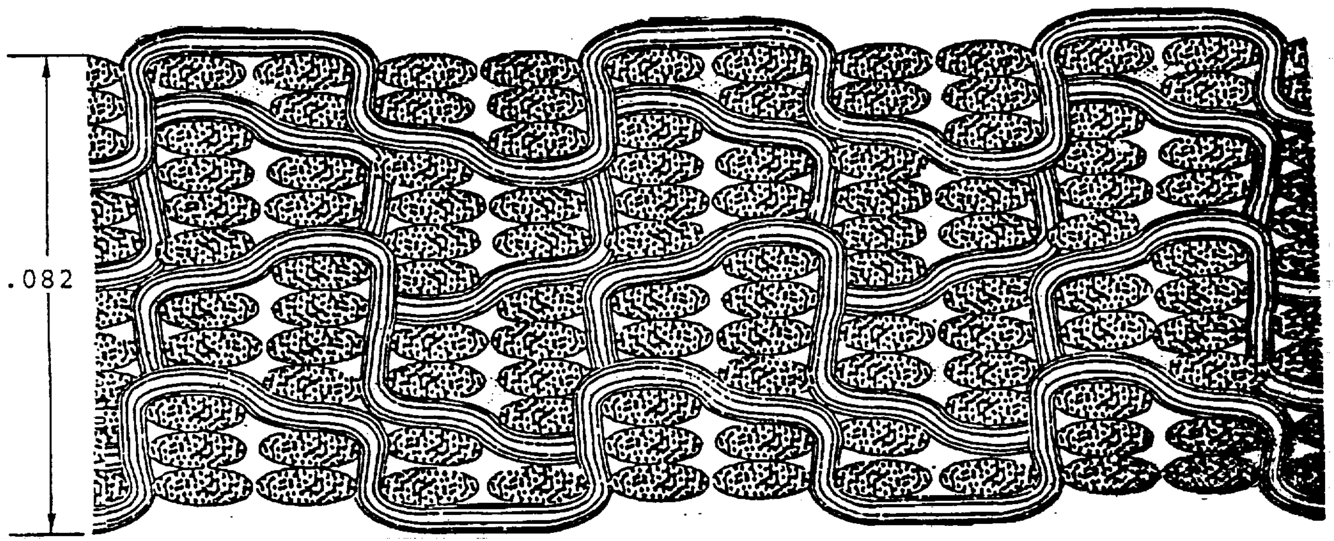

Nested Face and Internal Plies

Cell Volume = 4L x 10L x .082"
L = 1/18"

Figure 29. Nominal Nesting of Multi-Ply Revised Auxiliary Warp Constructions Indicating Magnitude of Through-the-Thickness Running and Overlapping Fill Yarns.

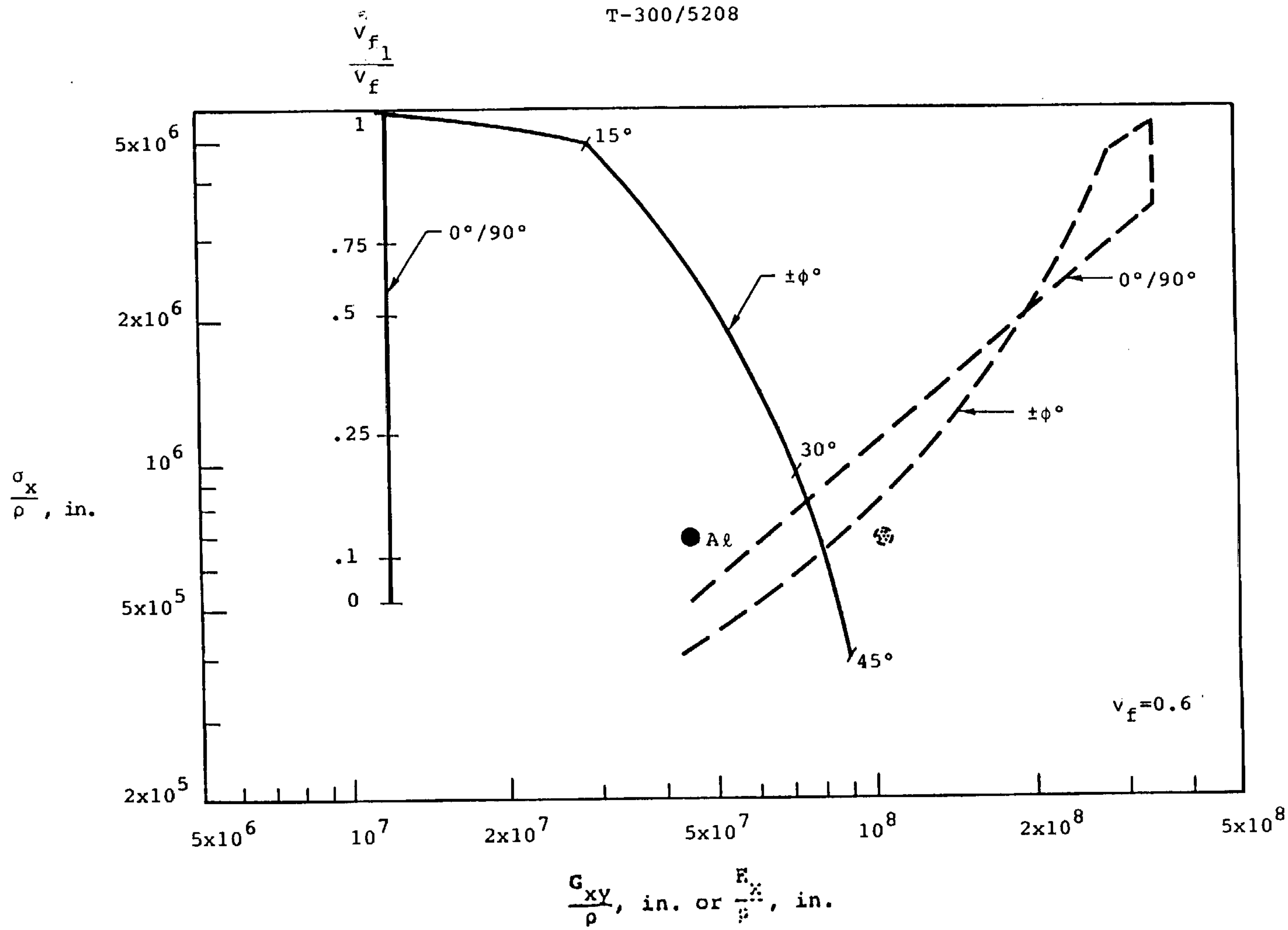

Figure 30. Evaluations of Intrinsic In-Plane Properties of Multi-Directional Reinforcements in Tension.-

I. T-300 0°/90° weaves and biaxial braids. The 0°/90° weave is characterized by minimal shear stiffnesses for all proportions. The braid (±φ° configuration) can have substantial shear stiffness combined with very high values of $\frac{\sigma_x}{\rho}$,-over seven times that of the aluminum alloy for the same shear stiffness/density ratio.

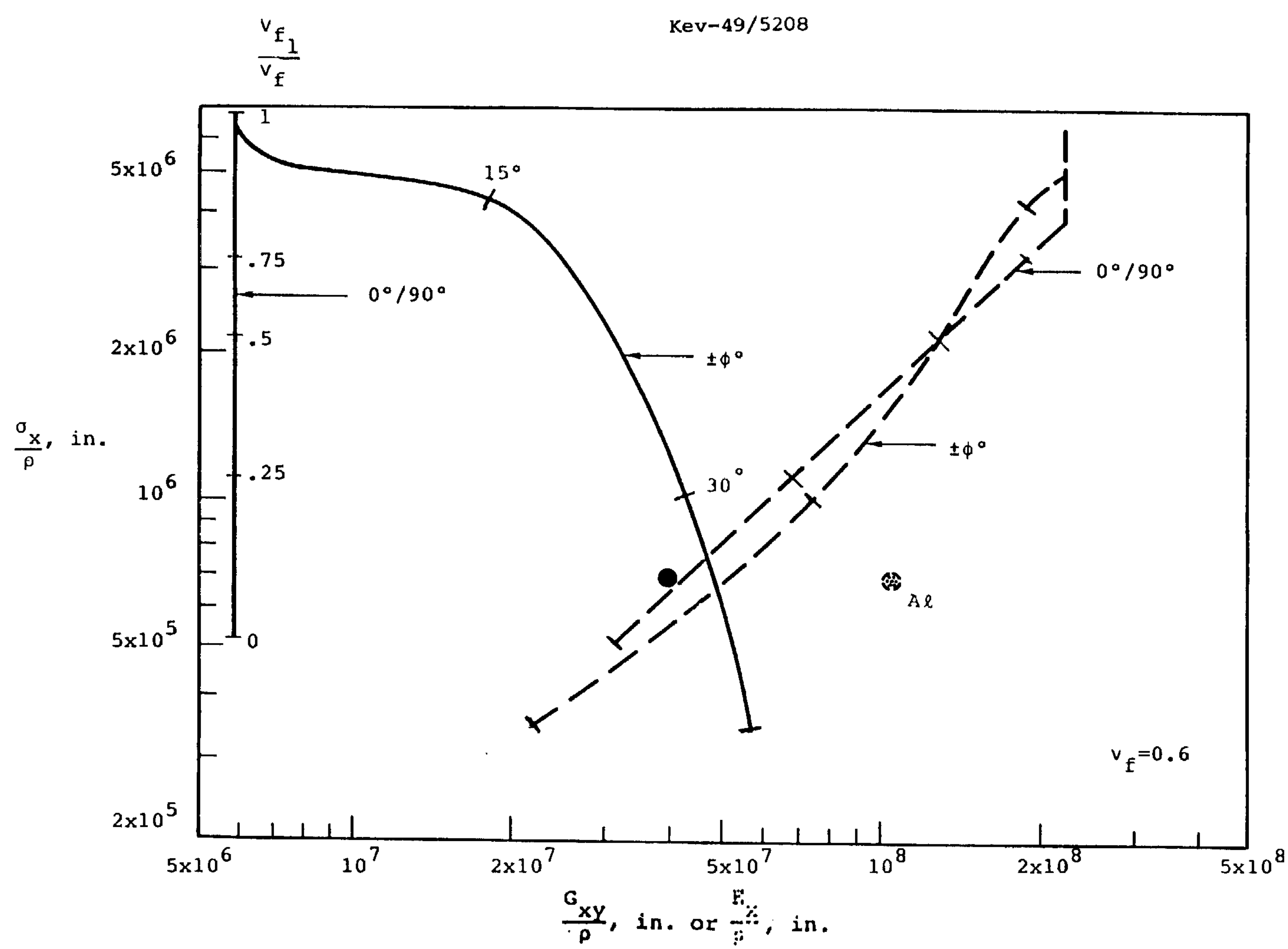

Figure 31. Evaluations of Intrinsic In-Plane Properties of Multi-Directional Reinforcements in Tension.-

II. Kevlar 0°/90° weaves and biaxial braids. The 0°/90° weave is characterized by minimal shear stiffnesses for all proportions. The braid ($\pm\phi°$ configuration) can have good shear stiffness combined with high values of $\frac{\sigma_x}{\rho}$,-nearly twice that of the aluminum alloy for the same shear stiffness/density ratio.

ORIGINAL PAGE IS OF POOR QUALITY

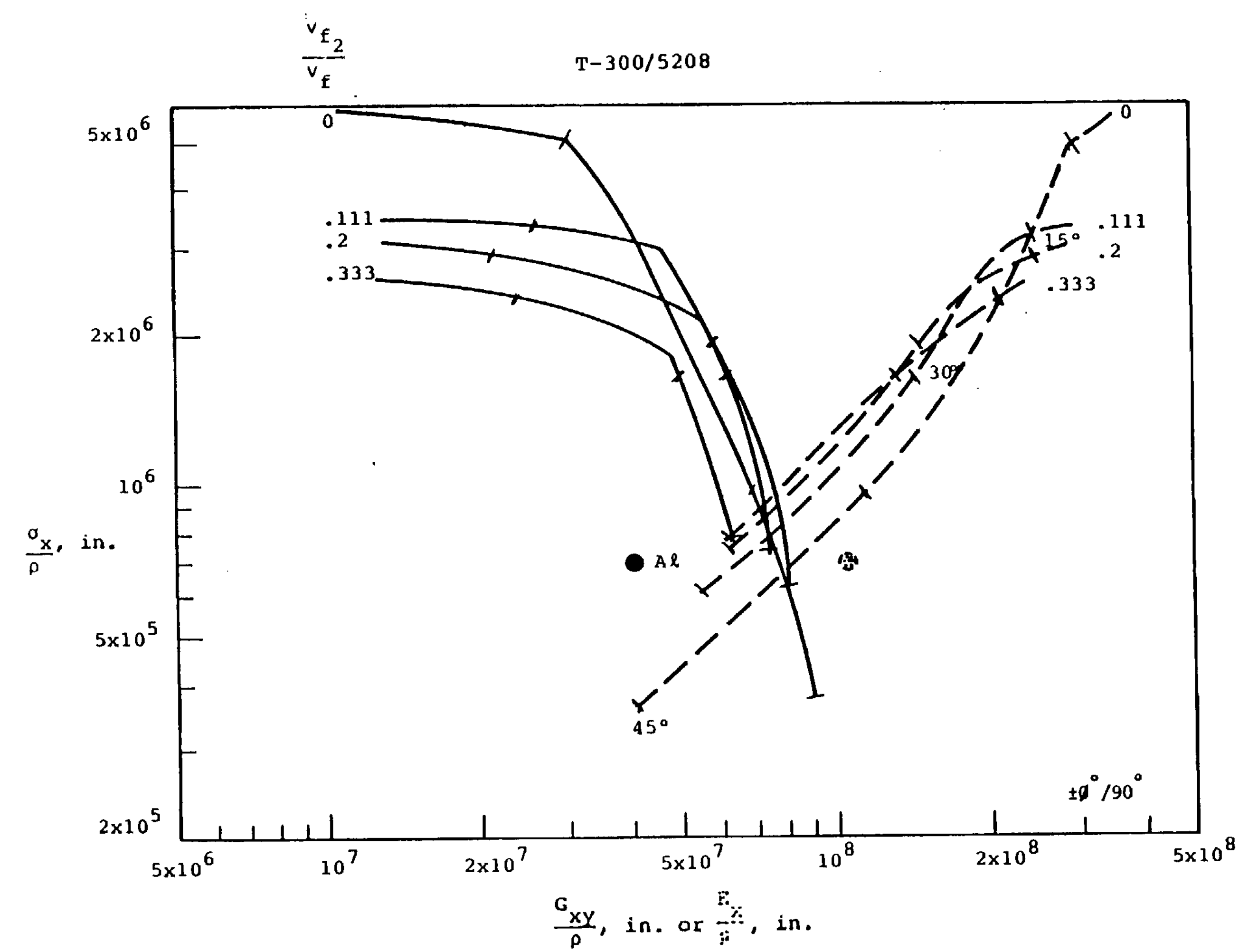

Figure 32. Evaluations of Intrinsic In-Plane Properties of Multi-Directional Reinforcements in Tension.-

III. T-300 $\pm\phi^\circ/90^\circ$ configurations. Addition of 90° reinforcement to the $\pm\phi^\circ$ configurations in small amounts decreases the values of $\frac{\sigma_x}{\rho}$ achieved and increases the shear stiffness/density ratios. Larger additions decrease both the tensile and shear properties. Fractions of 10% to 20% of the total reinforcement volume fraction appear to maximize the combined properties.

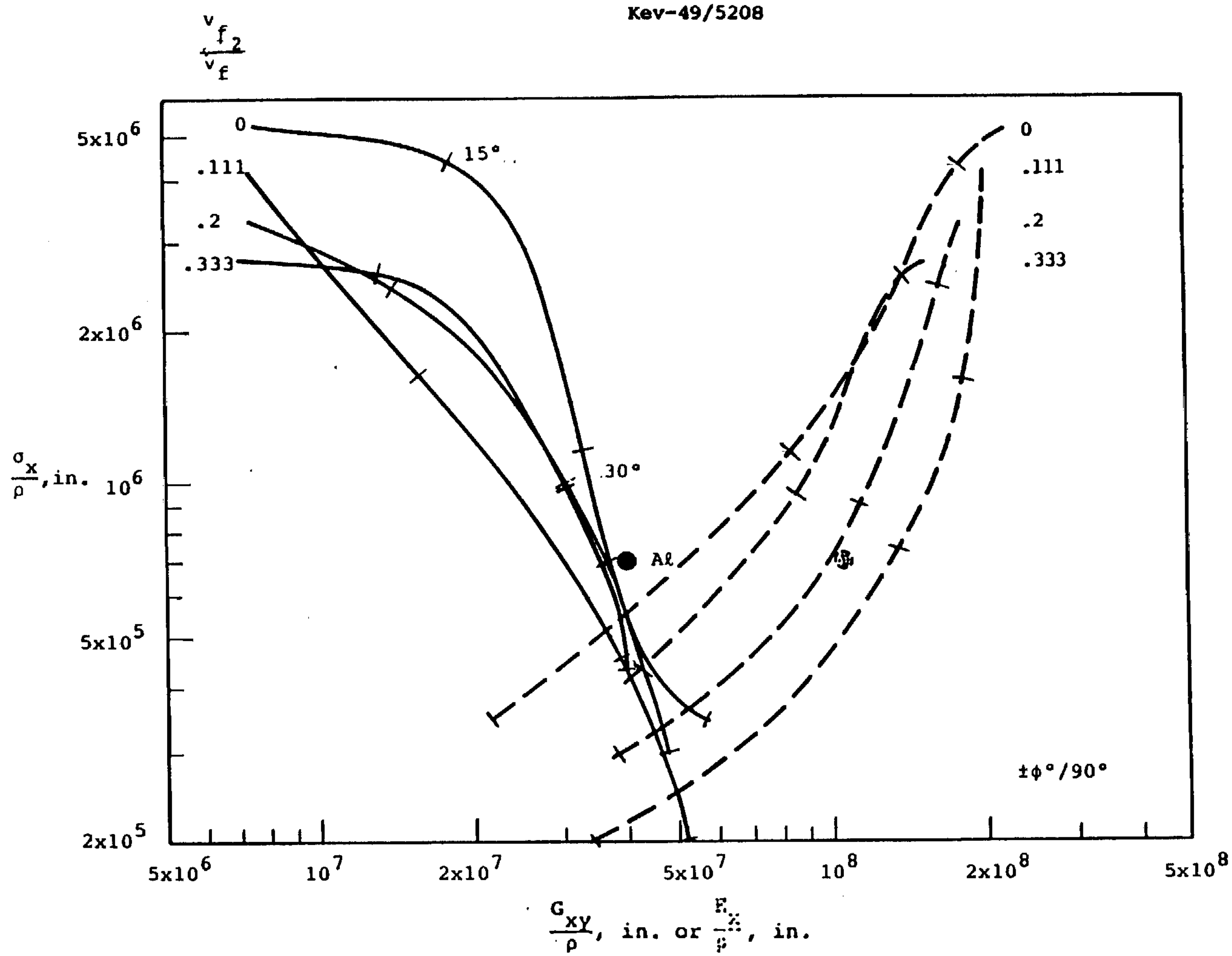

Figure 33. Evaluations of Intrinsic In-Plane Properties of Multi-Directional Reinforcement in Tension.-

IV. Kevlar $\pm\phi^\circ/90^\circ$ configurations. Addition of 90° reinforcement to the $\pm\phi^\circ$ configuration is not as salubrious as for T-300 (fig. 32). A compressive failure mode in the 90° filaments due to Poisson contraction is encountered in the low volume fraction 90° range found attractive in T-300. Kevlar reinforcements in any combination of proportions of the $\pm\phi^\circ/90^\circ$ configuration do not surpass the aluminum alloy properties for combined tension and shear stiffness.

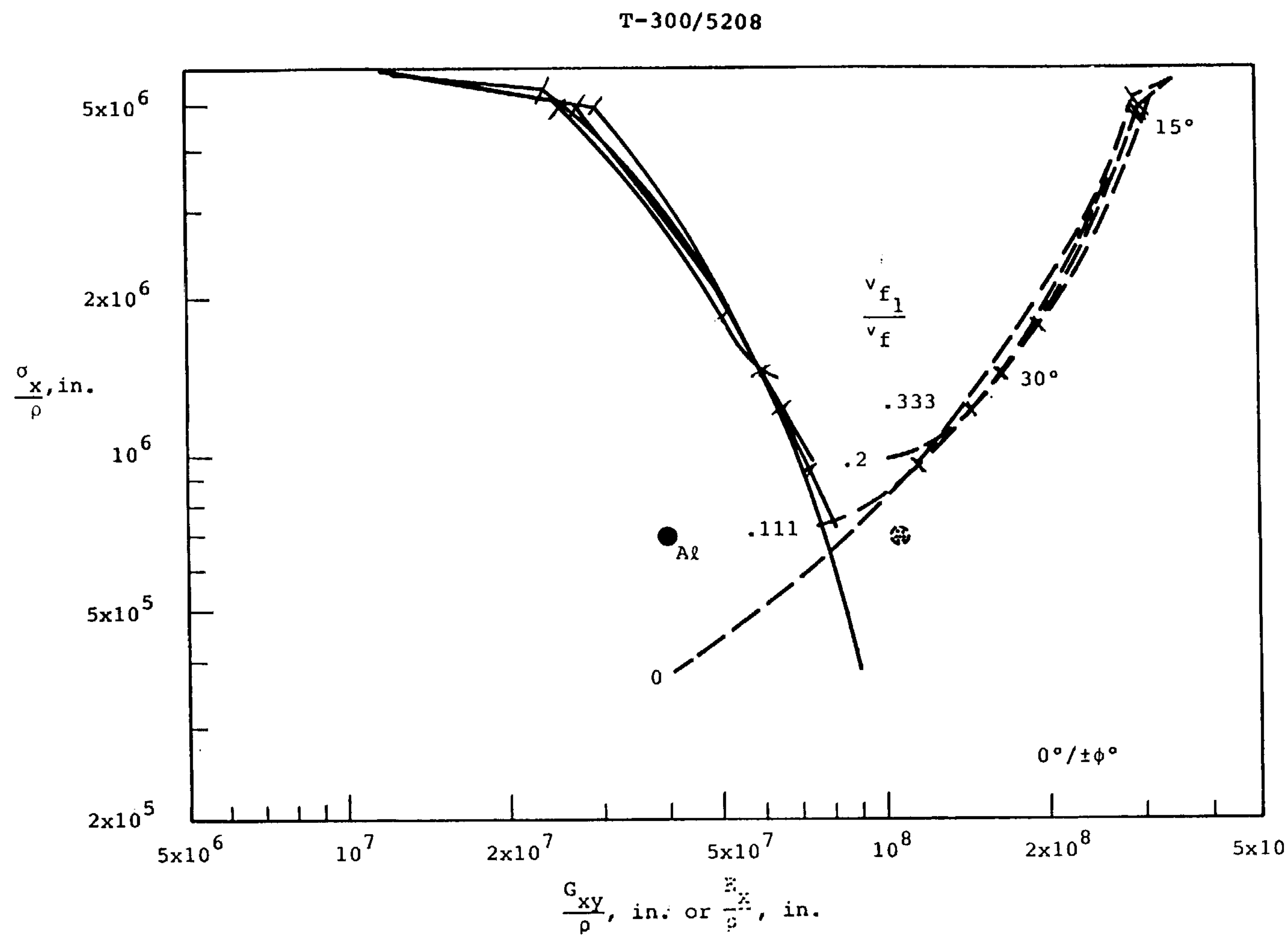

Figure 34. Evaluations of Intrinsic In-Plane Properties of Multi-Directional Reinforcements in Tension.-

V. T-300 $0^\circ/\pm\phi^\circ$ configurations are relatively insensitive to changes in proportions of filaments in the various directions. Optimal proportions provided slightly lower combined tension-shear stiffness/density ratios than $\pm\phi^\circ/90^\circ$ configurations but still yield values of $\frac{\sigma_X}{\rho}$ four times that of the aluminum alloy at the same shear stiffness/density ratio.

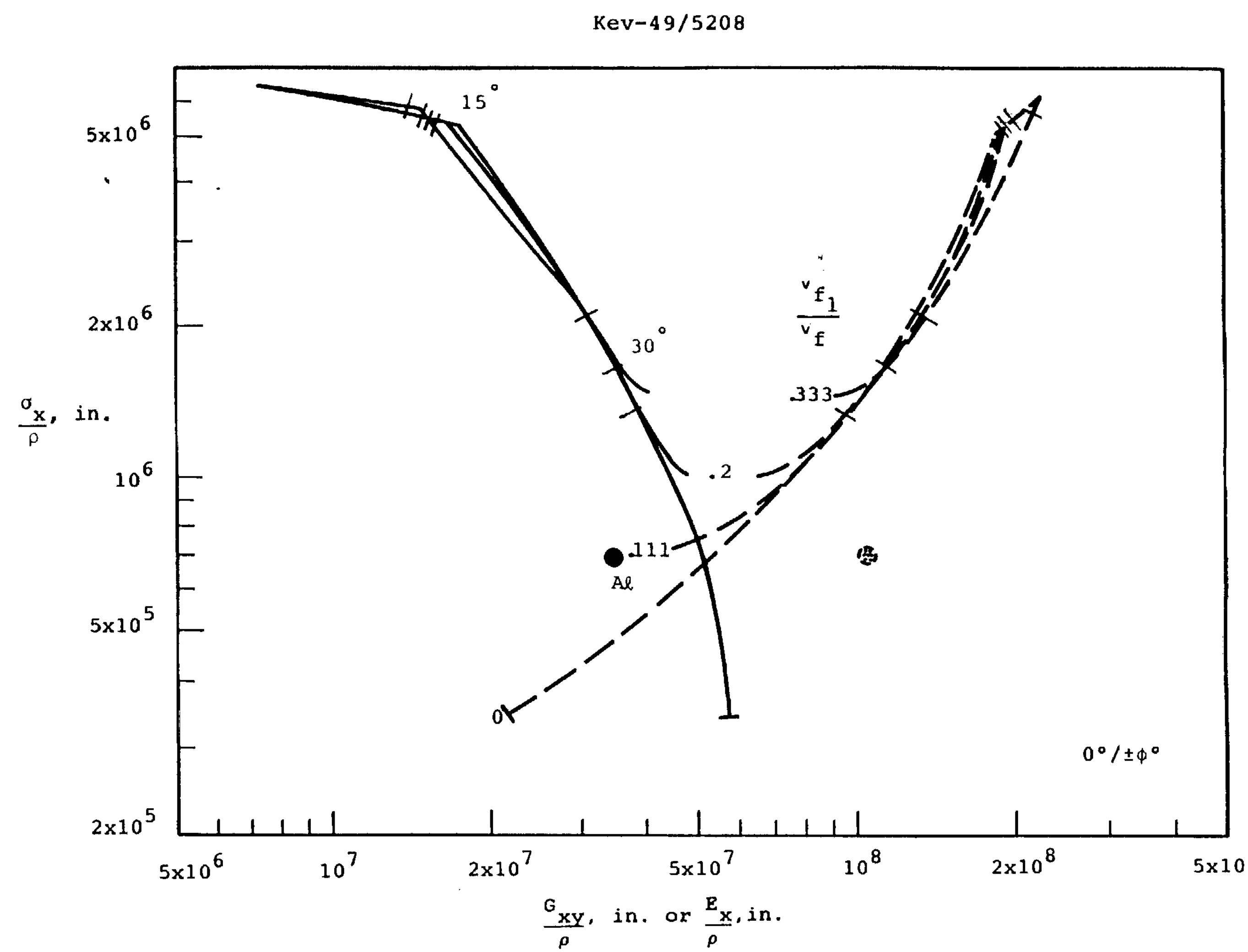

Figure 35. Evaluations of Intrinsic In-Plane Properties of Multi-Directional Reinforcements in Tension.-

VI. Kevlar $0^\circ/\pm\phi^\circ$ configurations are not susceptible to the compressive failures of the $\pm\phi^\circ/90^\circ$ reinforcements but even so are not competitive in performance with T-300 (c.f.Fig.32).

ORIGINAL PAGE IS OF POOR QUALITY

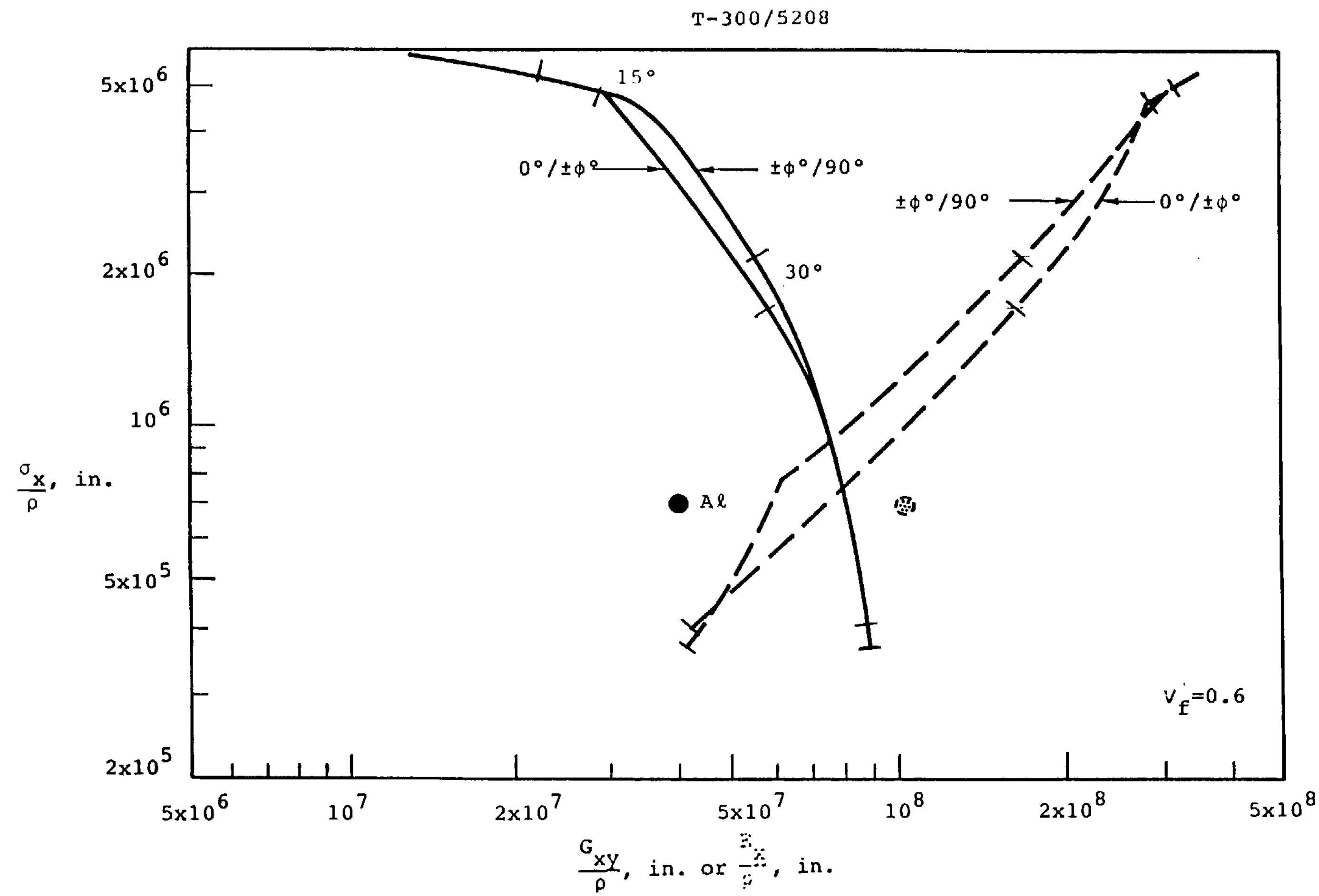

Figure 36. Overall Comparisons of $\mp\phi^\circ/90^\circ$ and $0^\circ/\mp\phi^\circ$ Configurations in Tension. Envelope curves for the various proportions evaluated show that the $0^\circ/\pm\phi^\circ$ configuration does not surpass the $\mp\phi^\circ/90^\circ$ configuration in combined tension-shear stiffness characteristics for any proportions. The coincidence of the curves at low shear stiffnesses represent proportions approaching 0°. At high shear stiffness $\mp 45^\circ$ reinforcing predominate. It is in the intermediate, mixed region that the $\mp\phi^\circ/90^\circ$ configuration shows slight superiority.

ORIGINAL PAGE IS
OF POOR QUALITY

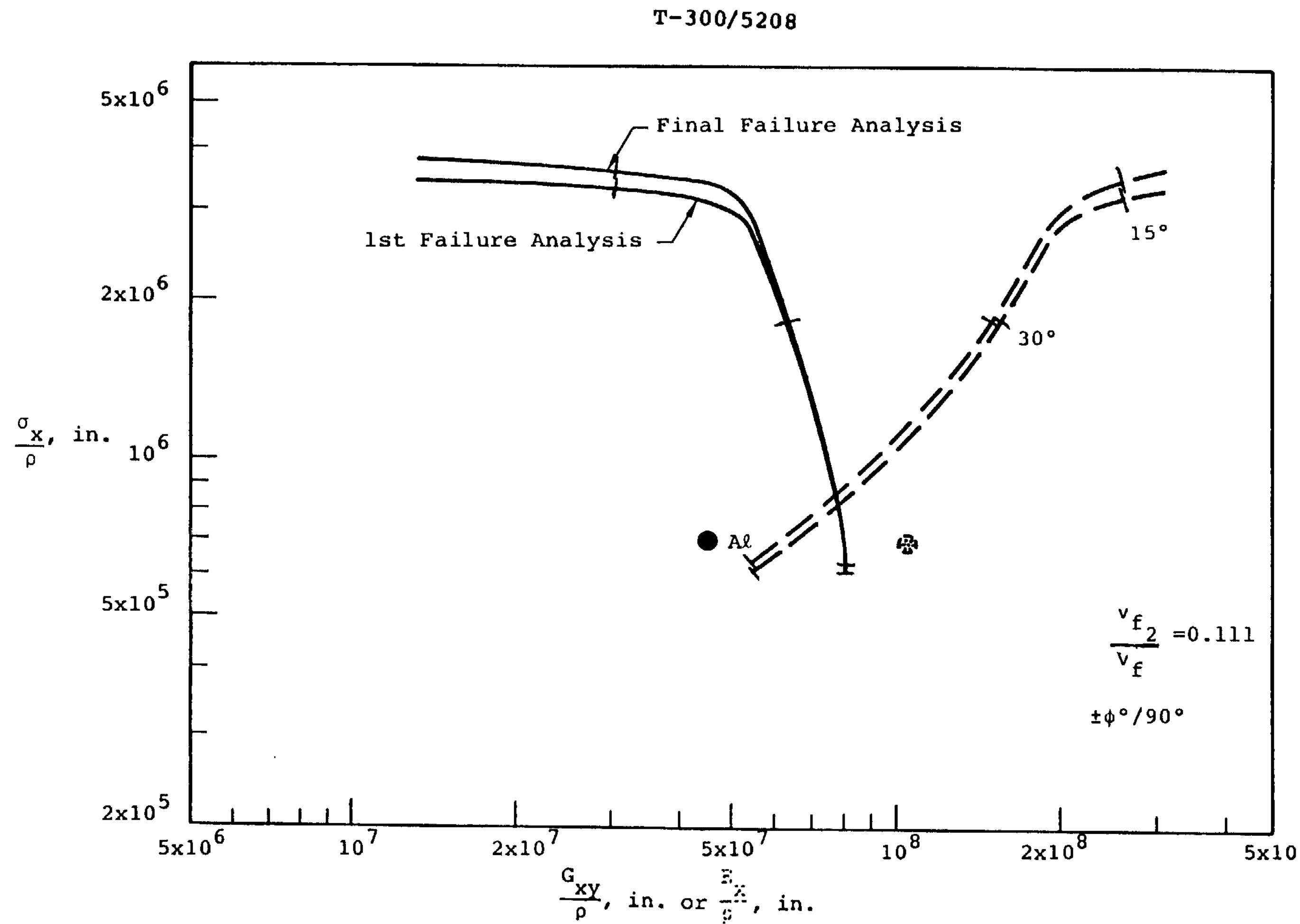

Figure 37. If Reinforcement Configurations and Properties Are Such that Premature First Failures Are Not Encountered, the Difference Between a First Failure Analysis and a Cumulative Failure Analysis is not Substantial, and, Importantly, the Configuration is Apt to Have Good Performance Characteristics, as Illustrated Here for the Well Proportioned T-300 $\pm\phi/90°$ Configuration.

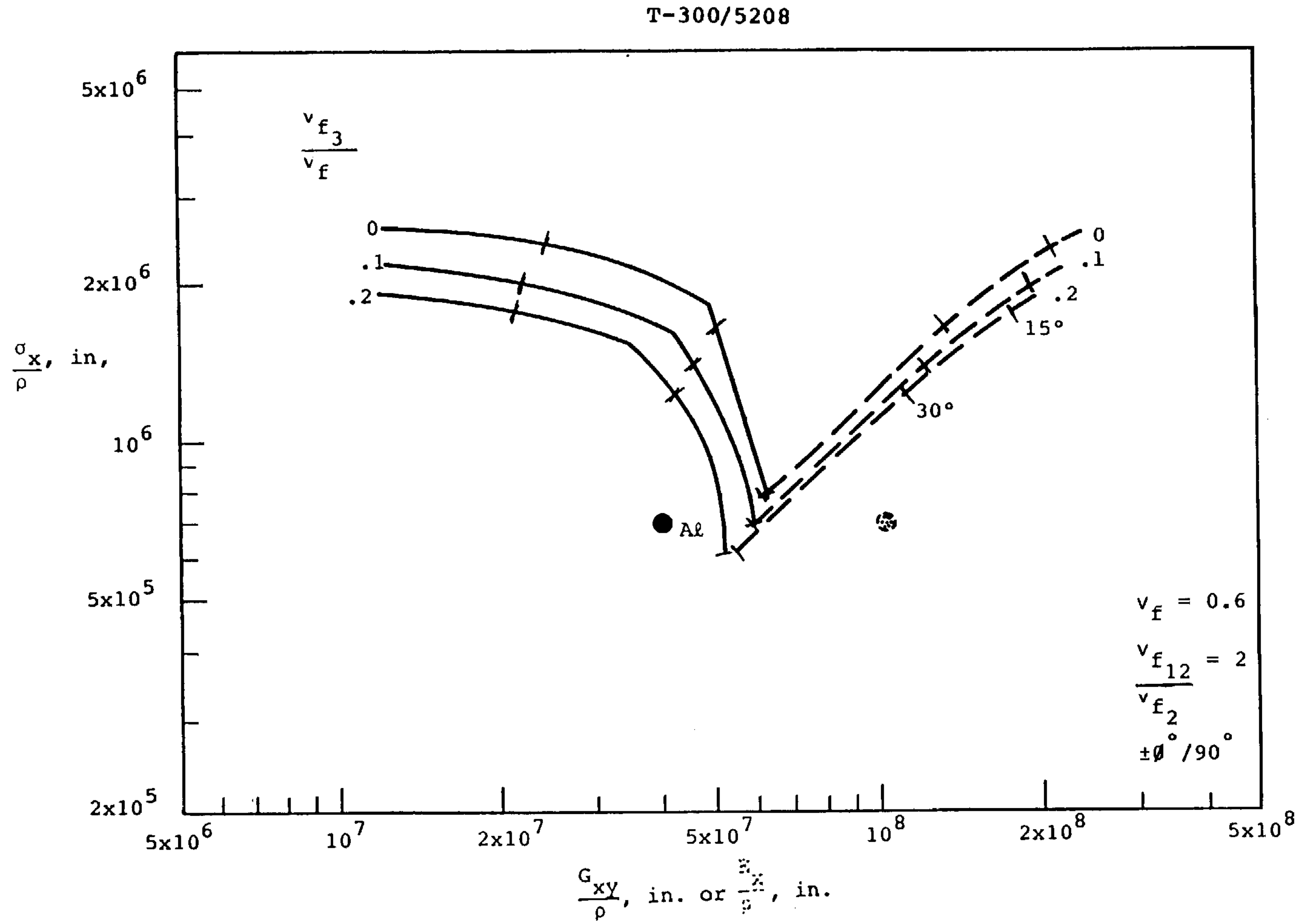

Figure 38. Evaluations of Effects of Thru the Thickness Reinforcement.-

I. Tension on a T-300/5208 $\pm\phi^\circ/90^\circ$ Configuration Having Equal In-Plane Reinforcements in All Three Directions, with Various Amounts of TTT Reinforcement. Failure modes are not affected by the addition of the TTT filaments; effects on strengths are orderly and percentagewise less than the percent TTT reinforcement.

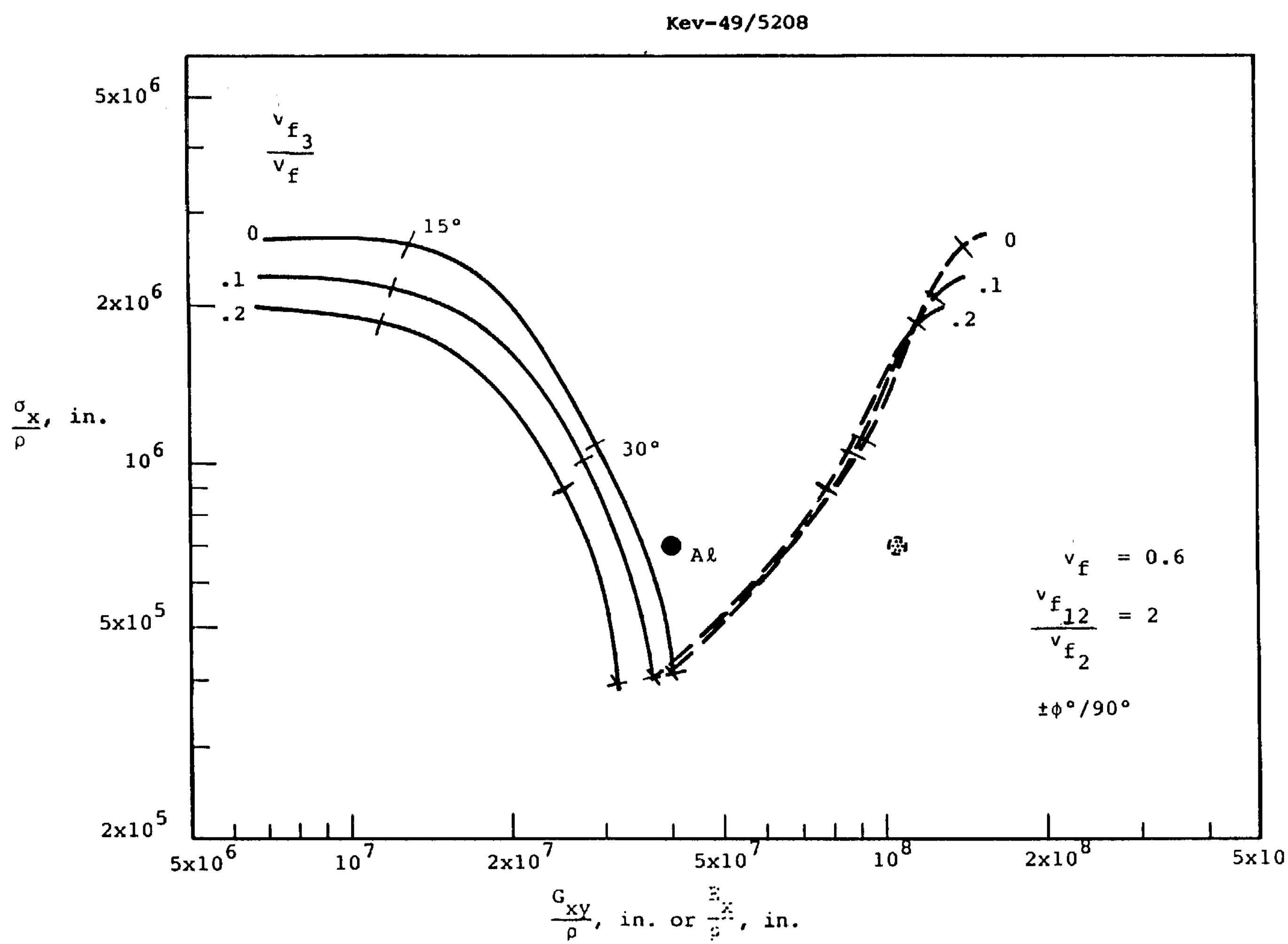

Figure 39. Evaluations of Effects of Thru the Thickness Reinforcement.-

II. Tension on a Kevlar/5208 $\pm\phi^\circ/90^\circ$ Configuration Having Equal In-Plane Reinforcements in All Three Directions, with Various Amount of TTT Reinforcement. Failure modes are not affected by the addition of the TTT filaments; effects on strengths are orderly and percentagewise less than the percent TTT reinforcement.

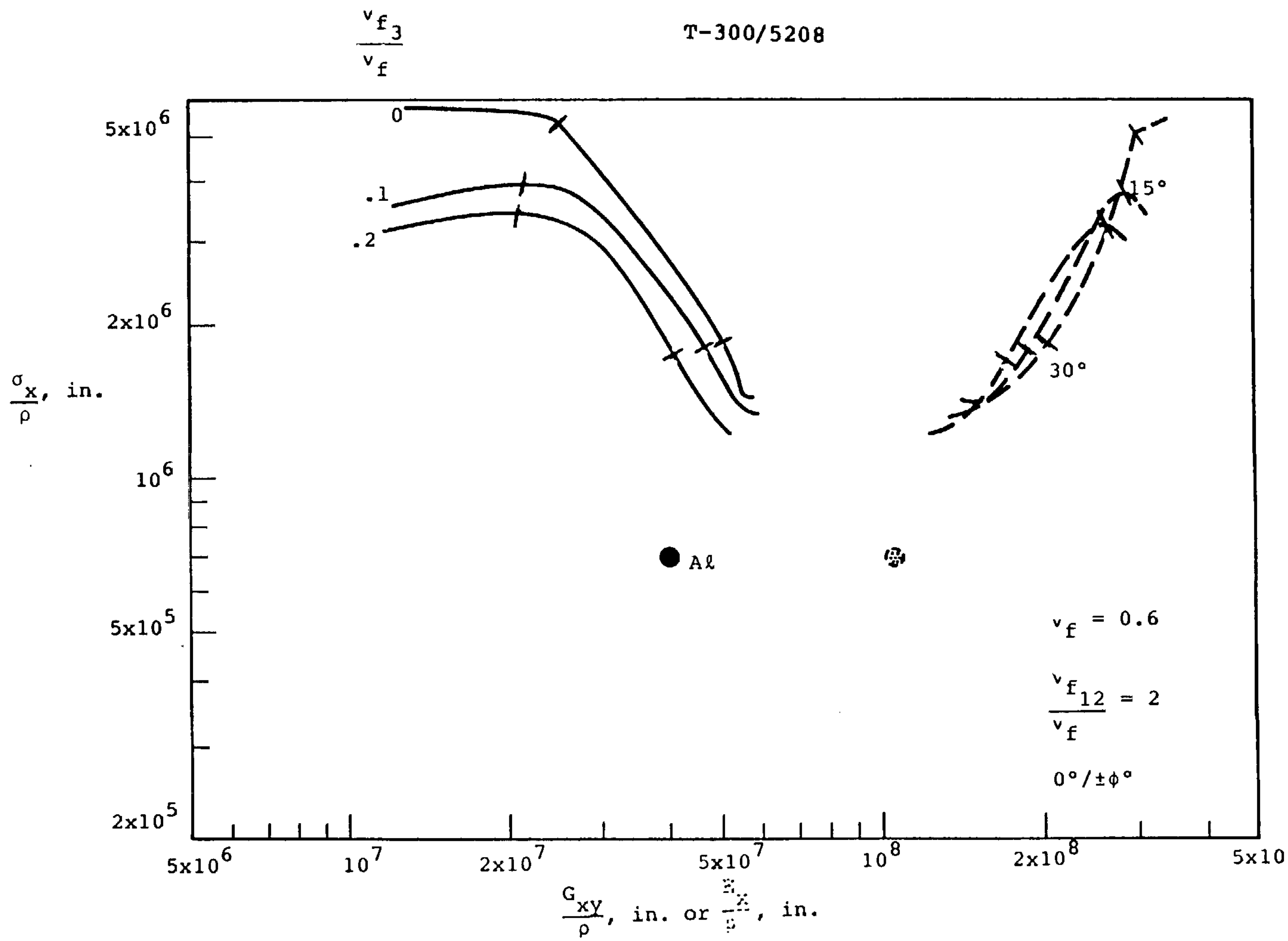

Figure 40. Evaluation of Effects of Thru the Thickness Reinforcement.-

III. Tension on a T-300 $0^\circ/\pm\phi^\circ$ configuration having equal reinforcements in all three directions, with various amounts of TTT reinforcement. Failure modes are affected by the addition of the TTT filaments; effects on strengths are most substantial for highest strength base configurations.

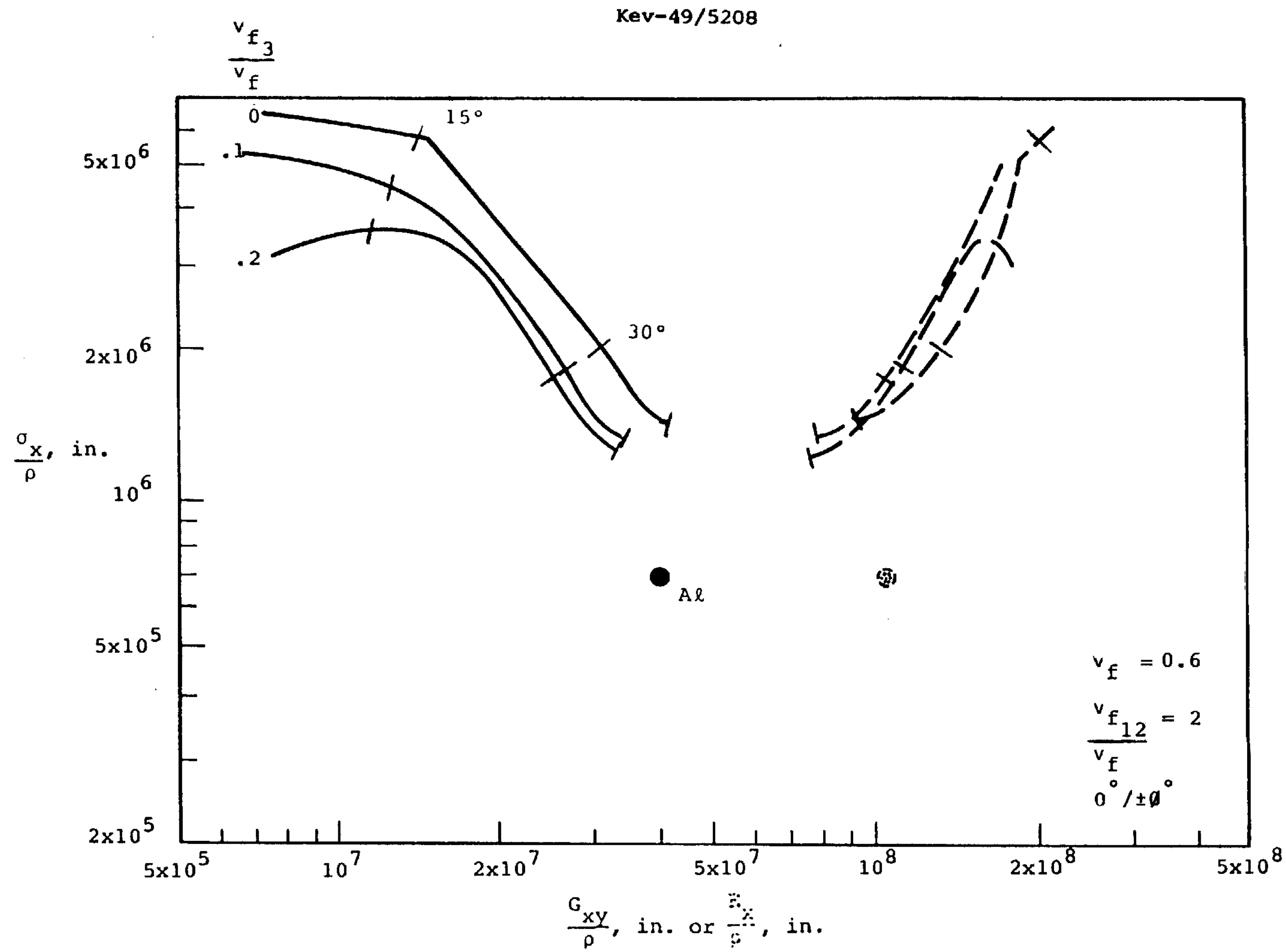

Figure 41. Evaluation of Effects of Thru the Thickness Reinforcement.-

IV. Tension on a Kevlar/5208 0°/±ϕ° configuration having equal reinforcements in all three directions, with various amounts of TTT reinforcement. Failure modes are affected by the addition of the TTT filaments; effects on strength are most substantial for highest strength base configurations at high TTT reinforcements.

ORIGINAL PAGE IS OF POOR QUALITY

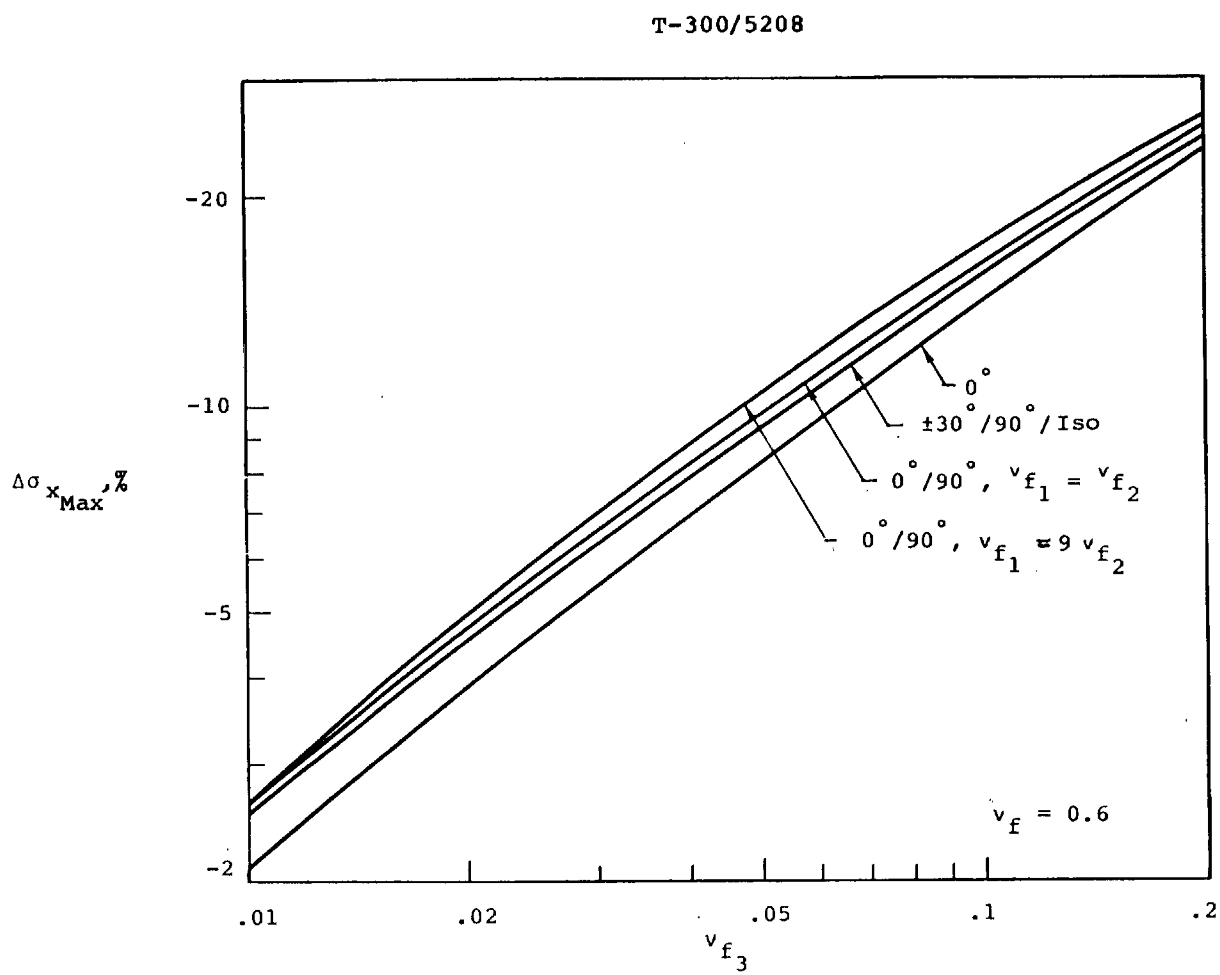

Figure 42. Summary of Effect of Thru the Thickness Reinforcement on Tensile Strengths,-Illustrated for T-300/5208 Composites Having Configurations That Have No Essential Changes in Mode of Failure with Changes in Amount of TTT Reinforcement.

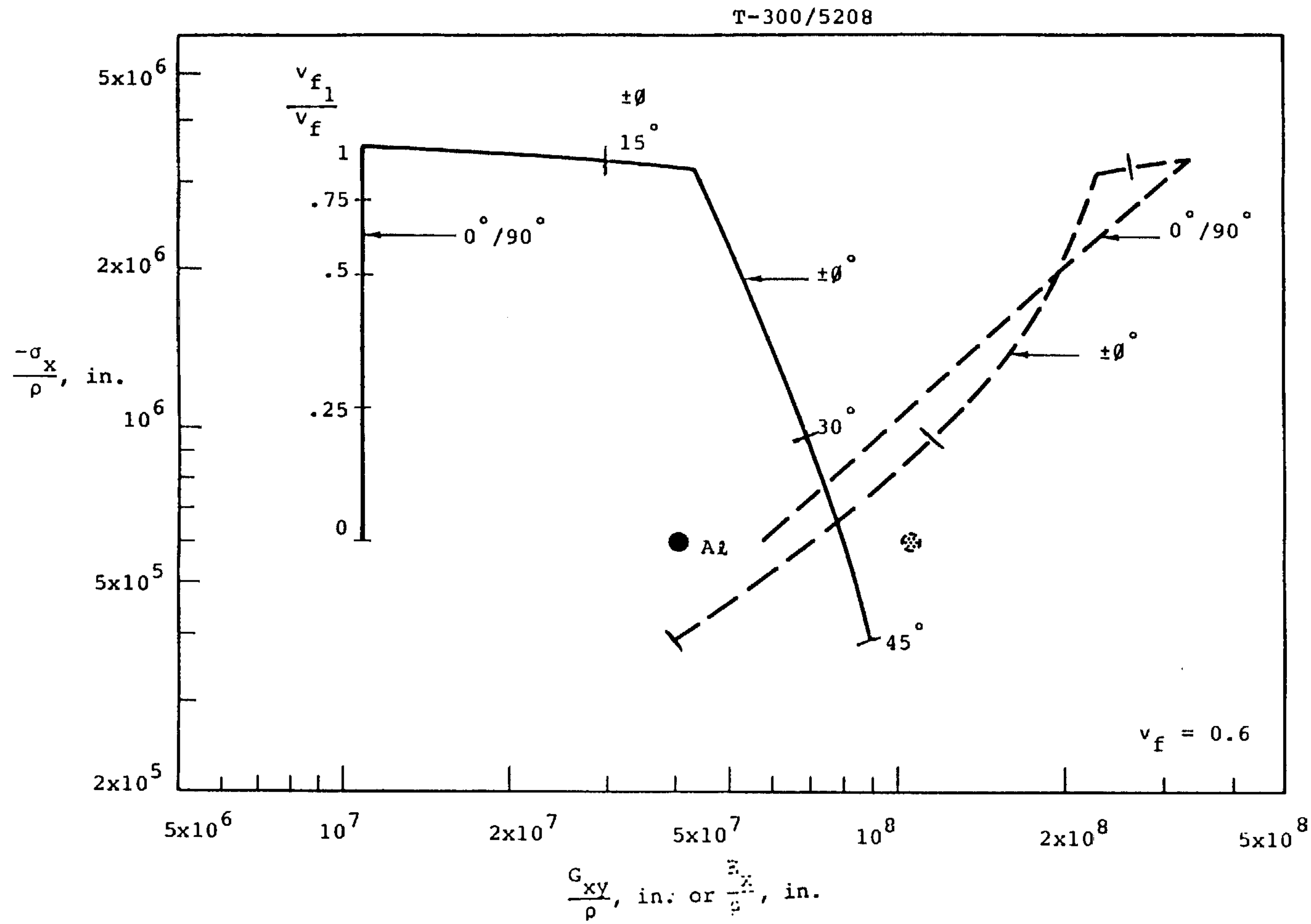

Figure 43. Evaluation of Intrinsic In-Plane Properties of Multi-Directional Reinforcements in Compression.-

I. T-300 long-float biaxial weaves and braids. The biaxial plain weave is characterized by minimal shear stiffnesses for all proportions. The braid ($\pm\phi°$ configuration) can have substantial shear stiffness combined with very high values of $\frac{-\sigma_x}{\rho}$ - over five times that of the aluminum alloy for the same shear stiffness/density ratio.

ORIGINAL PAGE IS
OF POOR QUALITY

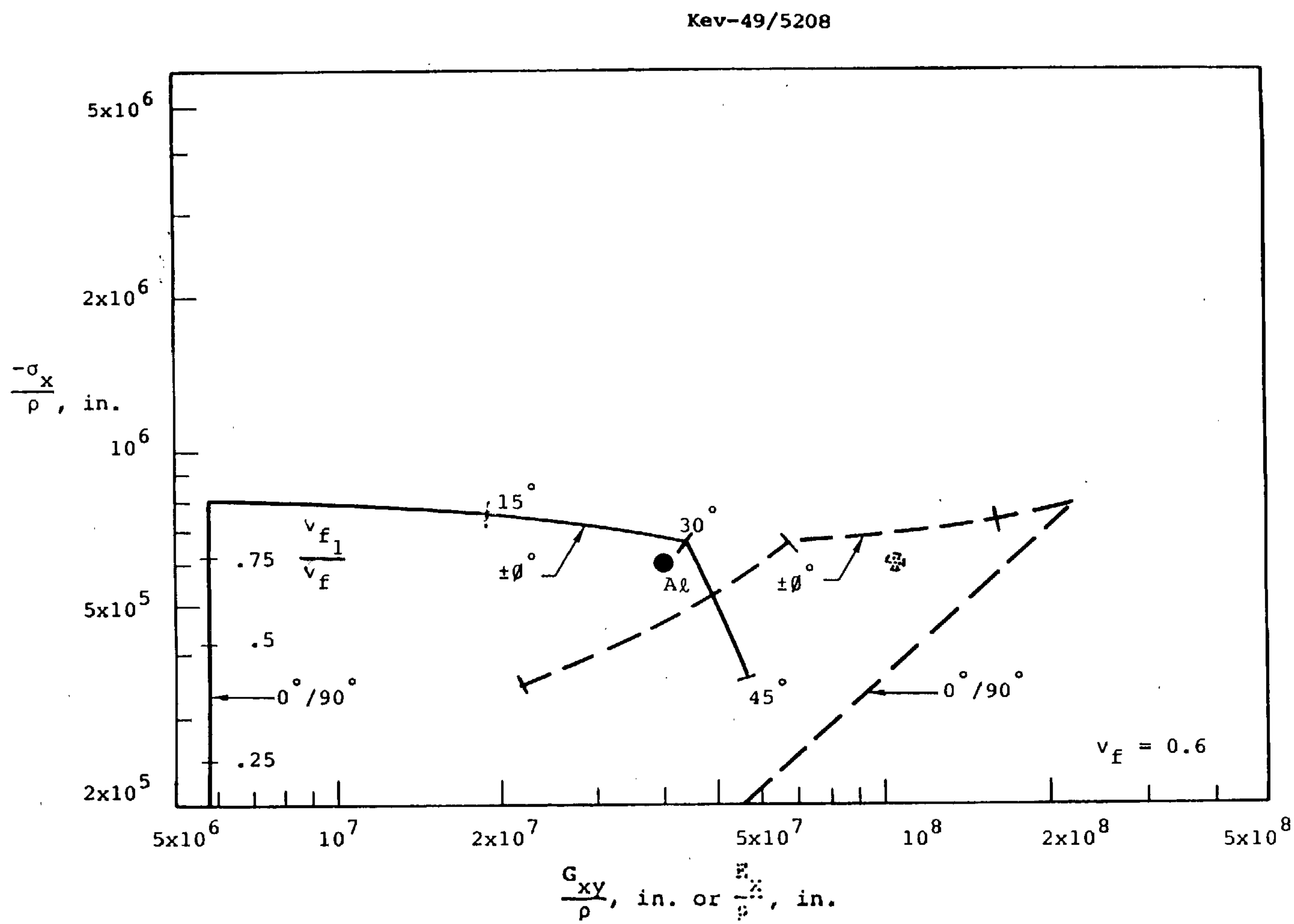

Figure 44. Evaluation of Intrinsic In-Plane Properties of Multi-Directional Reinforcements in compression.-

II. Kevlar long-float biaxial weaves and braids. The biaxial weave is characterized by minimal shear stiffnesses for all proportions; the braid by ($\pm\phi^{\circ}$ configuration) good shear stiffness combined with good values of $\frac{-\sigma_x}{\rho}$. - slightly better than that of the aluminum alloy for the same shear stiffness/density ratio.

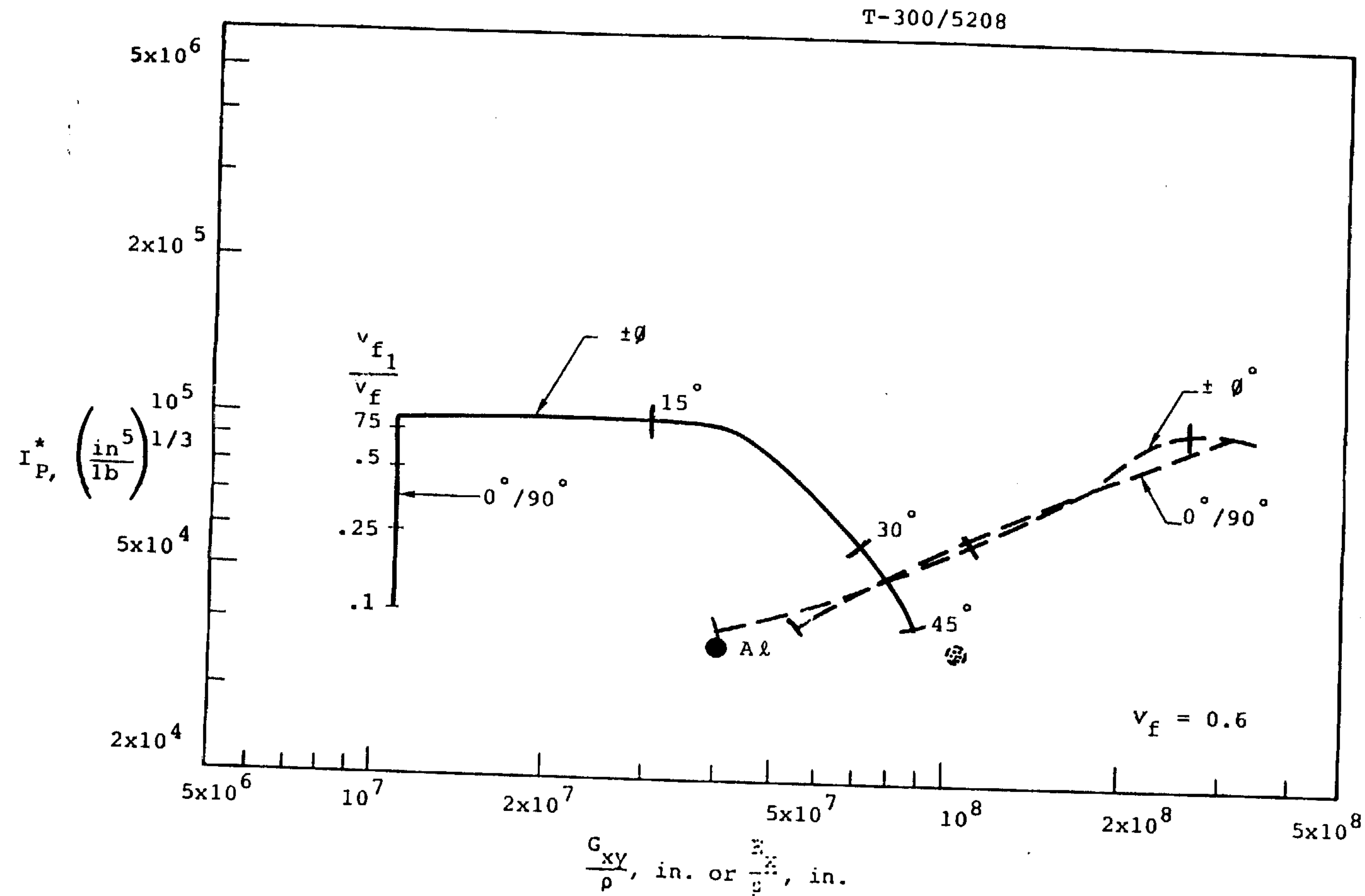

Figure 45. Evaluation of Intrinsic In-Plane Properties of Multi-Directional Reinforcements in Compression.-

III. T-300 long float biaxial weaves and braids as plate elements. For biaxial weaves, increases in the proportion of reinforcements in the 90° direction does nothing to increase the shear stiffness and decreases the value of I^*_P. For the braids, increasing the angle ϕ up to ±15° increases the shear stiffness/density ratio with no diminution of I^*_P. Resulting is a ratio of nearly three for the T-300 composite compared to the aluminum alloy at the same shear stiffness.

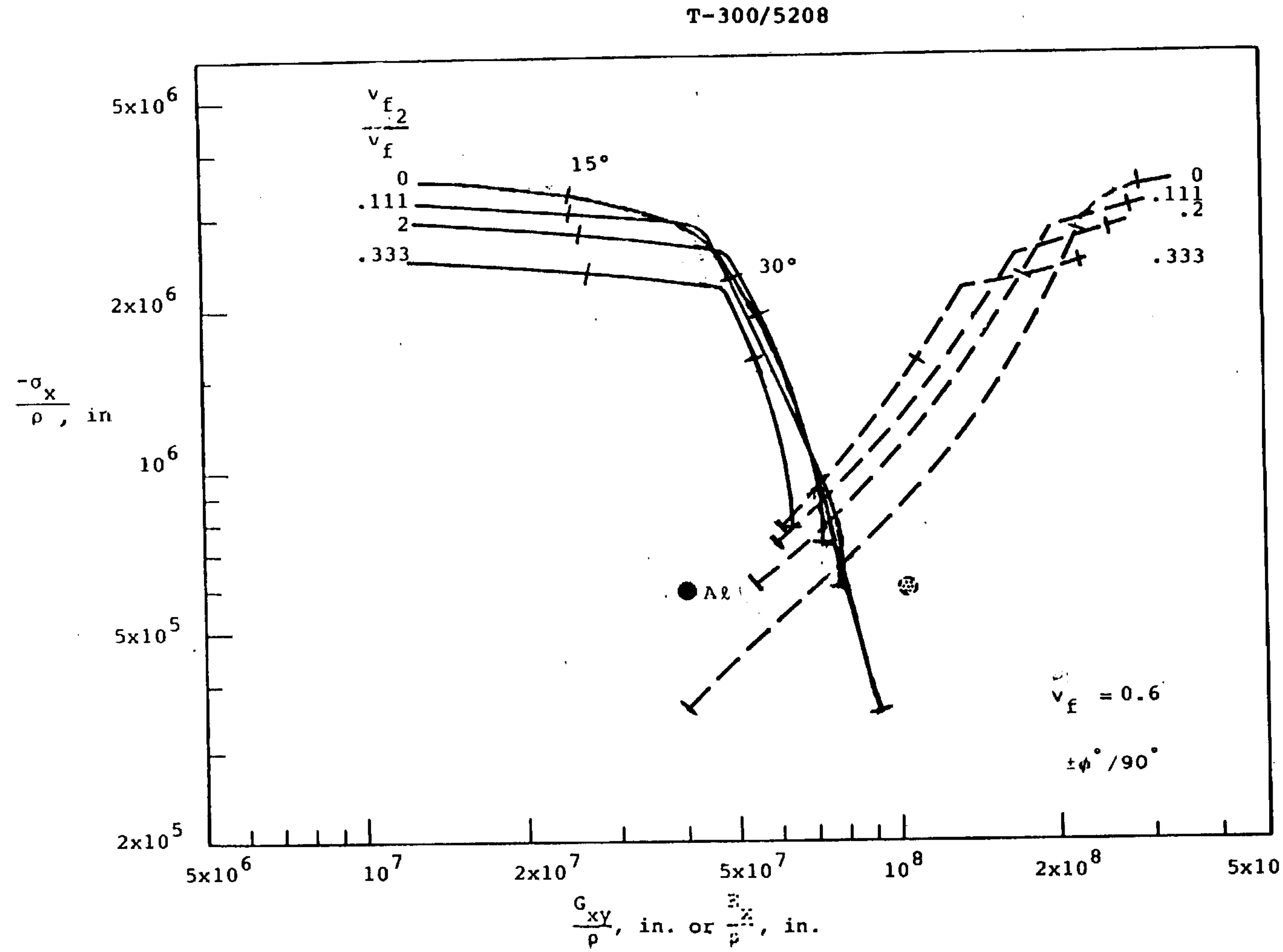

Figure 46. Evaluation of Intrinsic In-Plane Properties of Multi-Directional Reinforcements in Compression.-

IV. T-300 $\pm\phi°/90°$ configuration. Addition of 90° reinforcement to the $\pm\phi°$ configuration in small amounts decreases the values of $\frac{\sigma_x}{\rho}$ achieved and increases the shear stiffness/density ratios. Larger additions decrease both the tensile and shear properties. Fractions of 10% to 20% of the total reinforcement volume fraction appear to maximize the combined properties.

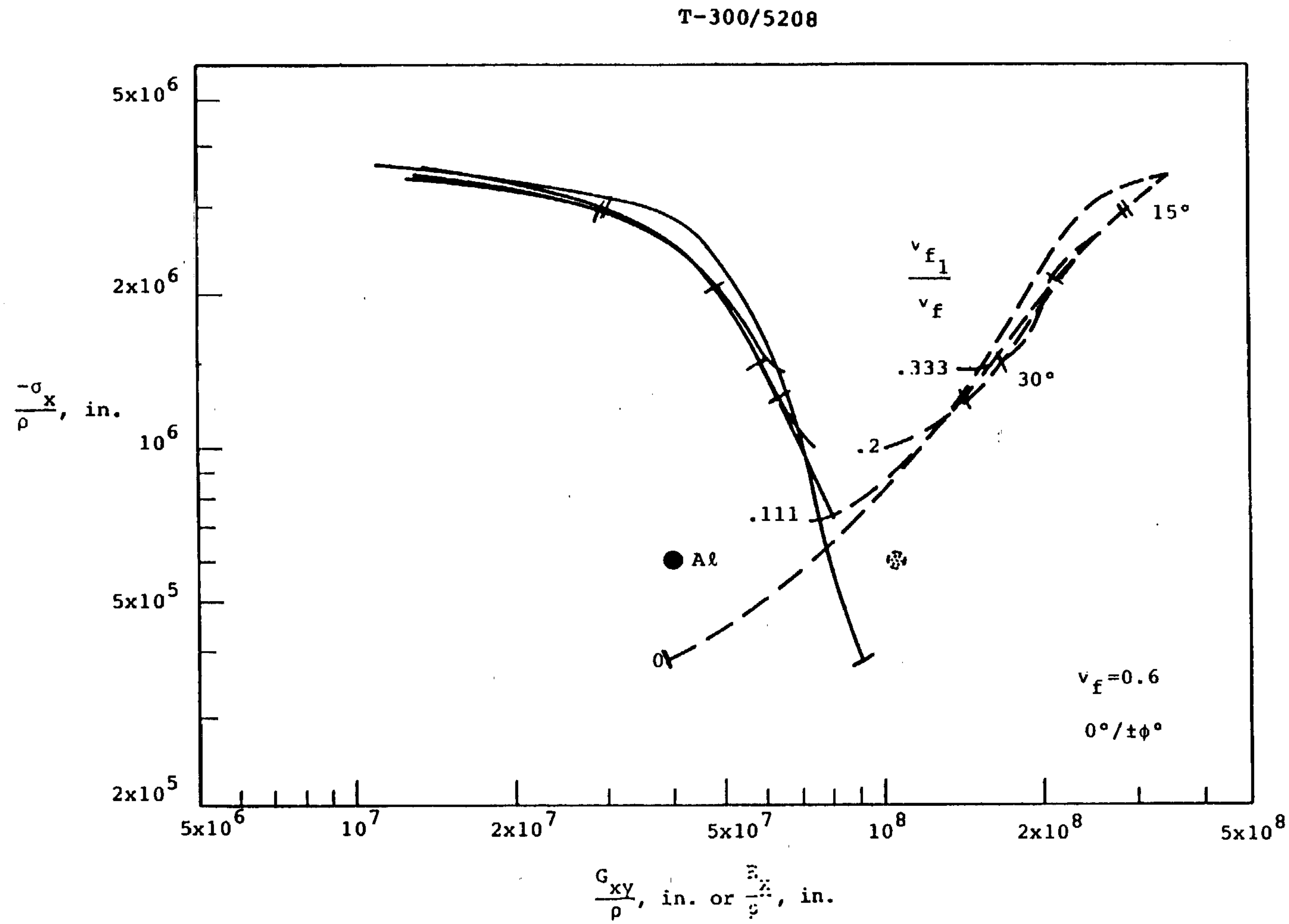

Figure 47. Evaluation of Intrinsic In-Plane Properties of Multi-Directional Reinforcements in Compression.-

V. T-300 $0^\circ/\pm\phi^\circ$ configurations are relatively insensitive to changes in proportions of filaments in the various directions. Optimal proportions provide slightly lower combined tension-shear stiffness/density ratios than $\pm\phi^\circ/90^\circ$ configurations but still yield values of $\frac{-\sigma_x}{\rho}$ four times that of the aluminum alloy at the same shear stiffness/density ratio.

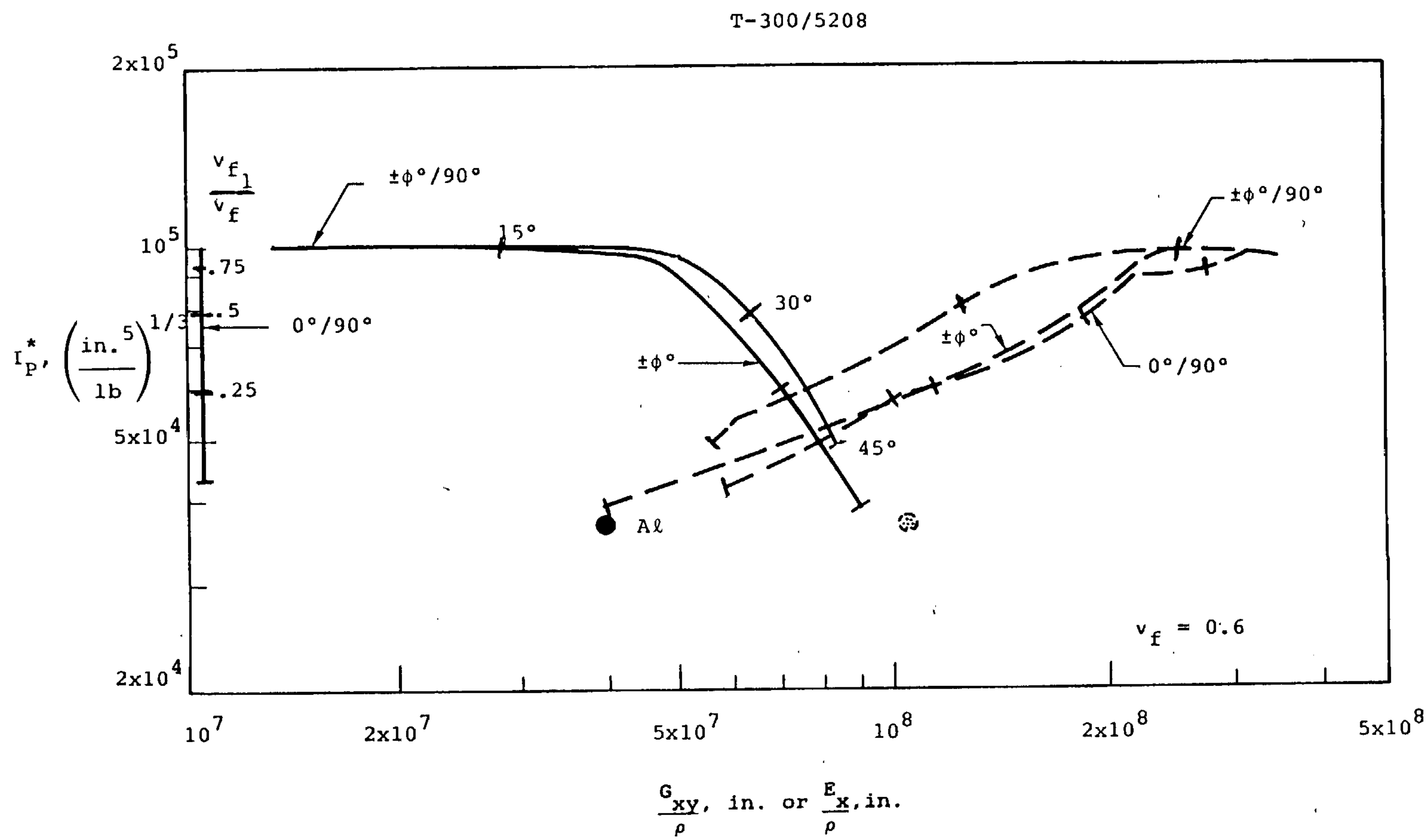

Figure 48. Evaluation of Intrinsic In-Plane Properties of Multi-Directional Reinforcements in Compression.-

VI. Overall comparisons of configurations. If shear stiffness requirement are non-existent or very low the simple-to-weave 0°/90° weave (or for that matter unidirectional tape) can yield as high values of I_p^* as the other configurations. The triaxial ±φ°/90° weave yields generally the highest combinations of I_p^* and $\frac{G_{xy}}{\rho}$.

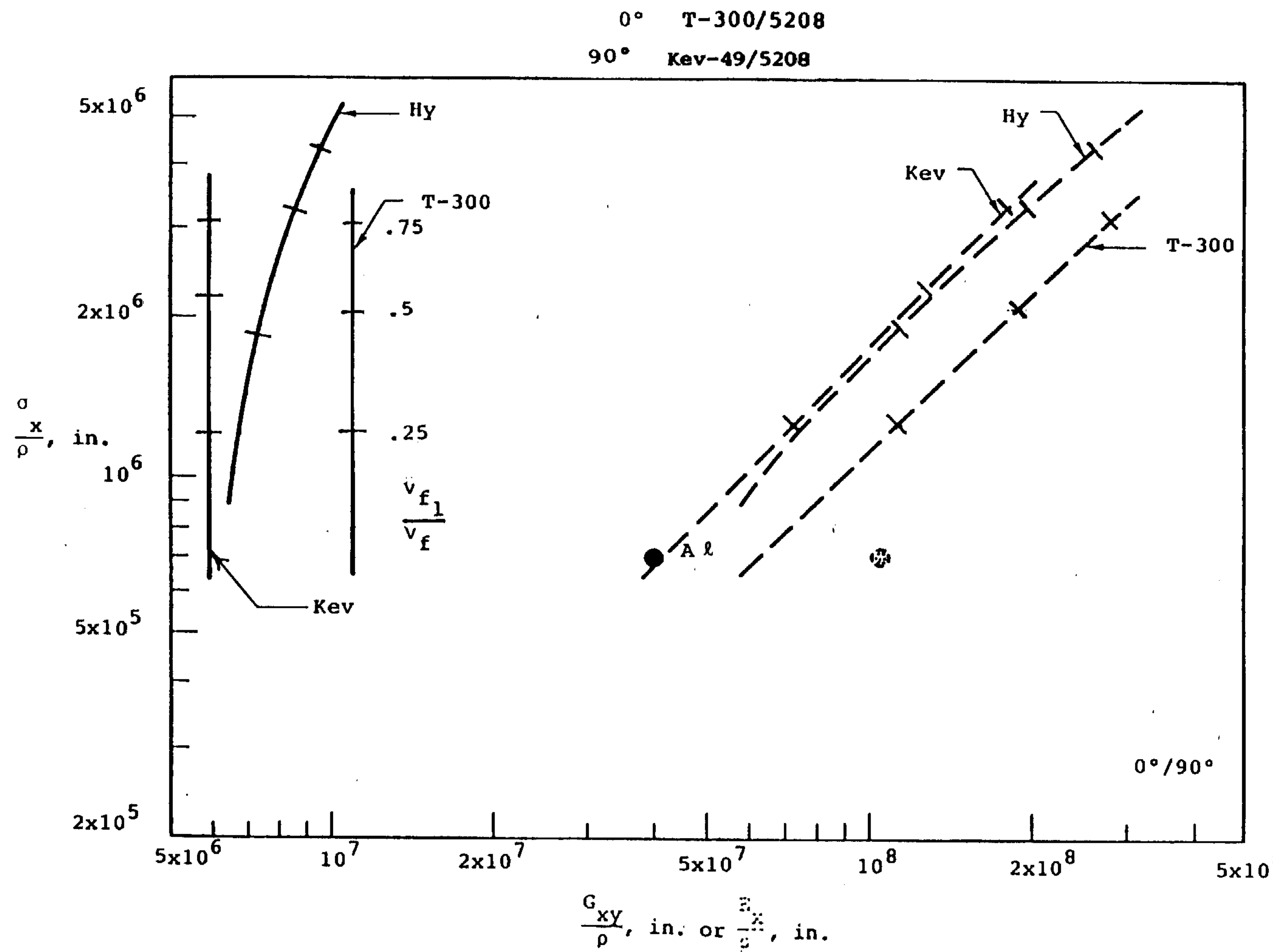

Figure 49. Evaluations of Hybrids.-

I. 0°/90° Weaves, T-300 in the warp (0°) direction, Kevlar in the fill, in tension. Both the all T-300 and the all Kevlar 0°/90° weaves are represented as weaves, not approaching unidirectional tapes, as $V_{f_1} \to 0$ or $V_{f_2} \to 0$. Thus the hybrid with Kevlar in the fill exceeds the all T-300 with an infinitesimal V_{f_2}, because of the greater transverse compliance of Kevlar. Apart from this rather hypothetical region no merit for the hybrid is apparent.

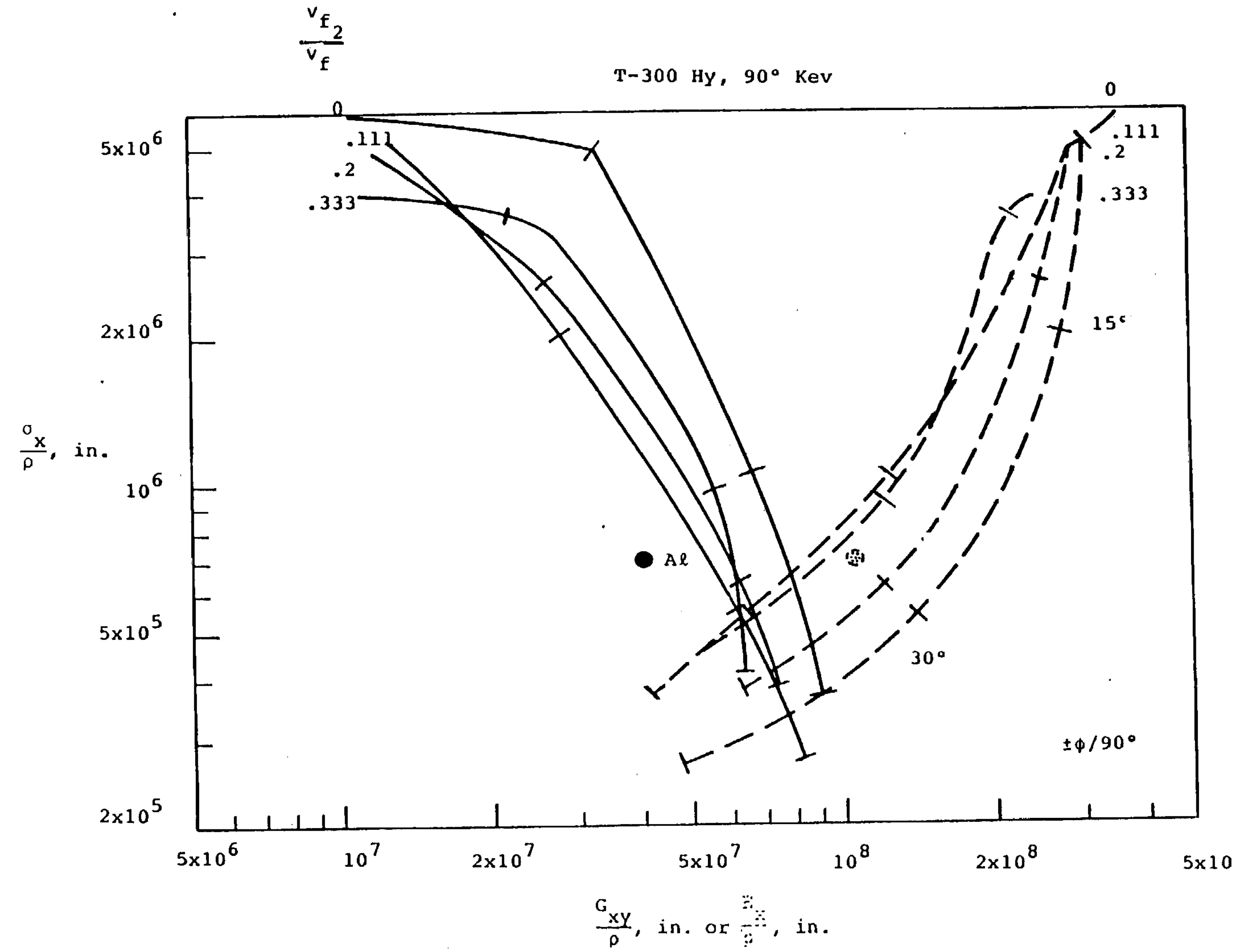

Figure 50. Evaluations of Hybrids.-

II. Triaxial Weave $\pm\phi^\circ/90^\circ$, Kevlar in the 90° direction, in tension. As in the all Kevlar $\pm\phi^\circ/90^\circ$ configurations (fig. 33) premature compressive failures are encountered in the 90° filaments with resulting poor values of $\frac{\sigma_x}{\rho}$.

ORIGINAL PAGE IS
OF POOR QUALITY

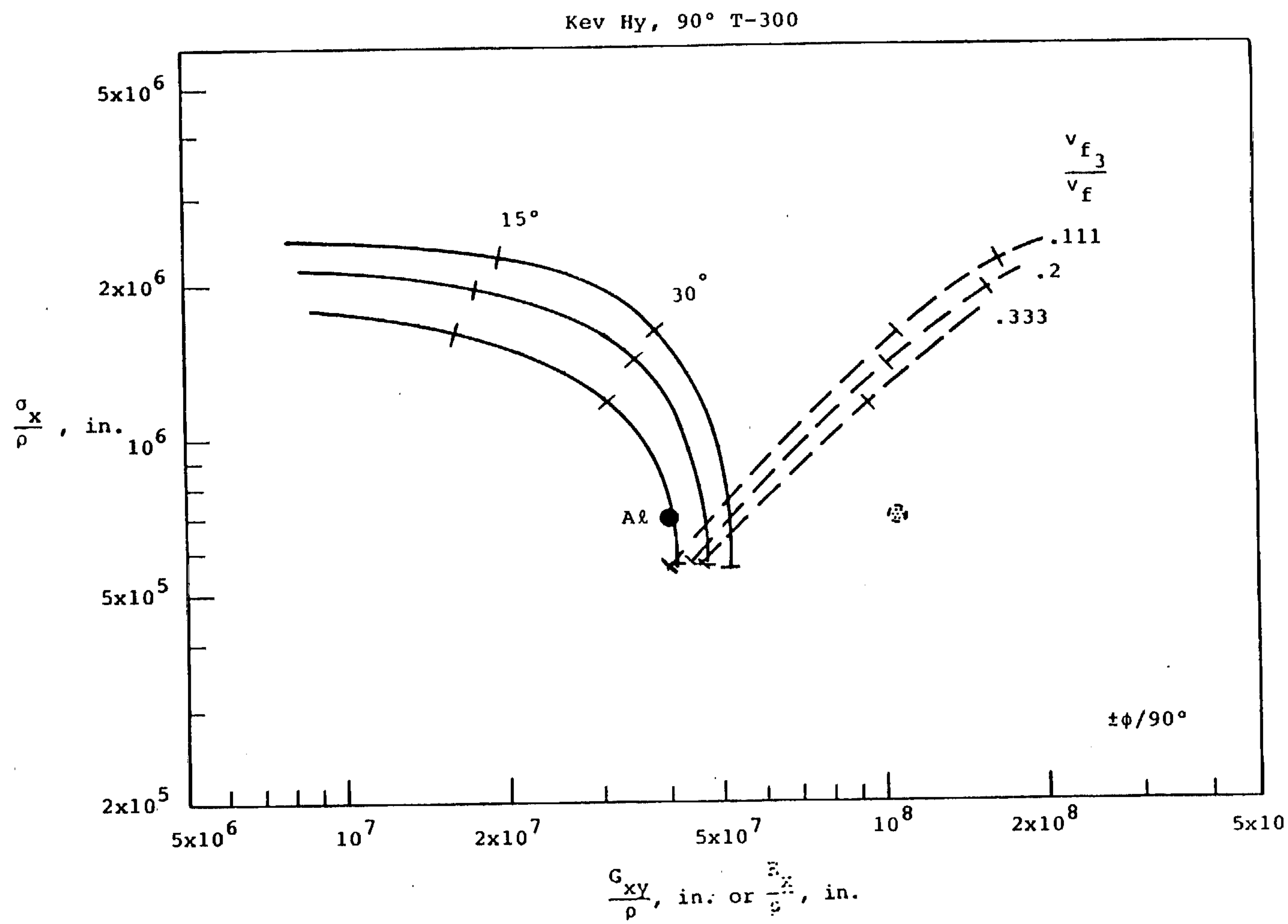

Figure 51. Evaluations of Hybrids.-

III. Triaxial Weave $\pm\phi^\circ/90^\circ$, T-300 in the 90° direction, in tension. Here premature failures transverse to the 90° fibers reduce the values of $\frac{\sigma_x}{\rho}$ compared to those for all Kevlar (Fig.33) at low values of $\frac{G_{xy}}{\rho}$ but avoid the even more deleterious effects of compression failure there shown for higher values of $\frac{G_{xy}}{\rho}$.

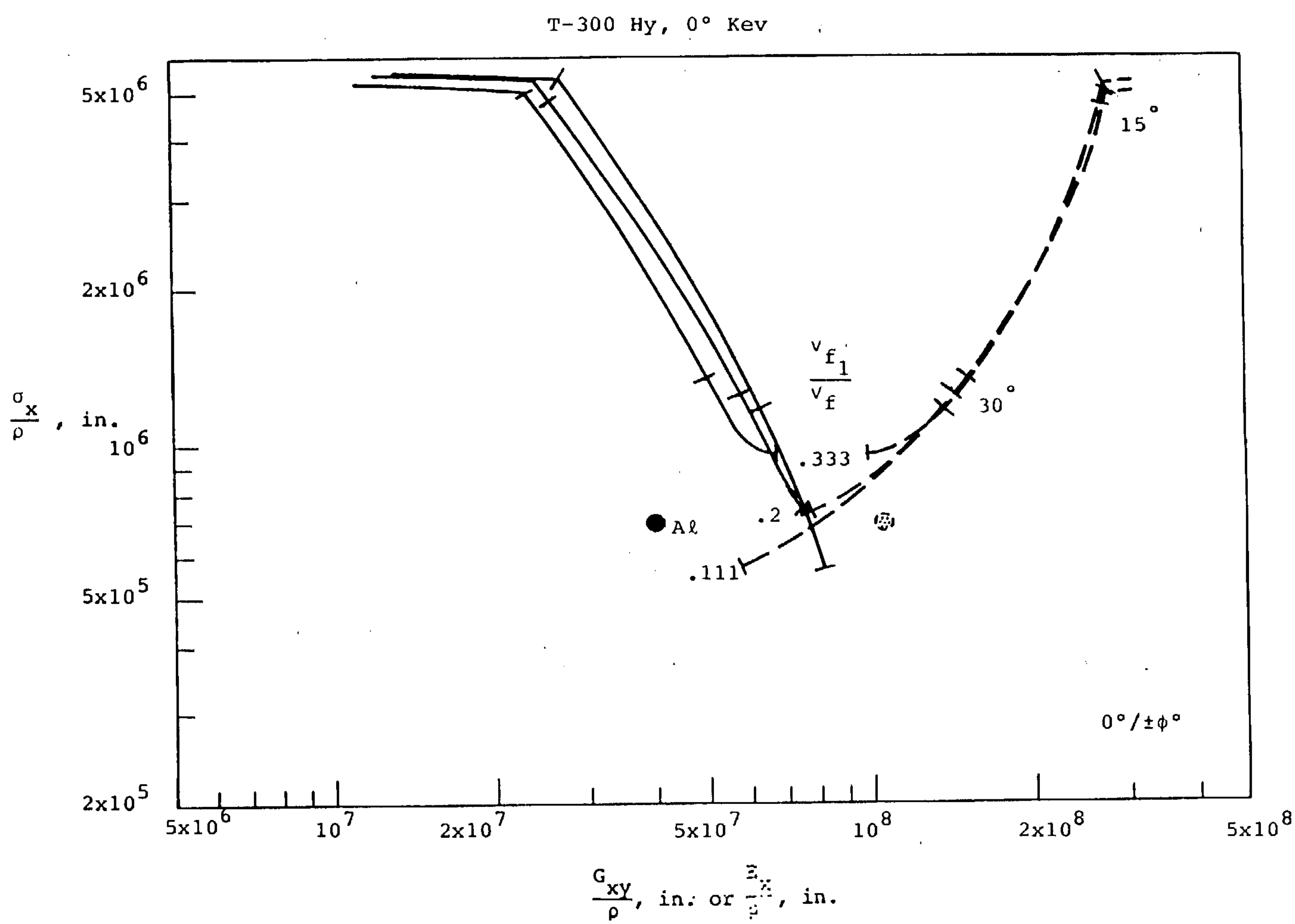

Figure 52. Evaluations of Hybrids.-

IV. Triaxial weave $0^\circ/\pm\phi^\circ$, Kevlar in the 0° direction, in tension. A generally effective configuration with no premature failure modes. Potential gains by a factor four compared to the aluminum alloy are evident.

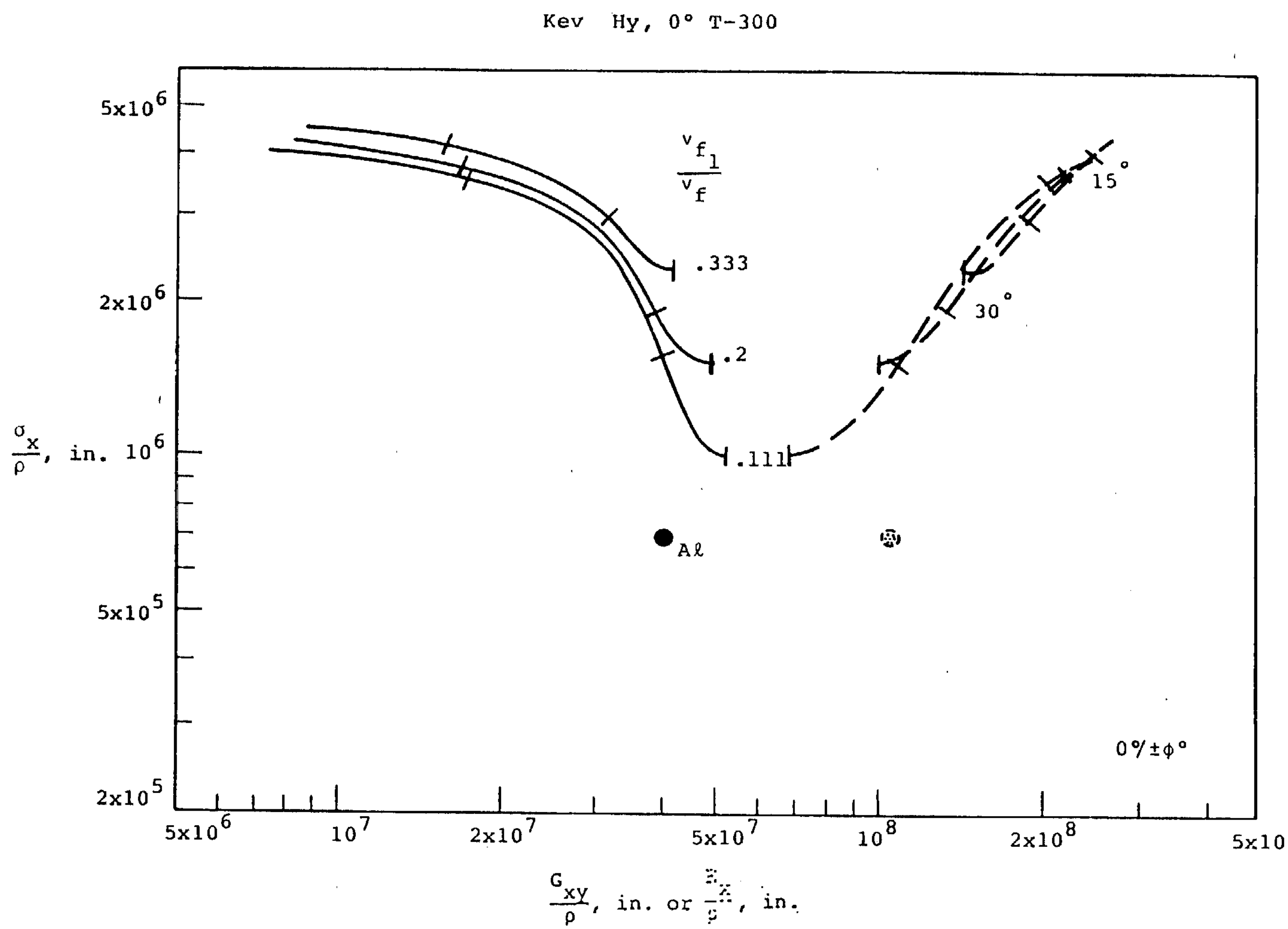

Figure 53. Evaluations of Hybrids.-

V. Triaxial Weave $0^\circ/\pm\phi^\circ$, T-300 in the 0° direction, in tension. A generally effective configuration with no premature failure modes. Potential gains by a factor greater than three are indicated.

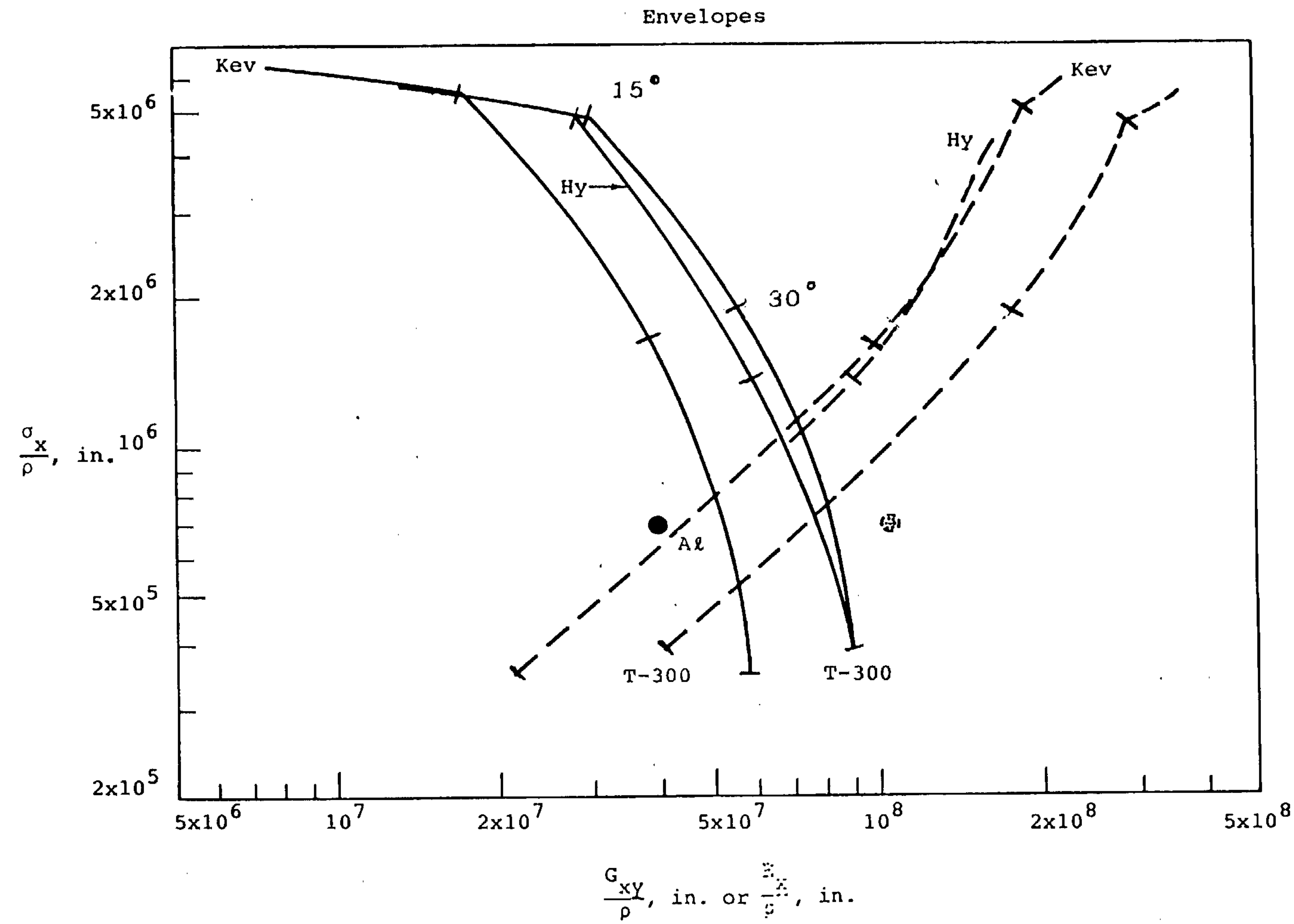

Figure 54. Evaluations of Hybrids.-

VI. Overall evaluations of $0°/\pm\phi°$ triaxial weaves in tension. Envelope curves drawn to the individual $0°/\pm\phi°$ curves of figures 34, 35, and 53 show that the hybrids fall between the all Kevlar and all T-300 constructions. The all T-300 has the highest values of $\frac{\sigma_x}{\rho}$ for high values of $\frac{G_{xy}}{\rho}$.

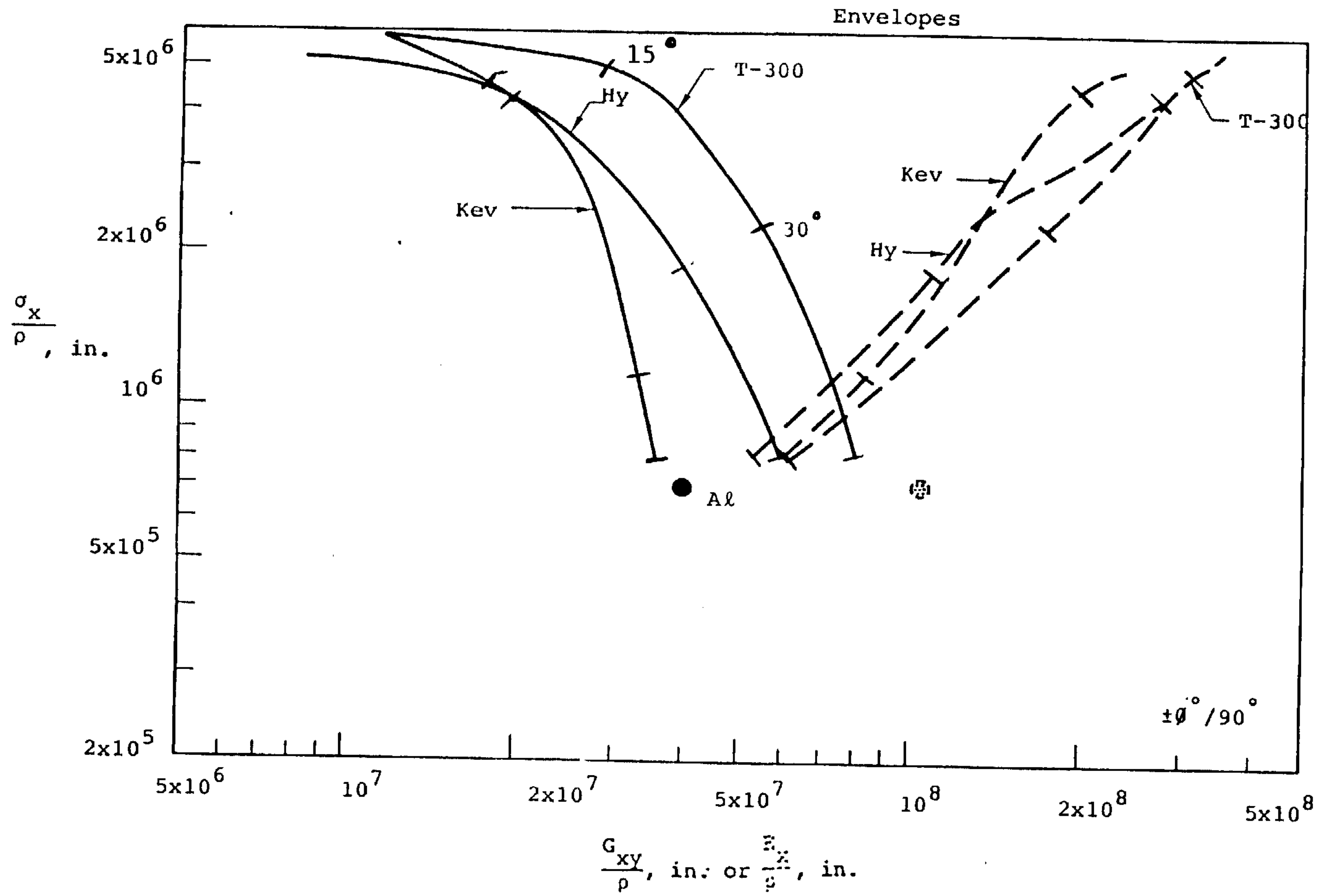

Figure 55. Evaluations of Hybrids.-

VII. Overall evaluations of $\pm\phi^\circ/90^\circ$ configurations, in tension.

Envelope curves drawn to the individual $\pm\phi^\circ/90^\circ$ curves of figure 32, 33 and 50 show that the hybrids fall between the all Kevlar and all T-300 constructions. The all T-300 has the highest values of $\frac{\sigma_x}{\rho}$ for all values of $\frac{G_{xy}}{\rho}$.

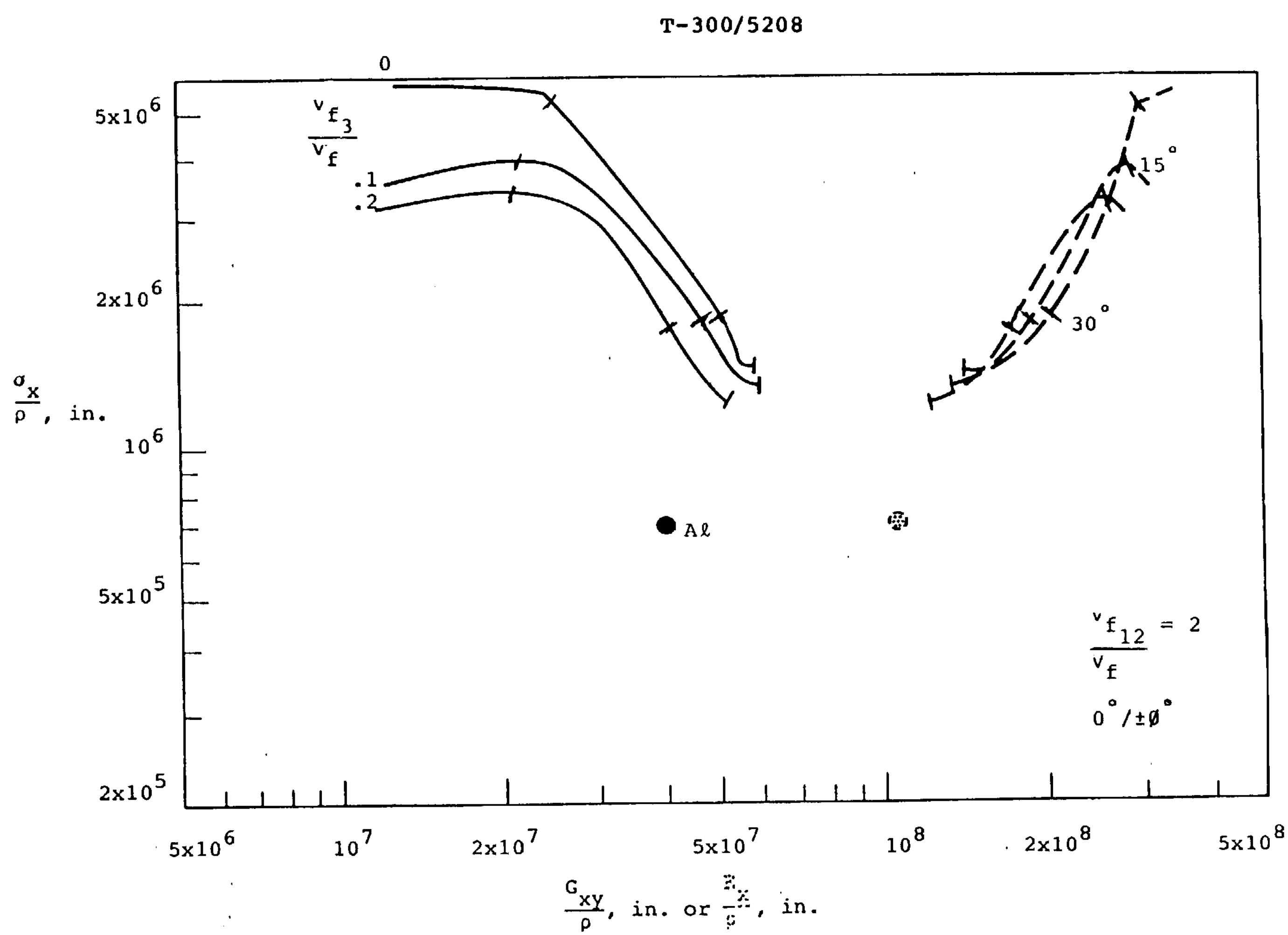

ORIGINAL PAGE IS OF POOR QUALITY

Figure 56. Evaluations of Hybrids.-

VIII. Effects of thru the thickness reinforcement in $0°/\pm\phi°$, in tension. The use of Kevlar TTT eliminates the premature failures induced by T-300 TTT(Fig.56) resulting in regions of improved performance.

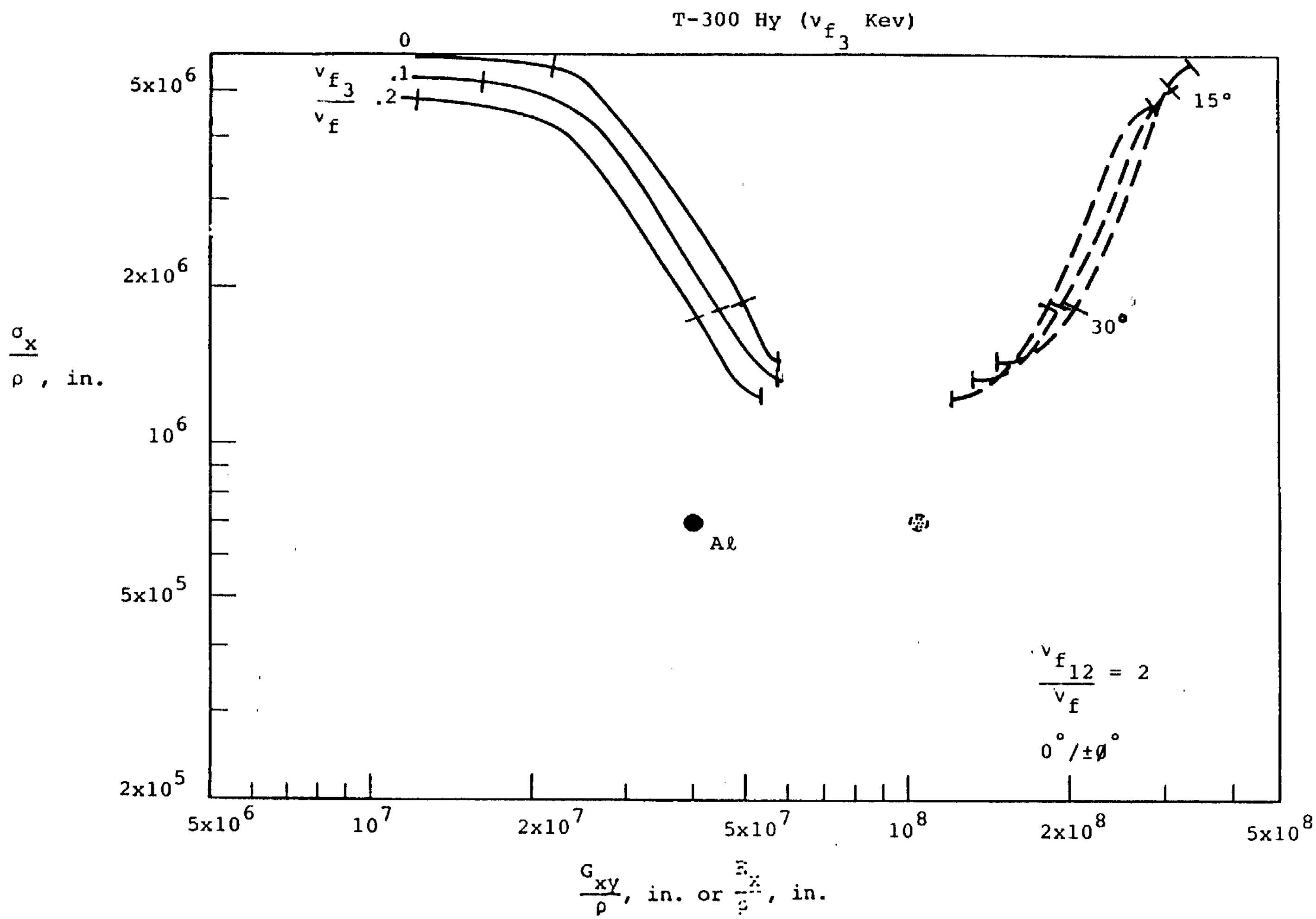

Figure 57. Evaluations of Hybrids.-

IX. Effects of thru the thickness reinforcement in 0°/±φ°, v_{f_3} Kevlar, in tension. The use of Kevlar TTT eliminates the premature failures induced by T-300 TTT (Fig.56) resulting in regions of improved performance.

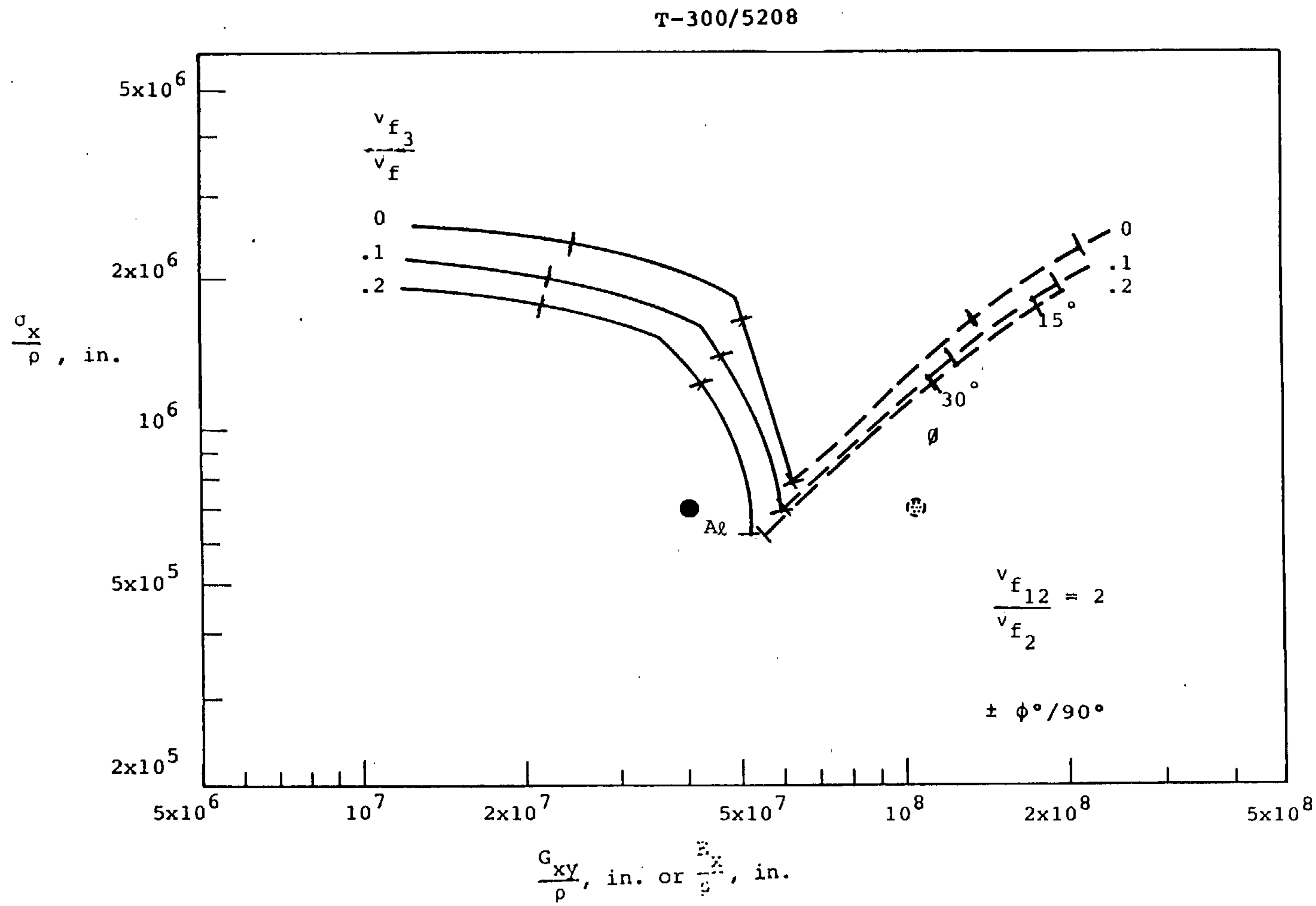

Figure 58. Evaluations of Hybrids.-

X. Effect of thru the thickness reinforcement, in $\pm\phi^\circ/90^\circ$ in tension. Baseline curves for all T-300 are reproduced (from Fig.38) here for convenience.

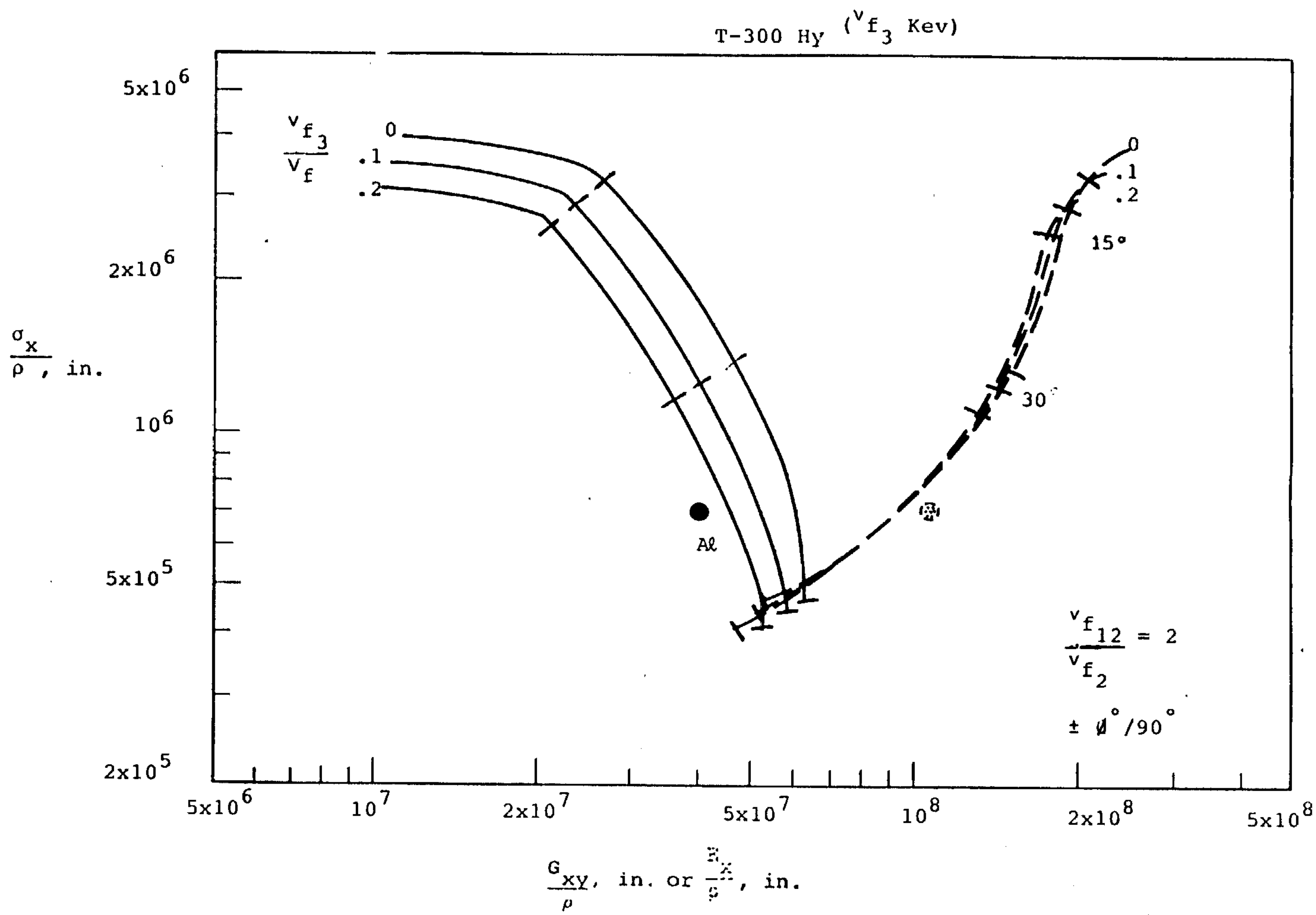

Figure 59. Evaluations of Hybrids.-

XI. Effects of thru the thickness reinforcement in $\pm\phi°/90°$, v_{f_3} Kevlar, in tension. The use of Kevlar is substantially less damaging to the performance of the reinforcement than T-300 TTT (see Fig. 58).

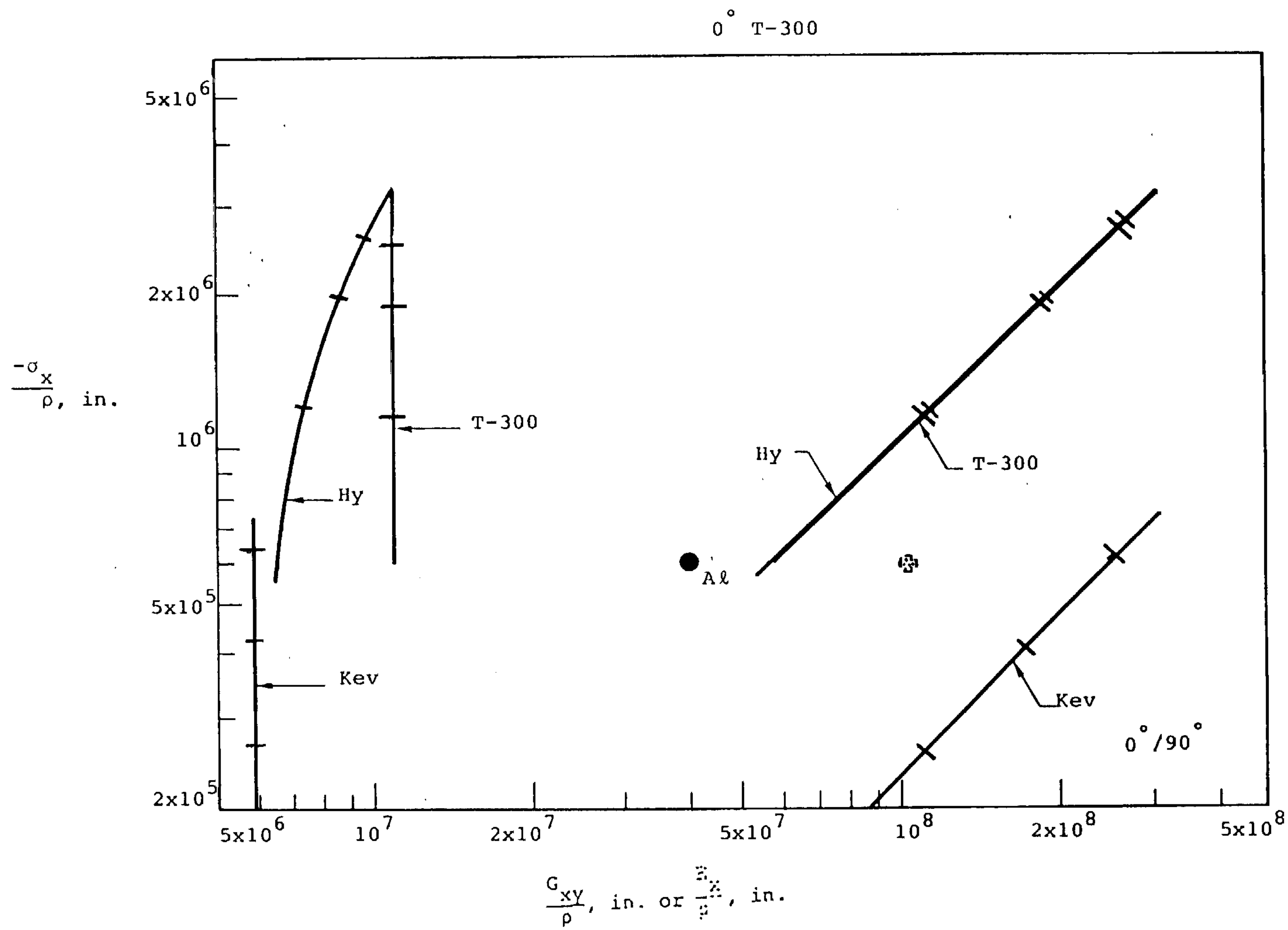

Figure 60. Evaluations of Hybrids.-

XII. 0°/90° weave, T-300 in the warp (0°) direction, Kevlar in the fill, in compression. No merit for the hybrid is evident.

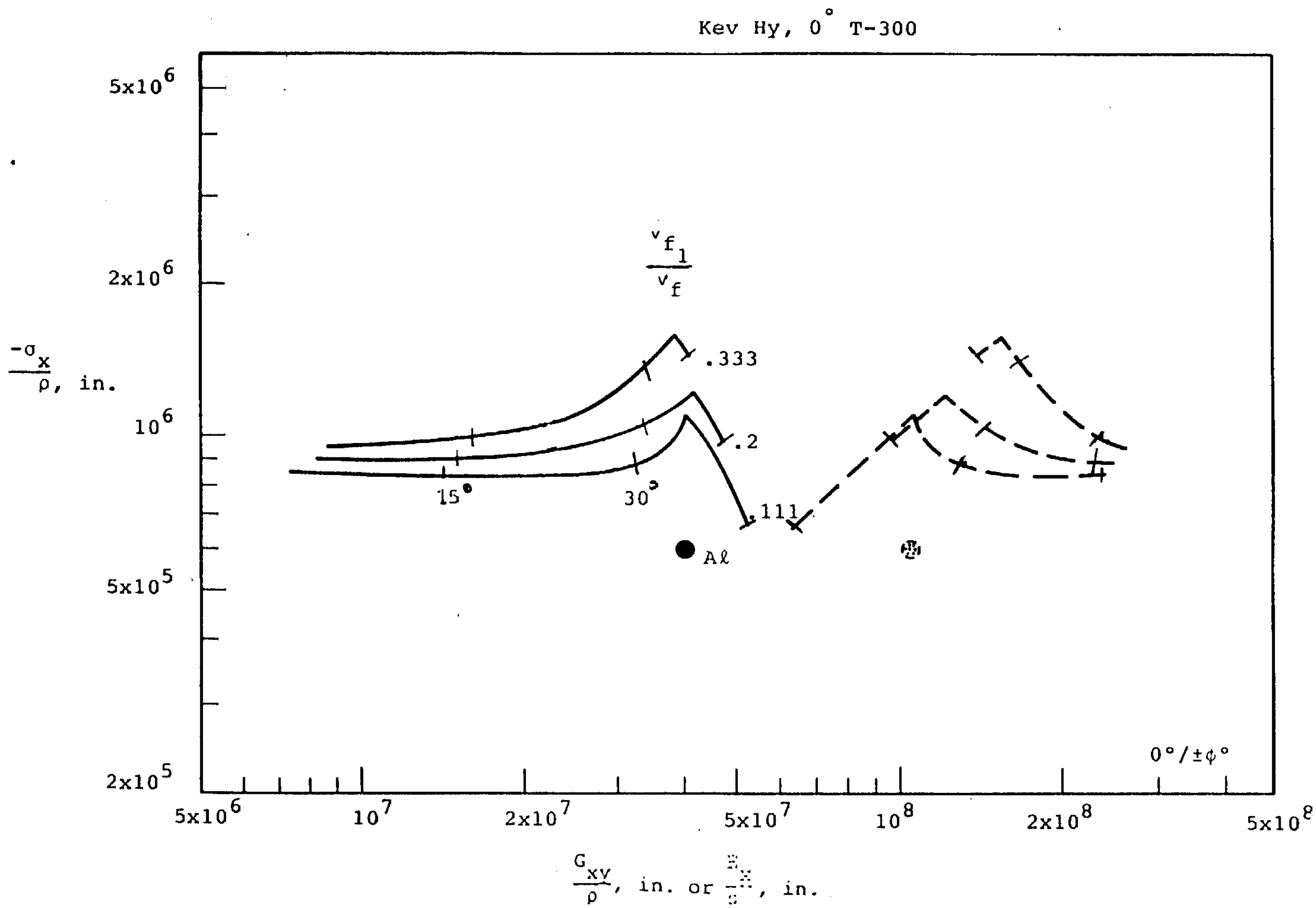

Figure 61. Evaluations of Hybrids.-

XIII. Triaxial weaves $0°/\pm\phi°$, T-300 in the 0° direction, in compression. Premature compressive failure in the $\pm\phi°$ Kevlar fibers make the performance undistinguished, though superior to the aluminum alloy because of the effectiveness of the 0° T-300 fibers.

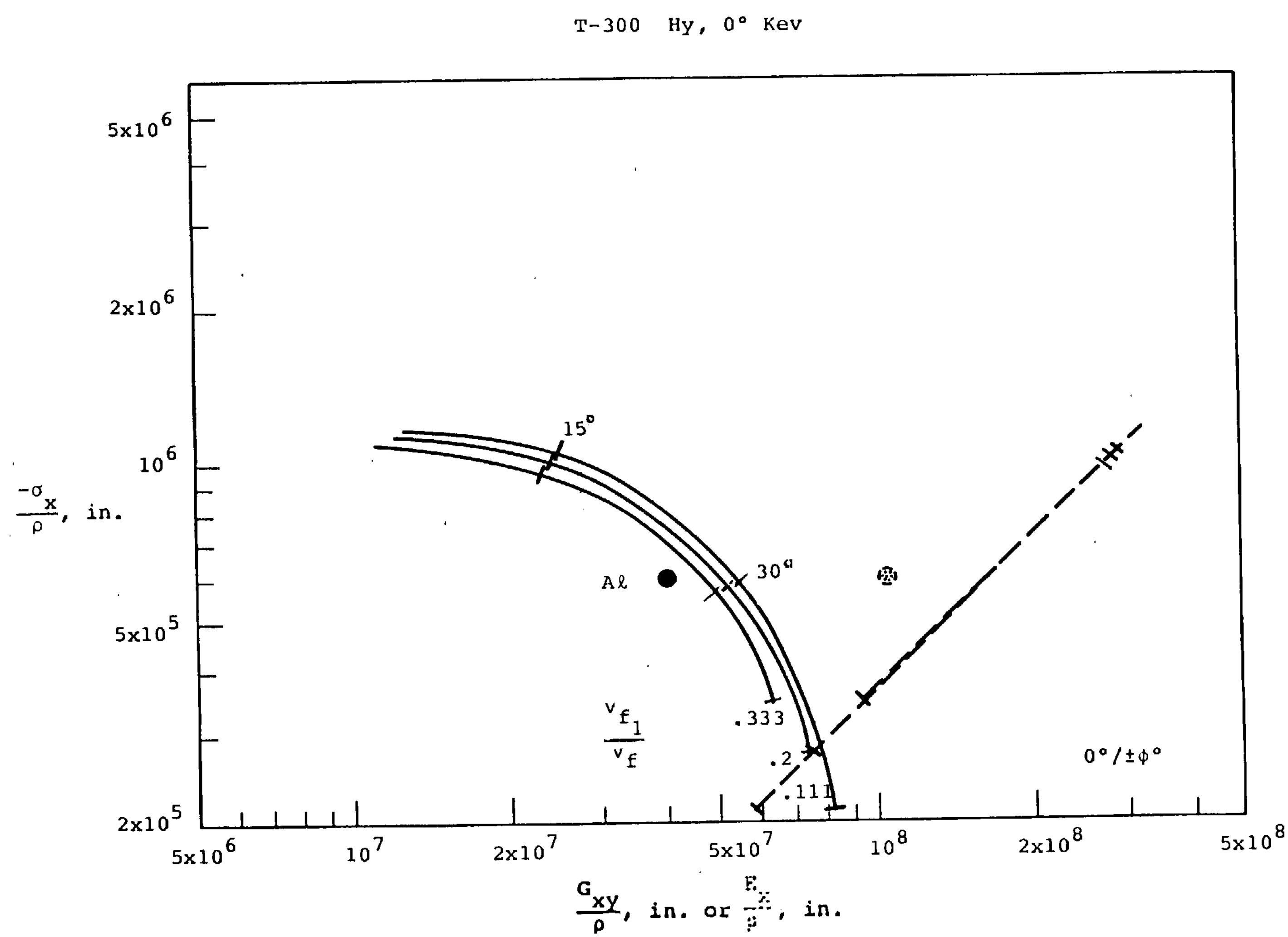

Figure 62. Evaluations of Hybrids.-

XIV. Triaxial weaves $0^\circ/\pm\phi^\circ$, Kevlar in the 0° direction, in compression. Here the premature failure occurs in the 0° Kevlar fibers. Performance is barely better than the aluminum alloy.

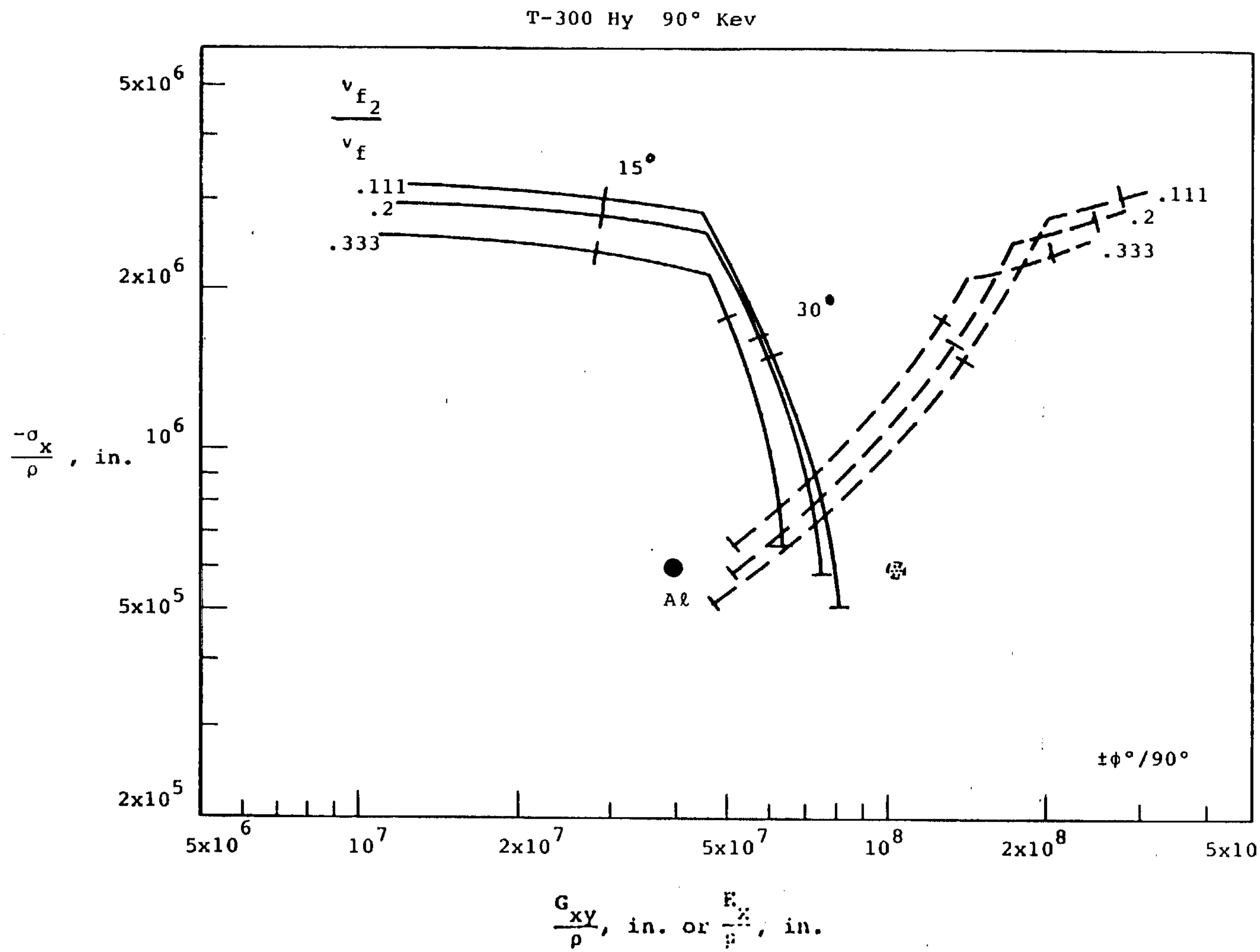

Figure 63. Evaluations of Hybrids.-

XV. Triaxial weaves $\pm\phi^\circ/90^\circ$, Kevlar in the 90° direction, in compression. Premature failure modes are not encountered and performance is excellent and similar to the related all T-300 configuration (Fig. 32.). The hybrid is slightly superior at the higher values of $\frac{G_{xy}}{\rho}$.

ORIGINAL PAGE IS
OF POOR QUALITY

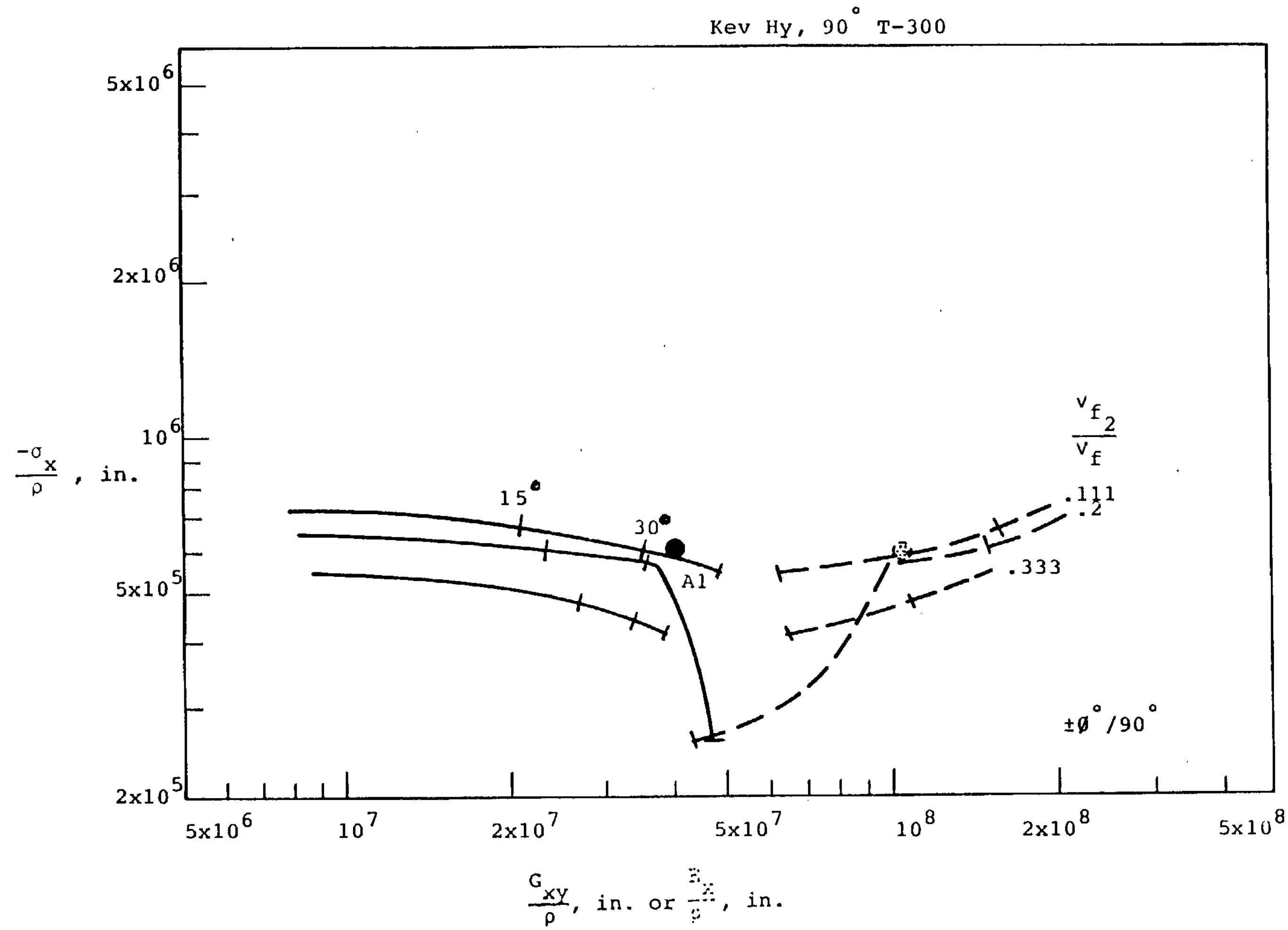

Figure 64. Evaluations of Hybrids.-

XVI. Triaxial weaves ±φ°/90°, T-300 in the 90° direction, in compression. Performance is limited by the low compressive strength of Kevlar. Not a configuration of much interest.

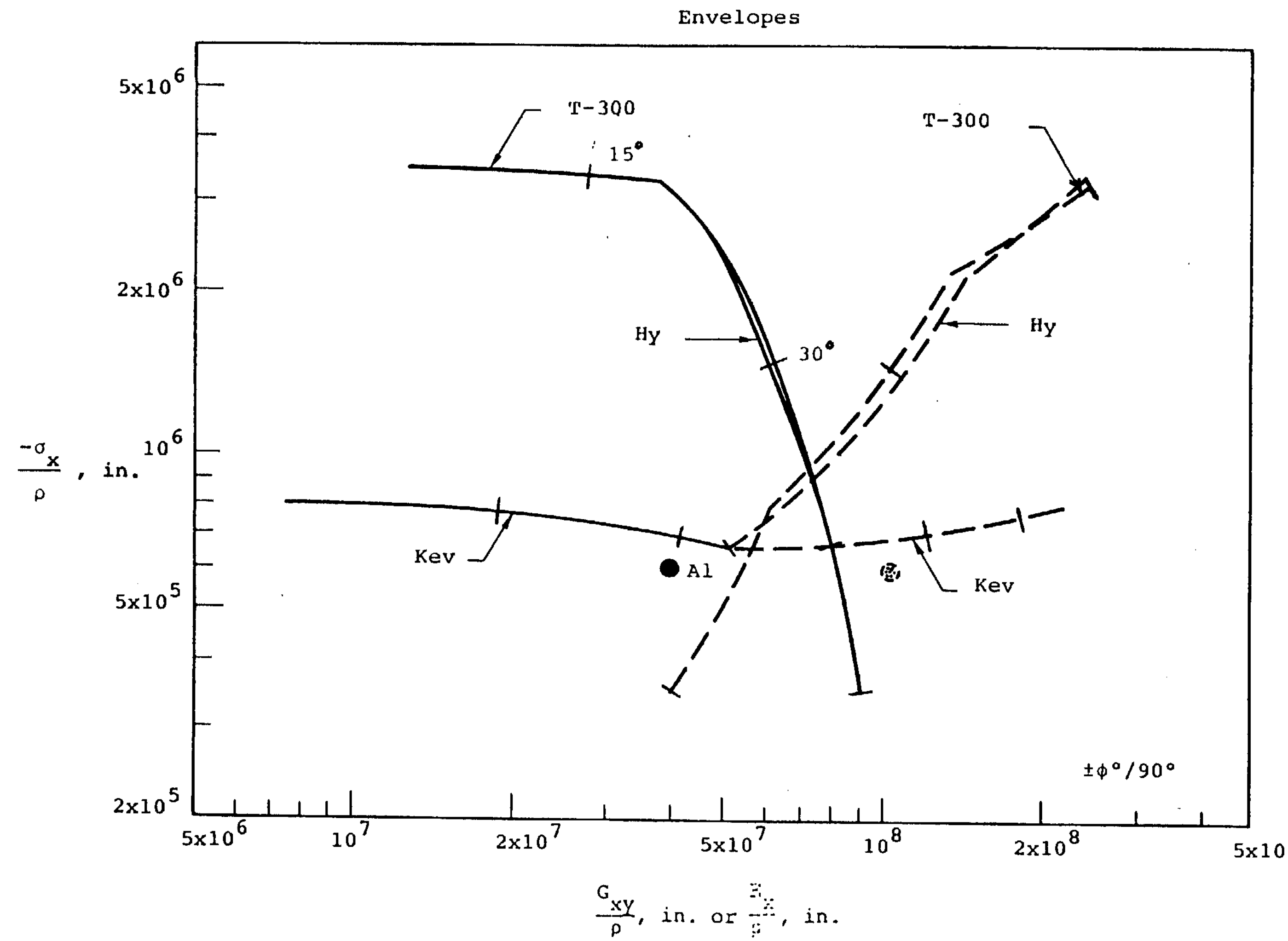

Figure 65. Evaluations of Hybrids.-

XVII. Overall evaluations of $\pm\phi^\circ/90^\circ$ triaxial weaves in compression. Envelope curves drawn to the individual curves of Figures 46 and 63 and calculated for all Kevlar show that the hybrids are somewhat below the all T-300 reinforcements. The all Kevlar is inappropriate for compressive loadings.

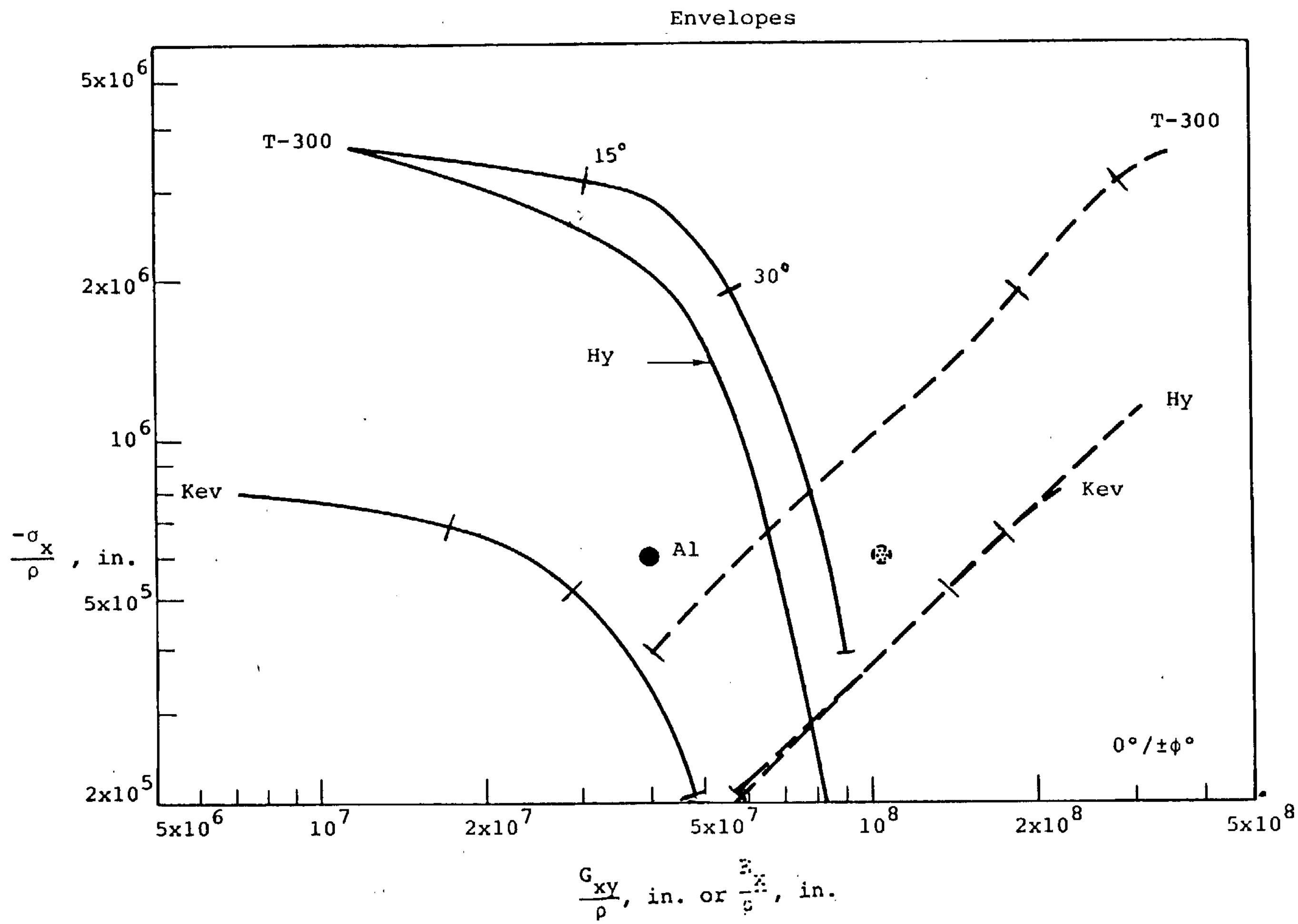

Figure 66. Evaluations of Hybrids.-

XVIII. Overall evaluations of $0^\circ/\pm\phi^\circ$ triaxial weaves in compression. Here the envelopes to curves of Figures 47 and 61 and calculated for all Kevlar are further below the all T-300 curves than for $\phi^\circ/90^\circ$ configurations. Again all Kevlar is not appropriate for compression.

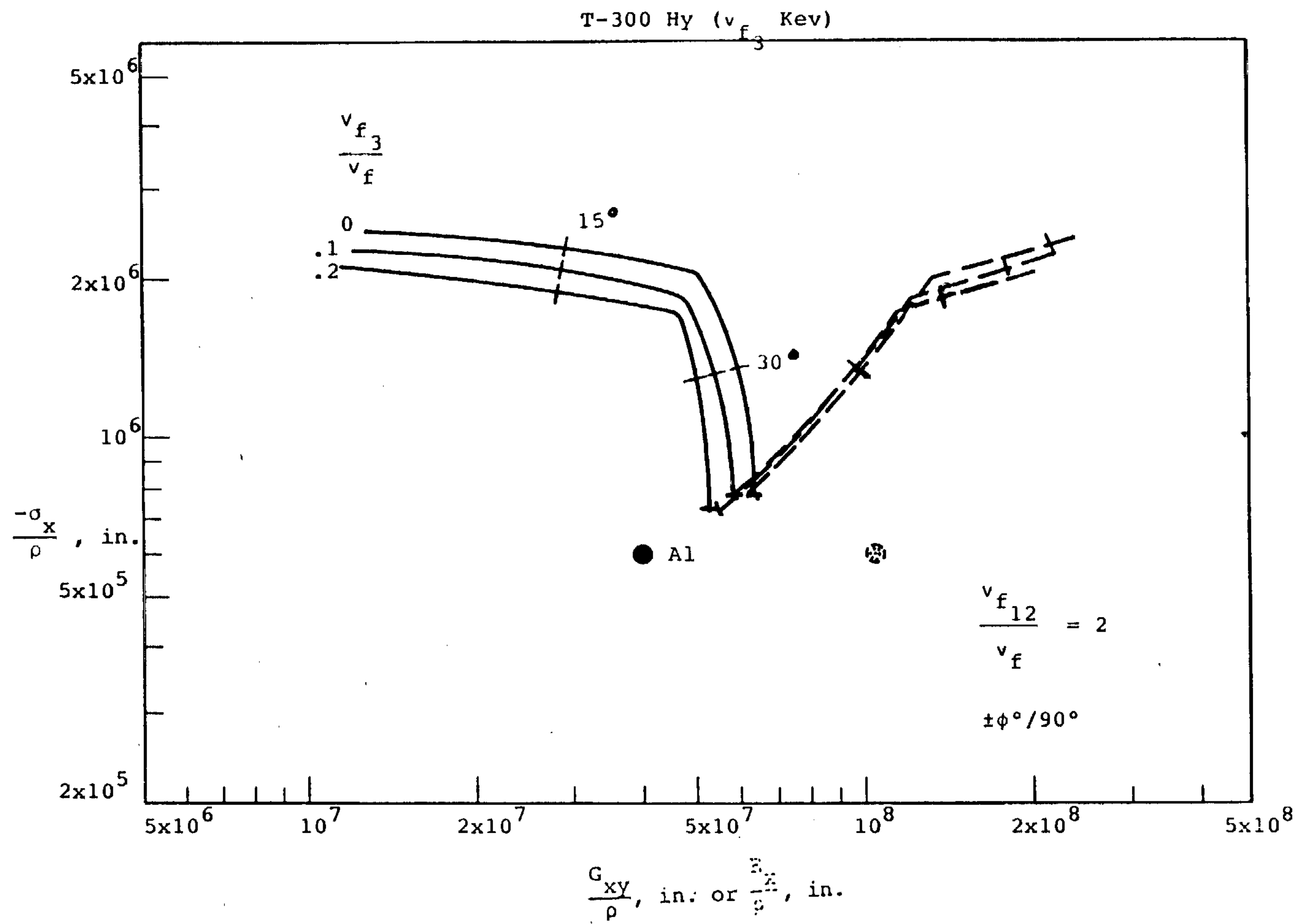

Figure 67. Evaluations of Hybrids.-

XIX. Effects of through-the-thickness reinforcement in compression.

(a) T-300, ±φ°/90° with Kevlar TTT. Losses due to TTT reinforcement are minimal, less than for a comparable all T-300 in tension (±φ°/90° with T-300 TTT, see Fig. 38).

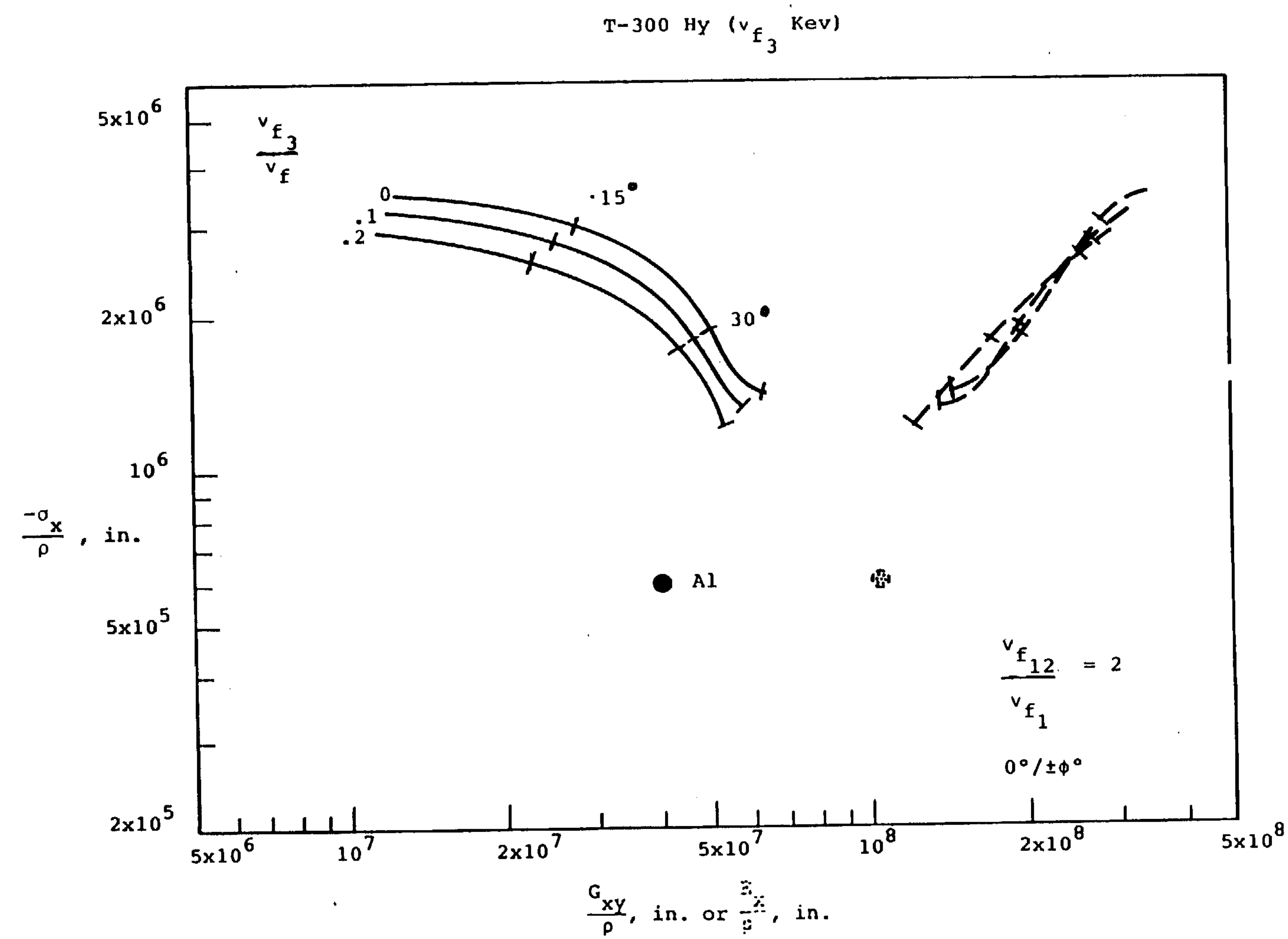

Figure 68. Evaluations of Hybrids.-

XX. Effects of thru the thickness reinforcement in compression.

(b) T-300, $0^\circ/\pm\phi^\circ$ with Kevlar TTT. Here the losses due to the Kevlar TTT are about the same as for all T-300 construction in tension - perhaps somewhat less at low values of $\frac{G_{xy}}{\rho}$ and somewhat more at high values of $\frac{G_{xy}}{\rho}$ (see Fig. 41). The comparison is complicated by the premature failure modes encountered by the $0^\circ/\pm\phi^\circ$ configuration).

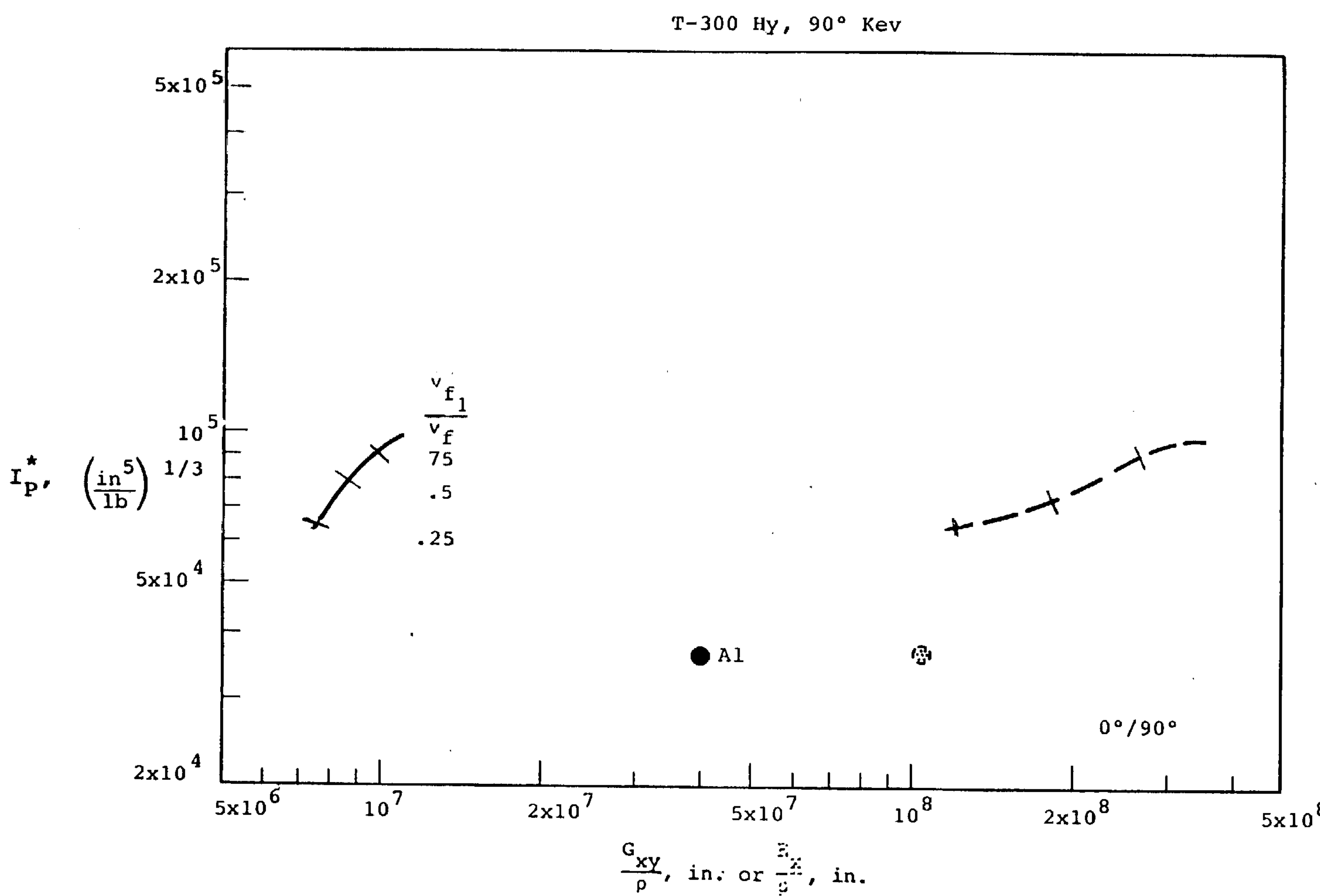

Figure 69. Evaluations of Hybrids.-

XXI. Use of indicator numbers to assess potentials for performance in compression.

(a) Simple plain weaves. While the plain weave T-300 hybrid can not provide shear stiffness/density ratios competitive with the aluminum alloy, for low stiffness requirements it offers promise of substantial weight savings.

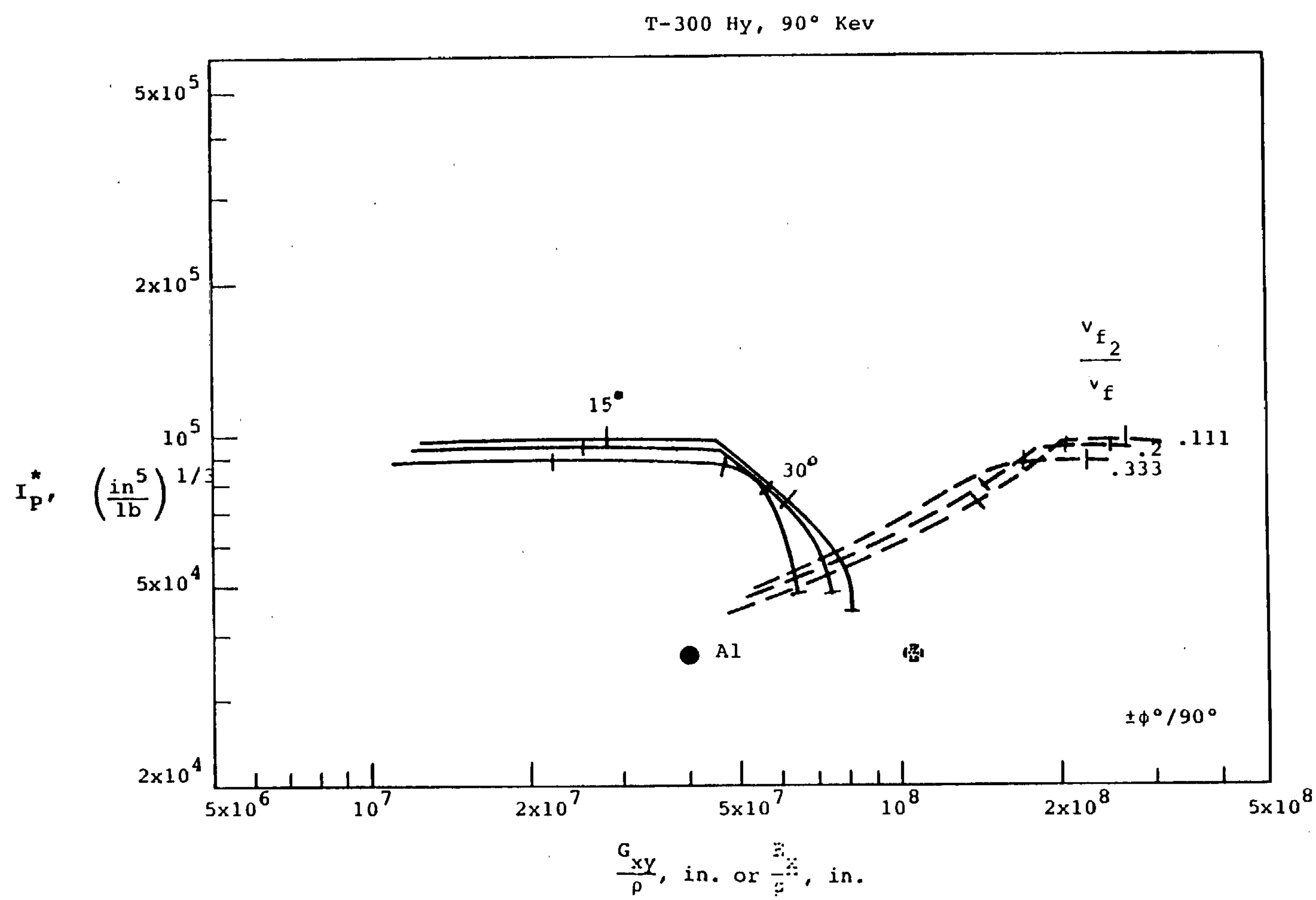

Figure 70. Evaluations of Hybrids.

XXII. Use of indicator numbers to assess potentials for performance in compression.

(b) Triaxial ±φ°/90° weaves, Kevlar in the 90° direction. These hybrids can provide shear stiffness/density ratios equal to or greater than the aluminum alloy with potential weight savings of over 60%.

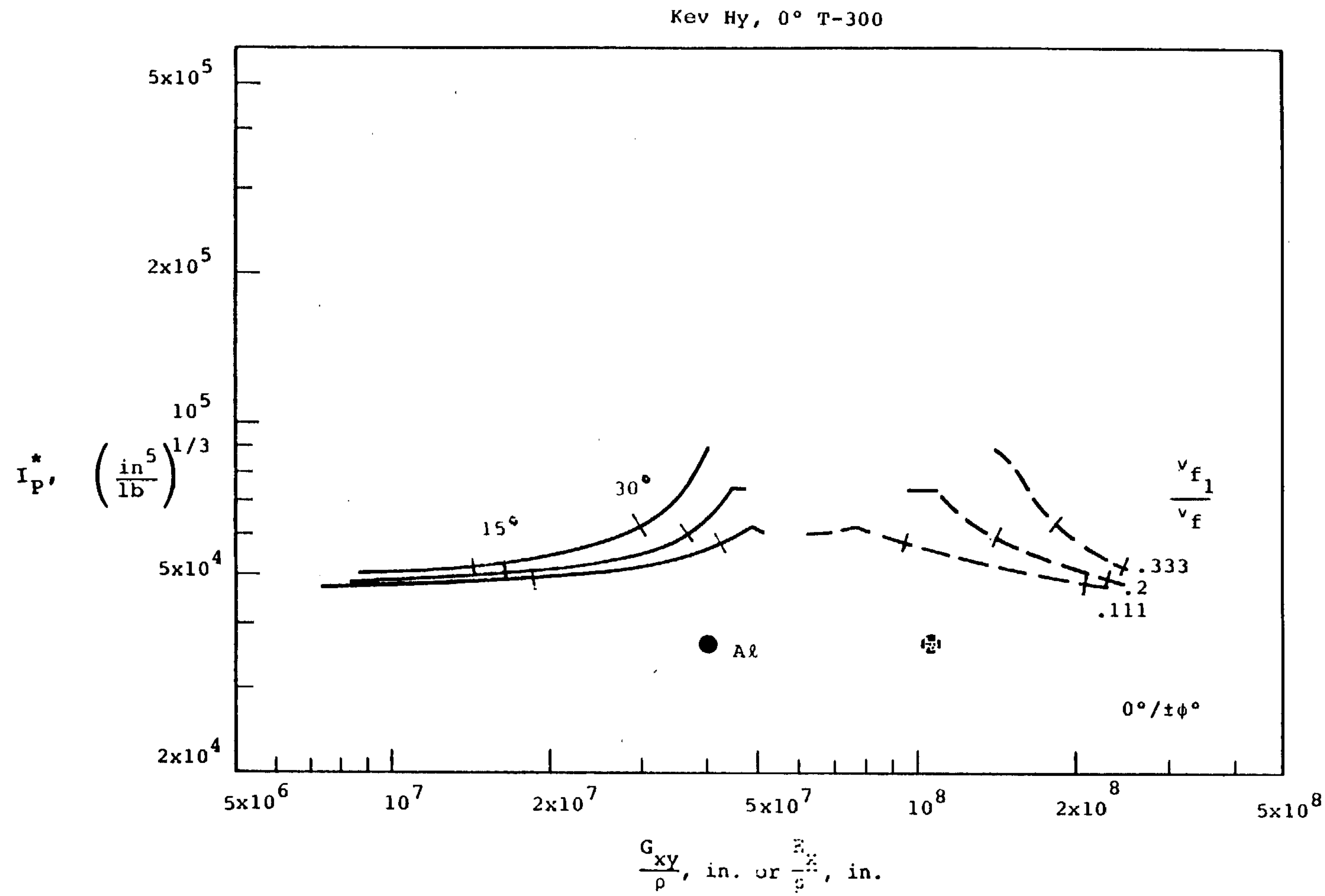

Figure 71. Evaluations of Hybrids.-

XXIII. Use of indicator numbers to assess potentials for performance in compression.

(c) Triaxial 0°/±φ° weaves, T-300 in the 0° direction. These hybrids, while less effective than the ±φ°/90° configuration, can provide significant weight savings over the aluminum alloy with comparable shear stiffness/density ratios.

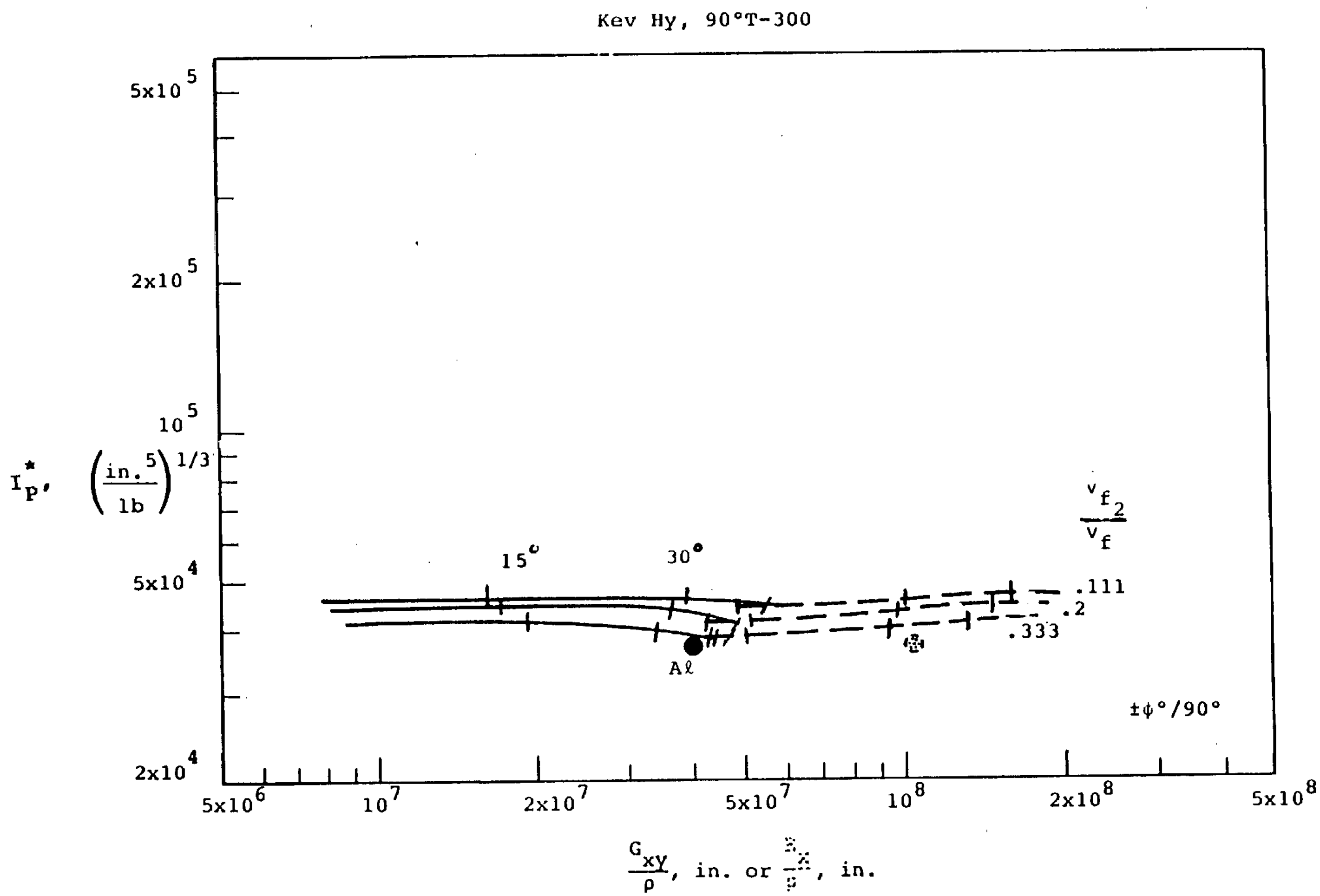

Figure 72. Evaluations of Hybrids.-

XXIV. Use of indicator numbers to assess potentials for performance in compression.

(d) Triaxial $\pm\phi^{\circ}/0^{\circ}$ weaves, T-300 in the 90° direction. As is to be expected because of the low compressive strength of Kevlar, these hybrids are not competitive with the corresponding $\pm\phi^{\circ}/90^{\circ}$ Kevlar in the 90° direction hybrids. Even so they have the potential to outperform the aluminum alloy.

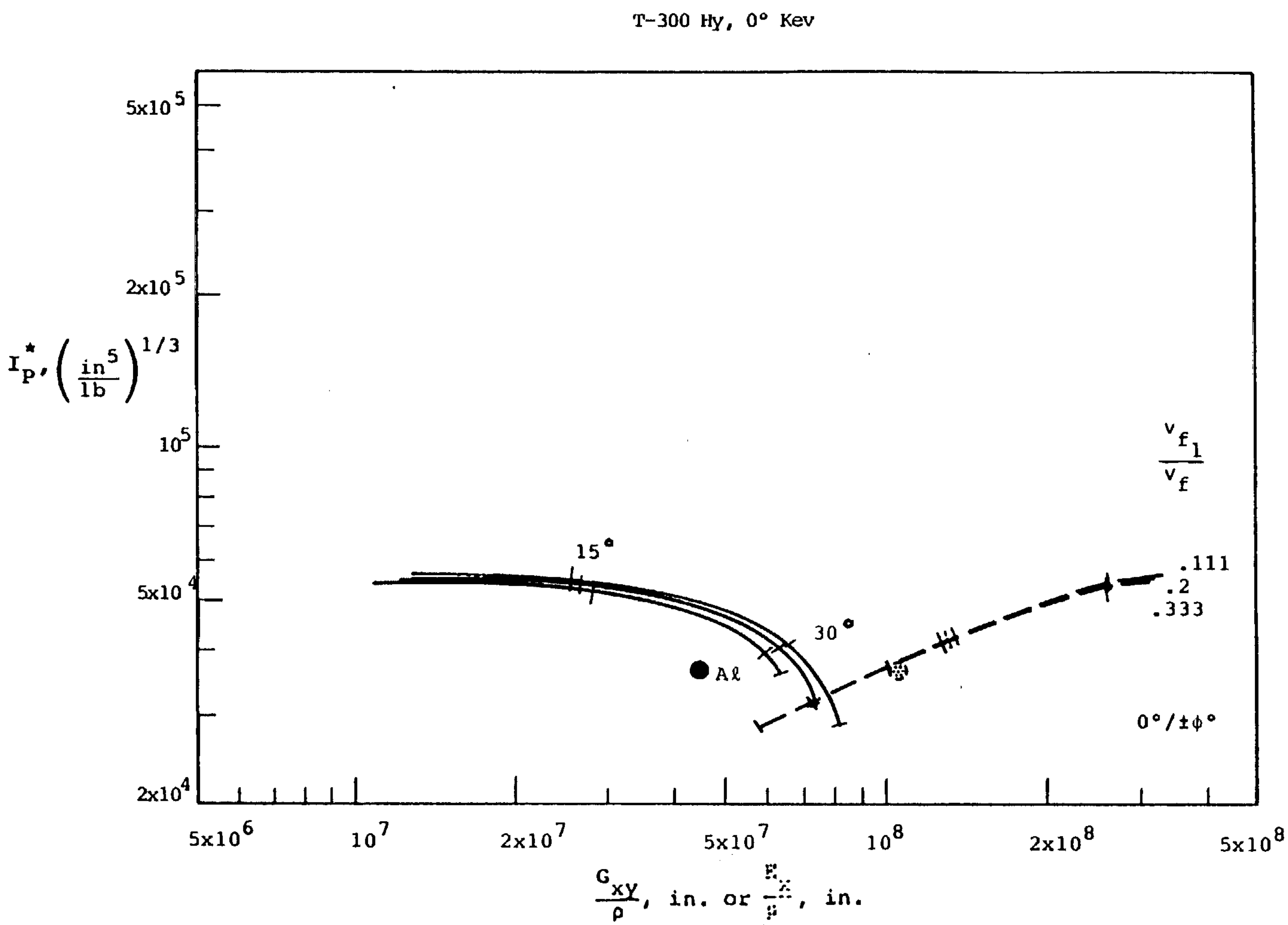

Figure 73. Evaluations of Hybrids.-

XXV. Use of indicator numbers to assess potentials for performance in compression.

(e) Triaxial 0°/90° weaves, Kevlar in the 0° direction. As in the case of the ±φ°/90° hybrids having T-300 in the 90° direction, the compressive strength of the 0° Kevlar limits the performance of these hybrids, though they have the potential to outperform the aluminum alloy by a substantial margin in both shear stiffness/density potential and weight.

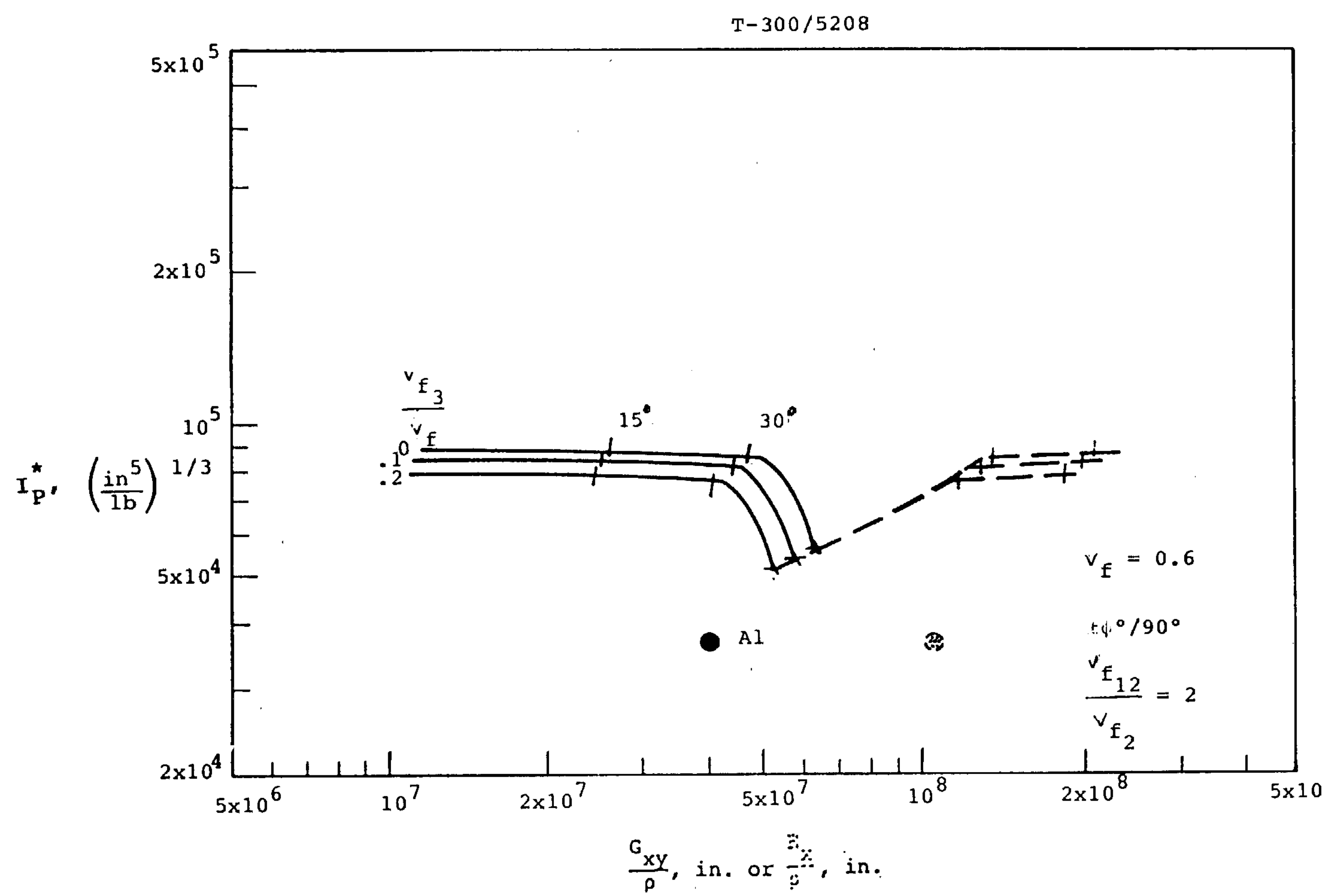

Figure 74. Evaluations of Hybrids.-

XXVI. Use of indicator numbers to assess potentials for performance in compression. A 16 2/3% increase in TTT reinforcement TTT produces 5% to 7% loss in I_p^* at shear stiffnesses up to that comparable to the aluminum alloy. For higher values the losses increase.

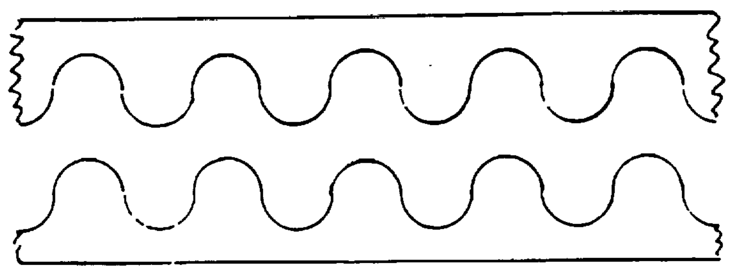

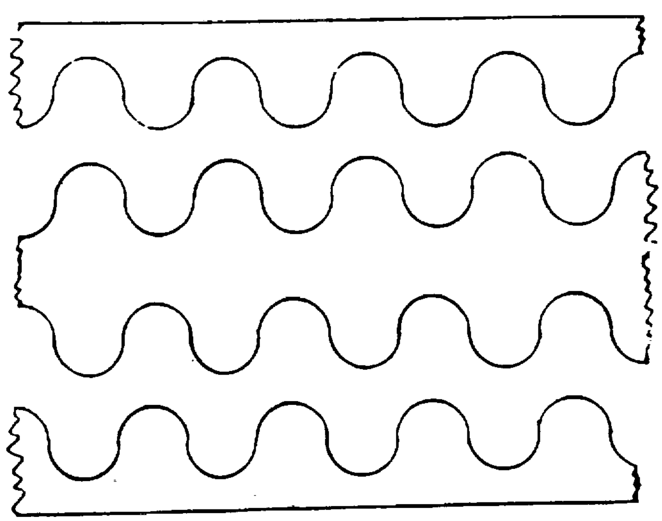

Figure 75. Bumpy Laminate Cross-Sectional Concept for Thru the Thickness Strength.

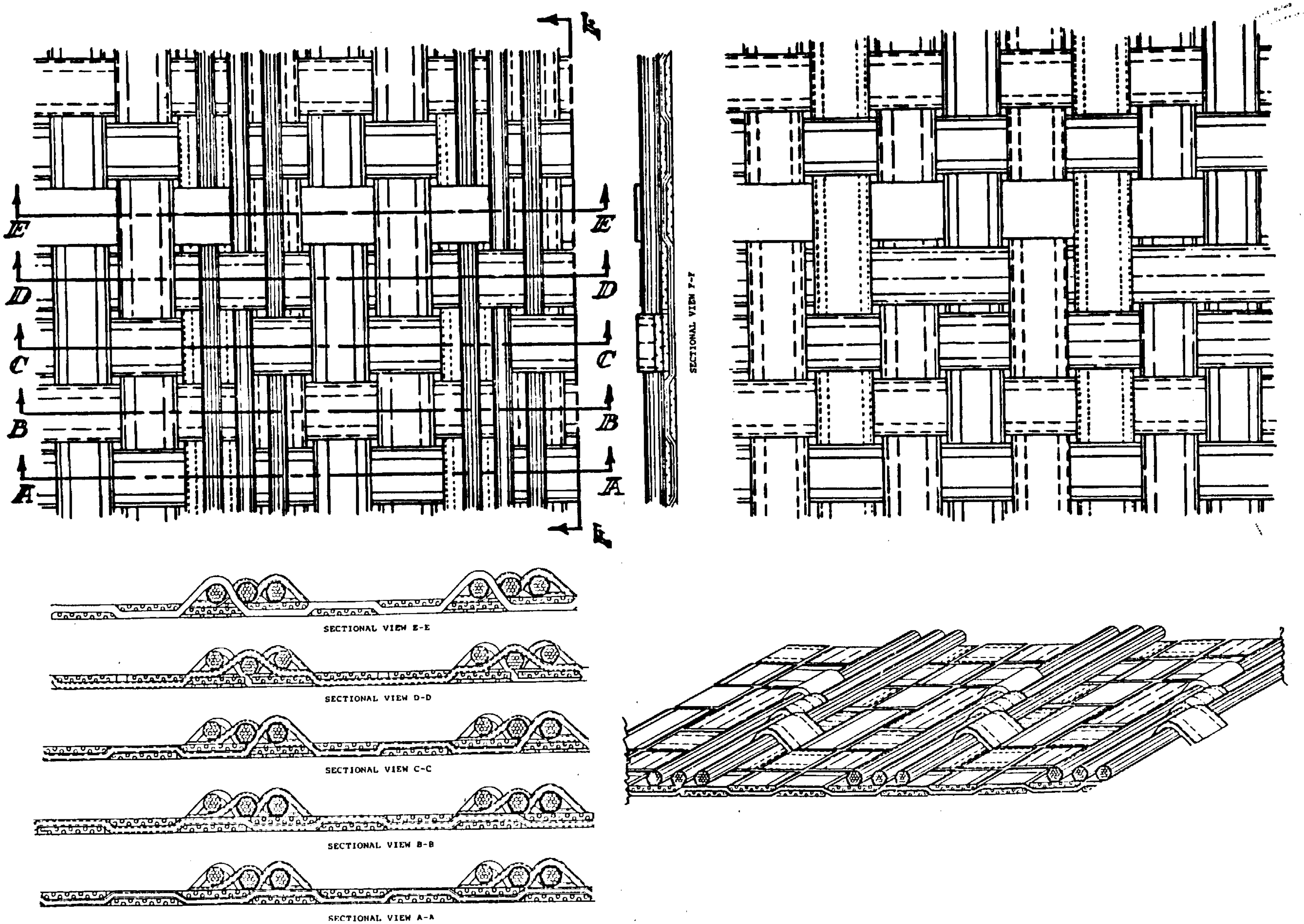

Figure 76. Even Though Twisted to Achieve Circular Cross Sections as Shown Here and in Figure 77, the Auxiliary Warps of This Initial Configuration Did Not Maintain Adequate Bumpiness when made into composites to Provide Substantial thru the thickness Reinforcement.

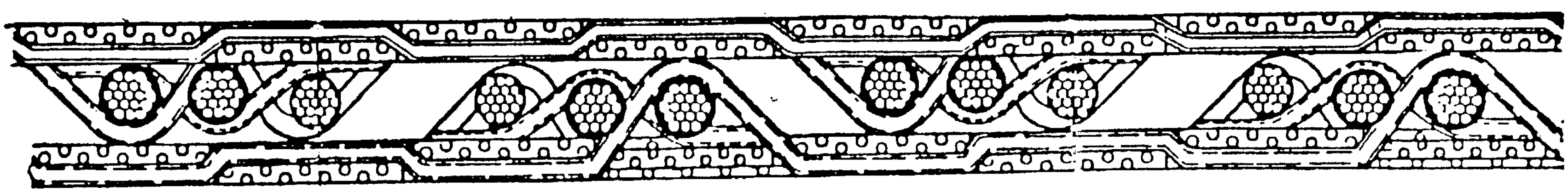

(a)

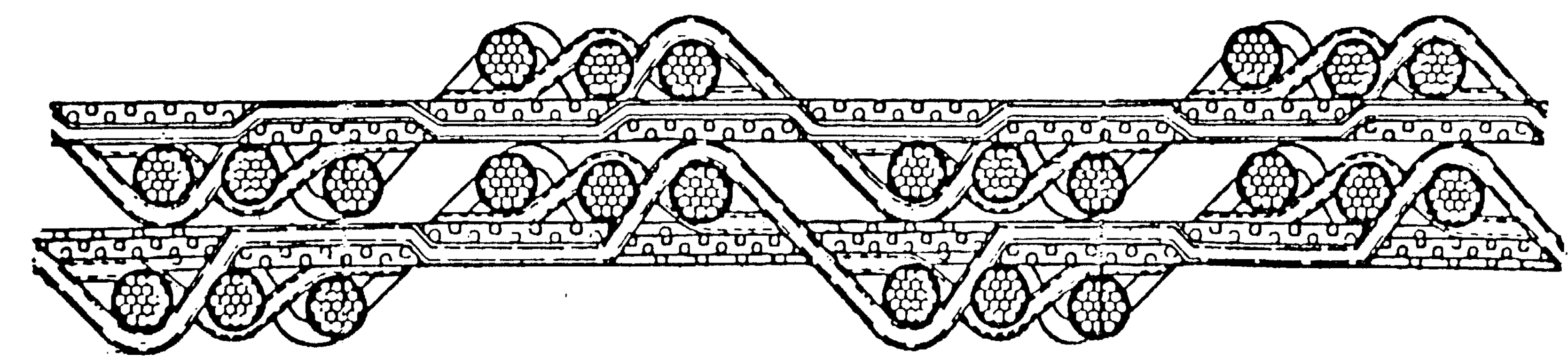

(b)

Figure 77. The Voids Evidenced Here in the Nominally Nested Configurations of the First Bumpy Construction May Have Contributed to the Lack of Substantial Through-the-Thickness Reinforcement of This Initial Bumpy-Fabric Construction.

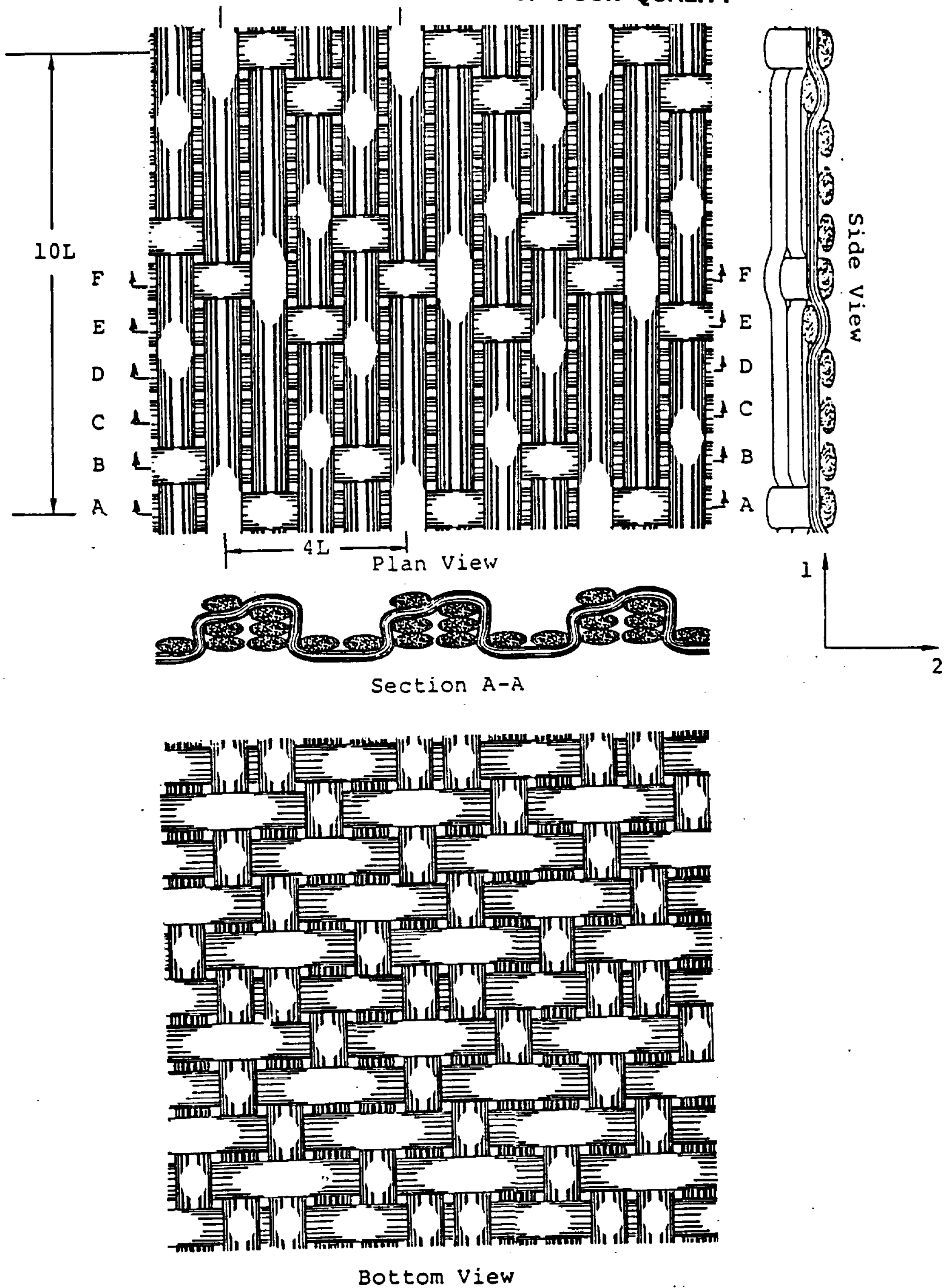

Figure 78. Revised (Mark II) Bumpy Fabric Stacked the Auxiliary Warps Two High, as Shown Here. Whether this is adequate to provide appreciable thru the thickness reinforcement is yet to be determined.

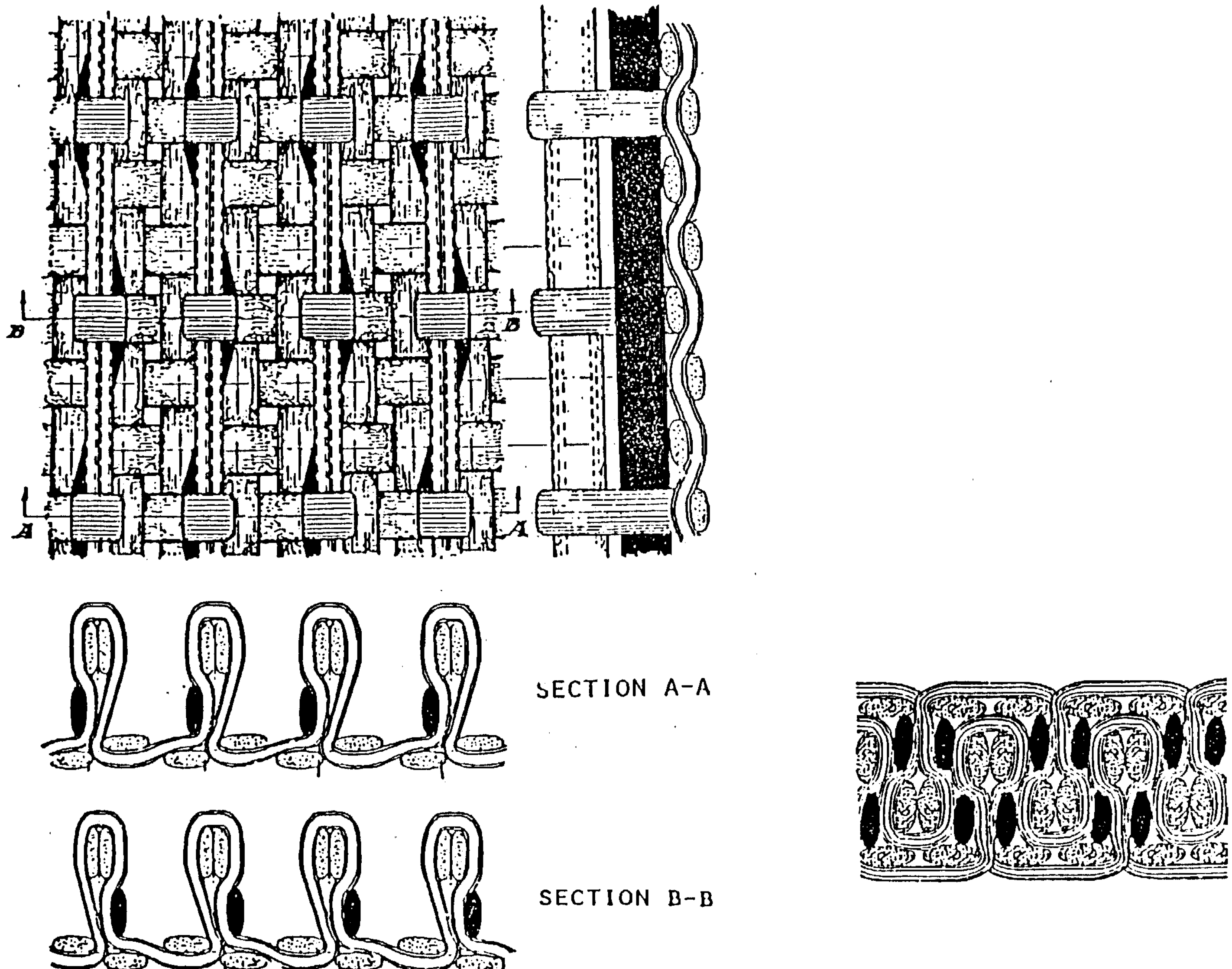

Figure 79. Advanced Bumpy Fabric Design Provides Nominally High Bumps, But as Drawn Relatively Low Volume Fraction Reinforcement . As in the preceding design, end volume fractions and performance are yet to be determined.

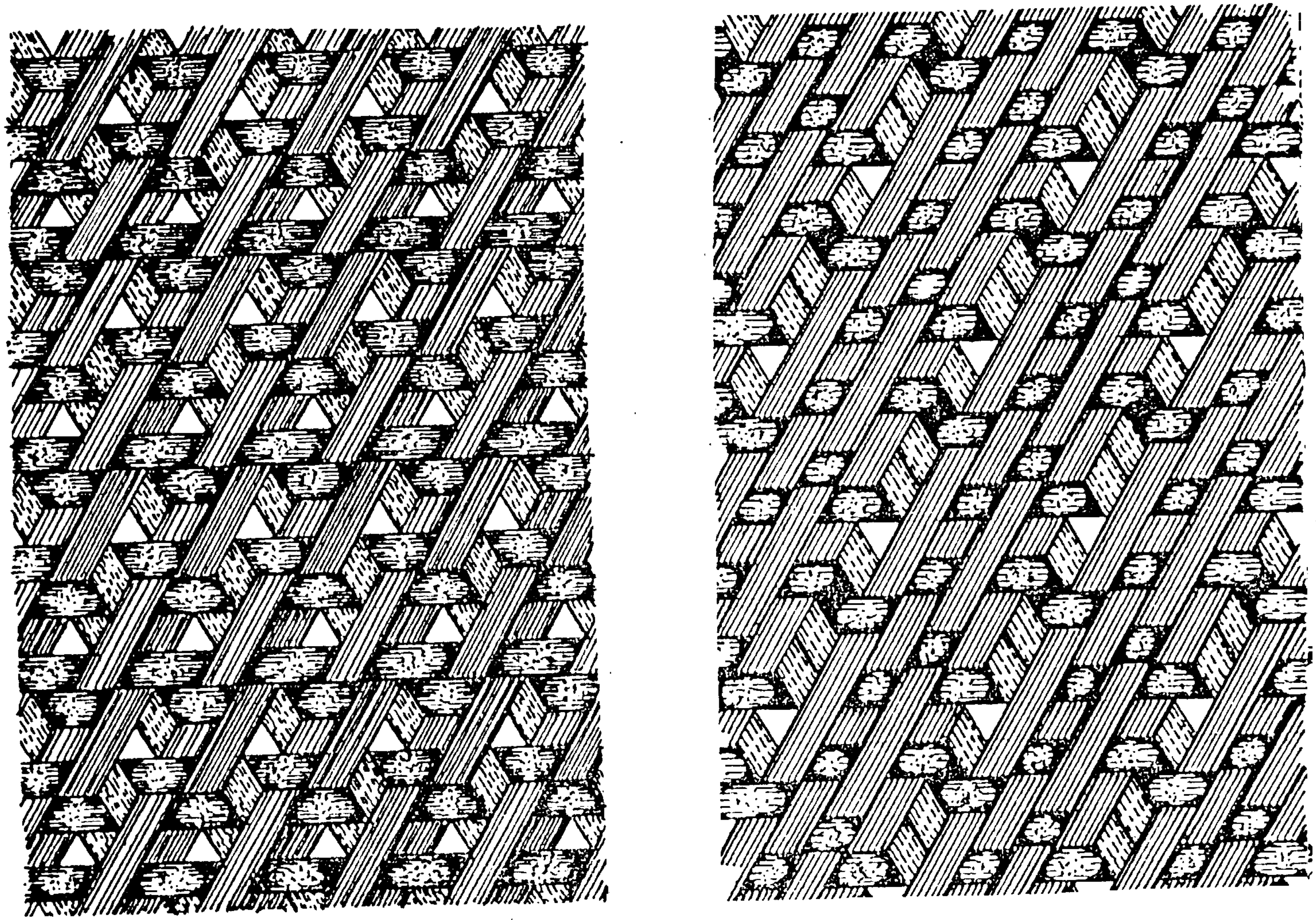

Figure 80. In These Example Stitchbase Weaves the Hole Spacings Are 2.3 and 4.6 yarn diameters. Other spacings are possible with different weave designs.

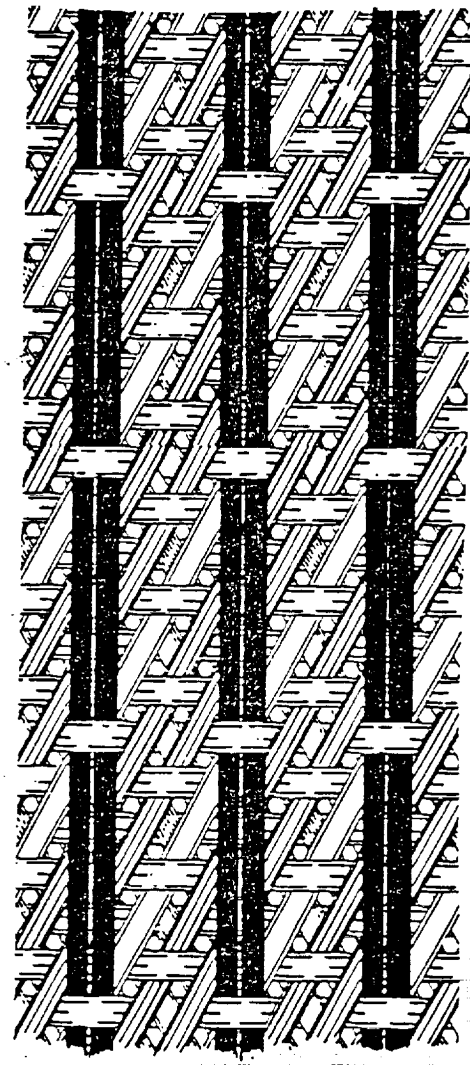

Figure 81. As Shown Here the Auxiliary Warps Have Relatively Long Floats. Alternatively, they could be woven to be tied in every second, fourth or other multiples of two fill yarns.

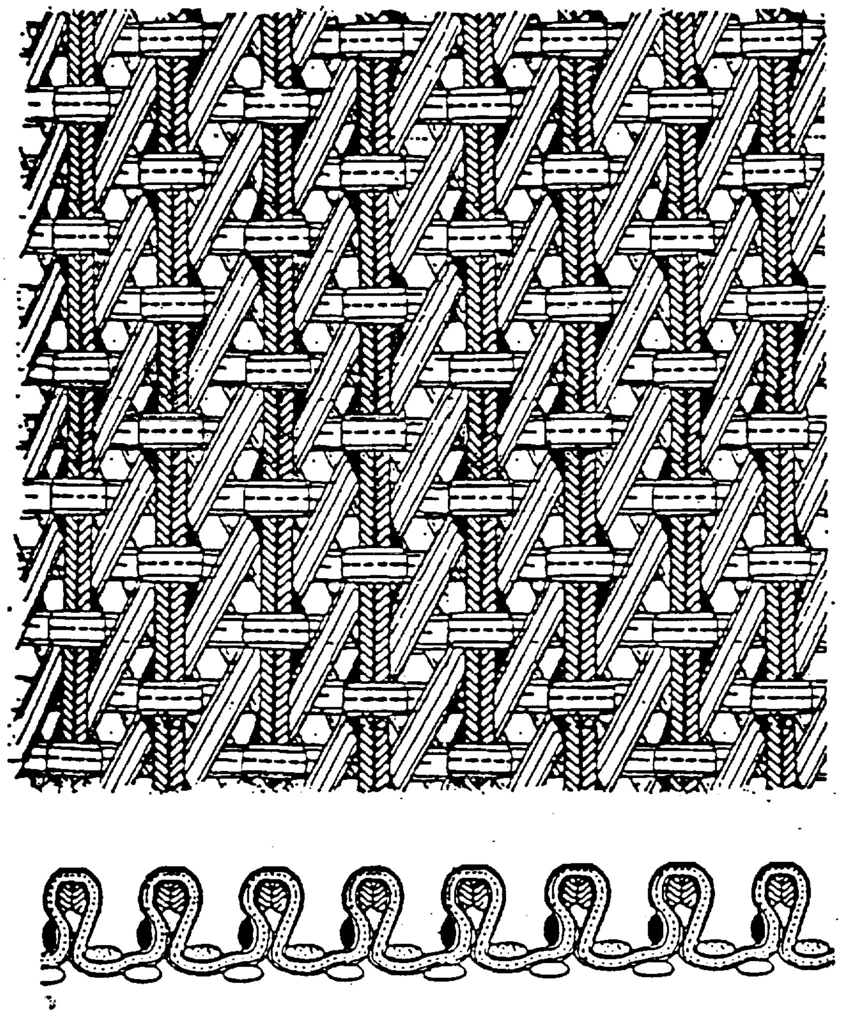

Figure 82. Nesting of Bulbous Blade Auxiliary Warps Atop Substrate Weave Fabric Constructions Is Different from that of Auxiliaries on Plain Weave Fabrics. The high Poisson's ratio of the Substrate Weave will permit some control of the width dimension by tensioning the fabrics. Truly compact nested configurations should be achievable.

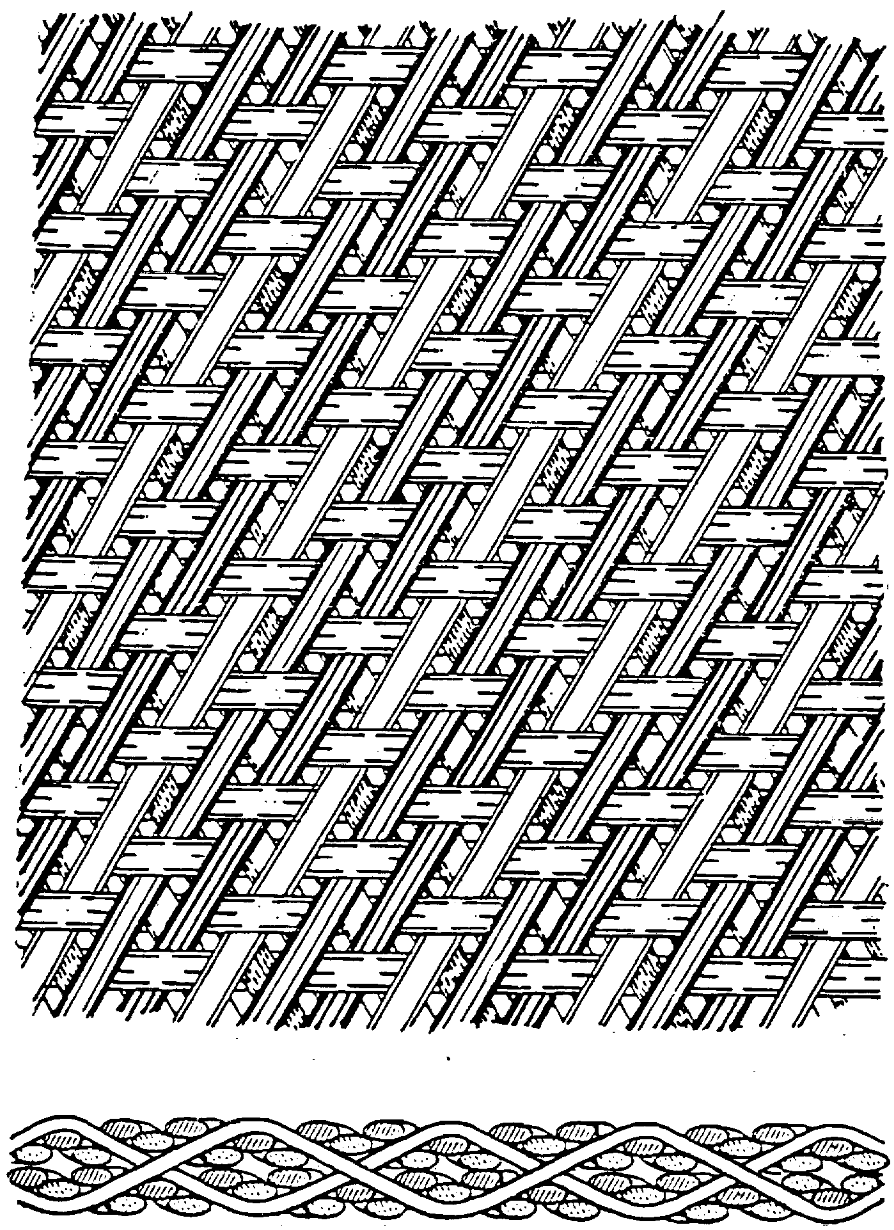

Figure 83. The Cross Section at the Bottom of the Figure Shows a Two Layer Construction. Up to four layers should be possible without difficulty.

ORIGINAL PAGE IS
OF POOR QUALITY

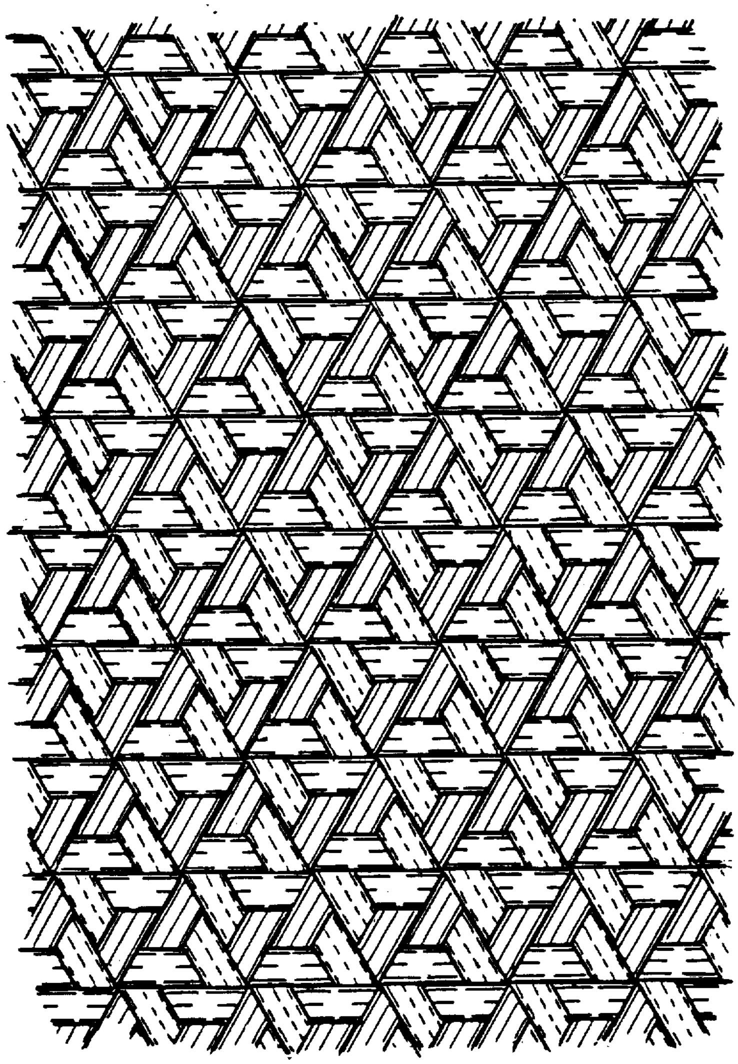

Figure 84. The Perfect Weave with Three-Way Symmetry, of Minor Interest for Composite Reinforcement Because of Short Float Lengths (1-up, 1-down in all three directions). Finely woven, however, it may have application in areas of stress concentration.

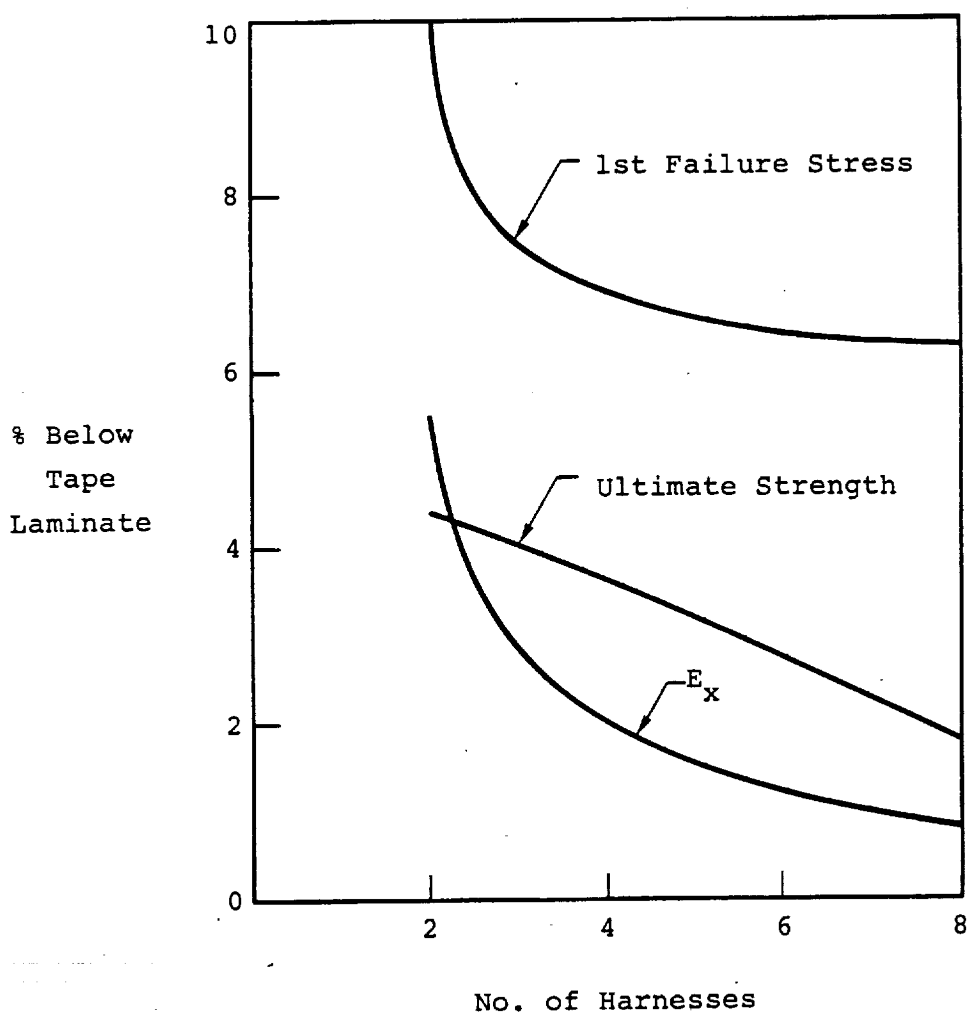

Figure 85. Losses in Properties in Tension Calculated by NDPROP for Biaxial Weaves Compared to 0°/90° Unidirectional Tape Laminates. Losses in E_x are in part compensated by increases in other elastic properties such as E_z and G_{xz}.

APPENDIX A

ANALYTICAL MODELS FOR THE CALCULATION OF WOVEN FABRIC PROPERTIES

LIST OF SYMBOLS

As used in Appendix A

A	area
A_{ij}	matrix relating in-plane stresses to strains
B_{ij}	matrix relating in-plane stresses to curvatures
C_{ij}	stiffness matrix
D_{ij}	matrix relating moments to curvatures
E	Young's modulus
G	shear modulus
h	thickness
L	thread count
S_{ij}	compliance matrix
ΔT	temperature difference from stress free temperature
U	strain energy
$\tilde{U}_c$	complementary energy
v_f	fiber volume fraction
α_i	thermal expansion coefficient vector
β_i	thermal curvature coefficient vector
Γ_i	vector relating strains due to applied temperature gradients to stresses
Δ_i	vector relating curvatures due to applied temperature gradients to stresses
ϵ_i	strain vector
κ	curvature vector
σ_i	stress vector
ν	Poisson's ratio

SUBSCRIPTS

L	longitudinal (fiber) direction
T	transverse (to fiber) direction
X	in-plane axial direction
Y	in-plane transverse direction
Z	thru the thickness direction

APPENDIX A

ANALYTICAL MODELS FOR THE CALCULATION OF WOVEN FABRIC PROPERTIES

The behavior of woven fabrics is dependent on several geometrical as well as material parameters. The analytical treatment of the woven fabric needs to be three-dimensional to account properly for the complicated reinforcement geometry of anisotropic fiber bundles. The mechanics of fabric reinforced composites are not as well defined as compared to laminated composite plates and hence our approach to the development of an analysis was to obtain bounds on the effective fabric properties based on energy principles. Various fabric models were considered and resulting calculations were compared with the results of finite element analyses in order to assess the validity of the different models. This appendix contains a brief description of each of the approaches and the results obtained.

LAYERED-PLATE FABRIC MODEL

The first step in analyzing the fabric was to define the geometry of a representative volume element. In this approach it was assumed that the yarn cross-sections remained circular. The overall structural behavior of the fabric was determined from the weave characteristics and properties computed for the representative volume element. The representative volume element of a five harness satin woven fabric is shown in figure A-1. The figure also shows several cross sections within the representative element. It can be observed from the figure that the weave is of the "over 4 under 1" pattern typical of the five harness satin weave. The cross-sections are similar to each other except for the relative position of the cross-over yarn.

A typical cross-section of the weave is shown in figure A-2. The cross-section of another weave would be similar except for the relative dimensions of the straight and cross-over yarns. The cross-section can be divided into several sub-layers each containing axial, transverse and oriented fiber bundles. The overall weave properties were computed by treating each sub-layer as a portion of a laminated plate and integrating through the ply thickness.

The elastic properties of the woven fabric were determined by this approach using three different assumptions. First, it was assumed that each of the sub-layers had a linear strain field thru the thickness and a constant strain field along its length yielding an upper bound on stiffnesses. The second assumption led to a reduced upper bound based on a constant strain field along the length and a state of plane stress for each sub-layer. The third assumption yielded a lower bound on the fabric stiffnesses by assuming a linear stress field thru the thickness and a constant stress field along the length for each sub-layer.Equations for the elastic properties under three different assumptions are presented in the following paragraphs.

Upper Bound Approximation

We assume that the element shown in figure A-3 is subjected to no surface tractions and that the assumed displacement fields hold everywhere inside the element. If the constitutive relations for the constituents are of the following form (in contracted notation)

$$\sigma_i = C_{ij}\,\epsilon_j + \gamma_i \Delta T \tag{1}$$

then noting that $\epsilon_{33} = \epsilon_{13} = \epsilon_{23} = 0$ everywhere, and summing the strain energies in all the constituents for the assumed displacement field, one obtains

$$U = \frac{A}{2}\left[A^1_{ij}\,\bar{\epsilon}_i\bar{\epsilon}_j + 2B^1_{ij}\,\bar{\epsilon}_i\,\bar{\kappa}_j + D^1_{ij}\,\bar{\kappa}_i\,\bar{\kappa}_j + \left(\Gamma^1_i\,\bar{\epsilon}_i + \Delta^1_i\,\bar{\kappa}_i\right)\Delta T\right] \tag{2}$$

where repeated indices indicate summation over indices 1, 2 and 6. The upper bound stiffness matrices A^1, B^1 and D^1 are calculated in the following manner.

$$\left(A_{ij}^{1},\ B_{ij}^{1},\ D_{ij}^{1}\right) = \frac{1}{A} \int_A \int_{-h/2}^{h/2} C_{ij}\ (1,z,z^2)\ dz$$

$$= \sum_{\ell=1}^{L} \left[(P^{\ell},\ Q^{\ell},\ R^{\ell}) \sum_{m=1}^{M(\ell)} C_{ij}^{\ell m}\ a^{\ell m}\right] \tag{3a}$$

$$\left(\Gamma_i^1,\ \Delta_i^1\right) = \frac{1}{A} \int_A \int_{-h/2}^{h/2} \gamma_i\ (1,z)\ dz$$

$$= \sum_{\ell=1}^{L} \left[(P^{L},\ Q^{L}) \sum_{m=1}^{M(\ell)} \gamma_i^{\ell m} a^{\ell m}\right] \tag{3b}$$

In equations (3) the superscripts ℓm indicate material, m, in layer, ℓ, and $M(\ell)$ is the number of materials in layer ℓ. L is the total number of layers. Further

$$P^{\ell} = h_{1\ell} - h_{2\ell}$$

$$Q^{\ell} = 1/2\ (h_{1\ell}^2 - h_{2\ell}^2) \tag{4}$$

$$R^{\ell} = 1/3\ (h_{1\ell}^3 - h_{2\ell}^3)$$

$h_{1\ell}$, $h_{2\ell}$ being the z-coordinates of top and bottom surfaces of layer ℓ.

A_{ij}^1, B_{ij}^1, D_{ij}^1, Γ_i^1 and Δ_i^1 yield approximate values of A_{ij}^*, B_{ij}^*, D_{ij}^* Γ_i^* and Δ_i^*, respectively. Moreover, the diagonal terms of the matrices A_{ij}^1 and D_{ij}^1 are upper bounds on the corresponding effective properties. Approximate expansions for average thermal expansions and curvatures can be obtained as

$$\begin{bmatrix} \alpha_i^{\,1} \\ \beta_i^{\,1} \end{bmatrix} = \begin{bmatrix} A^1 & B^1 \\ B^1 & D^1 \end{bmatrix}^{-1} \begin{bmatrix} \Gamma_i^{\,1} \\ \Delta_i^{\,1} \end{bmatrix} \tag{5}$$

Reduced Upper Bound Approximation

An assumption which is used in laminated plate theory is that the stress in the z direction is equal to zero. In the problem under consideration, we may make the same assumption and obtain approximate expressions A^2_{ij}, B^2_{ij}, D^2_{ij} for the effective properties by using reduced stiffnesses

$C'^{\ell m}_{ij} = C^{\ell m}_{ij} - C^{\ell m}_{i3}\, C^{\ell m}_{3j}/C^{\ell m}_{33}$ in place of $C^{\ell m}_{ij}$ in (3a). The expressions for the

diagonal terms of A^2 and D^2 matrices are not strictly upper bounds on the corresponding effective properties and, therefore, we have introduced the term reduced upper bound.

Lower Bound Aproximation

In this formulation, instead of choosing an approximate displacement field, we assume the following stress field in the representative area element

$$\sigma^{\ell}_{i} = \sigma^{\ell o}_{i} + z\, \sigma^{\ell 1}_{i} \quad , \quad \ell = 1,2, \ldots L, \quad i = 1,2,6 \tag{6a}$$

$$\text{and } \sigma^{\ell}_{3} = \sigma^{\ell}_{4} = \sigma^{\ell}_{5} = 0 \quad (\text{or, } \sigma^{\ell}_{33} = \sigma^{\ell}_{13} = \sigma^{\ell}_{23} = 0) \tag{6b}$$

where σ^{ℓ}_{i} = the stress component i in the ℓ^{th} layer each of which is independent of the x and y coordinates.

The complementary energy for the assumed stress field representative area element can be expressed as

$$\begin{aligned} U_c = \sum_{\ell=1}^{L} 1/2 \Big[F^{\ell}_{ij}\, \sigma^{\ell o}_{i}\, \sigma^{\ell o}_{j} + G^{\ell}_{ij} \left(\sigma^{\ell o}_{i}\, \sigma^{\ell 1}_{j} + \sigma^{\ell 1}_{i}\, \sigma^{\ell o}_{j} \right) \\ + H^{\ell}_{ij}\, \sigma^{\ell 1}_{i}\, \sigma^{\ell 1}_{j} \Big] + \left(e^{\ell}_{i}\, \sigma^{\ell o}_{i} + f^{\ell}_{i}\, \sigma^{\ell 1}_{i} \right) \Delta T \\ - \left\{ P^{\ell}\, \sigma^{\ell o}_{i}\, \bar{\epsilon}_{i} + Q^{\ell} \left(\sigma^{\ell o}_{i}\, \bar{\kappa}_{i} + \sigma^{\ell 1}_{i}\, \bar{\epsilon}_{i} \right) + R^{\ell}\, \sigma^{\ell 1}_{i}\, \bar{\kappa}_{i} \right\} \end{aligned} \tag{7}$$

where the repreated indices i, j indicate summation over 1, 2 and 6 and,

$$\left(F_{ij}^{\ell},\ G_{ij}^{\ell},\ H_{ij}^{\ell}\right) = \sum_{m=1}^{M(\ell)} \int_A \int_{-h/2}^{h/2} S_{ij}^{\ell m} \ (1,z,z^2) \ dz \ dA \tag{8}$$

$$= A\ (P^{\ell},\ Q^{\ell},\ R^{\ell}) \sum_{m=1}^{M(\ell)} a^{\ell m}$$

$$e_i^{\ell},\ f_i^{\ell} = \sum_{m=1}^{M(\ell)} \int_a \int_{-h/2}^{h/2} \sigma_i^{\ell m} \ (1,z) \ dz \ dA$$

$$= A\ (P^{\ell},\ Q^{\ell}) \sum_{m=1}^{M(\ell)} \sigma_i^{\ell m} \ a^{\ell m}$$

In equation (8) A is the area of the element P^{ℓ}, Q^{ℓ}, R^{ℓ} and $a^{\ell m}$ are defined for approximation 1, and $S_{ij}^{\ell m}$, $\alpha_i^{\ell m}$ are the complicances and thermal expansion coefficients for material m in layer ℓ. Minimization of U_c with respect to the unknows $\sigma_i^{\ell o}$, $\sigma_i^{\ell 1}$ ($i = 1,2,6$ and $\ell = 1, \ldots L$) yields

$$\begin{aligned} \sigma_i^{\ell o} &= F_{ij}^{\prime \ell} \left(-e_j^{\ell} \Delta T + P^{\ell} \bar{\epsilon}_j + Q^{\ell} \bar{\kappa}_j\right) \\ &\quad + G_{ij}^{\prime \ell} \left(-f_j^{\ell} \Delta T + Q^{\ell} \bar{\epsilon}_j + R^{\ell} \bar{\kappa}_j\right) \end{aligned} \tag{9}$$

$$\begin{aligned} \sigma_i^{\ell 1} &= G_{ij}^{\prime \ell} \left(-e_j^{\ell} \Delta T + P^{\ell} \bar{\epsilon}_j + Q^{\ell} \bar{\kappa}_j\right) \\ &\quad + H_{ij}^{\prime \ell} \left(-f_j^{\ell} \Delta T + Q^{\ell} \bar{\epsilon}_j + R^{\ell} \bar{\kappa}_j\right) \end{aligned}$$

where

$$\begin{bmatrix} F'^{\ell} & G'^{\ell} \\ G'^{\ell} & H'^{\ell} \end{bmatrix} = \begin{bmatrix} F^{\ell} & G^{\ell} \\ G^{\ell} & H^{\ell} \end{bmatrix}^{-1}$$

Substitution of equation (9) in (7) or evaluation of $\bar{N}_i$ and $\bar{M}_i$ with the help of (6a) and (9) yields the following approximate expressions for the effective properties.

$$A_{ij}^3 = \sum_{\ell=1}^{L} \left[F_{ij}^{'\ell} (P^\ell)^2 + 2 G_{ij}^{'\ell} P^\ell Q^\ell + H_{ij}^{'\ell} (Q^\ell)^2 \right]$$

$$B_{ij}^3 = \sum_{\ell=1}^{L} \left[F_{ij}^{'\ell} P^\ell Q^\ell + G_{ij}^{'\ell} \left\{ P^\ell R^\ell + (Q^\ell)^2 \right\} + H_{ij}^{'\ell} Q^\ell R^\ell \right]$$

$$D_{ij}^3 = \sum_{\ell=1}^{L} \left[F_{ij}^{'\ell} (Q^\ell)^2 + 2 G_{ij}^{'\ell} Q^\ell R^\ell + H_{ij}^{'\ell} (R^\ell)^2 \right] \qquad (10)$$

$$\Gamma_j^3 = \sum_{\ell=1}^{L} P^\ell \left[F_{ij}^{'\ell} e_j^{\ \ell} + G_{ij}^{'\ell} f_i^\ell \right] + Q^\ell \left[G_{ij}^{'\ell} e_j^{\ \ell} + H_{ij}^{'\ell} f_i^{\ 2} \right]$$

$$\Delta_j^3 = -\sum_{\ell=1}^{L} Q^\ell \left[F_{ij}^{'\ell} e_j^{\ \ell} + G_{ij}^{'\ell} f_i^\ell \right] + R^\ell \left[G_{ij}^{'\ell} e_j^{\ \ell} + H_{ij}^{'\ell} f_i^{\ 2} \right]$$

The appoximate effective thermal expansion coefficients and curvatures are then expressed as

$$\begin{bmatrix} \alpha_i^{\ 3} \\ \beta_i^{\ 3} \end{bmatrix} = \begin{bmatrix} A^3 & B^3 \\ B^3 & D^3 \end{bmatrix}^{-1} \begin{bmatrix} \Gamma_i^{\ 3} \\ \Delta_i^{\ 3} \end{bmatrix} \qquad (11)$$

In this formulation, the diagonal terms of the matrices A^3 and D^3 yield lower bounds for the diagonal terms of A^*, D^* respectively.

The yarn properties were obtained from the constituent fiber and matrix properties and the fiber volume fraction using UNI, a MSC fiber bundle property prediction code based on the composite cylinders assemblage. The T300/Epoxy properties used for the analyses are listed in table A-1.

The next step in this approach was the determination of amounts of yarn in the different orientations: axial, transverse and cross-over. This is illustrated in figure A-4. It can be observed that the angle of cross-over can be determined in terms of the fabric ply thickness and the distance between two consecutive yarns. The calculated volume fractions were then used along with the three different assumptions to yield bounds on the overall elastic properties of the woven fabric.

The results obtained by using the layered-plate fabric model for plain weave and 8 harness satin fabrics are shown in figure A-5. The results indicated very little difference in the in-plane elastic modulus between the plain weave and the 8 harness satin fabric based on both the upper and lower bounds. Also, the in-plane shear moduli of the fabrics were almost identical to the shear moduli of the unidirectional fiber bundles. The bounds were observed to be far apart so that it was not possible to ascertain the validity of the results. An improved lower bound was then obtained by subdividing the repeating element into layers parallel to the thru the thickness direction. This resulted in the fabric consisting of layers of 0/90 and crossover material for 3 and higher harness satin fabrics. Utilizing the geometry of the yarns as shown in figure A-2, appropriate volume fractions were calculated for the 0/90 material and segments of the crossover. The fabric in-plane modulus was then obtained through a lower bound formulation by considering the stiffnesses and the volume fractions of the sub-layers. This resulted in higher values as compared to the one obtained earlier because in this approach the oriented yarns only affect the stiffnesses of the crossover region. Thus, although the lower bound results for the plain weave (two harness satin) fabric were identical for both approaches, the 0/90 material without any crossover material improved the lower bound stiffnesses for higher harness number fabrics.

Another disadvantage with the layered-plate model was that the maximum prism volume fractions of the yarns was about 55-60%, which meant that the fabric contained large amounts of interstitial matrix. Examining photomicrographs of T300/5208 fabrics indicated that in actuality, the volume of interstitial matrix pockets was negligibly small and that the yarn flattened and changed shape along its length. Since the layered-plate fabric model did not yield very satisfactory results it was considered necessary to develop a geometrically compatible model. The following paragraphs contain a description of the approach and results obtained for the geometrically compatible model.

"NDPROP" MODEL

The basic assumption used in constructing the geometric model was that the yarn cross-sectional area remained unchanged while taking on various shapes along its length. Even though the shape of the cross-sections varied continuously, it was assumed that the transition sequence within one repeating element could be represented by a few discrete shapes.

Based on these considerations, representative area elements were identified for commonly used weaves. These are shown in figure A-6. It can be observed from the figure that the 8 harness satin weave element is of the "over 7 under 1" type and consists of 4 distinct shapes that the yarn must take along its length within its repeating length of 8L. Here "L" refers to the yarn count, i.e., the average distance between successive yarns. It was assumed that the actual distance between any two successive yarns could be different from L, in order to accommodate changes in length, while keeping the overall length of the representative element unchanged. The representative elements of the other weaves were defined in a similar manner. For 3 and higher harness satin fabrics the number of distinct shapes of the yarn cross-section were kept unchanged. The lengths in which the transitions occurred were selected according to the repeating element geometry. For the plain weave fabric, another intermediate cross-section, a rectangle, was introduced to make the transition more gradual and realistic.

The sequence of transition within the representative area element for two typical fabric constructions is shown in figure A-7. The sequences for the higher harness satins can be readily extrapolated from that of the 3 harness satin fabric.

The next step in the procedure consisted of determining the required dimensions to define the repeating element completely. The weave parameters which were utilized to do this were: yarn cross-sectional area, fabric ply thickness and yarn count. In addition to these, it was necessary to assume a few other dimensions in order to make the geometry determinate. However, these assumptions were made in non-critical dimensions so that the end results were not affected significantly. Once the leading dimensions of the cross-sections were determined, the yarn cross-over angle, prism volume fractions of the bundle segments and the volume of the interstitial matrix pockets could be calculated. The complete transition sequences for 3 harness and plain weave fabrics are shown in figure A-8.

In order to compute the properties of the yarn from the properties of the unidirectional fiber bundle, each cross-section was broken down into several segments by joining each vertex to the centroid of the cross-section. Each fiber bundle was assumed to exist from a segment of one cross-section to the corresponding segment of an adjoining cross-section. The procedure used to determine volume fractions and direction numbers is outlined in figure A-9. In the same manner the entire yarn could be broken down into various segments with their corresponding direction numbers and volume fractions. The volume fractions were normalized with respect to the repeating element volume and then multiplied by the total prism volume fraction to account for the interstitial matrix pockets.

The resulting set of volume fractions and direction numbers along with the unidirectional fiber bundle properties were fed into "NDPROP" which is an MSC computer code used to predict properties and strengths for a composite with multidirectional reinforcement. The upper bound properties were obtained by volume averaging globally transformed stiffnesses of the various bundle segments, corresponding to the constant strain assumption. The lower bound prediction of stiffnesses were obtained by volume averaging the transformed compliances of the bundle segments, the assumption being that the stresses in the longitudinal and transverse yarns are constant.

The upper and lower bound predictions of Young's moduli are shown for the plain weave and 8 harness satin fabrics in figures A-10 through A-13. The in-plane elastic modulus bounds are far apart even in this approach. The lower bound predictions for the two different fabric types are not significantly different for both in-plane and thru the thickness moduli. However according to the upper bound prediction, an increase in the in-plane modulus is accompanied by a decrease in the thru the thickness modulus for the 8 harness satin as compared to the plain weave. The elastic moduli can be expected to approach the 0/90 laminate moduli as the harness number increases.

The shear modulus predictions for the plain weave and 8 harness are shown in figures A-14 and A-15. The in-plane shear modulus predictions agree fairly well with the layered-plate fabric model predictions. For the plain weave, the transverse shear modulus is significantly higher than the in-plane shear modulus. The differences between in-plane and transverse shear moduli are much smaller for the 8 harness satin fabric.

The differences in the properties between the plain weave and 8 harness fabrics can be explained in general by the differences in amounts of thru the thickness reinforcement. The 8 harness satin properties are very similar to the properties of a cross-plied laminate, as Table 1 in the main body of the report indicates. Hence, the 8 and higher harness satin fabrics would have the best in-plane properties and the plain weave fabric would have the best thru the thickness properties.

Although this approach led to reasonable trends in the results, the far apart bounds in the in-plane elastic moduli were a cause for concern. In order to determine which of the bounds gave a better representation of the fabric behavior a finite element analysis was conducted. For this analysis the plain weave fabric was utilized due to modeling ease.

FINITE ELEMENT ANALYSIS

The finite element model was a symmetric section of the plain weave repeating element of the geometrically compatible model. Linear three-dimensional isoparametric finite elements were used in the analysis. Since the cross-section of the yarns varied within the repeating element, it was necessary to use solids with fairly complex geometries. Further, the interstitial matrix pockets were also modeled to prevent inaccuracies in the results due to the presence of voids in the model. The nature of the model and the applied boundary conditions resulted in stiffness matrices of very large bandwidth. Therefore, the finite model was made somewhat coarse (101 modes and 107 elements) for the sake of modeling ease and minimizing computer run times. The finite element model is shown schematically in figure A-16 along with the applied boundary conditions. The complete finite element model with all the element boundaries is shown in figure A-17.

The finite element results have been compared with the upper and lower bounds of the NDPROP model in figures A-18 and A-19. The analyses were conducted for four different volume fractions. Both the in-plane and thru the thickness moduli exhibited a consistent trend as can be observed from figures A-18 and A-19 respectively. The results appear to be reasonable and it can be observed that the finite element predictions are not significantly closer to either of the bounds. This indicates that neither the constant stress nor constant strain assumptions are good representations of fabric behavior. One of the reasons for the low in-plane elastic modulus obtained through the finite element analysis appeared to be the particular model geometry chosen with the high crossover angle of 53°. In order to study the effects of the crossover angle and thereby the relative amounts of horizontal and oriented yarn segments, two dimensional finite element analyses were conducted. The repeating element cross-sections shown in figure A-6 were modeled for plane strain analyses. The modulus from the 2-D analysis was about 5% lower than that from the 3-D analysis for the original geometry (crossover angle = 53°). The model was therefore verified to be accurate enough to compare effects of geometry changes. The plain weave moduli were observed to be very strong functions of the crossover angle. For example, the modulus for the T300/Epoxy Plain Weave fabric ($v_f = 0.60$) was calculated to be 4.10 Msi for a crossover angle of 53° and 6.96 Msi for an angle of 15°.

The 2-D plane strain analyses were also done for higher harness fabrics. The comparisons of the finite element results with those from the various approaches are presented at the end of this section.

Since the NDPROP and Layered-Plate model bounds were quite far apart, attempts were made to develop improved bounds based on a simplified fabric model. The following paragraphs described the analytical methodology and the results of this approach.

SIMPLIFIED FABRIC MODEL

The simplified fabric model consisted of four oriented yarn bundles with none of the bundles containing any straight horizontal segments. All four bundles were inclined at the same angle with respect to the thru the thickness direction and balanced in the in-plane direction, see figure A-20. An improved lower bound approach was formulated for this model based on the assumption that the transverse stresses in the bundles were the same as the state of stress in the interstitial matrix. Contributions of the longitudinal and transverse strands and the matrix material to the complementary strain energy were evaluated in terms of the applied in-plane stress in order to arrive at an improved lower bound for the in-plane elastic modulus. The upper bound calculations for this model were obtained in the same manner as for the NDPROP model.

The results of this approach are shown in figure A-21 for plain weave fabrics for different amounts of reinforcement. The orientation angle of the yarns was obtained from the fabric yarn count and ply thickness values used for the other models. The finite element results could not be compared to these results on the same basis since the geometries of the two models were different. The simplified model is, in fact, spatially compatible only up to a total yarn prism volume fraction of 75%. Accordingly, the results shown in figure A-21 are for a 75% prism volume fraction and a bundle volume fraction of 60%. The bounds predicted by this approach are indeed much closer together.

The same model was also utilized to calculate thru the thickness moduli. The results are shown in figure A-22. It can be observed from this figure, that the predicted values are in good agreement with earlier approaches and the bounds are quite close.

CONCLUSIONS FROM MODELING EFFORTS

The comparison between the results of the various approaches are shown in figure A-23. Also shown in figure A-23 are the results of the work done in this area by Ishikawa and Chou, reference A-1. A review of their work indicated that three different models were used by them for the prediction of fabric elastic properties. The first model, termed the mosaic model, assumed that the fabric composite could be modeled as a assemblage of pieces of cross-ply laminates. The effect of the inclined transition region of the fabric was neglected in the mosaic model. The fiber undulation model included this effect and hence was thought to be more realistic for plain weave fabrics. The third model was the bridging model which employed a two-dimensional repeating element of the fabric to account for the load transferring mechanisms in interlaced regions which are separate from one another, as in higher harness satin fabrics. The results of each of the three models are shown in Figure A-23.

It was observed from finite element analyses that the results approached the Upper Bound for low crossover angles. For fabrics of high quality (low interstitial matrix volume and low cross-over angles) the upper bound approaches will thus be appropriate. The "NDPROP" model is a geometrically compatible model and is a realistic three-dimensional representation of a woven fabric. Further, the "NDPROP" Upper Bound predicts trends that are reasonable and provides a complete set of fabric properties.

Therefore, the "NDPROP" Upper Bound was selected from among the various approaches to calculate woven fabric properties.

REFERENCES

A-1. Ishikawa, T. and Chou, T. W., "Stiffness and Strength Behavior of Woven Fabric Composites," Journal of Materials Science, 17, 1982.

Table A-1. Unidirectional T300/Epoxy Properties used for prediction of woven Fabric Properties

Property	$v_f = 0.2$	$v_f = 0.3$	$v_f = 0.4$	$v_f = 0.5$	$v_f = 0.6$
E_L, Msi	7.10	10.4	13.7	17.0	20.3
E_T, Msi	0.707	0.820	0.958	1.126	1.334
G_{LT}, Msi	0.275	0.332	0.404	0.499	0.630
ν_{LT}	0.3	0.3	0.3	0.3	0.3
ν_{TZ}	0.394	0.381	0.367	0.355	0.347

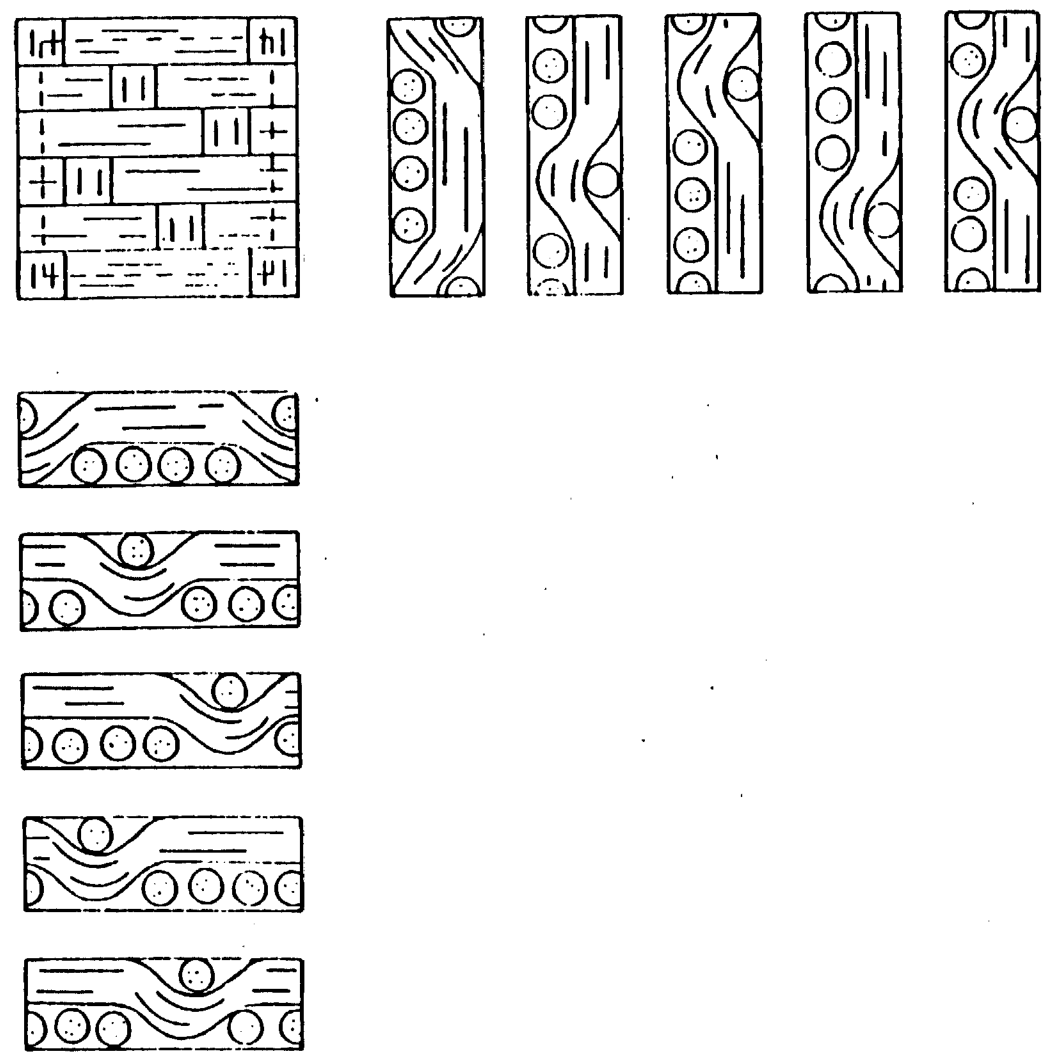

Figure A-1. Representative Volume Element of 5 Harness Satin Layered-Plate Fabric Model.

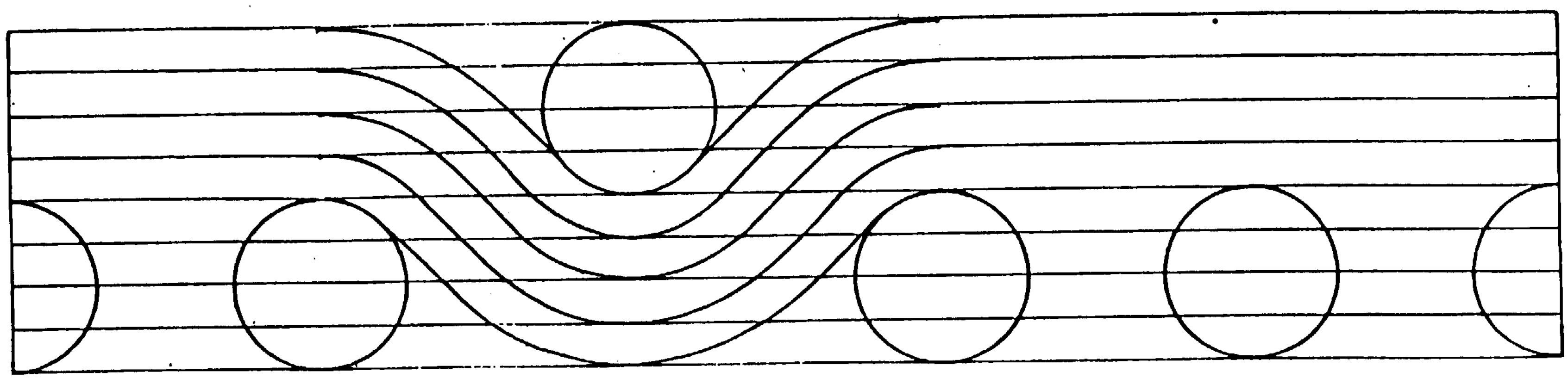

Figure A-2. Cross-Section of 5 Harness Satin Layered-Plate Fabric Model.

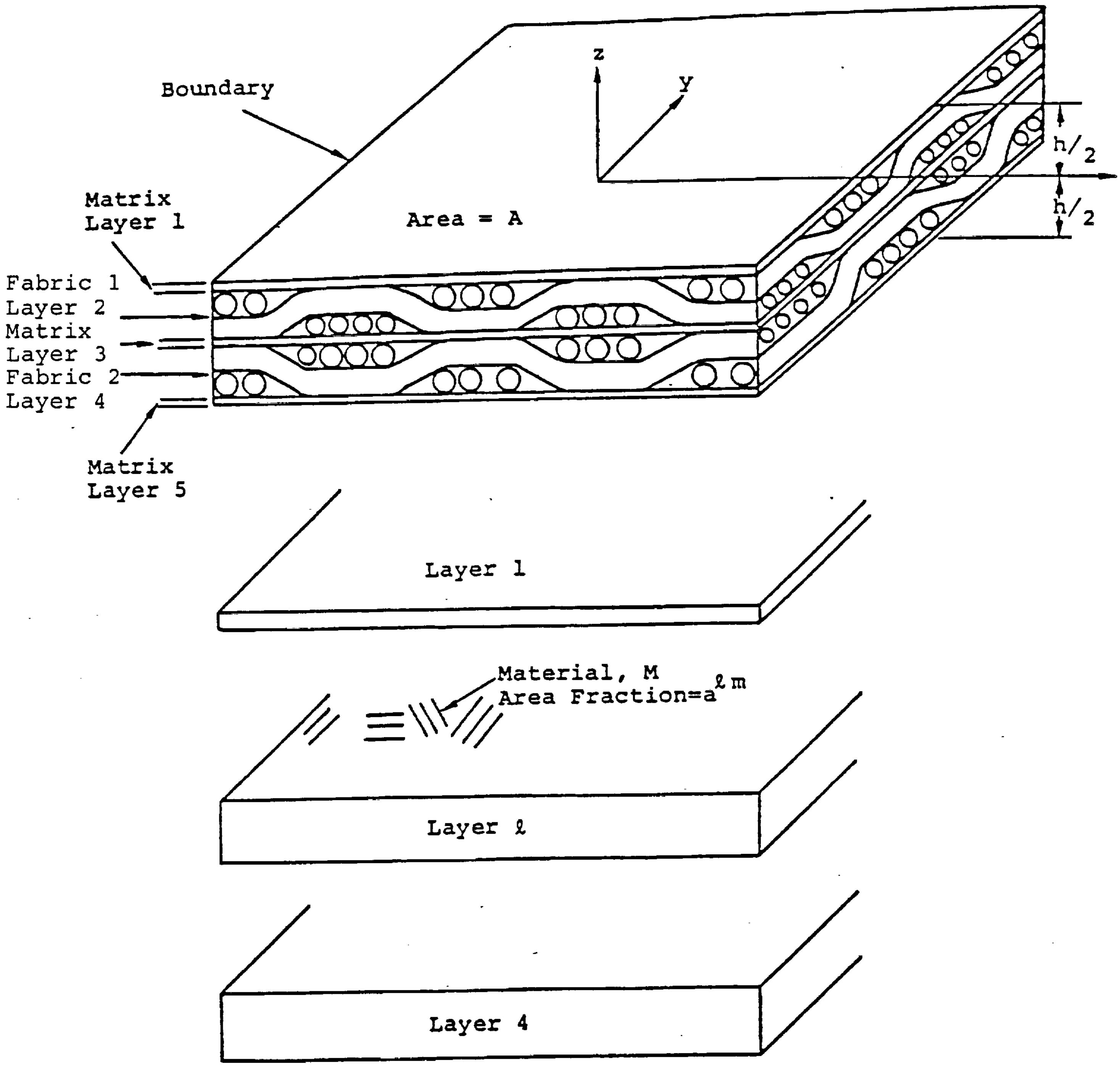

Figure A-3. Representative Area Element RAE Containing Several Layers for Layered-Plate Fabric Model

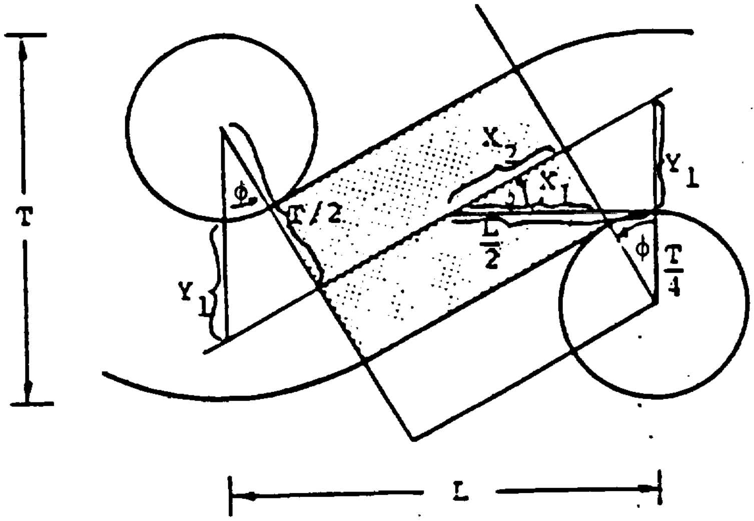

$$Y_1 = T\left(\frac{1}{2\cos\phi} - \frac{1}{4}\right); \quad X_1 = T\left(\frac{\frac{1}{\cos\phi} - \frac{1}{2}}{2\tan\phi} - \frac{1}{4}\tan\phi\right); \quad X_2 = X_1 \cos\phi$$

$$L = \frac{T}{\tan\phi}\left(\frac{1}{\cos\phi} - \frac{1}{2}\right)$$

ϕ can be determined from above equation given L and T

Volume of cross-over material: $(2\ X_2)\ (\frac{T}{2})\ (L)\ (2N)$

Volume of material in RVE: $T\ (NL)\ (NL)$

where N = Harness number of weave

Volume fraction of cross-over material:

$$v_\phi = \left(\frac{\beta}{2} - \frac{\tan\phi}{2}\right) \cos\phi/N\beta$$

where $\beta = \dfrac{\frac{1}{\cos\phi} - \frac{1}{2}}{\tan\phi}$

Figure A-4. Calculation of Volume Fraction of Cross-Over Material in Representative Volume Element, Layered-Plate Fabric Model.

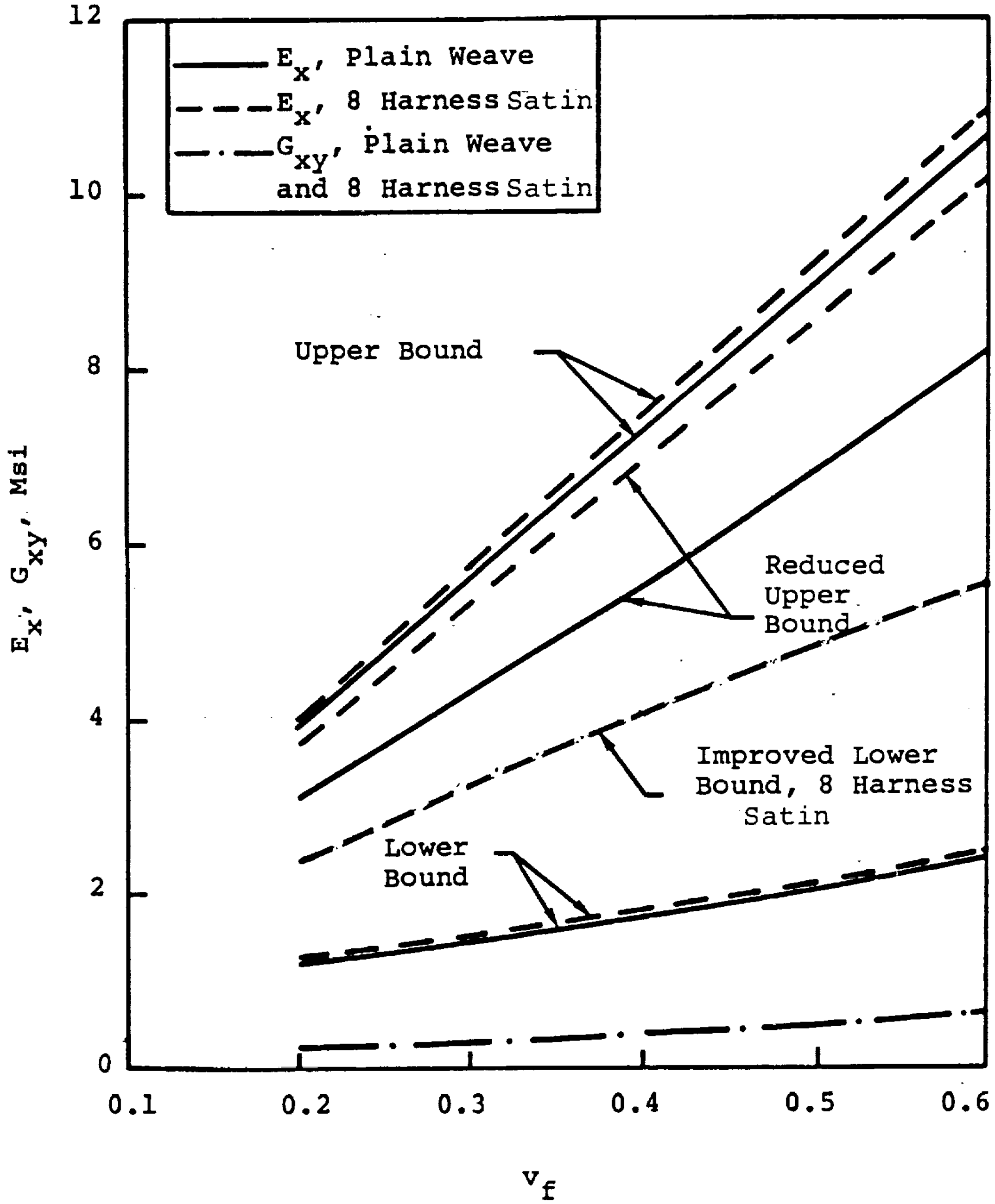

Figure A-5. Woven Fabric In-Plane Elastic Properties versus Fiber Content, Layered-Plate Fabric Model.

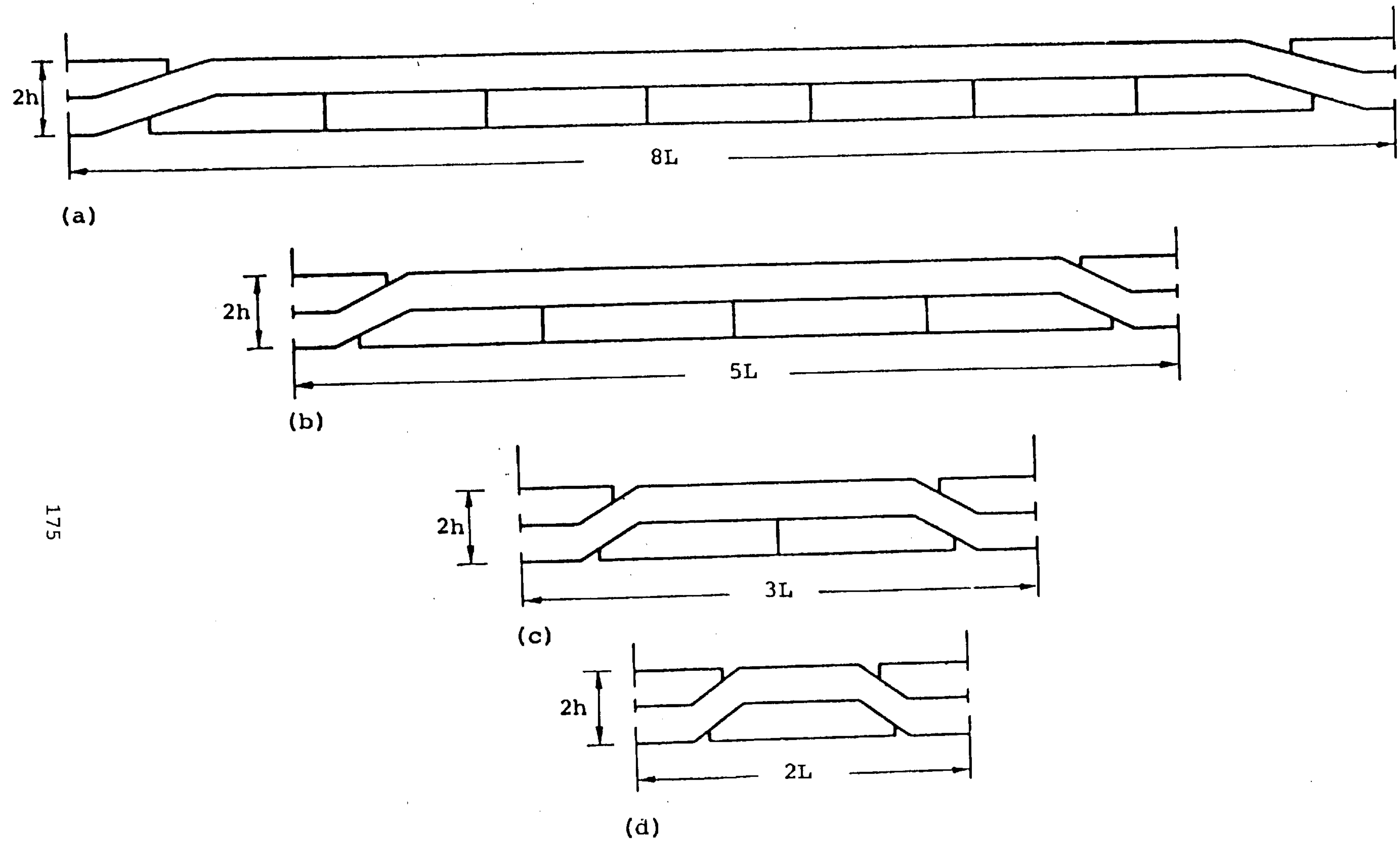

Figure A-6. Representative Area Element of (a) 8-Harness Satin, (b) 5-Harness Satin, (c) 3-Harness satin and (d) Plain Weave Woven Fabrics, NDPROP Model.

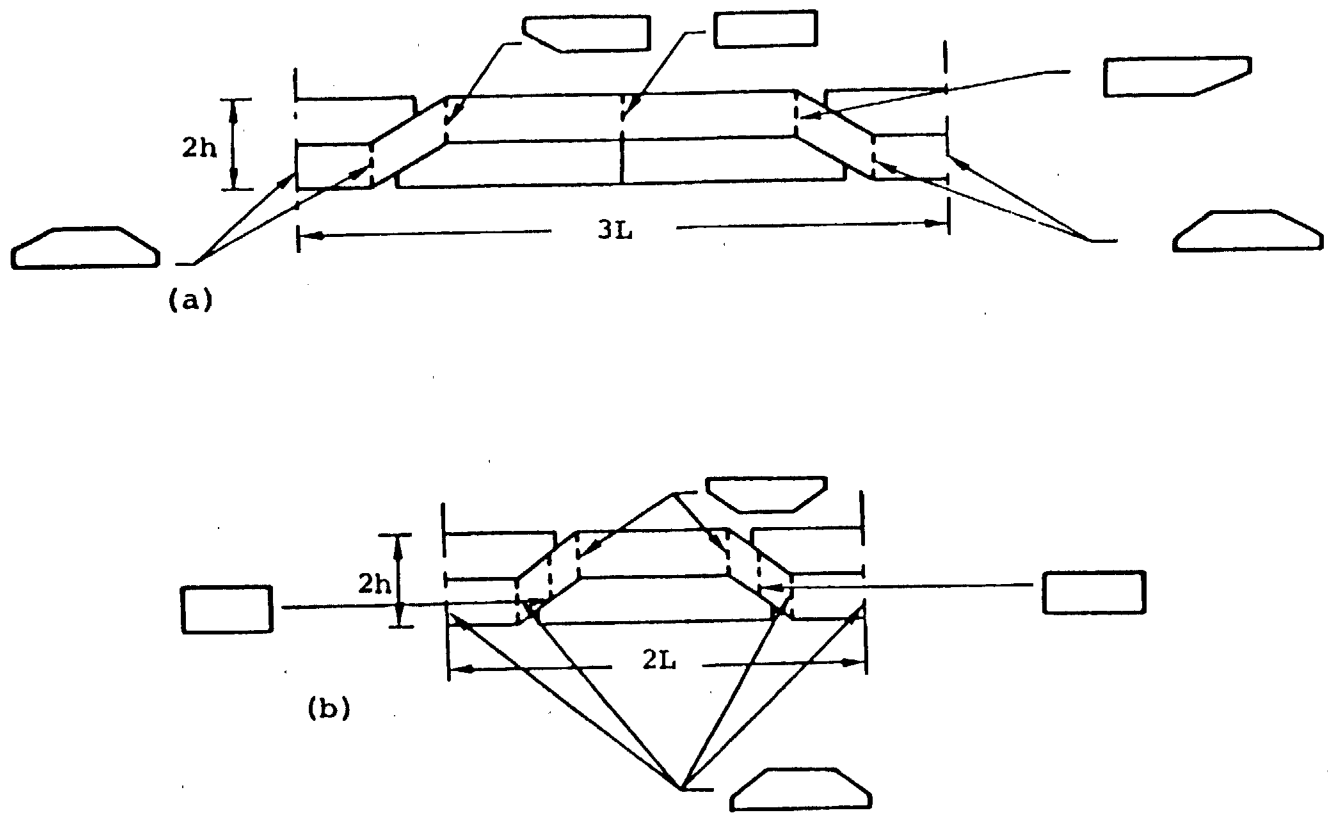

Figure A-7. Yarn Cross-Sections at Selected Locations for the Representative Area Element of (a) 3-Harness Satin and (b) Plain Weave Woven Fabrics, NDPROP Model.

NOTE: Indicated Cross-Sections are not drawn to scale.

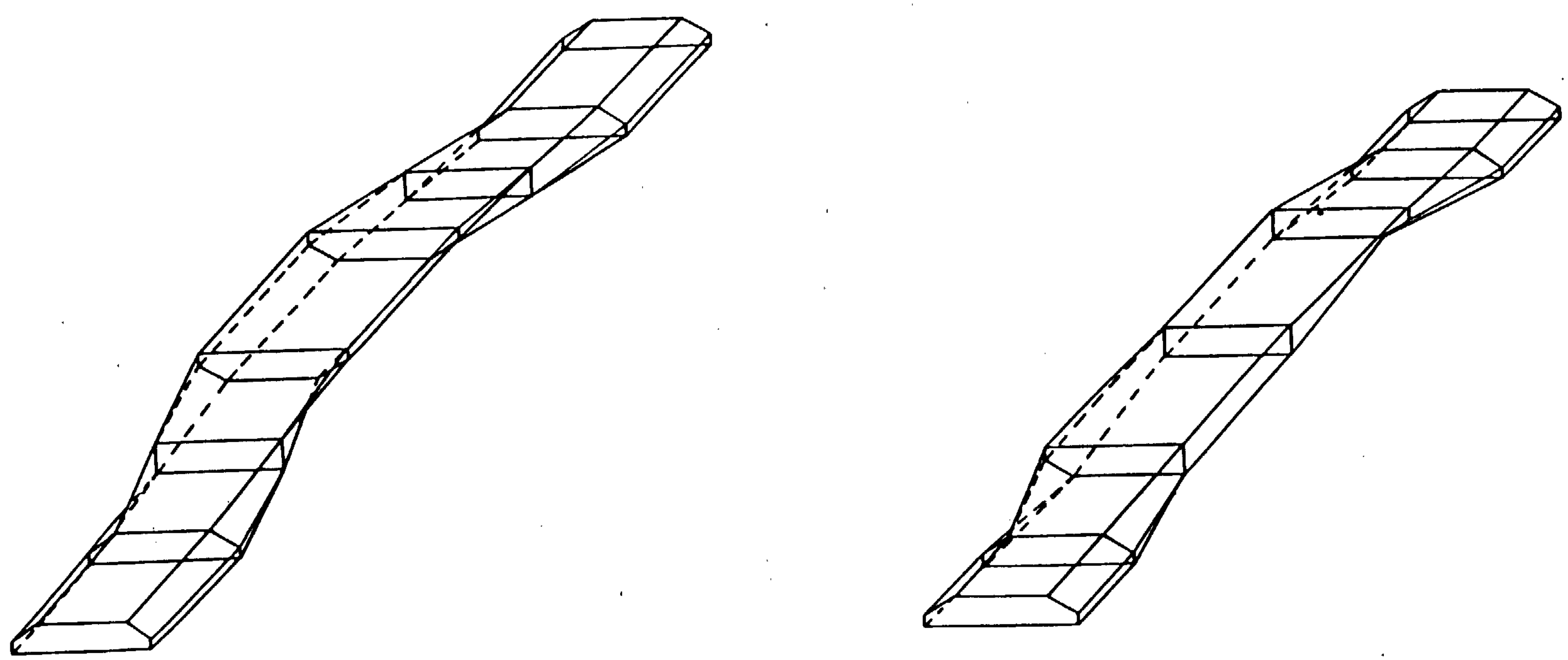

(a) (b)

FigureA-8. Transition sequences of (a) Plain Weave and (b) 3 Harness Satin Fabrics, NDPROP Model.

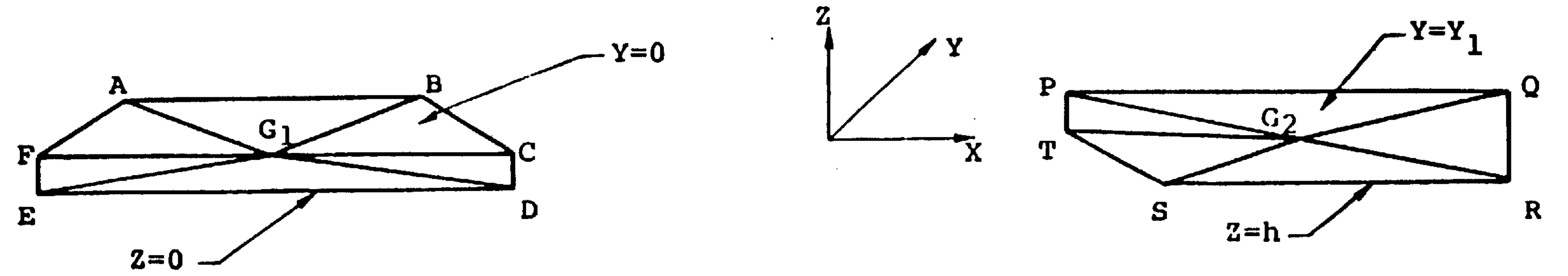

	Direction	Volume Fraction
Bundle 1:	$BG_1C \longrightarrow QG_2R$	$(BG_1C + QG_2R)/2A$
Bundle 2:	$CG_1D \longrightarrow RG_2$	$CG_1D/2A$
Bundle 3:	$DG_1E \longrightarrow RG_2S$	$(DG_1E + RG_2S)/2A$
Bundle 4:	$EG_1F \longrightarrow SG_2T$	$(EG_1F + SG_2T)/2A$
Bundle 5:	$FG_1A \longrightarrow TG_2P$	$(FG_1A + TG_2P)/2A$
Bundle 6:	$AG_1B \longrightarrow PG_2Q$	$(AG_1B + PG_2Q)/2A$

Where A = cross-sectional area of yarn

and h = one-half the fabric ply thickness.

Figure A-9. Approach for Calculating Direction Numbers and Volume Fractions for Various Segments within a Typical Yarn Section, NDPROP Model.

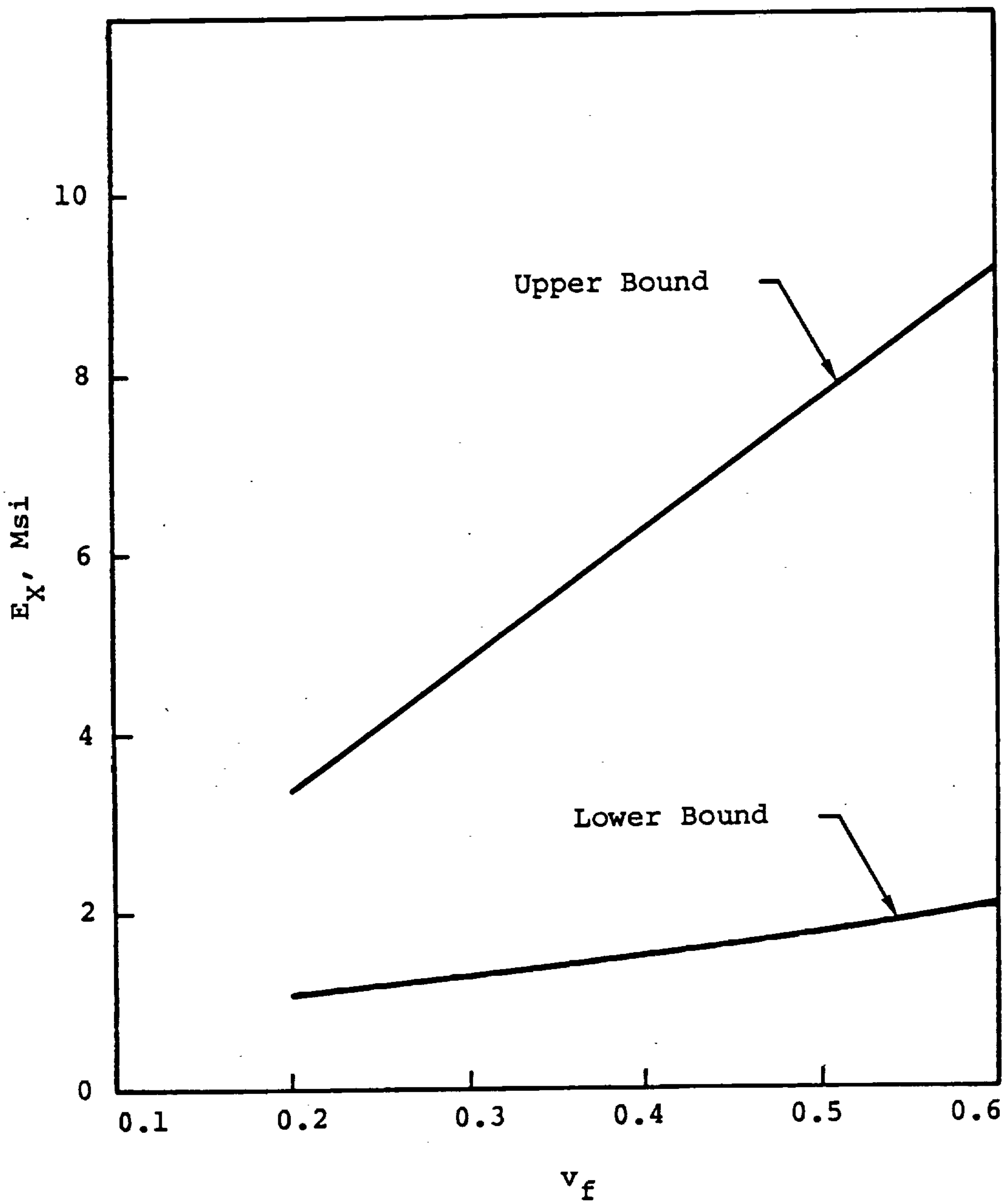

Figure A-10. Predicted Bounds for Plain Weave Fabric In-Plane Elastic Moduli, NDPROP Model.

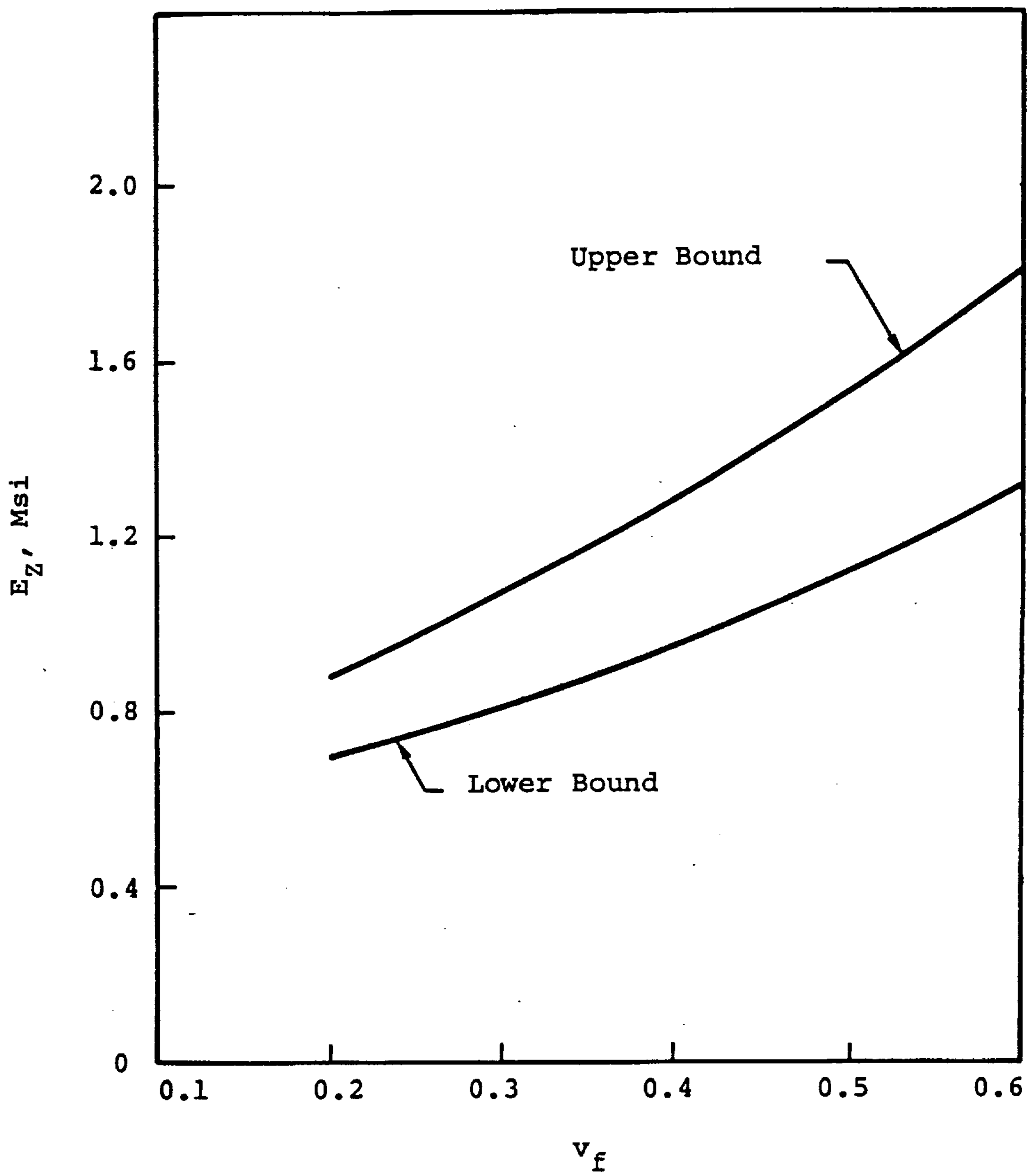

Figure A-11. Predicted Bounds for Plain Weave Fabric Through-the-thickness Elastic Moduli, NDPROP Model.

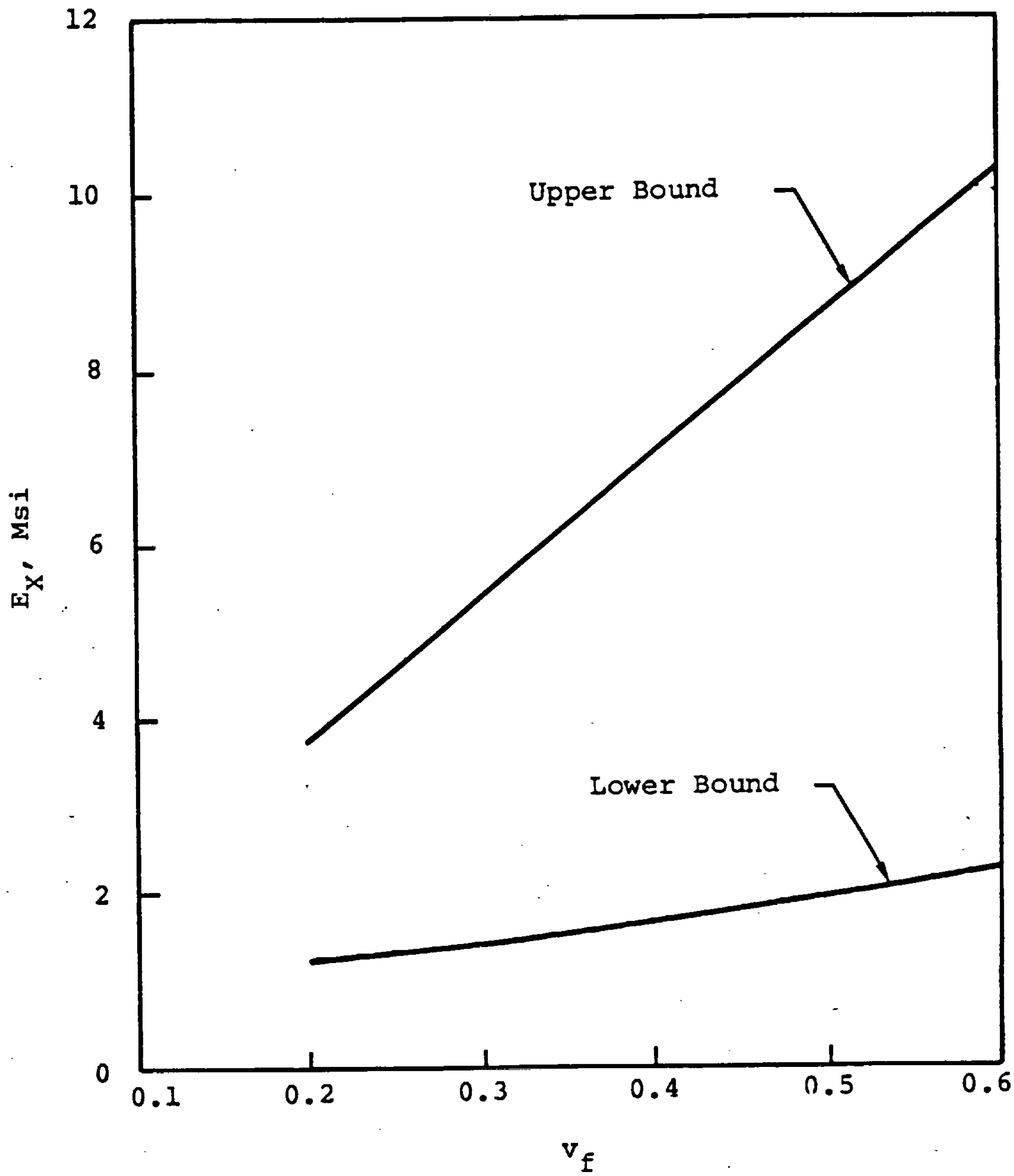

Figure A-12. Predicted Bounds for 8 Harness Satin Fabric In-Plane Elastic Moduli, NDPROP Model.

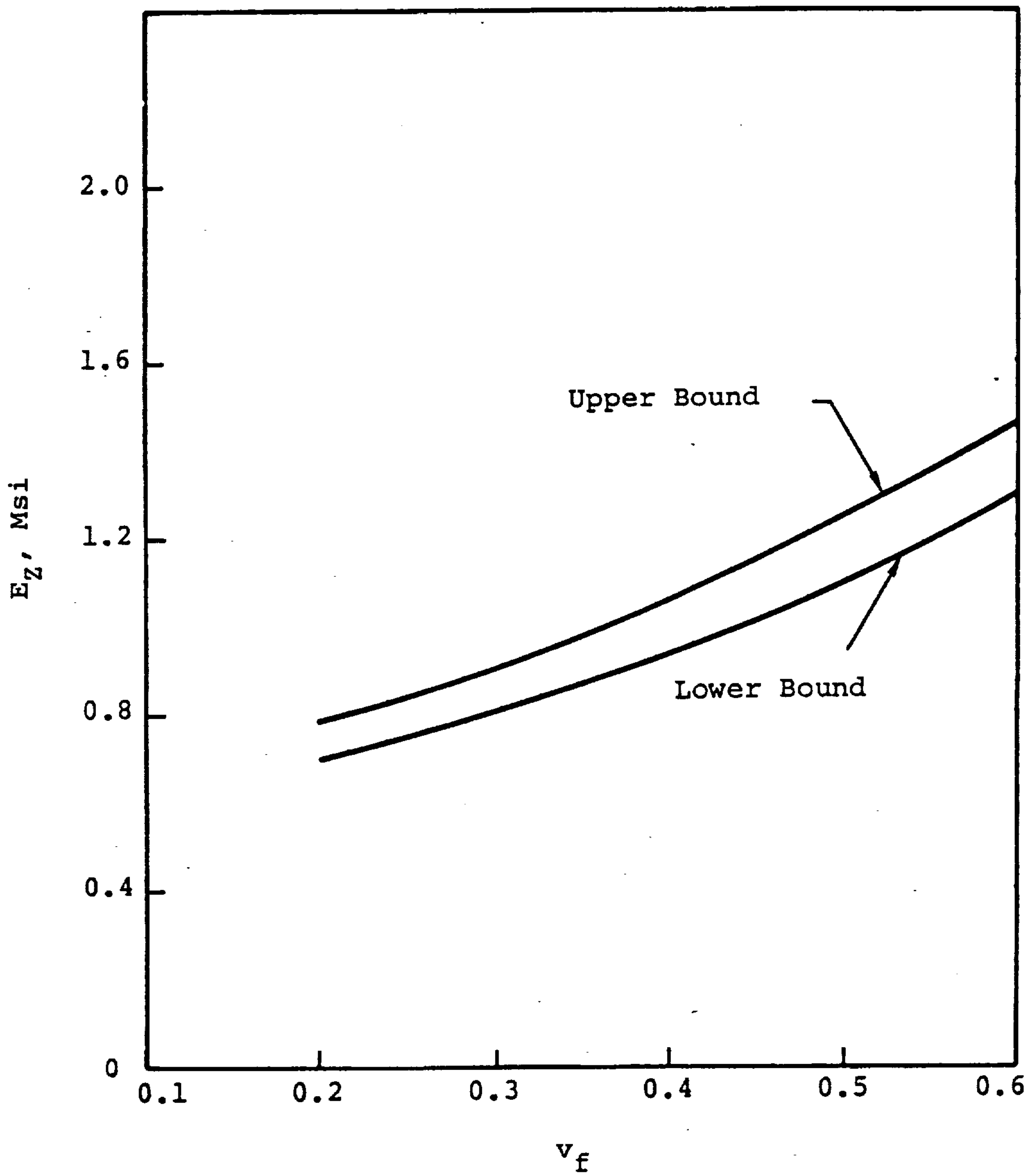

Figure A-13. Predicted Bounds for 8 Harness Satin Fabric Through-the-thickness Elastic Moduli, NDPROP Model.

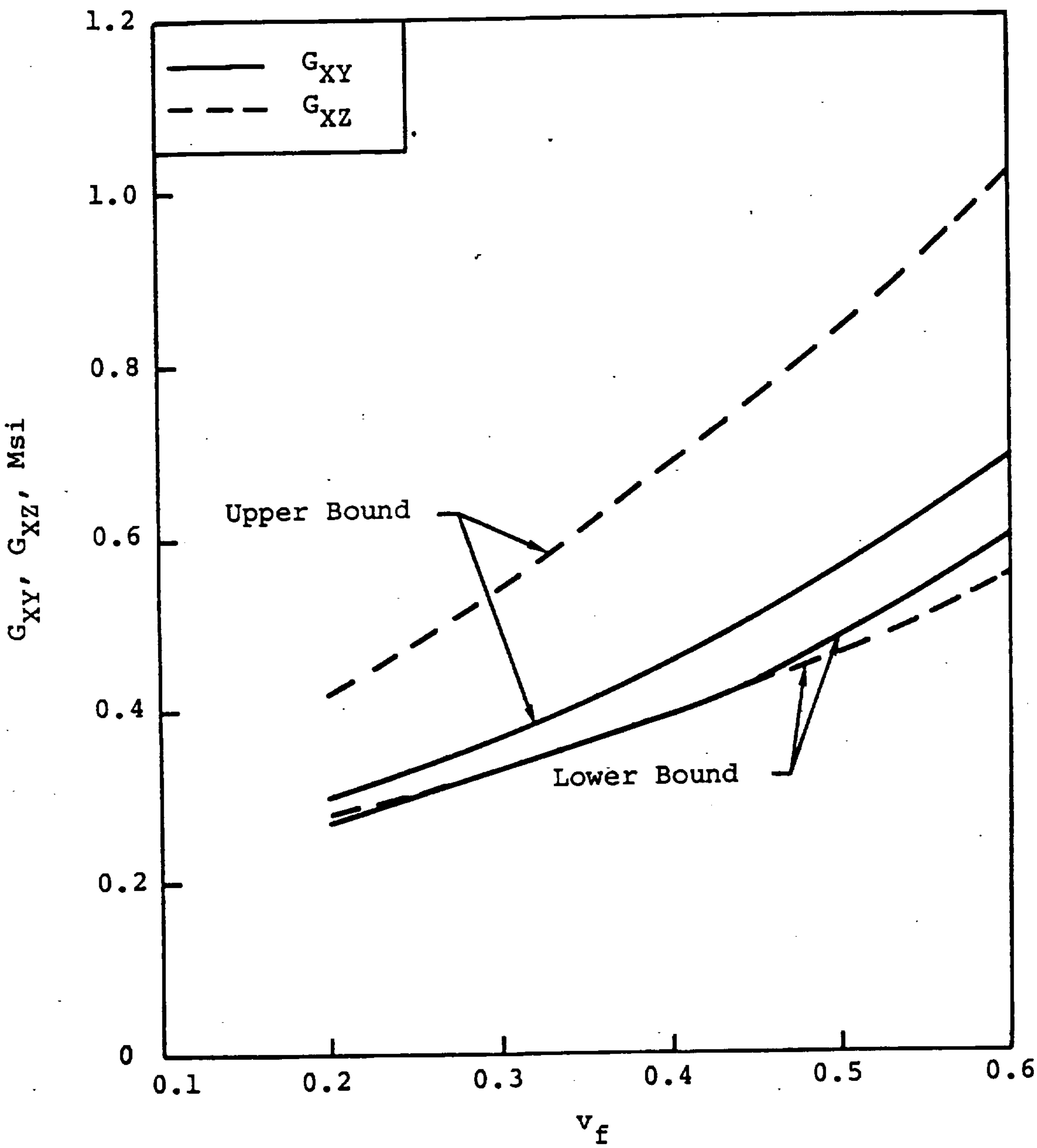

Figure A-14. Predicted Bounds for Plain Weave Fabric Shear Moduli, NDPROP Model.

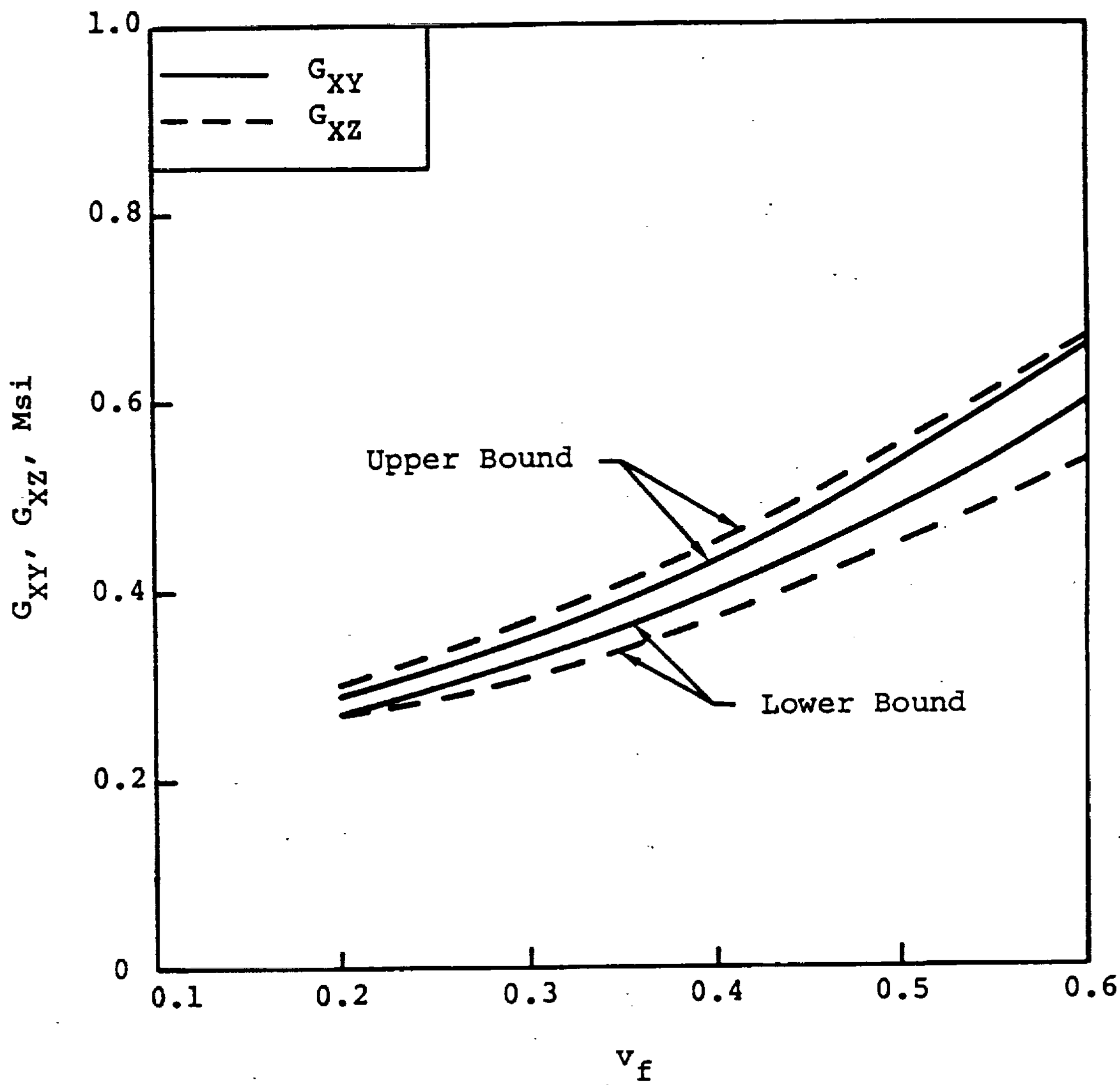

Figure A-15. Predicted Bounds for 8 Harness Satin Fabric Shear Moduli, NDPROP Model.

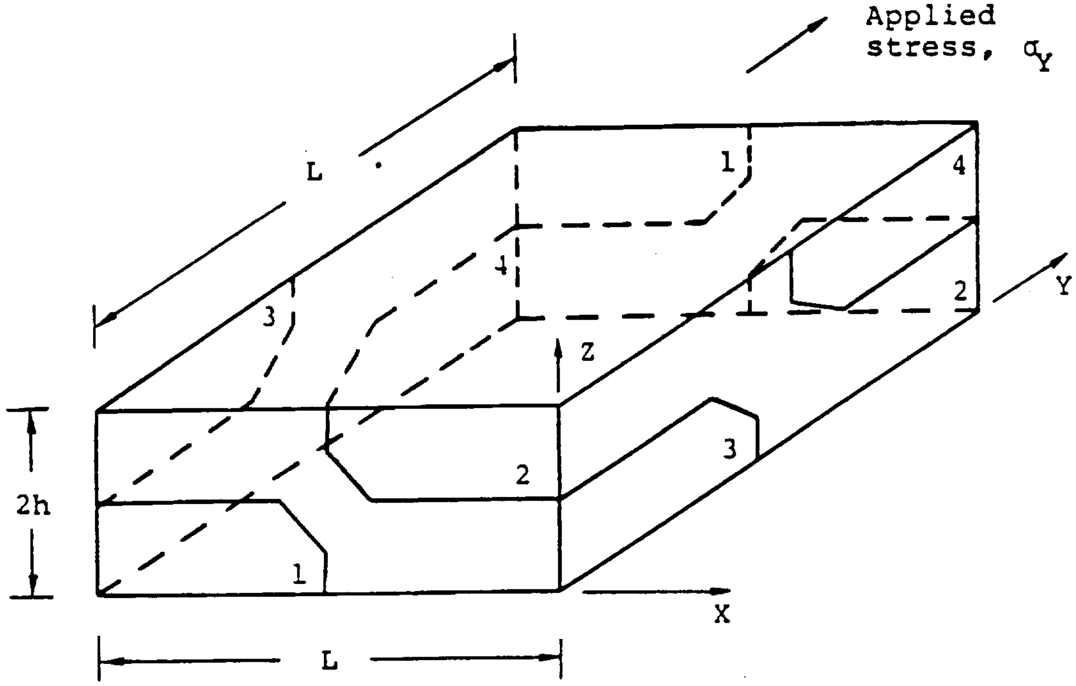

Boundary Conditions:

Surface X = 0, UX = 0

Surface Y = 0, UY = 0

Surface X = -L, UX uniform

Surface Y = L, UY uniform

At (0,0,0), UZ = 0

Figure A-16. Plain Weave Fabric Finite Element Model and Applied Boundary Conditions.

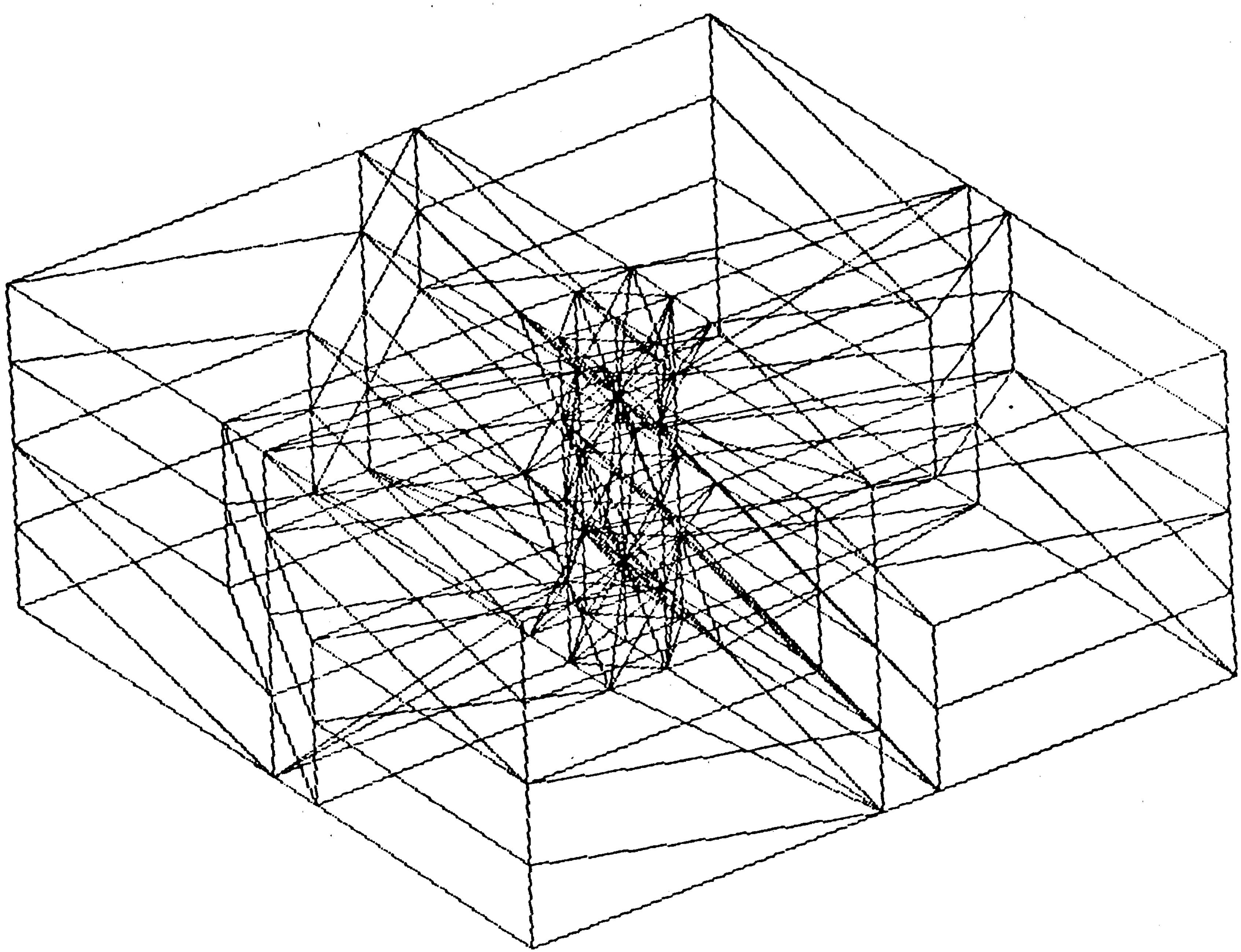

Figure A-17. Plain Weave Fabric Finite Element Model

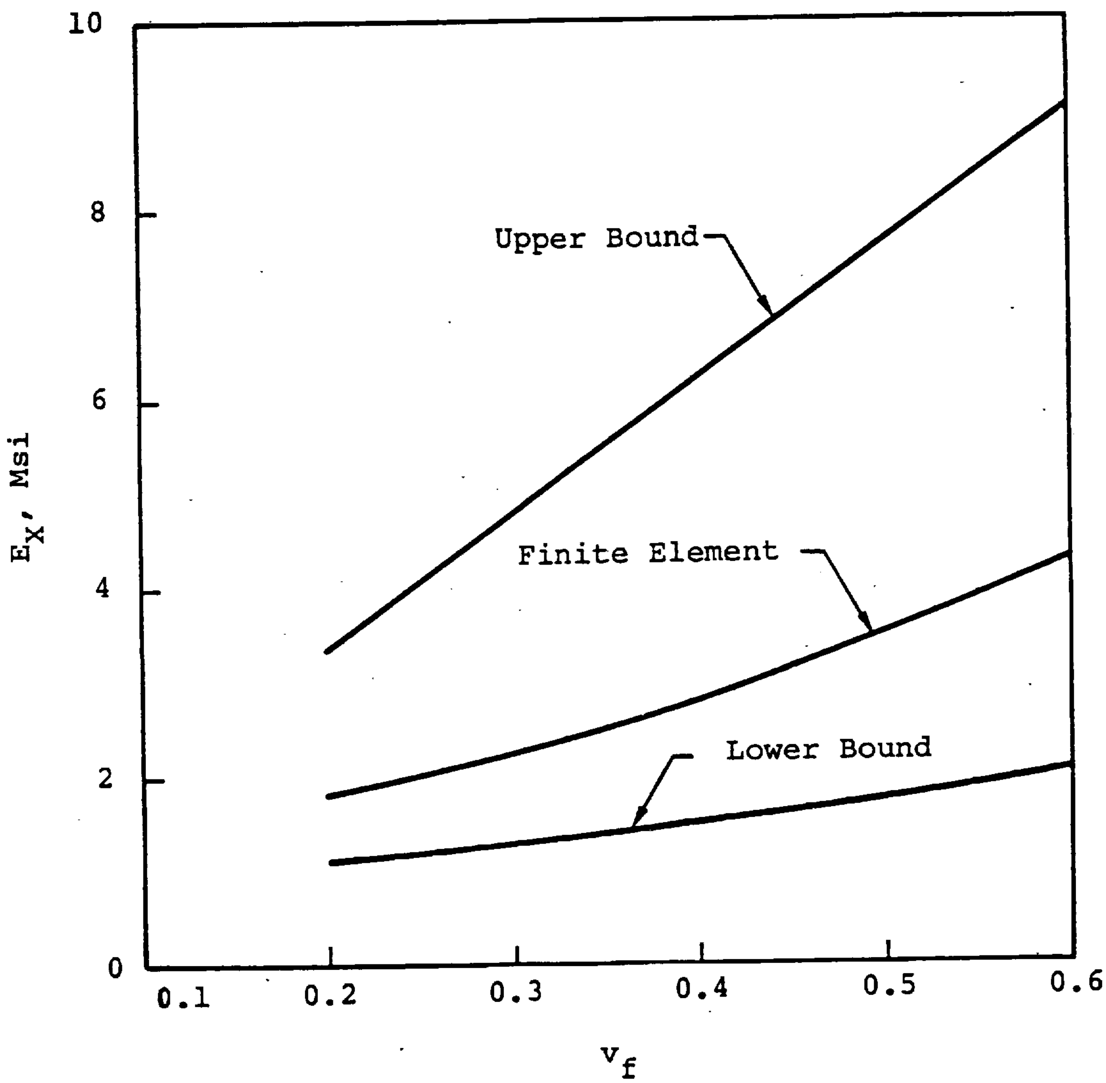

Figure A-18. Comparison of Plain Weave Fabric In-Plane Elastic Moduli Bounds with Finite Element Results, NDPROP Model.

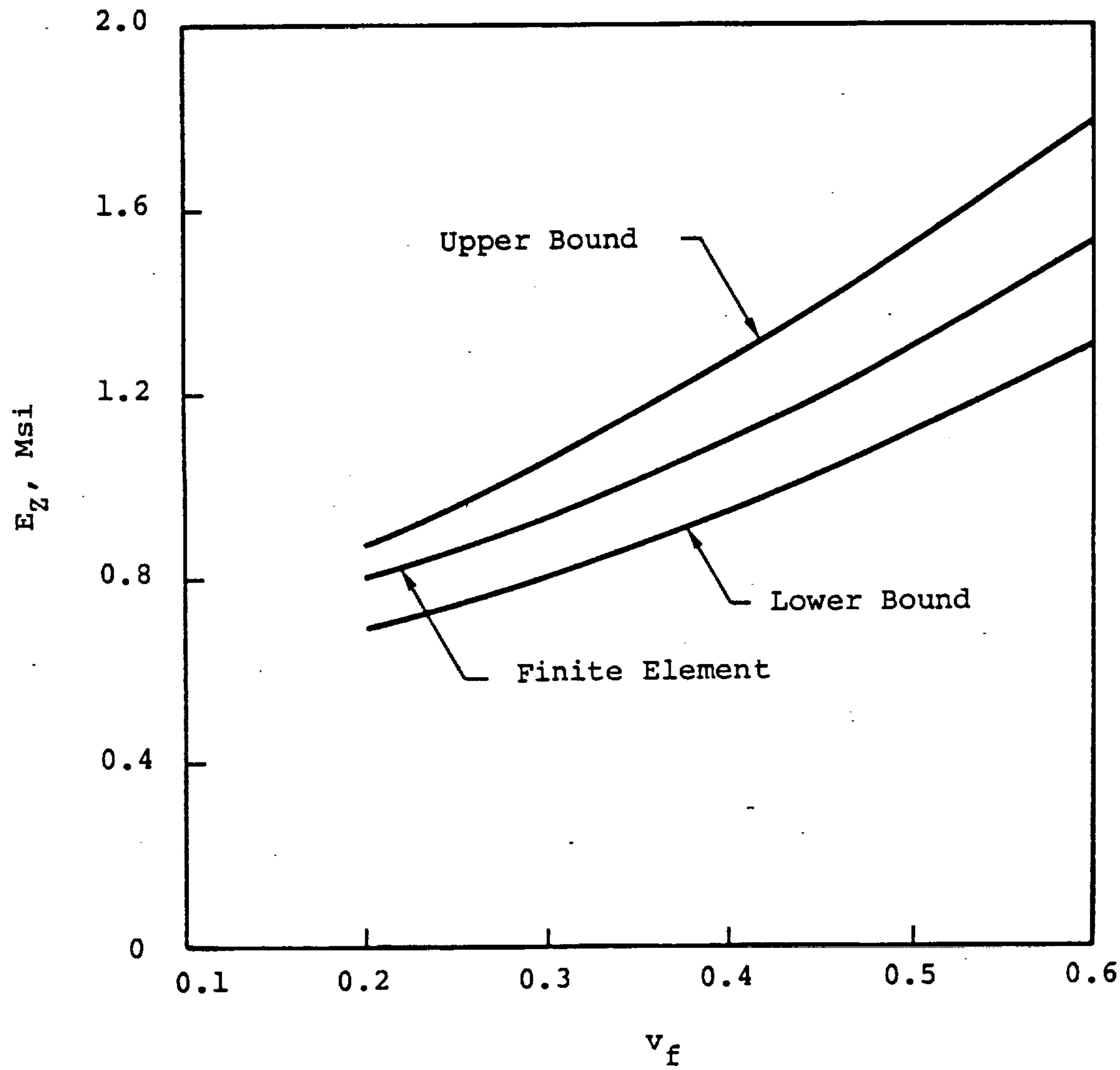

Figure A-19. Comparison of Plain Weave Fabric Thru the Thickness Elastic Moduli Bounds with Finitee Element Results, NDPROP Model.

C-3

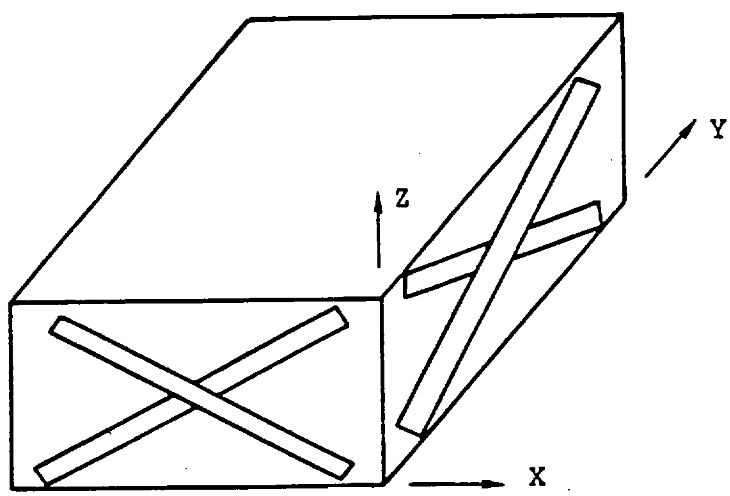

Figure A-20.Schematic Representation of Simplified Plain Weave Fabric Model

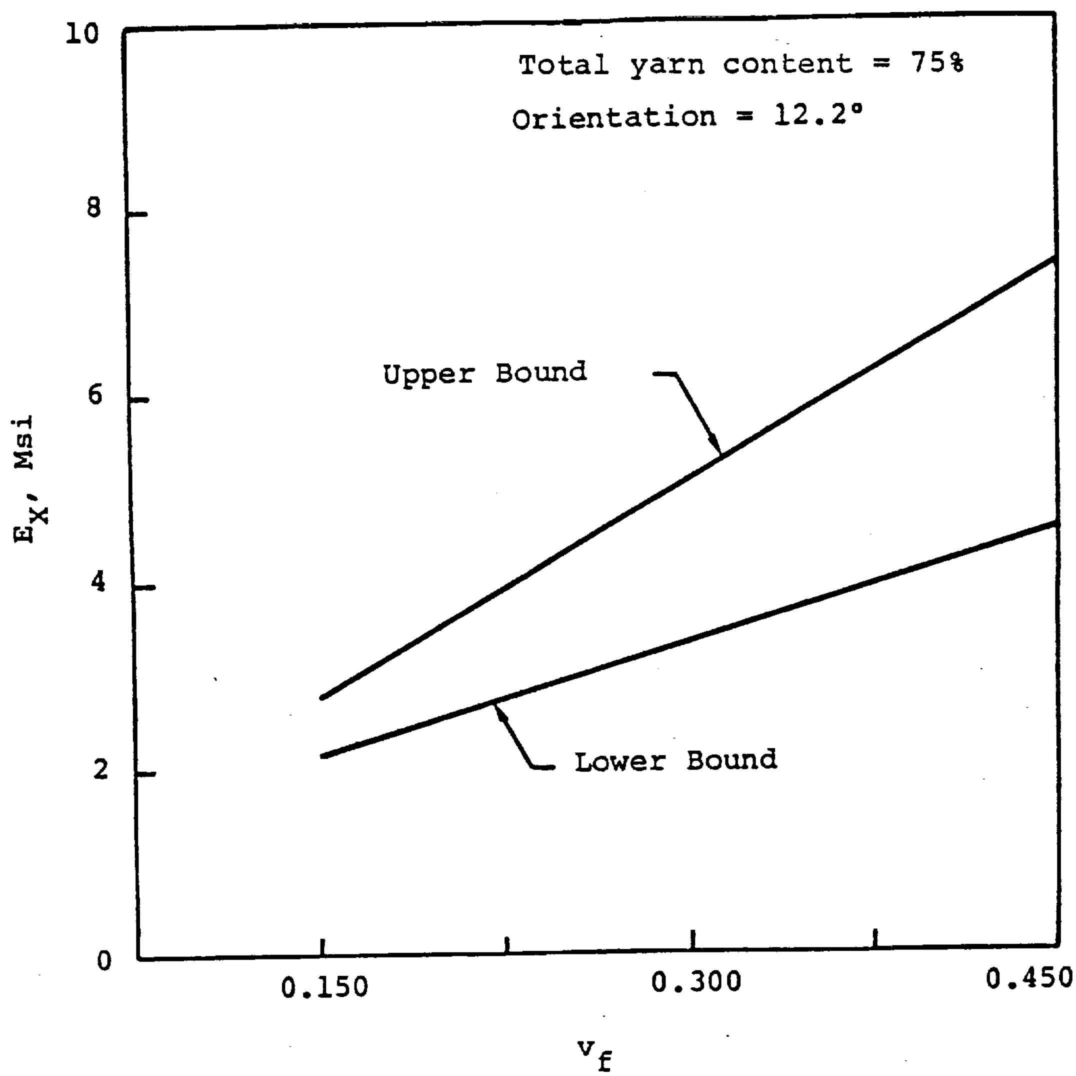

Figure A-21. Predicted Bounds for Plain Weave In-Plane Elastic Moduli, Simplified Model.

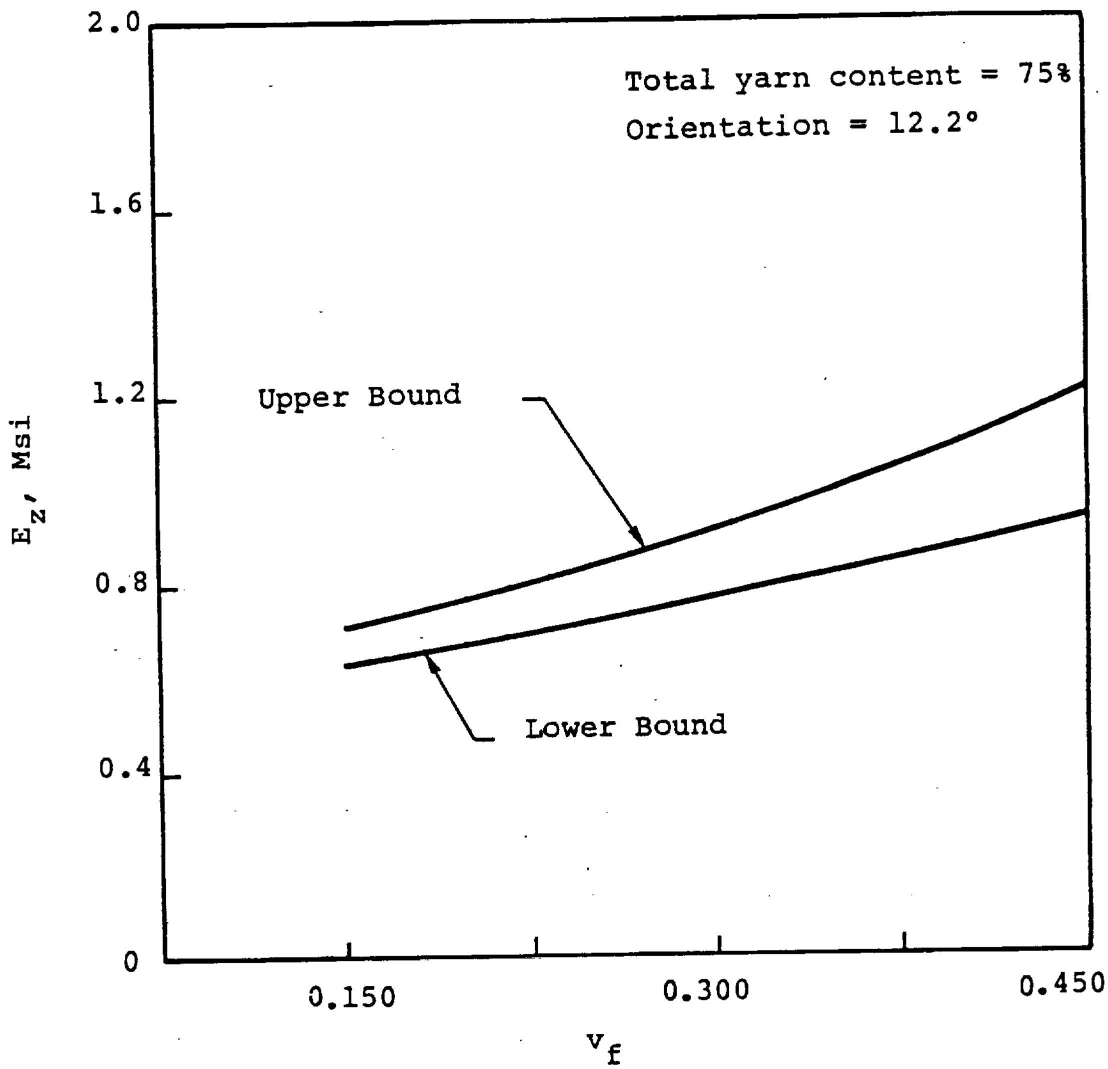

Figure A-22. Predicted Bounds for Plain Weave Thru the Thickness Elastic Moduli, Simplified Model.

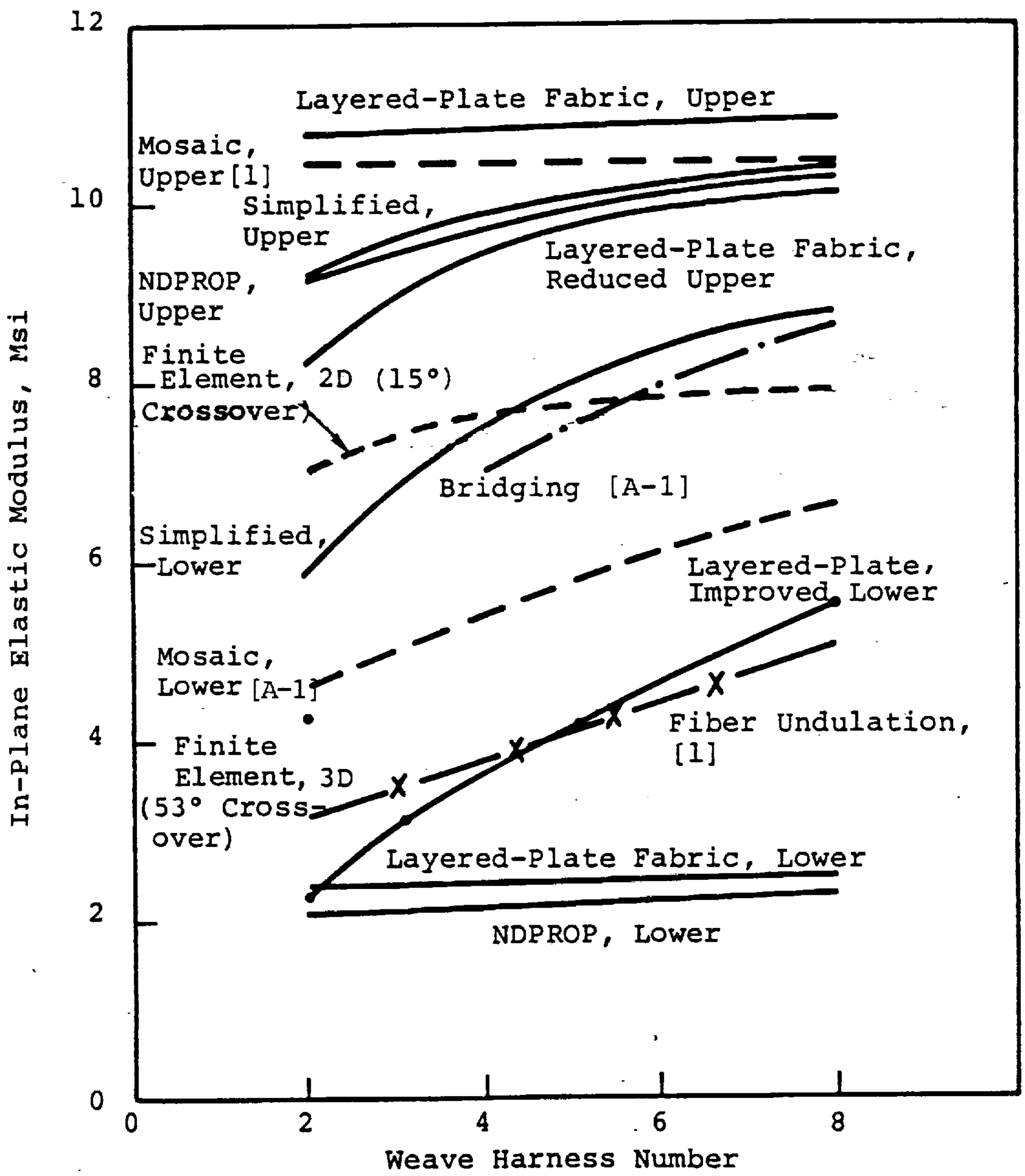

Figure A-23. Predicted In-Plane Elastic Moduli of T300/Epoxy Woven Fabrics (v_f = 0.60) as a Function of the Weave Harness Number through Various Approaches.

APPENDIX B

THE AVERAGE STRESS MODEL FOR THE ANALYSIS OF STRENGTHS OF WOVEN FABRIC COMPOSITES

LIST OF SYMBOLS

(As used in Appendix B)

E_L	longitudinal Young's Modulus
S_{ijkl}	compliance Matrix
v	volume fraction
ϵ_{ij}	strain tensor
σ_{ij}	stress tensor
σ_f	allowable fiber stress
σ_m	allowable matrix normal stress
τ_m	allowable matrix shear stress

SUPERSCRIPTS

f	fiber
m	matrix
*	unidirectional composite
+	tension
-	compression
tu	tensile ultimate
cu	compressive ultimate

APPENDIX B

THE AVERAGE STRESS MODEL FOR THE ANALYSIS OF STRENGTHS OF WOVEN FABRIC COMPOSITES

An approach to evaluate the strengths of fabric composites was formulated utilizing the "NDPROP" Upper Bound model, described in Appendix A and the "Average Stress Model". This appendix contains a description of the "Average Stress Model" approach.

Utilizing the fabric geometrical parameters such as yarn count and ply thickness, total fiber content and fiber cross-sectional area within the yarns, the inputs of direction numbers and volume fractions of yarn bundle segments could be generated. The elastic properties of the fabric were determined using this input and the "NDPROP" code. The same input geometry was then used as the basis for the strength analysis.

The first step of the procedure involved the determination of stresses and strains in the various yarn bundle segments due to the applied stresses in the fabric composite. Conventional three-dimensional stress analysis was therefore utilized for this purpose.

Since each (warp or fill) yarn had been discretized into several bundles, it was believed that the failure analysis would be more realistic if it was done on a fiber and matrix level rather than on a yarn bundle level. Accordingly, the next step involved the determination of stresses within the constituent fiber and matrix for the different yarn bundle segments comprising the fabric composite. The "Average Stress Model" was utilized for this purpose. This model postulates that although the stresses in the fiber and matrix vary from point to point, the failure stress level depends on the magnitudes of the average stress states within the fiber and matrix. The formulation of the "Average Stress Model" and the associated equations are shown in Table B-1. It can be observed from the table that the matrix stresses can be represented as a function of the volume fraction and compliance matrices of the fiber, matrix and unidirectional composite. The inputs required for the stress analysis are comprised of the allowable fiber stresses, σ_f^+ and σ_f^- and the allowable matrix stresses in tension, compression and shear, designated σ_m^+, σ_m^- and τ_m, respectively.

The maximum stress failure criterion was used in the strength analysis. The matrix stresses were converted into principal stresses and maximum shear stresses. Critical ratios were computed for matrix failure (tension, compression and shear) and fiber failure (tension, compression). Matrix failure corresponds to the initiation of cracking in the matrix and may not be catastrophic in most cases. Fiber failure, on the other hand, involves actual fiber breakage. In most cases, the composite can continue to carry loads even after the occurence of matrix failures. Therefore, the strength analysis procedure was of the sequential failure type. If the first failure was a matrix failure, the matrix properties for the appropriate yarn bundle were reduced and the analysis was continued until fiber axial failure occured. In some cases, fiber failure may not occur. In such cases, the strain may suddenly increase due to repeated matrix tensile and/or shear failures. Thus, ultimate strength was characterized either by fiber axial failure or the sudden increase in strain levels.

One of the limitations of this strength approach is that accurate constituent input strengths are needed. The fiber tensile allowable may be conveniently calculated from the measured fiber bundle tensile strength, σ_L^{tu}, according to the following equation

$$\sigma_f^{+} = \frac{\sigma_L^{tu} E_L^f}{E_L^*} \tag{B.1}$$

The neat resin tensile, compressive and shear allowables, are not as readily available. The matrix tensile and shear allowables used in this program were obtained from reference B-1 and were actually measured for the 3501-6 matrix material. The properties for the various brittle epoxies compatible with graphite fibers such as 5208, 914 and 934 are expected to be very similar. The matrix compressive allowable strength was obtained from manufacturer's data sheets on various resins and is not very significant because it is high enough to prevent any matrix compressive failures.

The fiber compressive strength allowable presents more problems, however. In the present program, the compressive allowable was calculated from the following equation:

$$\sigma_f^- = \frac{\sigma_L^{cu} E_L^f}{E_L^*} \qquad (B.2)$$

where σ_L^{cu} is the measured bundle compressive strength. The above equation will yield reasonable results if the available compressive strength data are for volume fractions close to those observed in the fabrics whose strengths are to be calculated and if the fabrics are not comprised of excessively wavy yarns. The compressive strength values used in (B.2) were for T300/Epoxy ($v_f = 0.6$) composites and hence the fiber compressive allowables used can be expected to yield reasonable values for only the higher harness satin fabrics. A consistent procedure to calculate compressive strengths of wavy yarn bundles based on the properties of the constituent fiber and matrix is required. This may then be used in (B.2) to obtain a reasonable value for σ_f^-. Typical values used for the strength analyses are shown in Table B-2.

REFERENCE

B-1. Zimmerman, R. S., Adams, D. F., and Walrath, D. E., "Investigation of the Relations Between Neat Resin and Advanced Composite Mechanical Properties", NASA CR-172303, November 1984.

Table B-1. Procedure for Determining Fiber and Matrix Stresses from Bundle Stresses Using the Average Stress Model

$$v_f \sigma_{ij}^{f} + v_m \sigma_{ij}^{m} = \sigma_{ij}^{*}$$

$$v_f \epsilon_{ij}^{f} + v_m \epsilon_{ij}^{m} = \epsilon_{ij}^{*}$$

$$\left.\begin{aligned} \epsilon_{ij}^{f} &= S_{ijkl}^{f} \sigma_{kl}^{f} \\ \epsilon_{ij}^{m} &= S_{ijkl}^{m} \sigma_{kl}^{m} \\ \epsilon_{ij}^{*} &= S_{ijkl}^{*} \sigma_{kl}^{*} \end{aligned}\right\} \text{ Constitutive Stress-Strain Relations}$$

$$\therefore \sigma_{ij}^{m} = \frac{1}{v_m} \left(B_{ijkl}\right)^{-1} \left[\left(S_{klmn}^{f} - S_{klmn}^{*}\right) \sigma_{mn}^{*} \right]$$

where $\left(B_{ijkl}\right)$ is the inverse of $\left(S_{ijkl}^{f} - S_{ijkl}^{m}\right)$

Table B-2. Input Fiber and Matrix Strengths used for Fabrics Strength Analysis

T-300:	$\sigma_f^+ = 350$ ksi
	$\sigma_f^- = 330$ ksi
Epoxy:	$\sigma_m^+ = 8.3$ ksi
	$\sigma_m^- = 27.0$ ksi
	$\tau_m = 8.0$ ksi

APPENDIX C.

CALCULATOR PROGRAMS

LIST OF SYMBOLS

(as used in Appendix C)

B	constant used in equations for stresses in phases of composites
E	Young's modulus
G	shear modulus
K	plane strain bulk modulus
$	stiffness constant
γ	shear strain
∇	increment in stiffness due to Poisson's effects
ϵ	extensional strain
ν	Poisson's ratio
σ	direct stress
τ	shear stress

SUBSCRIPTS AND SUPERSCRIPTS

G	relates to shearing resistance
h	hybrid
L	lengthwise
T	thicknesswise
W	widthwise
*	attached to B as $^*B$ indicates division by v_f, i.e, $^*B = \frac{B}{v_f}$
o	relates to properties for unidirectional reinforcements

APPENDIX C. CALCULATOR PROGRAMS

A programmable hand-held calculator, such as the Hewlett-Packard 41-C is adequate for preliminary surveys of properties of 3-D composites. Four programs developed for the 41-C for such surveys are included in this appendix, as follows:

UNI Elastic Constants for Unidirectionally Reinforced Composites

HYZ Elastic Constants and Strengths for $0°/\pm\phi°/90°_W/90°_T$ 3-D Reinforcement Configurations with Y- and Z- Direction Filaments Hybrids

HY Same as HYZ with only Y-Direction Filaments Hybrid

HZ Same as HYZ with only Z-Direction Filaments Hybrid

UNI, derived from the equations of reference C-1 is contained as a subroutine in the other three programs. HYZ, HY and HZ, utilizes algebraic extensions of the effectiveness coefficient analysis of reference C-2. Resulting equations are given in Tables C-1 to C-9.

These programs yield results identical to those obtained with NDPROP upper bound when the following restrictions apply:

(1) All filaments are straight and un-crimped.

(2) There is no unsymmetric divergence from the $0°/\pm\phi°/90°_W/90°_T$ configuration that produces coupling actions i.e. $0°/+30°/-45°/90°_W/90°_T$ is not permissible. As long as coupling is avoided, any arbitrary proportions of filaments may be used.

Printouts of the programs are given in Tables C-10 to C-12. Operational instructions are given in Tables C-13 to C-15.

REFERENCES

C-1 Rosen, B. W., Chatterjee, S. N., and Kibler, J. J., "An Analysis Model for Spatially Oriented Fiber Composites," ASTM STP 617, 1977.

C-2 Dow, N. F., "Directions for 3-D Composite Reinforcement I: Intimations of Isotropy," Proc. AIAA 21st Structural Dynamics, Structures and Materials Conference, May 1980.

Tables C-1. Equations for Unidirectional Stiffnesses

$$\$_{1_\circ} = \frac{E_L(1-\nu_{TW})}{1-\nu_{TW}-2\nu_{LW}\nu_{WL}}$$

$$\$_{2_\circ} = \frac{\nu_{LW}E_W}{1-\nu_{TW}-2\nu_{LW}\nu_{WL}}$$

$$\$_{3_\circ} = \frac{\nu_{LW}E_W}{1-\nu_{TW}-2\nu_{LW}\nu_{WL}}$$

$$\$_{4_\circ} = \frac{E_W(1-\nu_{LW}\nu_{WL})}{(1-\nu_{TW}-2\nu_{LW})(1+\nu_{TW})}$$

$$\$_{5_\circ} = \frac{E_W(\nu_{TW}+\nu_{LW}\nu_{WL})}{(1-\nu_{TW}-2\nu_{LW}\nu_{WL})(1+\nu_{TW})}$$

$$\$_{6_\circ} = \frac{E_W(1-\nu_{LW}\nu_{WL})}{(1-\nu_{TW}-2\nu_{LW}\nu_{WL})(1+\nu_{TW})}$$

$$\$_{7_\circ} = G_{LW}$$

$$\$_{8_\circ} = G_{TW}$$

$$\$_{9_\circ} = G_{LT}$$

Table C-2. Equations for 3-D $0°/\pm\phi°/90°_W/90°_T$ Stiffnesses:
(1) All Filaments of Same Material

$$\$_1 = \left(\frac{v_{f_{12}}}{v_f} \cos^4\phi + \frac{v_{f_1}}{v_f}\right) \$_{1_\circ} + \left(\frac{v_{f_{12}}}{v_f} \sin^4\phi + \frac{v_{f_2}}{v_f} + \frac{v_{f_3}}{v_f}\right) \$_{4_\circ}$$

$$+ \; 4 \left(\frac{v_{f_{12}}}{v_f} \sin^2\phi \cos^2\phi\right) \left(\$_{7_\circ} + \frac{\$_{2_\circ}}{2}\right)$$

$$\$_2 = \left[\frac{v_{f_{12}}}{v_f} (\sin^4\phi + \cos^4\phi) + \frac{v_{f_1}}{v_f} + \frac{v_{f_2}}{v_f}\right] \$_{2_\circ}$$

$$+ \left(\frac{v_{f_3}}{v_f}\right) \$_{5_\circ} + 4 \left(\frac{v_{f_{12}}}{v_f} \sin^2\phi \cos^2\phi\right) \left(\frac{\$_{1_\circ} + \$_{4_\circ}}{4} - \$_{7_\circ}\right)$$

$$\$_3 = \left(\frac{v_{f_{12}}}{v_f} \cos^2\phi + \frac{v_{f_1}}{v_f} + \frac{v_{f_3}}{v_f}\right) \$_{2_\circ}$$

$$+ \left(\frac{v_{f_{12}}}{v_f} \sin^2\phi + \frac{v_{f_2}}{v_f}\right) \$_{5_\circ}$$

$$\$_4 = \left(\frac{v_{f_{12}}}{v_f} \sin^4 + \frac{v_{f_2}}{v_f}\right) \$_{1_\circ} + \left(\frac{v_{f_{12}}}{v_f} \cos^4\phi + \frac{v_{f_1}}{v_f} + \frac{v_{f_3}}{v_f}\right) \$_{4_\circ}$$

$$+ \; 4 \left(\frac{v_{f_{12}}}{v_f} \sin^2\phi \cos^2\phi\right) \left(\$_{7_\circ} + \frac{\$_{2_\circ}}{2}\right)$$

$$\$_5 = \left(\frac{v_{f_{12}}}{v_f} \sin^2\phi + \frac{v_{f_2}}{v_f} + \frac{v_{f_3}}{v_f}\right) \$_{2_\circ} + \left(\frac{v_{f_{12}}}{v_f} \cos^2\phi + \frac{v_{f_1}}{v_f}\right) \$_{5_\circ}$$

Table C-2. (cont.) Equations for 3-D $0°/\pm\phi°/90°_W/90°_T$ Stiffnesses:
(1) All Filaments of Same Material

$$\$_6 = \left(\frac{v_{f_3}}{v_f}\right) \$_{1_\circ} + \left(\frac{v_{f_{12}}}{v_f} + \frac{v_{f_1}}{v_f} + \frac{v_{f_2}}{v_f}\right) \$_{4_\circ}$$

$$\$_7 = \left[\frac{v_{f_{12}}}{v_f}\,(1\text{-}4\ \mathrm{SIN}^2\phi\ \mathrm{COS}^2\phi) + \frac{v_{f_1}}{v_f} + \frac{v_{f_2}}{v_f}\right] \$_{7_\circ} + \left(\frac{v_{f_3}}{v_f}\right) \$_{8_\circ}$$

$$+ 4\left(\frac{v_{f_{12}}}{v_f}\ \mathrm{SIN}^2\phi\ \mathrm{COS}^2\phi\right)\left(\frac{\$_{1_\circ} + \$_{4_\circ}}{4} + \frac{\$_{2_\circ}}{2}\right)$$

$$\$_8 = \left(\frac{v_{f_{12}}}{v_f}\ \mathrm{SIN}^2\phi + \frac{v_{f_2}}{v_f} + \frac{v_{f_3}}{v_f}\right) \$_{7_\circ} + \left(\frac{v_{f_{12}}}{v_f}\ \mathrm{COS}^2\phi + \frac{v_{f_1}}{v_f}\right) \$_{8_\circ}$$

$$\$_9 = \left(\frac{v_{f_{12}}}{v_f}\ \mathrm{COS}^2\phi + \frac{v_{f_1}}{v_f} + \frac{v_{f_3}}{v_f}\right) \$_{7_\circ} + \left(\frac{v_{f_{12}}}{v_f}\ \mathrm{SIN}^2\phi + \frac{v_{f_2}}{v_f}\right) \$_{8_\circ}$$

Table C-3. Equations for 3-D $0°/\pm\phi°/90°_{W_h}/90°_T$ Configuration Stiffnesses: (2) 2-Direction Hybrid

$$\$_1 = \left(\frac{v_{f_{12}}}{v_f}\cos^4\phi + \frac{v_{f_1}}{v_f}\right)\$_{1_\circ} + \left(\frac{v_{f_{12}}}{v_f}\sin^4\phi + \frac{v_{f_3}}{v_f}\right)\$_{4_\circ} +$$

$$+ \left(\frac{v_{f_2}}{v_f}\right)\$_{4_{\circ h}} + 4\left(\frac{v_{f_{12}}}{v_f}\sin^2\phi\cos^2\phi\right)\left(\$_{7_\circ} + \frac{\$_{2_\circ}}{2}\right)$$

$$\$_2 = \left[\frac{v_{f_{12}}}{v_f}(\sin^4\phi + \cos^4\phi) + \frac{v_{f_1}}{v_f}\right]\$_{2_\circ} + \left(\frac{v_{f_2}}{v_f}\right)\$_{2_{\circ h}} + \left(\frac{v_{f_3}}{v_f}\right)\$_{5_\circ}$$

$$+ 4\left(\frac{v_{f_{12}}}{v_f}\sin^2\phi\cos^2\phi\right)\left(\frac{\$_{1_\circ} + \$_{4_\circ}}{4} - \$_{7_\circ}\right)$$

$$\$_3 = \left(\frac{v_{f_{12}}}{v_f}\cos^2\phi + \frac{v_{f_1}}{v_f} + \frac{v_{f_3}}{v_f}\right)\$_{2_\circ} + \left(\frac{v_{f_{12}}}{v_f}\sin^2\phi\right)\$_{5_\circ} + \left(\frac{v_{f_2}}{v_f}\right)\$_{5_{\circ h}}$$

$$\$_4 = \left(\frac{v_{f_{12}}}{v_f}\sin^4\phi\right)\$_{1_\circ} + \left(\frac{v_{f_2}}{v_f}\right)\$_{1_{\circ h}} + \left(\frac{v_{f_{12}}}{v_f}\cos^4\phi + \frac{v_{f_1}}{v_f} + \frac{v_{f_3}}{v_f}\right)\$_{4_\circ}$$

$$+ 4\left(\frac{v_{f_{12}}}{v_f}\sin^2\phi\cos^2\phi\right)\left(\$_{7_\circ} + \frac{\$_{2_\circ}}{2}\right)$$

Table C-3.(cont.) Equations for 3-D $0°/\pm\phi°/90°_{W_h}/90°_T$ Configuration Stiffnesses:(2) 2-Direction Hybrid

$$\$_5 = \left(\frac{v_{f_{12}}}{v_f}\ SIN^2\phi + \frac{v_{f_3}}{v_f}\right)\ \$_{2_{\circ_h}} + \left(\frac{v_{f_2}}{v_f}\right)\ \$_{2_{\circ_h}} + \left(\frac{v_{f_{12}}}{v_f}\ COS^2\phi + \frac{v_{f_1}}{v_f}\right)\ \$_{5_\circ}$$

$$\$_6 = \left(\frac{v_{f_3}}{v_f}\right)\ \$_{1_\circ} + \left(\frac{v_{f_{12}}}{v_f} + \frac{v_{f_1}}{v_f}\right)\ \$_{4_\circ} + \left(\frac{v_{f_2}}{v_f}\right)\ \$_{4_{\circ_h}}$$

$$\$_7 = \left[\frac{v_{f_{12}}}{v_f}\ (1\text{-}4\ SIN^2\phi\ \ COS^2\phi) + \frac{v_{f_1}}{v_f}\right]\ \$_{7_\circ} + \left(\frac{v_{f_2}}{v_f}\right)\ \$_{7_\circ}$$

$$+ \left(\frac{v_{f_3}}{v_f}\right)\ \$_{8_\circ} + 4\left(\frac{v_{f_{12}}}{v_f}\ SIN^2\phi\ COS^2\phi\right)\left(\frac{\$_{1_\circ} + \$_{4_\circ}}{4} + \frac{\$_{2_\circ}}{2}\right)$$

$$\$_8 = \left(\frac{v_{f_{12}}}{v_f}\ SIN^2\phi + \frac{v_{f_3}}{v_f}\right)\ \$_{7_\circ} + \left(\frac{v_{f_2}}{v_f}\right)\ \$_{7_{\circ_h}} + \left(\frac{v_{f_{12}}}{v_f}\ COS^2\phi + \frac{v_{f_1}}{v_f}\right)\ \$_{8_\circ}$$

$$\$_9 = \left(\frac{v_{f_{12}}}{v_f}\ COS^2\phi + \frac{v_{f_1}}{v_f} + \frac{v_{f_3}}{v_f}\right)\ \$_{7_\circ} + \left(\frac{v_{f_{12}}}{v_f}\ SIN^2\phi\right)\ \$_{8_\circ} + \left(\frac{v_{f_2}}{v_f}\right)\ \$_{8_{\circ_h}}$$

Table C-4. Equations for 3-D $0°/\pm\phi°/90°_W/90°_{T_h}$ Configuration Stiffnesses: (3) 3-Direction Hybrid

$$\$_1 = \left(\frac{v_{f_{12}}}{v_f} \cos^4\phi + \frac{v_{f_1}}{v_f}\right) \$_{1_\circ} + \left(\frac{v_{f_{12}}}{v_f} \text{SIN}^4\phi + \frac{v_{f_2}}{v_f}\right) \$_{4_\circ} + \left(\frac{v_{f_3}}{v_f}\right) \$_{4_{\circ_h}}$$

$$+ 4 \left(\frac{v_{f_{12}}}{v_f} \text{SIN}^2\phi \cos^2\phi\right) \left(\$_{7_\circ} + \frac{\$_{1_\circ}}{2}\right)$$

$$\$_2 = \left[\frac{v_{f_{12}}}{v_f} (\text{SIN}^4\phi + \cos^4\phi) + \frac{v_{f_1}}{v_f} + \frac{v_{f_2}}{v_f}\right] \$_{2_\circ} + \left(\frac{v_{f_3}}{v_f}\right) \$_{5_{\circ_h}}$$

$$+ 4 \left(\frac{v_{f_{12}}}{v_f} \text{SIN}^2\phi \cos^2\phi\right) \left(\frac{\$_{1_\circ} + \$_{4_\circ}}{4} - \$_{7_\circ}\right)$$

$$\$_3 = \left(\frac{v_{f_{12}}}{v_f} \cos^2\phi + \frac{v_{f_1}}{v_f}\right) \$_{2_\circ} + \left(\frac{v_{f_3}}{v_f}\right) \$_{2_{\circ_h}} + \left(\frac{v_{f_{12}}}{v_f} \text{SIN}^2\phi + \frac{v_{f_2}}{v_f}\right) \$_{5_\circ}$$

$$\$_4 = \left(\frac{v_{f_{12}}}{v_f} \text{SIN}^4\phi + \frac{v_{f_2}}{v_f}\right) \$_{1_\circ} + \left(\frac{v_{f_{12}}}{v_f} \cos^4\phi + \frac{v_{f_1}}{v_f}\right) \$_{4_\circ} + \left(\frac{v_{f_3}}{v_f}\right) \$_{4_\circ}$$

$$+ 4 \left(\frac{v_{f_{12}}}{v_f} \text{SIN}^2\phi \cos^2\phi\right) \left(\$_{7_\circ} + \frac{\$_{2_\circ}}{2}\right)$$

Table C-4.(cont.) Equations for 3-D $0°/\pm\phi°/90°_W/90°_{T_h}$ Configuration

Stiffnesses: (3) 3-Direction Hybrid

$$\$_5 = \left(\frac{v_{f_{12}}}{v_f}\,\mathrm{SIN}^2\phi + \frac{v_{f_2}}{v_f}\right)\$_{2_\circ} + \left(\frac{v_{f_3}}{v_f}\right)\$_{2_{\circ_h}} + \left(\frac{v_{f_{12}}}{v_f}\,\mathrm{COS}^2\phi + \frac{v_{f_1}}{v_f}\right)\$_{5_\circ}$$

$$\$_6 = \left(\frac{v_{f_3}}{v_f}\right)\$_{1_{\circ_h}} + \left(\frac{v_{f_{12}}}{v_f} + \frac{v_{f_1}}{v_f} + \frac{v_{f_2}}{v_f}\right)\$_{4_\circ}$$

$$\$_7 = \left[\frac{v_{f_{12}}}{v_f}\,(1\text{-}4\ \mathrm{SIN}^2\phi\ \mathrm{COS}^2\phi) + \frac{v_{f_1}}{v_f} + \frac{v_{f_2}}{v_f}\right]\$_{7_\circ} + \left(\frac{v_{f_3}}{v_f}\right)\$_{8_{\circ_h}}$$

$$+\ 4\left(\frac{v_{f_{12}}}{v_f}\,\mathrm{SIN}^2\phi\ \mathrm{COS}^2\phi\right)\left(\frac{\$_{1_\circ} + \$_{4_\circ}}{4} + \frac{\$_{2_\circ}}{2}\right)$$

$$\$_8 = \left(\frac{v_{f_{12}}}{v_f}\,\mathrm{SIN}^2\phi + \frac{v_{f_2}}{v_f}\right)\$_{7_\circ} + \left(\frac{v_{f_3}}{v_f}\right)\$_{7_{\circ_h}} + \left(\frac{v_{f_{12}}}{v_f}\,\mathrm{COS}^2\phi + \frac{v_{f_1}}{v_f}\right)\$_{8_\circ}$$

$$\$_9 = \left(\frac{v_{f_{12}}}{v_f}\,\mathrm{COS}^2\phi + \frac{v_{f_1}}{v_f}\right)\$_{7_\circ} + \left(\frac{v_{f_3}}{v_f}\right)\$_{7_{\circ_h}} + \left(\frac{v_{f_{12}}}{v_f}\,\mathrm{SIN}^2\phi + \frac{v_{f_2}}{v_f}\right)\$_{8_\circ}$$

Table C-5. Equations for 3-D $0°/\pm\phi°/90°_{W_h}/90°_{T_h}$ Configuration Stiffnesses: (4) 2- and 3- Directions Hybrids

$$\$_1 = \left(\frac{v_{f_{12}}}{v_f}\cos^2\phi + \frac{v_{f_1}}{v_f}\right)\$_{1_\circ} + \left(\frac{v_{f_{12}}}{v_f}\mathrm{SIN}^2\phi\right)\$_{4_\circ} + \left(\frac{v_{f_2}}{v_f} + \frac{v_{f_3}}{v_f}\right)\$_{4_{\circ_h}} + 4\left(\frac{v_{f_{12}}}{v_f}\mathrm{SIN}^2\phi\ \mathrm{COS}^2\phi\right)\left(\$_{7_\circ} + \frac{\$_{2_\circ}}{2}\right)$$

$$\$_2 = \left[\frac{v_{f_{12}}}{v_f}(\mathrm{SIN}^2\phi + \mathrm{COS}^2\phi) + \frac{v_{f_1}}{v_f}\right]\$_{2_\circ} + \left(\frac{v_{f_2}}{v_f}\right)\$_{2_{\circ_h}} + \left(\frac{v_{f_3}}{v_f}\right)\$_{5_{\circ_h}} + 4\left(\frac{v_{f_{12}}}{v_f}\mathrm{SIN}^2\phi\ \mathrm{COS}^2\phi\right)\left(\frac{\$_{1_\circ} + \$_{4_\circ}}{4} - \$_{7_\circ}\right)$$

$$\$_3 = \left(\frac{v_{f_{12}}}{v_f}\mathrm{COS}^2\phi + \frac{v_{f_1}}{v_f}\right)\$_{2_\circ} + \left(\frac{v_{f_3}}{v_f}\right)\$_{2_{\circ_h}} + \left(\frac{v_{f_{12}}}{v_f}\mathrm{SIN}^2\phi\right)\$_{5_\circ} + \left(\frac{v_{f_2}}{v_f}\right)\$_{5_{\circ_h}}$$

$$\$_4 = \left(\frac{v_{f_{12}}}{v_f}\mathrm{SIN}^4\phi\right)\$_{1_\circ} + \left(\frac{v_{f_2}}{v_f}\right)\$_{1_{\circ_h}} + \left(\frac{v_{f_{12}}}{v_f}\mathrm{COS}^4\phi + \frac{v_{f_1}}{v_f}\right)\$_{4_\circ} + \left(\frac{v_{f_3}}{v_f}\right)\$_{4_{\circ_h}} + 4\left(\frac{v_{f_{12}}}{v_f}\mathrm{SIN}^2\phi\ \mathrm{COS}^2\phi\right)\left(\$_{7_\circ} + \frac{\$_{2_\circ}}{2}\right)$$

Table C-5.(cont.) Equations for 3-D $0°/\pm\phi°/90°_{W_h}/90°_{T_h}$ Configuration Stiffnesses: (4) 2- and 3- Directions Hybrids

$$\$_5 = \left[\frac{v_{f_{12}}}{v_f} \text{SIN}^2\phi\right] \$_{2_\circ} + \left[\frac{v_{f_2}}{v_f} + \frac{v_{f_3}}{v_f}\right] \$_{2_{\circ_h}} + \left[\frac{v_{f_{12}}}{v_f} \text{COS}^2\phi + \frac{v_{f_1}}{v_f}\right] \$_{5_\circ}$$

$$\$_6 = \left[\frac{v_{f_3}}{v_f}\right] \$_{1_{\circ_h}} + \left[\frac{v_{f_{12}}}{v_f} + \frac{v_{f_1}}{v_f}\right] \$_{4_\circ} + \left[\frac{v_{f_2}}{v_f}\right] \$_{4_{\circ_h}}$$

$$\$_7 = \left[\frac{v_{f_{12}}}{v_f} (1\text{-}4\ \text{SIN}^2\phi\ \text{COS}^2\phi\ ) + \frac{v_{f_1}}{v_f}\right] \$_{7_\circ} + \left[\frac{v_{f_2}}{v_f}\right] \$_{7_{\circ_h}}$$

$$+ \left[\frac{v_{f_3}}{v_f}\right] \$_{8_{\circ_h}} + 4 \left[\frac{v_{f_{12}}}{v_f} \text{SIN}^2\phi\ \text{COS}^2\phi\right] \left[\frac{\$_{1_\circ} + \$_{4_\circ}}{4} + \frac{\$_{2_\circ}}{2}\right]$$

$$\$_8 = \left[\frac{v_{f_{12}}}{v_f} \text{SIN}^2\phi\right] \$_{7_\circ} + \left[\frac{v_{f_2}}{v_f} + \frac{v_{f_3}}{v_f}\right] \$_{7_{\circ_h}}$$

$$+ \left[\frac{v_{f_{12}}}{v_f} \text{COS}^2\phi + \frac{v_{f_1}}{v_f}\right] \$_{8_\circ}$$

Table C-5.(cont.) Equations for 3-D $0°/\pm\phi°/90°_{W_h}/90°_{T_h}$ Configuration Stiffnesses: (4) 2- and 3- Directions Hybrids

$$\$_9 = \left[\frac{v_{f_{12}}}{v_f} \cos^2\phi + \frac{v_{f_1}}{v_f} \right] \$_{7_\circ} + \left[\frac{v_{f_3}}{v_f} \right] \$_{7_{\circ_h}}$$

$$+ \left[\frac{v_{f_{12}}}{v_f} \mathrm{SIN}^2\phi \right] \$_{8_\circ} + \left[\frac{v_{f_2}}{v_f} \right] \$_{8_{\circ_h}}$$

Table C-6. Definitions of Constants Used in Equations for Average Stresses

$$B' = G_{f_{LW}} \left(\frac{G_{LW} - G_m}{G_{f_{LW}} - G_m} \right) = G_{f_{LW}} \beta' v_f \qquad \underset{-}{B}' = G_m \left(\frac{G_{f_{LW}} - G_{LW}}{G_{f_{LW}} - G_m} \right)$$

$$B'' = G_{f_{TW}} \left(\frac{G_{TW} - G_m}{G_{f_{TW}} - G_m} \right) = G_{f_{tw}} \beta'' v_f \qquad \underset{-}{B}'' = G_m \left(\frac{G_{f_{TW}} - G_{TW}}{G_{f_{TW}} - G_m} \right)$$

$$B_{LW} = \nu_{f_{LW}} K_f \left(\frac{K - K_m}{K_f - K_m} \right) = \nu_{f_{LW}} K_f \beta_{LW} v_f \qquad \underset{-}{B}_{LW} = \nu_m K_m \left(\frac{K_f - K}{K_f - K_m} \right)$$

$$B_L = \frac{v_f E_{f_L} + \nabla}{2} + 2\, \nu_{LW} B_{LW} \qquad B_{-L} = \frac{v_m E_m}{2} + 2\nu_{LW} B_{-LW}$$

$$B_T = \frac{1}{2} \left(\frac{B_{LW}}{\nu_{f_{LW}}} + B'' \right) \qquad B_{-T} = \frac{1}{2} \left(\frac{B_{LW}}{\nu_m} + \underset{-}{B}'' \right)$$

$$B_G = \frac{1}{2} \left(\frac{B_{LW}}{\nu_{f_{LW}}} - B'' \right) \qquad B_{-G} = \left(\frac{B_{LW}}{\nu_m} - \underset{-}{B}'' \right)$$

with

$$B' + \underset{-}{B}' = G_{LW} = \$_{7_\circ} = \$_{9_\circ}$$

$$B_T + B_{-T} = \frac{\$_{4_\circ}}{2} = \frac{\$_{6_\circ}}{2} = \left(\frac{1 - \nu_{LW}\nu_{WL}}{1+\nu_{TW}} \right) K_\circ$$

Table C-6.(cont.) Definitions of Constants Used in Equations for Average Stresses

$$B'' + B''_{-} = G_{TW} = \$_{8_\circ} \qquad\qquad B_G + B_{-G} = \frac{\$_{5_\circ}}{2}$$

$$B_{LW} + B_{-LW} = \frac{\$_{2_\circ}}{2} = \frac{\$_{3_\circ}}{2}$$

$$K_\circ = \$_{4_\circ} - \$_{8_\circ} = \frac{\$_{4_\circ} + \$_{5_\circ}}{2} = \$_{5_\circ} + \$_{8_\circ} = B_T + B_{-T} + B_G + B_{-G}$$

$$= 2\,[B_T + B_{-T} - (B'' + B''_{-})]$$

$$B_L + B_{-L} = \frac{\$_{1_\circ}}{2}$$

where the plane-strain bulk moduli are

$$K_\circ = \frac{\dfrac{v_f K_f}{K_f + G_M} + \dfrac{v_m K_m}{K_m + G_m}}{\dfrac{v_f}{K_f + G_m} + \dfrac{v_m}{K_m + G_m}} = \frac{E_W}{2(1 - \nu_{TW} - 2\nu_{LW}\nu_{WL})} = \$_{4_\circ} - \$_{8_\circ} = \frac{\$_{4_\circ} + \$_{5_\circ}}{2}$$

$$K_f = \frac{E_{f_W}}{2(1 - \nu_{f_{TW}} - 2\nu_{f_{LW}}\nu_{f_{WL}})}, \qquad K_M = \frac{E_m}{2\,(1 - \nu_m - 2\nu_m^2)} = \frac{G_m}{1 - 2\nu_m}$$

and

$$\nabla = 4v_f \frac{\left(\nu_{f_{LW}} - \nu_m\right)^2}{\dfrac{1}{K_f} + \dfrac{1}{v_m} \quad \left(\dfrac{v_f}{K_m} + \dfrac{1}{G_m}\right)}$$

Table C-7. Relationships Among Previously Identified Constants (ref.C-2) and Those Used Herein

$$\beta' v_f = \frac{G_{LW} - G_m}{G_{f_{LW}} - G_m}$$

$$\beta'' v_f = \frac{G_{TW} - G_m}{G_{f_{TW}} - G_m}$$

$$\beta_{LW} v_f = \frac{K - K_m}{K_f - K_m}$$

$$\beta_L v_f = \frac{B_L}{\dfrac{\nu_{f_{LW}}}{\nu_{f_{WL}}} \left(\dfrac{1 - \nu_{f_{LW}} \nu_{f_{WL}}}{1 + \nu_{f_{TW}}} \right) K_f} \qquad 1 - \beta_L v_f = \frac{B_L}{(1 - \nu_m) K_m}$$

$$\beta_T v_f = \frac{B_T}{\left(\dfrac{1 - \nu_{f_{LW}} \nu_{f_{WL}}}{1 + \nu_{f_{TW}}} \right) K_f} \qquad 1 - \beta_T v_f = \frac{B_T}{\nu_m K_m}$$

$$\beta_G v_f = \frac{B_G}{\nu_f K_f} \qquad 1 - \beta_G v_f = \frac{B_G}{\nu_m K_m}$$

Table C-8. Equations for Stresses in 3-D $0°/\pm\phi°/90°_W/90°_T$ Configurations: (1) All Filaments of Same Material

Along the $\pm\phi°$ filaments, for positive applied shear stresses -

$$\sigma_{f_{12_{L+}}} = \epsilon_{S_{L+}} * B_L + \left(\epsilon_{S_{W+}} + \epsilon_z\right) * B_{LW} \qquad \sigma_{m_{12_{L+}}} = \epsilon_{S_{L+}} * B_{-L} + \left(\epsilon_{S_{W+}} + \epsilon_z\right) * B_{LW} \quad (1)$$

Along the $\pm\phi°$ filaments, for negative applied shear stresses -

$$\sigma_{f_{12_{L-}}} = \epsilon_{S_{L-}} * B_L + \left(\epsilon_{S_{W-}} + \epsilon_z\right) * B_{LW} \qquad \sigma_{m_{12_{L-}}} = \epsilon_{S_{L-}} * B_{-L} + \left(\epsilon_{S_{W-}} + \epsilon_z\right) * B_{LW} \quad (2)$$

In plane, transverse to the $\pm\phi°$ filaments, for positive applied shear stresses -

$$\sigma_{f_{12_{W+}}} = \epsilon_{S_{L+}} * B_{LW} + \epsilon_{S_{W+}} * B_T + \epsilon_z * B_G \qquad \sigma_{m_{12_{W+}}} = \epsilon_{S_{L+}} * B_{-LW} + \epsilon_{S_{W+}} * B_T + \epsilon_z * B_{-G} \quad (3)$$

In plane, transverse to the $\pm\phi°$ filaments, for negative applied shear stresses -

$$\sigma_{f_{12_{W-}}} = \epsilon_{S_{L-}} * B_{LW} + \epsilon_{S_{W-}} * B_T + \epsilon_z * B_G \qquad \sigma_{m_{12_{W-}}} = \epsilon_{S_{L-}} * B_{-LW} + \epsilon_{S_{W-}} * B_T + \epsilon_z * B_{-G} \quad (4)$$

Thru the thickness transverse to the $\pm\phi°$ filaments, for positive applied shear stresses -

$$\sigma_{f_{12_{T+}}} = \epsilon_{S_{L+}} * B_{LW} + \epsilon_{S_{W+}} * B_G + \epsilon_z * B_T \qquad \sigma_{m_{12_{T+}}} = \epsilon_{S_{L+}} * B_{-LW} + \epsilon_{S_{W+}} * B_{-G} + \epsilon_z * B_{-T} \quad (5)$$

Table C-8.(cont.) Equations for Stresses in 3-D $0°/\pm\phi°/90°_W/90°_T$ Configurations: (1) All Filaments of Same Material

Thru the thickness transverse to the $\pm\phi°$ filaments, for negative applied shear stresses -

$$\sigma_{f_{12_{T-}}} = \epsilon_{S_{L-}} * B_{LW} + \epsilon_{S_{W-}} * B_G + \epsilon_z * B_T \qquad \sigma_{m_{12_{T-}}} = \epsilon_{S_{L-}} * B_{-LW} + \epsilon_{S_{W-}} * B_{-G} + \epsilon_z * B_{-T} \tag{6}$$

Along the 0° filaments -

$$\sigma_{f_{1_L}} = \epsilon_x * B_L + (\epsilon_y + \epsilon_z) * B_{LW} \qquad \sigma_{m_{1_L}} = \epsilon_x * B_{-L} + (\epsilon_y + \epsilon_z) * B_{-LW} \tag{7}$$

In plane transverse to the 0° filaments -

$$\sigma_{f_{1_W}} = \epsilon_x * B_{LW} + \epsilon_y * B_T + \epsilon_z * B_G \qquad \sigma_{m_{1_W}} = \epsilon_x * B_{-LW} + \epsilon_y * B_{-T} + \epsilon_z * B_{-G} \tag{8}$$

TTT transverse to the 0° filaments -

$$\sigma_{f_{1_T}} = \epsilon_x * B_{LW} + \epsilon_y * B_G + \epsilon_z * B_T \qquad \sigma_{m_{1_T}} = \epsilon_x * B_{-LW} + \epsilon_y * B_{-G} + \epsilon_z * B_{-T} \tag{9}$$

Along the in-plane 90° filaments -

$$\sigma_{f_{2_L}} = (\epsilon_x + \epsilon_z) * B_{LW} + \epsilon_y * B_L \qquad \sigma_{m_{2_L}} = (\epsilon_x + \epsilon_z) * B_{-LW} + \epsilon_y * B_{-L} \tag{10}$$

In-plane transverse to the in-plane 90° filaments -

$$\sigma_{f_{2_W}} = \epsilon_x * B_T + \epsilon_y * B_{LW} + \epsilon_z * B_G \qquad \sigma_{m_{2_W}} = \epsilon_x * B_{-T} + \epsilon_y * B_{-LW} + \epsilon_z * B_{-G} \tag{11}$$

TTT transverse to the in-plane 90° filaments -

$$\sigma_{f_{2_T}} = \epsilon_x * B_G + \epsilon_y * B_{LW} + \epsilon_z * B_T \qquad \sigma_{m_{2_T}} = \epsilon_x * B_{-G} + \epsilon_y * B_{-LW} + \epsilon_z * B_{-T} \tag{12}$$

Table C-8.(cont.) Equations for Stresses in 3-D $0°/\pm\phi°/90°_W/90°_T$ Configurations: (1) All Filaments of Same Material

Along the TTT 90° filaments -

$$\sigma_{f_{3_L}} = (\epsilon_x+\epsilon_y) *B_{LW}+\epsilon_z*B_L \qquad \sigma_{m_{3_L}} = (\epsilon_x+\epsilon_y) *B_{-LW}+\epsilon_z*B_{-L} \tag{13}$$

Transverse (y-direction) to the TTT 90° filaments -

$$\sigma_{f_{3_{W_y}}} = \epsilon_x*B_G+\epsilon_y*B +\epsilon_y*B_{LW} \qquad \sigma_{m_{3_{W_y}}} = \epsilon_x*B_{-G}+\epsilon_y*B_{-T}+\epsilon_z*B_{-LW} \tag{14}$$

Transverse (x-direction) to the TTT 90° filaments -

$$\sigma_{f_{3_{W_x}}} = \epsilon_x*B_T+\epsilon_y*B_G+\epsilon_z*B_{LW} \qquad \sigma_{m_{3_{W_x}}} = \epsilon_x*B_{-T}+\epsilon_y*B_{-G}+\epsilon_z*B_{-LW} \tag{15}$$

Table C-9 - Equations for Stresses in 3-D $0°/\pm\phi°/90°_W/90°_T$ Configurations: (2) 2- or 3-Direction Hybrid.

These equations have the same form as those in Table C-8, but the B quantities are those for the filaments in question. Thus, in all cases equations (1) - (9) are unchanged. Equations (10) - (12) become $\sigma_{f_{2_L}} = (\epsilon_x+\epsilon_z)*B_{LW_2} + \epsilon_y*B_L$, etc. if the in-plane 90° filaments are hybrids, and equations (13) - (15) become $\sigma_{f_{3_L}} = (\epsilon_x+\epsilon_y)*B_{LW_2}+\epsilon_z*B_{L_2}$, etc. if the thru the thickness filaments are of the second material.

Table C-10. Print-Out of Program HY

```
01◆LBL "HYX"
02 SF 01
03 GTO "HY"
04◆LBL "HYY"
05 SF 02
06◆LBL "HY"
07 .001
08 STO 37
09 STO 38
10 FS? 02
11 XEQ 01
12 XEQ 10
13 STO 58
14 STO 76
15 RCL 06
16 X<> 01
17 STO 11
18 RCL 07
19 X<> 02
20 STO 12
21 RCL 03
22 STO 13
23 RCL 09
24 X<> 04
25 STO 14
26 RCL 08
27 STO 71
28 RCL 67
29 STO 42
30 RCL 45
31 STO 44
32 RCL 51
33 STO 70
34 RCL 52
35 X<> 05
36 STO 15
37 RCL 53
38 STO 72
39 RCL 31
40 STO 73
41 RCL 68
42 STO 74
43 RCL 47
44 STO 77
45 RCL 79
46 STO 78
47 RCL 46
48 STO 39
49 FS? 01
50 XEQ 01
51 FS? 02
52 XEQ 01
53 XEQ 10
54 FS? 01
55 XEQ 01
56 CF 01
57 CF 02
58 RCL 16
59 STO 33
60 STO 34
61 STO 36
62 STO 37
63 ST* 66
64 1
65 RCL 26
66 STO 41
67 ST+ 41
68 COS
69 X↑2
70 STO 22
71 ST* 36
72 ST* 37
73 ST* 37
74 ST* 66
75 STO 75
76 -
77 ST* 33
78 STO 65
79 ST* 66
80 ST- 75
81 X↑2
82 *
83 STO 61
84 RCL 06
85 STO 55
86 *
87 RCL 37
88 RCL 17
89 +
90 ST* 06
91 RCL 19
92 +
93 RCL 09
94 *
95 +
96 RCL 18
97 ST* 04
98 RCL 01
99 +
100 +
101 STO 20
102 RCL 27
103 X<> 61
104 ST+ 37
105 RCL 19
106 +
107 RCL 09
108 *
109 ST+ 06
110 RCL 66
111 ST- 34
112 ST* 35
113 ST* 59
114 RCL 32
115 *
116 ST+ 06
117 ST+ 20
118 RCL 16
119 RCL 17
120 ST+ 34
121 ST+ 36
122 ST+ 37
123 +
124 ST* 09
125 RCL 04
126 ST+ 06
127 ST+ 09
128 RCL 19
129 RCL 55
130 *
131 ST+ 09
132 RCL 08
133 STO 03
134 STO 40
135 RCL 33
136 ST* 03
137 X<> 07
138 ST* 07
139 ST* 37
140 RCL 36
141 ST* 08
142 STO 55
143 RCL 19
144 +
145 X<>Y
146 *
147 ST+ 03
148 LASTX
149 RCL 19
150 *
151 ST+ 06
152 RCL 18
153 ST* 02
154 RCL 71
155 *
156 ST+ 03
157 RCL 02
158 ST+ 08
159 ST+ 37
160 RCL 07
161 ST+ 08
162 RCL 18
163 RCL 42
164 *
165 RCL 34
166 RCL 63
167 ST* 55
168 *
169 +
170 RCL 19
171 ST* 40
172 RCL 45
173 *
174 +
175 ST+ 35
176 RCL 67
177 RCL 33
178 *
179 RCL 42
180 RCL 18
181 ST* 44
182 *
183 +
184 RCL 19
185 RCL 63
186 *
187 ST+ 55
188 +
189 RCL 36
190 RCL 45
191 *
192 +
193 X<> 45
194 RCL 33
195 *
196 RCL 44
197 +
198 ST+ 55
199 RCL 40
200 ST+ 37
201 RCL 59
202 ST+ 37
203 RCL 37
204 RCL 09
205 *
206 RCL 03
207 RCL 08
208 *
209 -
210 STO 25
211 STO 40
212 RCL 03
213 RCL 20
214 *
215 RCL 37
216 RCL 08
217 *
218 -
219 STO 10
220 STO 60
221 RCL 06
222 RCL 08
223 *
224 RCL 37
225 RCL 03
226 *
227 -
228 STO 30
229 STO 50
230 RCL 20
231 RCL 09
232 *
233 RCL 08
234 X↑2
235 -
236 ST/ 10
237 ST/ 40
238 RCL 06
239 ST* 09
240 RCL 20
241 *
242 RCL 37
243 X↑2
244 -
245 ST/ 30
246 ST/ 60
247 RCL 09
248 RCL 03
249 X↑2
250 -
251 ST/ 25
252 ST/ 50
253 RCL 28
254 STO 62
255 CHS
256 STO 63
257 RCL 25
258 RCL 37
259 *
260 RCL 50
261 RCL 08
262 *
263 +
264 ST- 30
265 RCL 20
266 ST/ 62
267 RCL 50
268 /
269 ST* 30
270 ST/ 63
271 RCL 30
272 RCL 50
273 /
274 RCL 10
275 *
276 ST/ 61
277 X<> 10
278 RCL 61
279 *
280 ST- 63
281 RCL 61
282 RCL 62
283 RCL 25
284 *
285 ST- 61
286 RDN
287 RCL 40
288 *
289 ST- 62
290 RCL 65
291 RCL 62
292 STO 54
293 *
294 RCL 22
295 RCL 61
296 ST- 54
297 ST* 65
298 *
299 +
300 X<> 22
301 RCL 62
302 *
303 ST+ 65
304 RCL 29
305 RCL 35
306 /
307 STO 64
308 ST* 75
309 RCL 41
310 SIN
311 ST* 54
312 *
313 ST+ 22
314 ST- 65
315 STO 71
316 ST+ 71
317 RCL 54
318 RCL 75
319 ST+ 54
320 -
321 STO 66
322 STO 75
323 RCL 00
324 ST/ 05
325 ST/ 31
326 ST/ 51
327 ST/ 52
328 ST/ 53
329 ST/ 58
330 ST/ 70
331 ST/ 72
332 ST/ 73
333 ST/ 74
334 RCL 67
335 ST/ 39
336 ST/ 46
337 ST/ 47
338 ST/ 57
339 ST/ 58
340 ST/ 76
341 ST/ 77
342 ST/ 78
343 ST/ 79
344 RCL 61
345 STO 43
346 RCL 79
347 *
348 RCL 62
349 RCL 47
350 STO 07
351 STO 09
352 STO 59
353 *
354 +
355 STO 49
356 RCL 63
357 ST* 07
358 STO 37
359 RCL 53
360 STO 01
361 ST* 43
362 *
363 STO 44
364 RCL 62
365 ST* 01
366 ST+ 37
367 ST* 47
368 RCL 52
369 *
370 ST+ 43
371 +
372 RCL 61
373 ST* 09
374 RCL 37
375 X<> 31
376 STO 04
377 ST* 31
378 STO 33
379 *
380 ST+ 01
381 +
382 STO 41
383 RCL 61
384 RCL 46
385 STO 06
386 STO 36
387 ST* 37
388 *
389 ST+ 07
390 ST+ 47
391 RCL 63
392 STO 32
393 STO 38
394 RCL 79
395 *
396 ST+ 47
397 STO 56
398 RCL 61
399 ST+ 32
400 ST+ 38
401 RCL 05
402 *
403 RCL 62
404 STO 08
405 RCL 73
406 ST* 32
407 *
408 STO 02
409 +
410 RCL 63
411 RCL 72
412 *
413 +
414 STO 42
415 RCL 46
416 STO 34
417 X<> 39
418 ST* 08
419 ST* 38
420 RCL 63
421 ST* 34
422 RCL 78
423 *
424 RCL 08
425 +
426 RCL 61
427 ST* 78
428 RCL 77
429 *
430 +
431 STO 48
432 RCL 61
433 RCL 62
434 ST* 70
435 +
436 ST* 33
437 ST* 39
438 RCL 63
439 ST* 05
440 ST* 77
441 RCL 51
442 *
443 ST+ 33
444 RCL 61
445 STO 03
446 RCL 72
447 *
448 RCL 05
449 +
450 ST+ 02
```

ORIGINAL PAGE IS
OF POOR QUALITY

Table C-10 (cont.). Print-Out of Program HY

```
451 RCL 44
452 X<> 77
453 ST+ 08
454 RCL 62
455 ST* 76
456 RCL 79
457 *
458 ST+ 07
459 ST+ 09
460 RCL 78
461 ST+ 08
462 RCL 63
463 RCL 58
464 *
465 ST+ 39
466 RCL 63
467 ST* 73
468 RCL 52
469 ST* 83
470 *
471 ST+ 01
472 STO 05
473 RCL 62
474 RCL 53
475 *
476 RCL 63
477 RCL 04
478 *
479 ST+ 43
480 +
481 ST+ 03
482 RCL 34
483 ST+ 09
484 ST+ 49
485 RCL 61
486 RCL 57
487 *
488 ST+ 37
489 RCL 61
490 RCL 51
491 *
492 ST+ 31
493 RCL 76
494 ST+ 38
495 RCL 70
496 ST+ 32
497 RCL 65
498 RCL 63
499 +
500 ST* 36
501 RCL 04
502 STO 76
503 *
504 RCL 22
505 ST* 04
506 ST* 46
507 RCL 51
508 *
509 +
510 STO 34
511 RCL 04
512 RCL 65
513 RCL 52
514 *
515 +
516 ST+ 44
517 RCL 65
518 RCL 53
519 *
520 RCL 05
521 +
522 ST+ 04
523 RCL 46
524 RCL 65
525 RCL 79
526 *
527 +
528 X<> 06
529 STO 25
530 STO 78
531 RCL 56
532 RCL 65
533 RCL 59
534 *
535 +
536 ST+ 46
537 RCL 22
538 RCL 57
539 *
540 ST+ 36
541 RCL 71
542 ST- 22
543 ST+ 65
544 RCL 76
545 RCL 65
546 ST* 52
547 ST* 53
548 ST* 79
549 RCL 63
550 +
551 ST* 25
552 *
553 RCL 22
554 ST* 57
555 ST* 76
556 ST* 78
557 RCL 51
558 *
559 +
560 X<> 76
561 ST+ 05
562 RCL 52
563 +
564 ST+ 77
565 RCL 53
566 ST+ 05
567 RCL 78
568 RCL 63
569 RCL 59
570 ST* 65
571 *
572 ST+ 06
573 +
574 ST+ 79
575 RCL 57
576 ST+ 25
577 RCL 65
578 ST+ 78
579 RCL 56
580 ST+ 78
581 RCL 54
582 STO 56
583 RCL 68
584 STO 51
585 ST* 54
586 ST* 75
587 RCL 74
588 STO 52
589 RCL 64
590 ST* 51
591 ST* 52
592 STO 57
593 STO 58
594 RCL 14
595 RCL 00
596 /
597 ST/ 68
598 ST/ 74
599 RCL 69
600 CHS
601 ST* 68
602 ST- 68
603 ST* 74
604 ST- 74
605 RCL 67
606 ST/ 68
607 ST/ 74
608 RCL 68
609 ST* 56
610 ST* 57
611 ST* 66
612 RCL 74
613 ST* 58
614 RCL 10
615 RTN
616◆LBL 10
617 1
618 STO 07
619 STO 34
620 STO 36
621 STO 54
622 STO 60
623 RCL 23
624 ST+ 07
625 -
626 RCL 23
627 -
628 ST* 07
629 STO 79
630 CHS
631 STO 47
632 RCL 21
633 ST/ 07
634 RCL 07
635 ST+ 07
636 RCL 24
637 4
638 *
639 *
640 ST+ 54
641 RCL 54
642 STO 45
643 RCL 12
644 1/X
645 RCL 13
646 X↑2
647 RCL 11
648 /
649 -
650 4
651 STO 10
652 *
653 RCL 15
654 1/X
655 -
656 STO 33
657 2
658 *
659 RCL 15
660 *
661 1
662 +
663 RCL 24
664 STO 48
665 RCL 15
666 ST- 48
667 /
668 ST+ 45
669 ST- 60
670 *
671 ST- 54
672 1
673 STO 51
674 STO 67
675 +
676 ST/ 54
677 RCL 00
678 ST* 54
679 ST* 54
680 ST* 54
681 ST* 60
682 ST- 67
683 R↑
684 ST+ 51
685 ST- 54
686 RCL 60
687 ST+ 45
688 ST/ 45
689 RCL 54
690 ST* 45
691 ST* 51
692 RCL 67
693 X↑2
694 3
695 *
696 ST+ 45
697 RCL 45
698 RCL 51
699 -
700 ST/ 45
701 RCL 13
702 STO 31
703 ST+ 31
704 STO 51
705 STO 52
706 RCL 23
707 STO 20
708 -
709 RCL 24
710 ST* 45
711 1/X
712 RCL 07
713 ST/ 34
714 RCL 00
715 ST* 10
716 *
717 +
718 RCL 67
719 ST* 20
720 /
721 RCL 33
722 ST- 07
723 ST/ 36
724 +
725 /
726 ST* 07
727 *
728 ST* 10
729 RCL 13
730 ST+ 07
731 RCL 00
732 STO 06
733 ST* 07
734 RCL 11
735 *
736 STO 56
737 RCL 21
738 RCL 67
739 ST/ 06
740 *
741 +
742 ST+ 10
743 RCL 20
744 ST+ 07
745 RCL 24
746 RCL 14
747 STO 68
748 /
749 STO 63
750 RCL 06
751 RCL 67
752 1/X
753 +
754 ST+ 63
755 *
756 1
757 +
758 ST/ 63
759 RCL 24
760 RCL 45
761 -
762 RCL 48
763 /
764 ST* 47
765 ST* 79
766 RCL 06
767 RCL 24
768 RCL 34
769 +
770 RCL 24
771 STO 69
772 RCL 36
773 ST* 06
774 ST* 31
775 ST* 51
776 +
777 /
778 ST* 06
779 *
780 RCL 34
781 ST+ 06
782 ST- 36
783 RDN
784 1
785 STO 20
786 STO 46
787 +
788 ST/ 06
789 1
790 RCL 06
791 STO 09
792 STO 52
793 1/X
794 RCL 45
795 1/X
796 STO 57
797 +
798 4
799 ST* 51
800 STO 66
801 /
802 RCL 07
803 ST* 51
804 X↑2
805 RCL 10
806 ST* 06
807 /
808 +
809 ST* 06
810 ST/ 20
811 ST/ 57
812 LASTX
813 X<>Y
814 /
815 -
816 ST* 09
817 2
818 ST/ 57
819 RCL 57
820 ST/ 09
821 -
822 ST* 06
823 RCL 06
824 STO 57
825 ST+ 57
826 RCL 09
827 STO 08
828 +
829 2
830 ST* 06
831 ST* 09
832 /
833 STO 35
834 STO 59
835 RCL 45
836 ST- 08
837 RCL 52
838 ST* 07
839 RCL 34
840 -
841 RCL 36
842 /
843 ST* 31
844 ST- 46
845 ST- 47
846 ST* 51
847 ST- 79
848 2
849 ST* 08
850 RCL 23
851 RCL 23
852 +
853 ST* 46
854 ST+ 79
855 -
856 ST+ 47
857 RCL 34
858 ST* 46
859 ST* 47
860 ST* 79
861 RCL 08
862 RCL 79
863 -
864 STO 53
865 RCL 09
866 RCL 47
867 -
868 STO 52
869 RCL 56
870 ST+ 51
871 RCL 51
872 ST- 57
873 RCL 07
874 ST+ 07
875 STO 32
876 ST- 35
877 RCL 24
878 ST* 63
879 RCL 63
880 ST+ 32
881 ST- 59
882 -
883 ST* 68
884 RCL 24
885 RCL 14
886 -
887 ST/ 68
888 RCL 57
889 RTN
890◆LBL "L"
891 RCL 11
892 STO 01
893 RCL 12
894 STO 02
895 RCL 13
896 STO 03
897 RCL 14
898 STO 04
899 RCL 15
900 STO 05
901 RTN
902◆LBL 01
903 RCL 37
904 X<> 21
905 STO 37
906 RCL 38
907 X<> 24
908 STO 38
909 RTN
```

Table C-11. Print-Out of Program HZ

```
01♦LBL "HZX"
02 SF 01
03 GTO "HZ"
04♦LBL "HZY"
05 SF 02
06♦LBL "HZ"
07 .001
08 STO 37
09 STO 38
10 FS? 02
11 XEQ 01
12 XEQ 10
13 STO 58
14 STO 76
15 RCL 06
16 X<> 01
17 STO 11
18 RCL 07
19 X<> 02
20 STO 12
21 RCL 03
22 STO 13
23 RCL 09
24 X<> 04
25 STO 14
26 RCL 08
27 STO 71
28 RCL 63
29 STO 42
30 RCL 45
31 STO 44
32 RCL 51
33 STO 70
34 RCL 52
35 X<> 05
36 STO 15
37 RCL 53
38 STO 72
39 RCL 31
40 STO 73
41 RCL 66
42 STO 74
43 RCL 47
44 STO 77
45 RCL 79
46 STO 78
47 RCL 46
48 STO 39
49 FS? 01
50 XEQ 01
51 FS? 02
52 XEQ 01
53 XEQ 10
54 FS? 01
55 XEQ 01
56 CF 01
57 CF 02
58 RCL 16
59 STO 33
60 STO 36
61 STO 61
62 ST* 66
63 1
64 RCL 26
65 STO 41
66 ST+ 41
67 COS
68 X↑2
69 STO 22
70 ST* 36
71 ST* 61
72 ST* 61
73 ST* 66
74 STO 75
75 -
76 ST* 33
77 STO 65
78 ST* 66
79 ST- 75
80 X↑2
81 *
82 STO 37
83 RCL 18
84 ST+ 33
85 +
86 STO 20
87 RCL 16
88 RCL 17
89 ST+ 36
90 ST+ 61
91 +
92 STO 34
93 RCL 18
94 +
95 X<> 09
96 X<> 06
97 STO 55
98 ST* 26
99 X<>Y
100 STO 25
101 X<> 06
102 ST* 06
103 ST* 09
104 RCL 27
105 X<> 61
106 *
107 ST+ 20
108 LASTX
109 ST+ 37
110 RCL 55
111 *
112 ST+ 06
113 RCL 19
114 RCL 04
115 *
116 ST+ 06
117 ST+ 20
118 RCL 66
119 ST- 34
120 ST* 35
121 ST* 59
122 RCL 32
123 *
124 ST+ 06
125 ST+ 20
126 RCL 19
127 RCL 01
128 *
129 ST+ 09
130 RCL 08
131 STO 03
132 RCL 33
133 ST* 03
134 X<> 07
135 ST* 07
136 STO 40
137 ST* 37
138 RCL 36
139 ST* 08
140 STO 55
141 *
142 ST+ 03
143 RCL 19
144 RCL 02
145 *
146 ST+ 03
147 ST+ 08
148 RCL 59
149 ST+ 37
150 RCL 19
151 ST* 71
152 RCL 44
153 *
154 ST+ 35
155 RCL 07
156 ST+ 08
157 RCL 34
158 RCL 18
159 ST* 40
160 +
161 RCL 63
162 *
163 ST+ 35
164 RCL 33
165 RCL 63
166 ST* 55
167 *
168 RCL 19
169 RCL 42
170 *
171 ST+ 55
172 +
173 RCL 36
174 RCL 45
175 ST* 33
176 *
177 +
178 STO 45
179 RCL 33
180 ST+ 55
181 RCL 40
182 RCL 71
183 +
184 ST+ 37
185 RCL 37
186 RCL 09
187 *
188 RCL 03
189 RCL 08
190 *
191 -
192 STO 25
193 STO 40
194 RCL 03
195 RCL 20
196 *
197 RCL 37
198 RCL 08
199 *
200 -
201 STO 10
202 STO 60
203 RCL 06
204 RCL 08
205 *
206 RCL 37
207 RCL 03
208 *
209 -
210 STO 30
211 STO 50
212 RCL 20
213 RCL 09
214 *
215 RCL 08
216 X↑2
217 -
218 ST/ 10
219 ST/ 40
220 RCL 06
221 ST* 09
222 RCL 20
223 *
224 RCL 37
225 X↑2
226 -
227 ST/ 30
228 ST/ 60
229 RCL 09
230 RCL 03
231 X↑2
232 -
233 ST/ 25
234 ST/ 50
235 RCL 20
236 STO 62
237 CHS
238 STO 63
239 RCL 25
240 RCL 37
241 *
242 RCL 50
243 RCL 08
244 *
245 +
246 ST- 20
247 RCL 20
248 ST/ 62
249 RCL 50
250 /
251 ST* 30
252 ST/ 63
253 RCL 30
254 RCL 60
255 /
256 RCL 10
257 *
258 ST/ 61
259 X<> 10
260 RCL 61
261 *
262 ST- 63
263 RCL 61
264 RCL 62
265 RCL 25
266 *
267 ST- 61
268 RDN
269 RCL 40
270 *
271 ST- 62
272 RCL 65
273 RCL 62
274 STO 54
275 *
276 RCL 22
277 RCL 61
278 ST- 54
279 ST* 65
280 *
281 +
282 X<> 22
283 RCL 62
284 *
285 ST+ 65
286 RCL 29
287 RCL 35
288 /
289 STO 64
290 ST* 75
291 RCL 41
292 SIN
293 ST* 54
294 *
295 ST+ 22
296 ST- 65
297 STO 71
298 ST+ 71
299 RCL 54
300 RCL 75
301 ST+ 54
302 -
303 STO 66
304 STO 75
305 RCL 00
306 ST/ 05
307 ST/ 31
308 ST/ 51
309 ST/ 52
310 ST/ 53
311 ST/ 68
312 ST/ 70
313 ST/ 72
314 ST/ 73
315 ST/ 74
316 RCL 67
317 ST/ 39
318 ST/ 46
319 ST/ 47
320 ST/ 57
321 ST/ 58
322 ST/ 76
323 ST/ 77
324 ST/ 78
325 ST/ 79
326 RCL 61
327 STO 43
328 RCL 79
329 *
330 RCL 62
331 RCL 47
332 STO 07
333 STO 09
334 STO 59
335 *
336 +
337 STO 49
338 RCL 63
339 ST* 07
340 STO 37
341 RCL 53
342 STO 01
343 ST* 43
344 *
345 STO 44
346 RCL 62
347 ST* 01
348 ST* 37
349 ST* 47
350 RCL 52
351 *
352 ST+ 43
353 +
354 RCL 61
355 ST* 09
356 RCL 37
357 X<> 31
358 STO 04
359 ST* 31
360 STO 33
361 *
362 ST+ 01
363 +
364 STO 41
365 RCL 61
366 RCL 46
367 STO 06
368 STO 36
369 ST* 37
370 *
371 ST+ 07
372 ST+ 47
373 RCL 63
374 STO 32
375 STO 38
376 RCL 79
377 *
378 ST+ 47
379 STO 56
380 RCL 61
381 ST+ 32
382 ST+ 38
383 RCL 05
384 *
385 RCL 62
386 STO 08
387 RCL 73
388 ST* 32
389 *
390 STO 02
391 +
392 RCL 63
393 RCL 72
394 *
395 +
396 STO 42
397 RCL 46
398 STO 74
399 X<> 39
400 ST* 05
401 ST* 38
402 RCL 63
403 ST* 34
404 RCL 78
405 *
406 RCL 08
407 +
408 RCL 61
409 ST* 78
410 RCL 77
411 *
412 +
413 STO 48
414 RCL 61
415 RCL 62
416 ST* 70
417 +
418 ST* 33
419 ST* 39
420 RCL 63
421 ST* 05
422 ST* 77
423 RCL 51
424 *
425 ST+ 33
426 RCL 61
427 STO 03
428 RCL 72
429 *
430 RCL 05
431 +
432 ST+ 02
433 RCL 44
434 X<> 77
435 ST+ 08
436 RCL 62
437 ST* 76
438 RCL 79
439 *
440 ST+ 07
441 ST+ 09
442 RCL 78
443 ST+ 08
444 RCL 63
445 RCL 58
446 *
447 ST+ 39
448 RCL 63
449 ST* 73
450 RCL 52
```

Table C-11 (cont.). Print-Out of Program HZ

```
451 ST* 03
452 *
453 ST+ 01
454 STO 05
455 RCL 62
456 RCL 53
457 *
458 RCL 63
459 RCL 04
460 *
461 ST+ 43
462 +
463 ST+ 03
464 RCL 34
465 ST+ 09
466 ST+ 49
467 RCL 61
468 RCL 57
469 *
470 ST+ 37
471 RCL 61
472 RCL 51
473 *
474 ST+ 31
475 RCL 76
476 ST+ 36
477 RCL 70
478 ST+ 32
479 RCL 65
480 RCL 63
481 +
482 ST* 36
483 RCL 04
484 STO 76
485 *
486 RCL 22
487 ST* 04
488 ST* 46
489 RCL 51
490 *
491 +
492 STO 34
493 RCL 04
494 RCL 65
495 RCL 52
496 *
497 +
498 ST+ 44
499 RCL 65
500 RCL 53
501 *
502 RCL 05
503 -
504 ST+ 04
505 RCL 46
506 RCL 65
507 RCL 79
508 *
509 +
510 X<> 06
511 STO 25
512 STO 79
513 RCL 56
514 RCL 65
515 RCL 59
516 *
517 +
518 ST+ 46
519 RCL 22
520 RCL 57
521 *
522 ST+ 36
523 RCL 71
524 ST- 22
525 ST+ 65
526 RCL 76
527 RCL 65
528 ST* 52
529 ST* 53
530 ST* 79
531 RCL 63
532 +
533 ST* 25
534 *
535 RCL 22
536 ST* 57
537 ST* 76
538 ST* 78
539 RCL 51
540 *
541 +
542 X<> 76
543 ST+ 05
544 RCL 52
545 +
546 ST+ 77
547 RCL 53
548 ST+ 05
549 RCL 78
550 RCL 63
551 RCL 59
552 ST* 65
553 *
554 ST+ 06
555 +
556 ST+ 79
557 RCL 57
558 ST+ 25
559 RCL 65
560 ST+ 78
561 RCL 56
562 ST+ 78
563 RCL 54
564 STO 56
565 RCL 68
566 STO 51
567 ST* 54
568 ST* 75
569 RCL 74
570 STO 52
571 RCL 64
572 ST* 51
573 ST* 52
574 STO 57
575 STO 58
576 RCL 14
577 RCL 00
578 /
579 ST/ 68
580 ST/ 74
581 RCL 69
582 CHS
583 ST* 68
584 ST- 68
585 ST* 74
586 ST- 74
587 RCL 67
588 ST/ 68
589 ST/ 74
590 RCL 68
591 ST* 56
592 ST* 57
593 ST* 66
594 RCL 74
595 ST* 58
596 RCL 10
597 RTN
598•LBL "UNI
599 SF 00
600•LBL 10
601 1
602 STO 07
603 STO 34
604 STO 36
605 STO 54
606 STO 60
607 RCL 23
608 ST+ 07
609 -
610 RCL 23
611 -
612 ST* 07
613 STO 79
614 CHS
615 STO 47
616 RCL 21
617 ST/ 07
618 RCL 07
619 ST+ 07
620 RCL 24
621 4
622 *
623 *
624 ST+ 54
625 RCL 54
626 STO 45
627 RCL 12
628 1/X
629 RCL 13
630 X↑2
631 RCL 11
632 /
633 -
634 4
635 STO 10
636 *
637 RCL 15
638 1/X
639 -
640 STO 33
641 2
642 *
643 RCL 15
644 *
645 1
646 +
647 RCL 24
648 STO 48
649 RCL 15
650 ST- 48
651 /
652 ST+ 45
653 ST- 60
654 *
655 ST- 54
656 1
657 STO 51
658 STO 67
659 +
660 ST/ 54
661 RCL 00
662 ST* 54
663 ST* 54
664 ST* 54
665 ST* 60
666 ST- 67
667 R↑
668 ST+ 51
669 ST- 54
670 RCL 60
671 ST+ 45
672 ST/ 45
673 RCL 54
674 ST* 45
675 ST* 51
676 RCL 67
677 X↑2
678 3
679 *
680 ST+ 45
681 RCL 45
682 RCL 51
683 -
684 ST/ 45
685 RCL 13
686 STO 31
687 ST+ 31
688 STO 51
689 STO 52
690 RCL 23
691 STO 20
692 -
693 RCL 24
694 ST* 45
695 1/X
696 RCL 07
697 ST/ 34
698 RCL 00
699 ST* 10
700 *
701 +
702 RCL 67
703 ST* 20
704 /
705 RCL 33
706 ST- 07
707 ST/ 36
708 +
709 /
710 ST* 07
711 *
712 ST* 10
713 RCL 13
714 ST+ 07
715 RCL 00
716 STO 06
717 ST* 07
718 RCL 11
719 *
720 STO 56
721 RCL 21
722 RCL 67
723 ST/ 06
724 *
725 +
726 ST+ 10
727 RCL 20
728 ST+ 07
729 RCL 24
730 RCL 14
731 STO 68
732 /
733 STO 35
734 RCL 06
735 RCL 67
736 1/X
737 +
738 ST+ 35
739 *
740 1
741 +
742 ST/ 35
743 RCL 24
744 ST* 35
745 RCL 45
746 -
747 RCL 48
748 /
749 ST* 47
750 ST* 79
751 RCL 06
752 RCL 24
753 RCL 34
754 +
755 RCL 24
756 STO 69
757 RCL 36
758 ST* 06
759 ST* 31
760 ST* 51
761 +
762 /
763 ST* 06
764 *
765 RCL 34
766 ST+ 06
767 ST- 36
768 RDN
769 1
770 STO 20
771 STO 46
772 +
773 ST/ 06
774 1
775 RCL 06
776 STO 09
777 STO 52
778 1/X
779 RCL 45
780 1/X
781 STO 57
782 +
783 4
784 ST* 51
785 STO 66
786 /
787 RCL 07
788 STO 40
789 ST* 51
790 X↑2
791 RCL 10
792 ST* 06
793 /
794 +
795 ST* 06
796 ST/ 20
797 FS? 00
798 GTO "K"
799 ST/ 57
800 LASTX
801 X<>Y
802 /
803 -
804 ST* 09
805 2
806 ST/ 57
807 RCL 57
808 ST/ 09
809 -
810 ST* 06
811 RCL 06
812 STO 57
813 ST+ 57
814 RCL 09
815 STO 08
816 +
817 2
818 ST* 06
819 ST* 09
820 /
821 STO 63
822 STO 59
823 RCL 45
824 ST- 08
825 RCL 52
826 ST* 07
827 RCL 34
828 -
829 RCL 36
830 /
831 ST* 31
832 ST- 46
833 ST- 47
834 ST* 51
835 ST- 79
836 2
837 ST* 08
838 RCL 23
839 RCL 23
840 +
841 ST* 46
842 ST+ 79
843 -
844 ST+ 47
845 RCL 34
846 ST* 46
847 ST* 47
848 ST* 79
849 RCL 08
850 RCL 79
851 -
852 STO 53
853 RCL 09
854 RCL 47
855 -
856 STO 52
857 RCL 56
858 ST+ 51
859 RCL 51
860 ST- 57
861 RCL 07
862 ST+ 07
863 STO 32
864 ST- 63
865 RCL 24
866 RCL 63
867 X<> 35
868 ST+ 32
869 ST- 59
870 STO 63
871 -
872 ST* 68
873 RCL 24
874 RCL 14
875 -
876 ST/ 68
877 RCL 57
878 RTN
879•LBL "K"
880 CF 00
881 RCL 10
882 RTN
883•LBL "L"
884 RCL 11
885 STO 01
886 RCL 12
887 STO 02
888 RCL 13
889 STO 03
890 RCL 14
891 STO 04
892 RCL 15
893 STO 05
894 RTN
895•LBL 01
896 RCL 37
897 X<> 21
898 STO 37
899 RCL 38
900 X<> 24
901 STO 38
902 RTN
```

Table C-12. Print-Out of Program HYZ

```
01♦LBL "HYZX"
02 SF 01
03 GTO "HYZ"
04♦LBL "HYZY"
05 SF 02
06♦LBL "HYZ"
07 .001
08 STO 37
09 STO 38
10 FS? 02
11 XEQ 01
12 XEQ 10
13 STO 58
14 STO 76
15 RCL 06
16 X<> 01
17 STO 11
18 RCL 07
19 X<> 02
20 STO 12
21 RCL 03
22 STO 13
23 RCL 09
24 X<> 04
25 STO 14
26 RCL 08
27 STO 71
28 RCL 63
29 STO 42
30 RCL 45
31 STO 44
32 RCL 51
33 STO 70
34 RCL 52
35 X<> 05
36 STO 15
37 RCL 53
38 STO 72
39 RCL 31
40 STO 73
41 RCL 68
42 STO 74
43 RCL 47
44 STO 77
45 RCL 79
46 STO 78
47 RCL 46
48 STO 39
49 FS? 01
50 XEQ 01
51 FS? 02
52 XEQ 01
53 XEQ 10
54 FS? 01
55 XEQ 01
56 CF 01
57 CF 02
58 RCL 16
59 STO 33
60 STO 34
61 STO 36
62 STO 37
63 ST* 66
64 1
65 RCL 26
66 STO 41
67 ST+ 41
68 COS
69 X↑2
70 STO 22
71 ST* 36
72 ST* 37
73 ST* 37
74 ST* 66
75 STO 75
76 -
77 ST* 33
78 STO 65
79 ST* 66
80 ST- 75
81 X↑2
82 *
83 STO 61
84 RCL 06
85 *
86 RCL 37
87 RCL 17
88 +
89 ST* 06
90 RCL 09
91 *
92 +
93 RCL 19
94 RCL 04
95 *
96 ST+ 06
97 +
98 RCL 18
99 ST* 04
100 RCL 01
101 *
102 +
103 STO 20
104 RCL 27
105 X<> 61
106 ST+ 37
107 RCL 09
108 *
109 ST+ 06
110 RCL 66
111 ST- 34
112 ST* 35
113 ST* 59
114 RCL 32
115 *
116 ST+ 06
117 ST+ 20
118 RCL 16
119 RCL 17
120 ST+ 34
121 ST+ 36
122 ST+ 37
123 +
124 ST+ 05
125 RCL 04
126 ST+ 06
127 ST+ 09
128 RCL 19
129 RCL 01
130 *
131 ST+ 09
132 RCL 06
133 STO 03
134 RCL 33
135 ST* 03
136 X<> 07
137 ST* 07
138 ST* 37
139 RCL 36
140 ST* 08
141 STO 55
142 *
143 ST+ 03
144 RCL 19
145 RCL 02
146 *
147 ST+ 03
148 ST+ 08
149 RCL 18
150 ST* 02
151 RCL 71
152 *
153 ST+ 03
154 RCL 02
155 ST+ 08
156 ST+ 37
157 RCL 07
158 ST+ 08
159 RCL 18
160 RCL 42
161 *
162 RCL 34
163 RCL 63
164 ST* 55
165 *
166 +
167 RCL 19
168 RCL 44
169 *
170 +
171 ST+ 35
172 RCL 63
173 RCL 33
174 *
175 RCL 42
176 RCL 18
177 ST* 44
178 RCL 19
179 ST* 42
180 ST* 71
181 +
182 *
183 +
184 RCL 36
185 RCL 45
186 *
187 +
188 X<> 45
189 RCL 33
190 *
191 RCL 44
192 +
193 ST+ 55
194 RCL 42
195 ST+ 55
196 RCL 71
197 ST+ 37
198 RCL 59
199 ST+ 37
200 RCL 37
201 RCL 09
202 *
203 RCL 07
204 RCL 08
205 *
206 -
207 STO 25
208 STO 40
209 RCL 03
210 RCL 20
211 *
212 RCL 37
213 RCL 08
214 *
215 -
216 STO 10
217 STO 60
218 RCL 06
219 RCL 08
220 *
221 RCL 37
222 RCL 03
223 *
224 -
225 STO 30
226 STO 50
227 RCL 20
228 RCL 69
229 *
230 RCL 08
231 X↑2
232 -
233 ST/ 10
234 ST/ 40
235 RCL 06
236 ST* 09
237 RCL 20
238 *
239 RCL 37
240 X↑2
241 -
242 ST/ 30
243 ST/ 60
244 RCL 09
245 RCL 03
246 X↑2
247 -
248 ST/ 25
249 ST/ 50
250 RCL 20
251 STO 62
252 CHS
253 STO 63
254 RCL 25
255 RCL 37
256 *
257 RCL 50
258 RCL 08
259 *
260 +
261 ST- 20
262 RCL 20
263 ST/ 62
264 RCL 50
265 /
266 ST* 30
267 ST/ 63
268 RCL 30
269 RCL 60
270 /
271 RCL 10
272 *
273 ST/ 61
274 X<> 10
275 RCL 61
276 *
277 ST- 63
278 RCL 61
279 RCL 62
280 RCL 25
281 *
282 ST- 61
283 RDN
284 RCL 40
285 *
286 ST- 62
287 RCL 65
288 RCL 62
289 STO 54
290 *
291 RCL 22
292 RCL 61
293 ST- 54
294 ST* 65
295 *
296 +
297 X<> 22
298 RCL 62
299 *
300 ST+ 65
301 RCL 29
302 RCL 35
303 /
304 STO 64
305 ST* 75
306 RCL 41
307 SIN
308 ST* 54
309 *
310 ST+ 22
311 ST- 65
312 STO 71
313 ST+ 71
314 RCL 54
315 RCL 75
316 ST+ 54
317 -
318 STO 66
319 STO 75
320 RCL 00
321 ST/ 05
322 ST/ 31
323 ST/ 51
324 ST/ 52
325 ST/ 53
326 ST/ 68
327 ST/ 70
328 ST/ 72
329 ST/ 73
330 ST/ 74
331 RCL 67
332 ST/ 39
333 ST/ 46
334 ST/ 47
335 ST/ 57
336 ST/ 58
337 ST/ 76
338 ST/ 77
339 ST/ 78
340 ST/ 79
341 RCL 47
342 STO 07
343 STO 59
344 RCL 63
345 ST* 07
346 STO 37
347 RCL 53
348 STO 01
349 *
350 STO 44
351 RCL 62
352 ST* 01
353 ST+ 37
354 ST* 47
355 RCL 52
356 *
357 +
358 RCL 61
359 RCL 37
360 X<> 31
361 STO 04
362 ST* 31
363 *
364 ST+ 01
365 +
366 STO 41
367 RCL 61
368 RCL 46
369 STO 06
370 STO 36
371 ST* 37
372 *
373 ST+ 07
374 ST+ 47
375 RCL 63
376 STO 32
377 STO 38
378 RCL 79
379 *
380 ST+ 47
381 STO 56
382 RCL 61
383 ST+ 32
384 ST+ 36
385 RCL 05
386 STO 43
387 *
388 STO 03
389 RCL 62
390 STO 08
391 STO 09
392 RCL 73
393 ST* 32
394 *
395 STO 02
396 +
397 RCL 63
398 RCL 72
399 *
400 +
401 STO 42
402 RCL 39
403 ST* 08
404 STO 34
405 ST* 38
406 RCL 63
407 ST* 34
408 RCL 78
409 ST* 09
410 *
411 RCL 08
412 +
413 RCL 61
414 ST* 78
415 RCL 77
416 STO 49
417 *
418 ST+ 09
419 +
420 STO 48
421 RCL 63
422 ST* 05
423 ST* 58
424 ST* 77
425 RCL 70
426 *
427 RCL 61
428 RCL 62
429 ST* 43
430 ST* 70
431 +
432 ST* 39
433 RCL 73
434 *
435 +
436 STO 33
437 RCL 61
438 RCL 72
439 *
440 ST+ 43
441 RCL 05
442 +
443 ST+ 02
444 RCL 44
445 X<> 77
446 ST+ 08
447 RCL 63
448 ST* 49
449 ST* 72
450 ST* 76
```

ORIGINAL PAGE IS
OF POOR QUALITY

Table C-12 (cont.). Print-Out of Program HYZ

451 RCL 79	501 RCL 52	551 +	601 ST* 58	651 RCL 24	701 ST/ 34	751 /	801 X<>Y	850 RCL 79
452 *	502 *	552 ST+ 77	602 RCL 10	652 STO 48	702 RCL 00	752 ST* 47	802 /	851 -
453 ST+ 07	503 +	553 RCL 53	603 RTN	653 RCL 15	703 ST* 10	753 ST* 79	803 -	852 STO 53
454 RCL 78	504 ST+ 44	554 ST+ 05	604♦LBL 10	654 ST- 48	704 *	754 RCL 06	804 ST* 09	853 RCL 09
455 ST+ 08	505 RCL 65	555 RCL 78	605 1	655 /	705 +	755 RCL 24	805 2	854 RCL 47
456 ST+ 49	506 RCL 53	556 RCL 63	606 STO 07	656 ST+ 45	706 RCL 67	756 RCL 34	806 ST/ 57	855 -
457 RCL 58	507 *	557 RCL 59	607 STO 34	657 ST- 60	707 ST* 20	757 +	807 RCL 57	856 STO 52
458 ST+ 39	508 RCL 05	558 ST* 65	608 STO 36	658 *	708 /	758 RCL 24	808 ST/ 09	857 RCL 56
459 RCL 63	509 +	559 *	609 STO 54	659 ST- 54	709 RCL 33	759 STO 69	809 -	858 ST+ 51
460 ST* 73	510 ST+ 04	560 ST+ 06	610 STO 60	660 1	710 ST- 07	760 RCL 36	810 ST* 06	859 RCL 51
461 RCL 52	511 RCL 46	561 +	611 RCL 23	661 STO 51	711 ST/ 36	761 ST* 06	811 RCL 06	860 ST- 57
462 *	512 RCL 65	562 ST+ 79	612 ST+ 07	662 STO 67	712 +	762 ST* 31	812 STO 57	861 RCL 07
463 ST+ 01	513 RCL 79	563 RCL 57	613 -	663 +	713 /	763 ST* 51	813 ST+ 57	862 ST+ 07
464 STO 05	514 *	564 ST+ 25	614 RCL 23	664 ST/ 54	714 ST* 07	764 +	814 RCL 09	863 STO 32
465 RCL 72	515 +	565 RCL 65	615 -	665 RCL 00	715 *	765 /	815 STO 08	864 ST- 35
466 RCL 73	516 X<> 06	566 ST+ 78	616 ST* 07	666 ST* 54	716 ST* 10	766 ST* 06	816 +	865 RCL 24
467 ST+ 43	517 STO 25	567 RCL 56	617 STO 79	667 ST* 54	717 RCL 13	767 *	817 2	866 ST* 63
468 +	518 STO 76	568 ST+ 78	618 CHS	668 ST* 54	718 ST+ 07	768 RCL 34	818 ST* 06	867 RCL 63
469 ST+ 03	519 RCL 56	569 RCL 54	619 STO 47	669 ST* 60	719 RCL 00	769 ST+ 06	819 ST* 09	868 ST+ 32
470 RCL 34	520 RCL 65	570 STO 56	620 RCL 21	670 ST- 67	720 STO 06	770 ST- 36	820 /	869 ST- 55
471 ST+ 09	521 RCL 59	571 RCL 68	621 ST/ 07	671 R↑	721 ST* 07	771 RDN	821 STO 35	870 -
472 ST+ 49	522 *	572 STO 51	622 RCL 07	672 ST+ 51	722 RCL 11	772 1	822 STO 59	871 ST* 68
473 RCL 61	523 -	573 ST* 54	623 ST+ 07	673 ST- 54	723 *	773 STO 29	823 RCL 45	872 RCL 24
474 RCL 57	524 ST+ 46	574 ST* 75	624 RCL 24	674 RCL 60	724 STO 56	774 STO 46	824 ST- 08	873 RCL 14
475 *	525 RCL 22	575 RCL 74	625 4	675 ST+ 45	725 RCL 21	775 +	825 RCL 52	874 -
476 ST+ 37	526 RCL 57	576 STO 52	626 *	676 ST/ 45	726 RCL 67	776 ST/ 06	826 ST* 07	875 ST/ 68
477 RCL 61	527 *	577 RCL 64	627 *	677 RCL 54	727 ST/ 06	777 1	827 RCL 34	876 RCL 57
478 RCL 51	528 ST+ 36	578 ST* 51	628 ST+ 54	678 ST* 45	728 *	778 RCL 06	828 -	877 RTN
479 *	529 RCL 71	579 ST* 52	629 RCL 54	679 ST* 51	729 +	779 STO 09	829 RCL 36	878♦LBL "L"
480 ST+ 31	530 ST- 22	580 STO 57	630 STO 45	680 RCL 67	730 ST+ 10	780 STO 52	830 /	879 RCL 11
481 RCL 76	531 ST+ 65	581 STO 58	631 RCL 12	681 X↑2	731 RCL 20	781 1/X	831 ST* 31	880 STO 01
482 ST+ 38	532 RCL 76	582 RCL 14	632 1/X	682 3	732 ST+ 07	782 RCL 45	832 ST- 46	881 RCL 12
483 RCL 78	533 RCL 65	583 RCL 00	633 RCL 13	683 *	733 RCL 24	783 1/X	833 ST- 47	882 STO 02
484 ST+ 32	534 ST* 52	584 /	634 X↑2	684 ST+ 45	734 RCL 14	784 STO 57	834 ST* 51	883 RCL 13
485 RCL 65	535 ST* 53	585 ST/ 68	635 RCL 11	685 RCL 45	735 STO 63	785 +	835 ST- 79	884 STO 03
486 RCL 63	536 ST* 79	586 ST/ 74	636 /	686 RCL 51	736 /	786 4	836 2	885 RCL 14
487 +	537 RCL 63	587 RCL 69	637 -	687 -	737 STO 63	787 ST* 51	837 ST* 08	886 STO 04
488 ST* 36	538 +	588 CHS	638 4	688 ST/ 45	738 RCL 06	788 STO 66	838 RCL 23	887 RCL 15
489 RCL 04	539 ST* 25	589 ST* 68	639 STO 10	689 RCL 13	739 RCL 67	789 /	839 RCL 23	888 STO 05
490 STO 76	540 *	590 ST- 68	640 *	690 STO 31	740 1/X	790 RCL 07	840 +	889 RTN
491 *	541 RCL 22	591 ST* 74	641 RCL 15	691 ST+ 31	741 +	791 ST* 51	841 ST* 46	890♦LBL 01
492 RCL 22	542 ST* 57	592 ST- 74	642 1/X	692 STO 51	742 ST+ 63	792 X↑2	842 ST+ 79	891 RCL 37
493 ST* 04	543 ST* 76	593 RCL 67	643 -	693 STO 52	743 *	793 RCL 10	843 -	892 X<> 21
494 ST* 46	544 ST* 78	594 ST/ 68	644 STO 33	694 RCL 23	744 1	794 ST* 06	844 ST+ 47	893 STO 37
495 RCL 51	545 RCL 51	595 ST/ 74	645 2	695 STO 20	745 +	795 /	845 RCL 34	894 RCL 38
496 *	546 *	596 RCL 68	646 *	696 -	746 ST/ 63	796 +	846 ST* 46	895 X<> 24
497 +	547 +	597 ST* 56	647 RCL 15	697 RCL 24	747 RCL 24	797 ST* 06	847 ST* 47	896 STO 38
498 STO 34	548 X<> 76	598 ST* 57	648 *	698 ST* 45	748 RCL 45	798 ST/ 20	848 ST* 79	897 RTN
499 RCL 04	549 ST+ 05	599 ST* 66	649 1	699 1/X	749 -	799 ST/ 57	849 RCL 08	
500 RCL 65	550 RCL 52	600 RCL 74	650 +	700 RCL 07	750 RCL 48	800 LASTX		

Table C-13. Operational Instructions for HY, HZ, and HYZ. (Size 80 registers.)

Inputs

Filament properties	MAIN		HYBRID	
Longitudinal Young's modulus	E_{f_L}	STO 01	$E_{f_{L_2}}$	STO 11
Transverse Young's modulus	E_{f_W}	STO 02	$E_{f_{W_2}}$	STO 12
Longitudinal Poisson's ratio	$\nu_{f_{LW}}$	STO 03	$\nu_{f_{LW_2}}$	STO 13
Longitudinal shear modulus	$G_{f_{LW}}$	STO 04	$G_{f_{LW_2}}$	STO 14
Transverse shear modulus	$G_{f_{TW}}$	STO 05	$G_{f_{TW_2}}$	STO 15

Matrix properties

Young's modulus	E_m	STO 21
Poisson's ratio	ν_m	STO 23
Shear modulus	G_m	STO 24

Volume fraction reinforcement (total)	v_f	STO 00 (1)
Volume fraction in 12-direction	$\frac{v_{f_{12}}}{v_f}$	STO 16
Volume fraction in 1-direction(2)	$\frac{v_{f_1}}{v_f}$	STO 17
Volume fraction in 2-direction	$\frac{v_{f_2}}{v_f}$	STO 18
Volume fraction in 3-direction	$\frac{v_{f_3}}{v_f}$	STO 19

Angle of skew direction, deg.	ϕ	STO 26
Applied stresses	σ_x	STO 27
	σ_y	STO 28
	τ_{xy}	STO 29

Table C-13.(cont.) Operational Instructions for HY, HZ, and HYZ. (Size 80 registers.)

Outputs

See table C-14.

Notes

(1) $$\frac{v_{f_{12}}}{v_f} + \frac{v_{f_1}}{v_f} + \frac{v_{f_2}}{v_f} + \frac{v_{f_3}}{v_f} = 1$$

(2) 1-direction = x- direction, 2- = y, 3- = z.

Table C-14. Operational Instructions for UNI. (Size 45 registers.)

<u>Inputs</u>

Filament properties			
Longitudinal Young's modulus	E_{f_L} (1)	STO	11
Transverse Young's modulus	$E_{f_W} = E_{f_T}$	STO	12
Longitudinal Poisson's ratio	ν_{LW}	STO	13
Longitudinal shear modulus	$G_{f_{LW}}$	STO	14
Transverse shear modulus	$G_{f_{TW}}$ (2)	STO	15
Matrix properties			
Young's modulus	E_m (1)	STO	21
Poisson's ratio	ν_m	STO	23
Shear modulus	G_m (3)	STO	24
Volume fraction reinforcement	v_f	STO	00

<u>Outputs</u>

Longitudinal Young's modulus of composite	E_L	RCL	10
Transverse Young's modulus	E_W	RCL	20
Longitudinal Poisson's ratio of composite	ν_{LW}	RCL	30
Tranverse Poisson's ratio of composite	ν_{TW}	RCL	40
Longitudinal (in-plane) shear modulus of composite	G_{LW}	RCL	35
Transverse shear modulus of composite	G_{TW}	RCL	45

<u>Note</u>

(1) $E_{f_L} > E_m$

(2) Filaments assumed transversely isotropic. - i.e.

$$G_{f_{TW}} = \frac{E_{f_W}}{2(1+\nu_{TW})}$$

(3) Matrix assumed isotropic: - i.e. $G_m = \dfrac{E_m}{2(1+\nu_m)}$

Table C-15. Outputs from HY, HZ and HYZ

Register	00	10	20	30	40	50	60	70
Output	v_f	E_x	E_y	E_z	ν_{xy}	ν_{yz}	ν_{zx}	-
Register	01	11	21	31	41	51	61	71
Output	$\sigma_{f_{1_T}}$	E_{f_L}	E_m	$\sigma_{f_{1_L}}$	$\sigma_{f_{1_W}}$	$\tau_{f_{1LW}}$	ϵ_x	-
Register	02	12	22	32	42	52	62	72
Output	$\sigma_{f_{2_T}}$	E_{f_W}	$\epsilon_{S_L}^{-}$	$\sigma_{f_{2_L}}$	$\sigma_{f_{2_W}}$	$\tau_{f_{2LW}}$	ϵ_y	-
Register	03	13	23	33	43	53	63	73
Output	$\sigma_{f_{3_{W_x}}}$	$\nu_{f_{LW}}$	ν_m	$\sigma_{f_{3_L}}$	$\sigma_{f_{3_{W_y}}}$	-	ϵ_z	-
Register	04	14	24	34	44	54	64	74
Output	$\sigma_{f_{12_T^+}}$	$G_{f_{LW}}$	G_m	$\sigma_{f_{12_L^+}}$	$\sigma_{f_{12_W^+}}$	$\tau_{f_{12_{LW}^+}}$	γ_{xy}	-
Register	05	15	25	35	45	55	65	75
Output	$\sigma_{f_{12_T^-}}$	$G_{f_{TW}}$	$\sigma_{m_{12_L^-}}$	G_{xy}	G_{yz}	G_{zx}	-	$\tau_{f_{12_L^-}}$
Register	06	16	26	36	46	56	66	76
Output	$\sigma_{m_{12_T^+}}$	$\frac{v_{f_{12}}}{v_f}$	ϕ	$\sigma_{m_{12_L^+}}$	$\sigma_{m_{12_W^+}}$	$\tau_{m_{12_{LW}^+}}$	$\tau_{m_{12_{LW}^+}}$	$\sigma_{f_{12_L^-}}$
Register	07	17	27	37	47	57	67	77
Output	$\sigma_{m_{1_T}}$	$\frac{v_{f_1}}{v_f}$	σ_x	$\sigma_{m_{1_L}}$	$\sigma_{m_{1_W}}$	$\tau_{m_{1_{LW}}}$	v_m	$\sigma_{f_{12_W^-}}$
Register	08	18	28	38	48	58	68	78
Output	$\sigma_{m_{2_T}}$	$\frac{v_{f_2}}{v_f}$	σ_y	$\sigma_{m_{2_L}}$	$\sigma_{m_{2_W}}$	$\tau_{m_{2_{LW}}}$	-	$\sigma_{m_{12_W}}$
Register	09	19	29	39	49	59	69	79
Output	$\sigma_{m_{3_W}}$	$\frac{v_{f_3}}{v_f}$	τ_{xy}	$\sigma_{m_{3_L}}$	$\sigma_{m_{3_W}}$	-	-	$\sigma_{m_{12_T}}$

NASA Contractor Report 178275
Distribution List
NAS1-17205

NASA, Langley Research Center
ATTN: Research Information Office,
Mail Stop 151
Hampton, VA 23665-5225

NASA Ames Research Center
ATTN: Library, Mail Stop 202-3
Moffett Field, CA 94035

NASA, Langley Research Center
ATTN: H. Benson Dexter,
Mail Stop 188B
Hampton, VA 23665-5225

Jet Propulsion Laboratory
4800 Oak Grove Drive
ATTN: Library, Mail 111-113
Pasadena, CA 91103

NASA John F. Kennedy Space Center
ATTN: Library, NWSI-D
Kennedy Space Center, FL 32899

NASA Lewis Research Center
21000 Brookpark Road
ATTN: Library, Mail Stop 60-3
Cleveland, OH 44135

National Aeronautics and Space Admin.
ATTN: RM/Samual Venneri
Washington, DC 20546

Air Force Wright Aeronautical Lab.
ATTN: F.D. Cherry, AFWAL/MLB
Wright-Patterson Air Force Base,
OH 45433

Air Force Wright Aeronautical Lab.
ATTN: Larry G. Kelly, AFWAL/FIBC
Wright-Patterson Air Force Base,
OH 45433

Air Force Wright Aeronautical Lab.
ATTN: T.J. Reinhart, AFWAL/MLSE
Wright-Patterson Air Force Base,
OH 45433

U.S. Army Research & Tech. Lab.
Applied Technology Lab. (AVSCOM)
ATTN: J. Shipley
Fort Eustis, VA 23604

U.S. Army Aerostructures Directorate
(AVSCOM), Mail Stop 266
NASA Langley Research Center
Hampton, VA 23665-5225

Department of the Navy
Naval Air Systems Command
ATTN: Mike Dubberley, Code AIR 530
Room 980 JP2
Washington, DC 20361

Beech Aircraft Corporation
9709 East Central Avenue
ATTN: Ed Hooper
Wichita, KS 67201

The Boeing Company
Commercial Airplane Group
P.O. Box 3707
ATTN: J.T. Quinlivan, MS 6C-11
Seattle, WA 98124

The Boeing Company
Commercial Airplane Group
P.O. Box 3707
ATTN: J.M. Hopper, MS 6C-11
Seattle, WA 98124

Bell Helicopter Company
Box 482
ATTN: Charles Rogers
Fort Worth, TX 76101

General Dynamics Corporation
Fort Worth Division
P.O. Box 748
ATTN: W.D. Buntin, MZ 2633
Fort Worth, TX 76101

General Electric Commpany
Space Division
P.O. Box 8555
ATTN: C. Zweben
Philadelphia, PA 19101

Grumman Aerospace Corporation
ATTN: Sam Dastin, MS B10, Plant 25
Bethpage, NY 11714

L.J. Broutman & Associates
10 West 35th Street
ATTN: K.E. Hofer, Jr.
Chicago, IL 60616

Lockheed Aircraft Corporation
Lockheed-Georgia Company
86 South Cobb Drive
ATTN: W.E. Harvill, Dept. 72-77
Bldg. B-95, Zone 450
Marietta, GA 30063

McDonnell Aircraft Company
P.O. Box 516
ATTN: J.F. Harrell, Dept. 112D
Bldg. 220
St. Louis, MO 63166

Lockheed-Aircraft Corporation
Lockheed-California Company
ATTN: C.F. Griffin, Dept. 76-20
Bldg. 199
Burbank, CA 91520

Rockwell International Corporation
International Airport
ATTN: Dr. Leslie M. Lackman
Code 115001, GD14
Los Angeles, CA 90009

Northrop Corporation
3901 West Broadway
ATTN: C. Rosenkranz, Manager
Department 3851/82
Hawthorne, CA 90250

Texas A&M University
Aerospace Engineering Department
ATTN: W.J. Horn
College Station, TX 77843

Gulfstream Aerospace Corporation
P.O. Box 2206
ATTN: G.S. Viteritti
Savannah, GA 31402

Lockheed Georgia Company
Department 72-77/Zone 450
ATTN: Sherrill Biggers
Marietta, GA 30063

Atlantic Research Corporation
5390 Cherokee Avenue
ATTN: Dick T. Brown
Alexandria, VA 22314

University of Delaware
Dept. of Mechanical Engineering
ATTN: Tsu-Wei Chou
Newark, DE 19716

University of Delaware
Dept of Mechanical Engineering
ATTN: Scott Fowser
Newark, DE 19716

Office of Naval Research
Code 1131
800 N. Quincy Street
ATTN: L. H. Peebles
Arlington, VA 22217

VPI&SU
ESM Department
ATTN: Robert Simonds
Blacksburg, VA 24061

University of Delaware
Center for Composite Materials
201 Spencer Lab
ATTN: Dale Wilson
Newark, DE 19716

Naval Research Laboratory
Code 6383
ATTN: Irv Wolock
Washington, DC 20375

University of Maryland
Mechanical Engineering Department
ATTN: M.W. Hyer
College Park, MD 20742

David Taylor Naval Ship R&D Cntr.
Code 2844
ATTN: Tom Juska
Annapolis, MD 21402

David Taylor Naval Ship R&D Cntr.
Code 2844
ATTN: Roger M. Crane
Annapolis, MD 21402

Naval Air Development Center
Code 6043
ATTN: Lee W. Gause
Warminster, PA 18974

Pepin Associates
97A Exchange Street, Suite 302
ATTN: John Pepin
Portland, MA 04101

Naval Surface Weapons Center
Nometallics Materials Division
ATTN: Dick Weller
Silver Spring, MD 20910

Drexel University
Department of Materials Engineering
32nd & Chestnut Streets
ATTN: Christopher Pastore
Philadelphia, PA 19104

Fiber Materials, Inc.
Biddeford Industrial Park
ATTN: John Herrick
Biddeford, ME 04005

VPI&SU
ESM Department
ATTN: Robert Jones
Blacksburg, VA 24061

Clemson University
Department of Mechanical Engineering
ATTN: John Kennedy
Clemson, SC 29631

Drexel University
Materials Engineering Department
32nd & Chestnut Streets
ATTN: M.J. Koczak
Philadelphia, PA 19104

Textile Technologies, Inc.
ATTN: Ted Lynch
Hatboro, PA 19040

Textile Products
2512 West Woodland Drive
ATTN: John McGrath
Anaheim, CA 92801

David Taylor Naval Ship R&D Cntr.
Code 1720
ATTN: Alex Macander
Bethesda, MD 20084

NASA Goddard Space Flight Center
ATTN: Library
Greenbelt, MD 20771

Bell Helicopter Company
Box 482
ATTN: Henry Wilson
Fort Worth, TX 76101

NASA Dryden Flight Research Center
ATTN: Library
Edwards, CA 93523
Stratford, CT 06497

United Technologies Corporation
Sikorsky Aircraft Division
ATTN: Dave Lowry

NASA Lyndon B. Johnson Space Center
ATTN: JM6/Library
Houston, TX 77058

Hexcel Corporation
11711 Dublin Blvd.
ATTN: Jim Bumgarner
Dublin, CA 94566

NASA Marshall Space Flight Center
ATTN: AS24L/Library
Marshall Space Flight Center, AL 35812

David Taylor Naval Ship R&D Cntr.
Code 2844
ATTN: E.T. Camponeschi
Annapolis, MD 21402

Office, Chief of Research & Dev.
Physical & Engineering Sciences Div.
Department of the Army
ATTN: Richard L. Ballard
Washington, DC 20310

Lockheed Georgia Company
Department 72-77/Zone 450
ATTN: John Dickson
Marietta, GA 30063

Air Force Wright Aeronautical Lab.
ATTN: R.C. Tomashot, AFWAL/MLTN
Wright-Patterson Air Force Base,
OH 45433

Douglas Aircraft Company
Dept. E-84, Mail Code 36-90
3855 Lakewood Blvd.
ATTN: Ray Palmer
Long Beach, CA 90846

U.S. Army Materials Tech.Lab.
ATTN: D.W. Oplinger
Watertown, MA 02172-2719

Atlantic Research Corporation
5390 Cherokee
ATTN: Della Scott
Alexandria, VA 22314

The Boeing Company
Commercial Airplane Group
P.O. Box 3707
ATTN: Randy Coggeshall, MS 6C-11
Seattle, WA 98124

The Boeing Company
Vertol Division
P.O. Box 16858
ATTN: Erwin Durchlaub
Philadelphia, PA 19142

General Dynamics Corporation
Convair Division
P.O. Box 85357
ATTN: Dennis R. Dunbar, MZ 21-9501
San Diego, CA 92138

McDonnell Douglas Helicopter Company
Centinela and Teale Sts.
ATTN: Donald H. Mancill,
Bldg. 12, MS T136
Culver City, CA 90230

Martin Marietta Corporation
P.O. Box 179
ATTN: John Lager
Denver, CO 80201

McDonnell Douglas Corporation
3855 Lakewood Blvd.
ATTN: Matt Stolle C1-E84, MC 36-52
Long Beach, CA 90846

NASA Scientific and Technical
Information Facility
P.O. Box 8757
Baltimore/Washington Int'l. Airport
Maryland 21240

University of Delaware
Center for Composite Materials
201 Spencer Lab
ATTN: D. Wilkins
Newark, DE 19716

Office of Naval Research
Code 1132-SM
800 N. Quincy Street
ATTN: Y. Rajapakse
Arlington, VA 22217

General Dynamics
Convair Division
ATTN: Paul Hertzberg
San Diego, CA 92123

JR&E
P.O. Box 7200
ATTN: Julius Jortner
Costa Mesa, CA 92626

Drexel University
Materials Engineering Department
32nd & Chestnut Streets
ATTN: Frank Ko
Philadelphia, PA 19104

Textile Technologies, Inc.
ATTN: Janice Maiden
Hatboro, PA 19040

Standard Bibliographic Page

1. Report No. NASA CR-178275	2. Government Accession No.	3. Recipient's Catalog No.
4. Title and Subtitle Analysis of Woven Fabrics for Reinforced Composite Materials		5. Report Date August, 1987
		6. Performing Organization Code
7. Author(s) Norris F. Dow, V. Ramnath, and B. Walter Rosen		8. Performing Organization Report No. MSC TFR 1715/0210
9. Performing Organization Name and Address Materials Sciences Corporation Gwynedd Plaza II, Bethlehem Pike Spring House, PA 19477		10. Work Unit No.
		11. Contract or Grant No. NAS1-17205
12. Sponsoring Agency Name and Address National Aeronautics and Space Administration Langley Research Center Hampton, VA 23665		13. Type of Report and Period Covered FINAL 11/3/82 - 4/30/87
		14. Sponsoring Agency Code
15. Supplementary Notes Langley Technical Monitor: H. Benson Dexter Final Report		

16. Abstract

The use of woven fabrics as reinforcements for composites are considered in depth. Methods of analysis of properties are reviewed and extended, with particular attention paid to three-dimensional constructions having thru the thickness reinforcements. Methodology developed is used parametrically to evaluate potentials for performance of a wide variety of reinforcement constructions including hybrids. Comparisons are made of predicted and measured properties of representative composites having biaxial and triaxial woven, and laminated tape lay-up reinforcements. Overall results are incorporated in advanced weave designs.

17. Key Words (Suggested by Authors(s)) Fiber reinforced composites, Fabrics Mechanical properties, Laminates, Impact resistance.		18. Distribution Statement Unclassified - Unlimited	
19. Security Classif.(of this report) Unclassified	20. Security Classif.(of this page) Unclassified	21. No. of Pages 243	22. Price

For sale by the National Technical Information Service, Springfield, Virginia 22161

NASA Langley Form 63 (June 1985)